Primordial black holes and their gravitational-wave signatures

Eleni Bagui, Sebastien Clesse, Valerio de Luca, Jose María Ezquiaga, Gabriele Franciolini, Juan García-Bellido, Cristian Joana, Rajeev Kumar Jain, Sachiko Kuroyanagi, Ilia Musco, et al.

Living Reviews in Relativity (2025)28:1
https://doi.org/10.1007/s41114-024-00053-w

REVIEW ARTICLE

Primordial black holes and their gravitational-wave signatures

Eleni Bagui[1] · Sébastien Clesse[1] · Valerio De Luca[2] · Jose María Ezquiaga[3] · Gabriele Franciolini[4] · Juan García-Bellido[5] · Cristian Joana[6,7] · Rajeev Kumar Jain[8] · Sachiko Kuroyanagi[5,9] · Ilia Musco[10,11] · Theodoros Papanikolaou[12,13,14] · Alvise Raccanelli[4,15,16,17] · Sébastien Renaux-Petel[18] · Antonio Riotto[19] · Ester Ruiz Morales[5,20] · Marco Scalisi[21] · Olga Sergijenko[22,23,24,25] · Caner Ünal[26,27,28] · Vincent Vennin[29] · David Wands[30] · For the LISA Cosmology Working Group

Received: 22 December 2023 / Accepted: 5 November 2024

Abstract

In the recent years, primordial black holes (PBHs) have emerged as one of the most interesting and hotly debated topics in cosmology. Among other possibilities, PBHs could explain both some of the signals from binary black hole mergers observed in gravitational-wave detectors and an important component of the dark matter in the Universe. Significant progress has been achieved both on the theory side and from the point of view of observations, including new models and more accurate calculations of PBH formation, evolution, clustering, merger rates, as well as new astrophysical and cosmological probes. In this work, we review, analyze and combine the latest developments in order to perform end-to-end calculations of the various gravitational-wave signatures of PBHs. Different ways to distinguish PBHs from stellar black holes are emphasized. Finally, we discuss their detectability with LISA, the first planned gravitational-wave observatory in space.

Keywords Black holes · Primordial black holes · Cosmology · Gravitational waves · LISA

List of symbols

ζ	Curvature fluctuation
δ	Density fluctuation
$\mathcal{P}_\zeta$	Primordial curvature power spectrum (dimensionless)
$\mathcal{P}_\delta$	Primordial density power spectrum (dimensionless)
n_s	Scalar spectral index of the power spectrum

Extended author information available on the last page of the article

Published online: 23 January 2025

P	Probability density function of curvature/density fluctuations
σ	Variance of P
a	Scale factor
H	Hubble parameter
N	E-fold number
$m_{\rm Pl}$	Planck mass
$M_{\rm PI}$	Reduced Planck mass
$m_{\rm PBH}$	PBH mass
$\mathcal{M}_{\rm c}$	Chirp mass of a binary
$M_{\rm tot}$	Total binary mass
m_1	Primary mass of a binary
m_2	Secondary mass of a binary
$M_{\rm H}$	Horizon mass at horizon crossing
$t_{\rm H}$	Horizon crossing time
γ	Ratio between PBH initial mass and hubble mass at horizon crossing
χ	PBH spin parameter
$f_{\rm PBH}$	Total dark matter fraction made of PBHs
ψ, ψ_1	Normalised PBH density distribution (per unit PBH mass interval)
f	Normalised PBH density distribution (per unit neperian logarithmic PBH mass interval)
β	PBH density distribution at formation (per neperian logarithmic mass interval)
$\Omega_{\rm GW}$	GW background amplitude
$\Omega_{\rm DM}$	DM density parameter
$\rho_{\rm GW}$	Energy density associated to GWs
$\delta_{\rm c}$	Overdensity threshold for PBH formation
$\delta_{\rm m}$	Matter perturbation amplitude
$\rho_{\rm PBH}$	PBH energy density profile
$n_{\rm PBH}$	PBH number density per comoving volume
w	Equation of state parameter
$\rho_{\rm c}$	Critical energy density of a spatially flat Universe
$f_{\rm NL}$	Non-Gaussianity parameter
$R_{\rm EB/LB}$	Merger rate in a comoving volume for early/late binaries (per neperian logarithmic PBH mass interval)

Contents

1 Introduction

1.1 A brief history of primordial black holes (PBHs)

The idea that black holes could have been formed in the early Universe dates back to the late 1960s with the pioneering work of Zel'dovich and Novikov (1967) and to the early 1970s with the work of Hawking (1971). This triggered Hawking's famous discovery of black hole evaporation (Hawking 1975). Subsequently, Carr, Hawking's PhD student at the time, continued to investigate PBHs (Carr and Hawking 1974; Carr 1975). Already in Hawking (1971), Carr and Hawking (1974), Chapline (1975), it was suggested that such primordial black holes (PBHs) could contribute to the suspected Dark Matter (DM) in the Universe or to the seeds of supermassive black holes. The first formation scenarios in the context of inflation were proposed in the 1990s (Dolgov and Silk 1993; Carr and Lidsey 1993; Carr et al. 1994; Ivanov et al. 1994; García-Bellido et al. 1996; Kim and Lee 1996; Kawasaki et al. 1998; Green and Liddle 1997; Ivanov 1997; Yokoyama 1998; Kotok and Naselsky 1998), but these usually led to (evaporating) PBHs of very small mass, except for García-Bellido et al. (1996) who predicted solar mass PBHs that could account for the MACHO microlensing events observed towards the Magellanic clouds (Aubourg et al. 1993; Alcock et al. 1997). Other mechanisms were also proposed, e.g., based

on phase transitions (Jedamzik 1997; Niemeyer and Jedamzik 1998), an early matter era (Khlopov and Polnarev 1980; Polnarev and Khlopov 1985; Green et al. 1997), scalar field instabilities (Khlopov et al. 1985), collapse of topological defects (Polnarev and Zembowicz 1991), modified gravity (Barrow and Carr 1996; Kawai and Kim 2021; Zhang 2022), string theory (Cicoli et al. 2018; Nanopoulos et al. 2020; Mavromatos et al. 2022), bouncing cosmological scenarios (Copeland et al. 1998; Carr and Coley 2011; Quintin and Brandenberger 2016; Chen et al. 2017; Banerjee et al. 2022; Papanikolaou et al. 2024a) as well as quantum gravity setups (Papanikolaou 2023a). In the late 1990s, stellar-mass PBHs were seriously considered as a dark matter candidate, following the possible detection in the MACHO survey (Aubourg et al. 1993; Alcock et al. 1997) of several microlensing events towards the Magellanic clouds. However, the EROS (Tisserand et al. 2007) and OGLE (Wyrzykowski et al. 2010, 2011a, b; Calchi Novati et al. 2013) surveys later set more stringent limits on the PBH abundance, and at the same time, very stringent constraints from cosmic microwave background (CMB) observations were claimed in Ricotti et al. (2008).

Despite some pioneering numerical studies (Novikov and Polnarev 1978, 1980; Bicknell and Henriksen 1979), only more recently it has become possible to fully understand the mechanism of PBH formation with detailed spherically-symmetric numerical simulations (Shibata and Sasaki 1999; Musco et al. 2005; Polnarev and Musco 2007), showing that superhorizon cosmological perturbations would collapse to PBHs after re-entering the cosmological horizon, if their amplitude δ is larger than a certain threshold value δ_c. This quantity, measured at horizon crossing, was initially estimated with a simplified Jeans length argument in Newtonian gravity (Carr 1975), giving $\delta_c \sim c_s^2$, where $c_s^2 = 1/3$ is the sound speed of the cosmological radiation fluid measured in units of the speed of light. More recently this argument has been generalized within general relativity using a three-zone model (Harada et al. 2013; Papanikolaou 2022b) which gives $\delta_c \simeq 0.4$ for a radiation-dominated Universe. Numerical simulations showed that the mechanism of critical collapse characterizing perfect fluids (Neilsen and Choptuik 2000) arises naturally in the context of PBH formation (Yokoyama 1998; Niemeyer and Jedamzik 1998; Jedamzik and Niemeyer 1999; Musco et al. 2005). In particular, the collapse is characterized by a relativistic wind which progressively separates the collapsing perturbation from the expanding background, approaching a self-similar critical solution characterizing the threshold (Musco et al. 2009; Musco and Miller 2013). Finally, a very recent detailed study has found a clear relation between the value of the threshold, δ_c, and the initial configuration of the curvature (or energy density) profile used to set the initial condition of the numerical simulations, with $0.4 \leq \delta_c \leq 2/3$, where the shape is identified by a single parameter (Musco 2019; Escrivà et al. 2020). This range is reduced to $0.4 \leq \delta_c \lesssim 0.6$ when the initial perturbations are computed, using peak theory (Bardeen et al. 1986), from the primordial power spectrum of cosmological perturbations (Musco et al. 2021).

Since 2016, the real game-changer that has rekindled the idea that PBHs may exist and constitute a significant fraction to the total dark matter (Bird et al. 2016; Clesse and García-Bellido 2017b; Sasaki et al. 2016) has been the first gravitational-wave

(GW) detection from a black hole merger by LIGO/Virgo (Abbott et al. 2016). Initially, the merger rate of early PBH binaries seemed to only allow a small fraction of the dark matter to be made of PBHs (Sasaki et al. 2016), but N-body simulations later showed that these rates are in fact significantly suppressed (Raidal et al. 2019; Trashorras et al. 2021). Nowadays, the importance of the different PBH binary formation channels, the possible abundance of PBHs, their viable mass function, are a subject of intense activity and are hotly debated (for recent reviews, see e.g. Carr and Kuhnel 2020; Carr et al. 2021c). Recent analysis based on the rate and mass (Clesse and García-Bellido 2018; Raidal et al. 2019; Carr et al. 2021b; Hall et al. 2020; Jedamzik 2020, 2021; Clesse and García-Bellido 2022; Hütsi et al. 2021c; Escrivà et al. 2023), or spin (Fernandez and Profumo 2019; De Luca et al. 2020e; García-Bellido et al. 2021c), or both (De Luca et al. 2020d, 2021c; Wong et al. 2021; Franciolini 2021; Franciolini et al. 2022a, b, e; Franciolini and Pani 2022) distributions of compact binary coalescences observed in the first, second (Abbott et al. 2019b) and third (Abbott et al. 2021a, 2023a) observing runs of the LIGO/Virgo/Kagra collaboration (LVK), suggest that some black holes may be primordial. Some are based on a Bayesian approach (Clesse and García-Bellido 2018; Raidal et al. 2019; Hall et al. 2020; Hütsi et al. 2021c; Wong et al. 2021; De Luca et al. 2021a, c; Kritos et al. 2021; Franciolini et al. 2022a, e; Franciolini 2021; Fernandez and Profumo 2019; García-Bellido et al. 2021c) that will ultimately allow us to compare statistically the different possible origins and scenarios.

Most of population analysis studies have concluded, for the considered scenarios, that only a fraction of dark matter of order of 10^{-3} made of PBHs in the LIGO/Virgo black hole mass range is allowed. While there is a rather general consensus among the community that PBHs of more than ten solar masses cannot explain the dark matter, the exact constraints on their abundance from GW obsevations at the solar-mass scale – motivated by the expected softening of the collapse threshold at the QCD transition – is still debated. On the one hand, the merger rates inferred from LIGO/Virgo are higher and still uncertain. On the other hand, the theoretical predictions for PBH merger rates are quite model dependent. There are also several sources of uncertainties in the rate prescriptions for broad PBH mass distributions, notably the importance of binary disruptions in the early Universe. Therefore, due to the broad variety of PBHs and astrophysical models as well as the large theoretical and observational uncertainties, it is still premature to firmly affirm (or deny) a PBH origin of GW observations or to relate them to a particular value of the PBH dark matter fraction. In this context, the next generation of GW detectors like Einstein Telescope (Maggiore et al. 2020), Cosmic Explorer (Reitze et al. 2019) and the Laser Interferometer Space Antenna (LISA) (Amaro-Seoane et al. 2017; Colpi et al. 2024) will play a crucial role. Also, the development of ultra-high frequency GW detectors may additionally complement the search for GW signatures of asteroid-mass PBHs (Herman et al. 2023; Franciolini et al. 2022d) (see also e.g. Aggarwal et al. 2021; Ringwald et al. 2021; Berlin et al. 2022a, b; Domcke et al. 2022).

Important progress has also been made on the limits on the allowed PBH abundance set by various types of observations. Shortly after the first GW detection, the CMB limits were re-analysed and found to be much less stringent than initially

thought (Ali-Haïmoud and Kamionkowski 2017), thereby re-opening the stellar mass region. At the same time, the degree of validity of the microlensing limits has been questioned (Hawkins 2015; Clesse and García-Bellido 2015; García-Bellido and Clesse 2018; Green 2017; Calcino et al. 2018; Carr et al. 2021b) for more realistic scenarios than monochromatic and homogeneous distributions of PBHs. New probes, like ultra-faint-dwarf galaxies (Brandt 2016; Green 2016; Li et al. 2017) and X-ray sources towards the galactic center (Gaggero et al. 2017), have revived the mass region between 1 and 100 $M_\odot$, while the constraining power of other probes like high-cadence microlensing (Niikura et al. 2019b), neutron stars (Capela et al. 2013a) and white dwarves (Capela et al. 2013b), have been reduced, which has reopened the asteroid-mass region (Smyth et al. 2020). Finally, a series of recent microlensing events from OGLE (Niikura et al. 2019a; Wyrzykowski and Mandel 2020), HSC (Niikura et al. 2019b), as well as quasars (Hawkins 1993, 2020a, b, 2022), may hint at the existence of an important population of planetary-mass and solar-mass dark compact objects. The unexplained spatial correlations between infrared and X-ray backgrounds at high redshift (Kashlinsky et al. 2005) could also be due to an important population of stellar-mass PBHs (Kashlinsky 2016; Kashlinsky et al. 2018; Cappelluti et al. 2022).

Furthermore, since PBHs are formed by the collapse of large density fluctuations, there is an associated stochastic GW background (SGWB) sourced by these perturbations at second-order. It has been calculated (Ando et al. 2018; García-Bellido et al. 2017) that if BHs detected by LVK have a primordial origin, there is an inevitable accompanying SGWB peaking around pulsar-timing-array frequencies. In September 2020, NANOGrav claimed the possible detection of a SGWB at nanohertz frequency using pulsar timing arrays (Arzoumanian et al. 2020), which may have been sourced by primordial density perturbations which could be the origin of stellar-mass PBH formation (Vaskonen and Veermäe 2021; De Luca et al. 2021g; Kohri and Terada 2021). Remarkably, such claim was confirmed by more recent pulsar timing array data released in 2023 by the NANOGrav (Agazie et al. 2023b, c), EPTA (in combination with InPTA) (Antoniadis et al. 2023a, b, 2024), PPTA (Reardon et al. 2023a, b; Zic et al. 2023) and CPTA (Xu et al. 2023) collaborations, who found evidence for a Hellings and Downs angular correlation, typical of an homogeneous spin-2 GW background and consistent with the quadrupolar nature of GWs in GR (Hellings and Downs 1983).

On the theory side, a plethora of new models have been proposed in the last four years. Most of them are still subject to fine-tuning issues related to the amplitude of fluctuations required to form PBHs with a significant abundance. Nevertheless, one should explore a new class of models that do not require a modification of the primordial power spectrum on the cosmological scale. That is, one in which the PBH formation is related to an exponential, rather than Gaussian, tail of the distribution of primordial perturbations on small scales (Ezquiaga et al. 2020; Carr et al. 2021a), which do not affect the observations on CMB scales. In these models, a large population of PBHs could arise much more naturally. PBH masses of order of the solar mass and around 30 $M_\odot$ could also arise naturally due to the thermal history of the Universe and the change in the equation of state at the QCD epoch (Jedamzik 1997; Niemeyer and Jedamzik 1998; Byrnes et al. 2018; Carr et al. 2021b;

Franciolini et al. 2022e; Escrivà et al. 2023), which should strongly boost PBH formation. Finally, besides explaining the dark matter or a significant fraction of it, PBHs could also be related to baryogenesis and different mechanisms have been proposed (Dolgov et al. 2000; Baumann et al. 2007b; García-Bellido et al. 2021a; Carr et al. 2021a; García-Bellido 2019; De Luca et al. 2021b).

Any firm detection would open a new window on the physics at play in the very early Universe and a possible way to solve various long-standing astrophysical and cosmological puzzles (Clesse and García-Bellido 2018; Carr et al. 2021b). Ultimately, the best way to distinguish PBHs from stellar black holes would be to detect sub-solar-mass black holes. Recently, four sub-solar black hole triggers have been found in the second observing run of LVK (Phukon et al. 2021; Morras et al. 2023), and three in the third observing run (Abbott et al. 2023c). These are not statistically significant enough to claim a firm detection, but if confirmed, these would strongly support a PBH origin of some LVK black holes and make a significant contribution to the dark matter in the Universe.

1.2 Why a(nother) review on PBHs?

There already exist a few recent and relatively complete review articles dedicated to PBHs, see e.g. Sasaki et al. (2018), García-Bellido (2017), Carr and Kuhnel (2020), Carr et al. (2021c, 2024). Earlier reviews that pre-date the first GW detection also exist, see e.g. Khlopov (2010), Carr et al. (2010). All of them are written by only a few authors. It has therefore been quite challenging for them to include detailed discussions and analysis of the broad range of topics covered by PBHs. Indeed, these include early Universe cosmology, numerical relativity, dark matter, astrophysics, celestial mechanics, GW astrophysics, etc. Those reviews therefore summarize some of the results obtained in these topics but do not include model specific A-to-Z calculations of PBH related observables. Very often, some of the most recent developments like the precise determination of the critical threshold density leading to PBH formation, which is highly model-dependent and varies with the evolution of the equation of state of the Universe, or the rate suppression/boost linked to Poisson clustering, are not always considered when models are compared to observations.

The goal of this paper is to review these most recent developments and discuss how they impact the GW signatures of PBHs. Compared to other recent reviews, we aim at integrating together the most recent and accurate models, e.g., of PBH formation, evolution, clustering, merger rates, in order to compute the GW signatures of PBHs, and to explore their detectability. For this purpose, we have developed in parallel a numerical code that implements all those models and recent scenarios. The code will be released soon in a separate publication, but it has been already used in this paper in order to produce the key figures. The task of including these increasingly complex models has been eased by the specific expertise of many authors, who have actively contributed to these developments, covering a broad range of topics.

Finally, another original aspect of this work is the fact that we plan to have a *living* review format, with bi-yearly updates of the present manuscript, in order to track the rapid progress in this very active field of research and provide at all times an up-to-

date reference publication. In future, this review could be expanded to include new sections on the detectability by PTAs and ground-based GW detectors, or on the cosmological signatures of PBH scenarios.

All of this encourages us to go beyond the present state, and provide a new kind of review on PBHs.

1.3 Probing PBHs with LISA

This project is hosted by the cosmology working group of the LISA consortium. Therefore our discussion has been focused on the GW signatures of PBHs in the particular context of the LISA mission.

PBHs cover a very wide range of masses and therefore frequency ranges of GWs. In particular, LISA will be sensitive to a broad band around the millihertz GW frequencies (García-Bellido et al. 2017; Cai et al. 2019a; Bartolo et al. 2019b; Ünal 2019), which is complementary to the ground-based GW detectors (Maggiore et al. 2020; Reitze et al. 2019) and electromagnetic probes (Kashlinsky et al. 2019). One of the positive prospects for LISA is the measurement of a SGWB spectrum which, if proven to have a cosmological origin, could provide some information on the physics of the early universe. One channel for example involves GWs from PBH formation in the radiation era. While it would be much more involved to robustly claim a connection to PBH formation, the search for a SGWB from PBH formation could allow to constrain their existence in different mass ranges, for example in the interesting asteroid-mass range around $10^{-12}\,M_\odot$ (Saito and Yokoyama 2009; García-Bellido et al. 2017; Cai et al. 2019a; Bartolo et al. 2019b; Ünal 2019). Moreover, the coalescence of the heavy seeds of supermassive black holes (SMBH) in the late Universe could leave clear signatures of their primordial origin, or even detect individual events at high redshift which could not have arisen from astrophysical mechanisms.

The great sensitivity of LISA at mHz frequencies (Baibhav et al. 2021; Amaro-Seoane et al. 2023; Arun et al. 2022; Karnesis et al. 2024) opens the possibility to detect the mergers of $10^3 - 10^4\,M_\odot$ PBHs all the way to $z \simeq 100$. Furthermore, the isotropic SGWB from the coalescence of PBHs since recombination should have an amplitude and spectral shape that will make it easily detectable by LISA. In this review, we will describe the different features of known PBH scenarios that can be probed with LISA.

LISA will not only probe the GWs from individual PBH mergers and we will review numerous other types of signatures of PBHs that can be probed with LISA. Among them, the GW background from second order curvature fluctuations will probe the very interesting asteroid-mass range. Other backgrounds include the one from ultralight, evaporated PBHs, the ones from early and late PBH binaries as well as from hyperbolic encounters. GW from individual sources could also be observed by LISA, for instance from intermediate-mass PBH mergers, including at high-redshifts, as above mentioned, or from inspirals with extreme mass ratios which are expected for extended PBH mass distributions. LISA will also have a key role if data are combined to LVK or other detector observations at higher frequencies, for long-

duration signals including mergers with a subsolar component. Subsolar-mass PBHs could also produce detectable quasi-monochromatic continuous waves in the LISA frequency range. Finally, a more exotic possibility is to use LISA as a detector of near-Earth asteroid-mass PBHs.

1.4 Outline of this review

This review is organized as follows. In Sect. 2, we present the different classes of theoretical PBH formation scenarios, with a focus on recent inflation models but including a discussion of other production mechanisms such as (p)reheating, curvatons, phase transitions, topological defects and primordial magnetic fields. Among inflationary scenarios, we especially focus on recent proposals in which the usual Gaussian distribution of primordial curvature fluctuations is modified in a more complex way than can be described in terms of conventional non-Gaussian deviation parameters ($f_{\rm NL}$, etc). Ultimately this could be one possible way to resolve the long-standing fine-tuning issue for primordial fluctuations as the origin of PBHs (Cole et al. 2023b).

Section 3 is dedicated to PBH formation and the computation of the PBH mass distribution. We start with the standard formation formalism but then we summarize and include in our calculations the results of the most recent and accurate studies based on simulations in numerical relativity, such as non-linear and non-Gaussian effects, the impact of the shape of the spectrum and the curvature/overdensity profiles, the changes in the equation of state linked to the thermal history, the mass and spin evolution after formation, etc.

Once the PBH mass distribution is known, the next important step is the calculation of PBH merger rates, covered in Sect. 4. PBH mergers are due to two dominant channels: early binaries that are formed before matter-radiation equality, and late binaries formed in PBH clusters. We use the latest prescriptions, e.g., based on N-body simulations, in order to derive merger rates for different mass scales and for some representative models, including for very low mass ratios and intermediate-mass BH mergers. Finally, we consider the case of hyperbolic encounters in PBH clusters that can also lead to a large number of GW burst events.

In Sect. 5, we review the different sources of stochastic backgrounds related to PBHs. One particularly relevant source of SGWB comes from the curvature fluctuations that source GWs at second order in perturbation theory. Other SGWBs are due to early or late PBH binaries as well as due to PBH isocurvature fluctuations.

In Sect. 6, we review the possible ways to use the cross-correlations between gravitational wave observations of individual mergers or the stochastic background, and large-scale structure (LSS), in order to constrain the existence and abundance of PBHs.

The current limits on the abundance of PBHs from various probes, including GWs, are reviewed and discussed in Sect. 7. In particular, we aim to present them in a model-dependent way. We emphasize and comment on the underlying hypotheses and discuss how these limits change according to the different classes of models.

Finally, the detectability of various GW signatures from PBHs with LISA is discussed in Sect. 8, including individual merger events with extreme mass ratios or

intermediate-masses, hyperbolic encounters, stochastic backgrounds, continuous waves, high-redshift signals, signal combination with other ground-based detectors, etc.

At the end of each section, we provide an augmented discussion of recent results, the current limitations and pave the way for future analyses by listing some interesting perspectives. Our conclusions are presented in Sect. 9.

2 Theoretical models

In this section, we provide an overview of the principal mechanisms that can lead to large curvature fluctuations and PBH formation. We start with inflationary scenarios (see Özsoy and Tasinato 2023 for a recent review), either in single-field (quasi-inflection point) or multi-field realisations (hybrid inflation, turns in field space, gauge field interactions, etc.). Where possible, we provide some general formulae for the calculation of the primordial power spectrum. Then we consider recent models relying on quantum diffusion of the inflaton or of a stochastic spectator field, generically leading to non-Gaussian distributions of the curvature fluctuations. The third part of this section is dedicated to other models of PBH formation, due to curvaton fields, preheating, phase transitions, early matter era, cosmic strings, domain walls and primordial magnetic fields. When PBH form due to primordial overdensities, one typically requires order one fluctuations to form PBHs due to their gravitational collapse, when they re-enter inside the Hubble horizon. One can therefore relate the PBH mass $m_{\rm PBH}$, being of the order of the mass in the Hubble horizon, to the fluctuation wavenumber k, the formation redshift and the Universe temperature at that time, as sketched in Fig. 1.

2.1 Single-field inflationary models

In the following, we provide a review of the main production mechanisms of primordial black holes in the context of single-field inflationary models.

2.1.1 The basic idea and the slow-roll approximation

The inflationary epoch provides an ideal setting for producing PBHs in the very early Universe, with single-field inflation being the minimal framework. While a nearly scale-invariant spectrum of primordial curvature perturbations is remarkably consistent with the observations of CMB temperature anisotropies at large scales, the spectrum on smaller scales remains largely unconstrained. When small-scale perturbations with sufficiently large overdensities re-enter the expanding horizon during the radiation-dominated epoch, their gradients induce a gravitational collapse that cannot be overcome even by the radiation pressure of the expanding plasma, thereby producing PBHs with a mass of the order of the horizon mass at the time of re-entry of a given wavemode, k. The abundance of PBHs crucially depends on the collapse process and the nature of primordial curvature perturbations, which are discussed later. If PBHs start evaporating due to Hawking radiation right after their

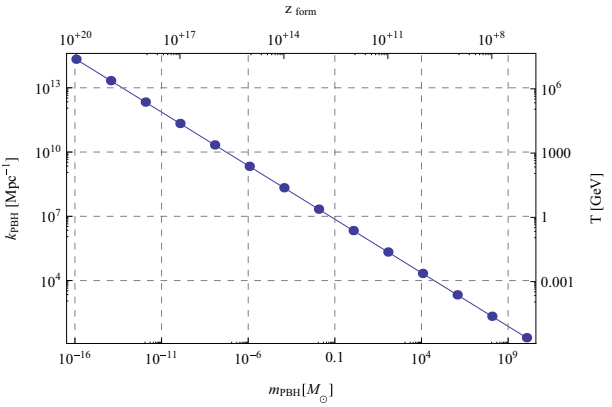

Fig. 1 Relation between the PBH mass (here being set equal to the mass in the Hubble horizon), the wave-number k associated to the primordial overdensity at the origin of the PBH formation, the Universe temperature and the redshift when this mode re-enters inside the Hubble radius. Image reproduced from Clesse et al. (2018) Image reproduced with permission

production, one finds that PBHs with mass $m_{\rm PBH} \gtrsim 10^{-18}\, M_\odot$ will survive until today and dominate the expansion of the Universe at matter-radiation equality unless their initial abundance is strongly suppressed.

Since single-field slow-roll inflationary models typically predict a nearly scale-invariant power spectrum of curvature perturbations on all scales, most slow-roll single-field inflation models do not produce PBHs, because a significant abundance of PBHs requires a substantial growth of the power spectrum on small scales. Nevertheless, a large positive running of the scalar primordial power spectrum can lead to PBH formation (Carr et al. 1994). Another possibility is to have a transition in the slope of the potential, with the scalar field slowly rolling towards a region of almost constant potential, as one gets for instance in the original hybrid inflation model along the valley. But the difficulty is then to end inflation in a limited number of e-folds while, in order to produce a large power, the potential is extremely flat. Another possibility for producing PBHs in single-field inflation is through the violation of the usual slow-roll conditions (Ivanov et al. 1994; García-Bellido and Ruiz Morales 2017; Motohashi and Hu 2017; Inomata et al. 2021b, 2022, 2023), although one should then pay a special attention to perturbative control (Inomata

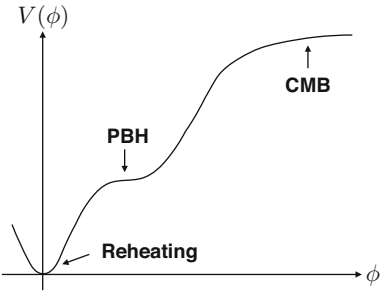

Fig. 2 A schematic plot of the inflationary potential with an inflection point. Image adapted from García-Bellido (2017) Image reproduced with permission

et al. 2023). Moreover, not all single-field inflationary models can produce the relevant abundance of PBHs as it crucially depends on the shape of the potential and various model parameters. This typically leads to a high degree of fine-tuning of model parameters.

The power spectrum of curvature perturbations in single-field models is given at first order and in the slow-roll approximation, by

$$\mathcal{P}_\zeta(k) = \frac{H_*^2}{\pi m_{\rm PI}^2 \epsilon_{1*}} \left[1 - 2(C+2)\epsilon_{1*} + C\epsilon_{2*} - (2\epsilon_{1*} + \epsilon_{2*}) \ln\left(\frac{k}{k_*}\right)\right], \qquad (1)$$

where $C = 0.578 + 2\ln 2 - 2$, $\epsilon_1 \equiv -\dot{H}/H^2$ is the first slow-roll Hubble-flow parameter, $\epsilon_2 \equiv \mathrm{d}\ln\epsilon_1/\mathrm{d}N$ is the second Hubble-flow parameter, $m_{\rm PI}$ is the Planck mass (and $M_{\rm PI} = \sqrt{8\pi}\, m_{\rm PI}$ denotes the reduced Planck mass) and a star denotes a quantity evaluated at the time the comoving wavenumber, k_*, crosses the Hubble radius during inflation when $k_* = a_* H_*$. Therefore, one can naively expect that an enhancement of $\mathcal{P}_\zeta$ can occur if there is a dynamical phase during the inflationary expansion in which ϵ_1 becomes much smaller than unity. Such an epoch is often called an *ultra slow-roll* (USR) phase which can be achieved by means of a plateau region in the inflationary potential, which slows down the inflaton field more rapidly than in slow roll, before ending inflation. An efficient and interesting way to produce this plateau is with the introduction of an inflection point in the potential. However, one must ensure that the inflaton does not stay too long at the inflection point otherwise all the inflationary fluctuations that had successfully imprinted the metric perturbations on large scales to explain the CMB anisotropies will be expanded away. A schematic plot of the potential with an inflection point is shown in Fig. 2.

2.1.2 Inflection point potentials

The simplest way to achieve an inflection or a near-inflection point in the potential is to use a suitable polynomial potential or ratio of polynomials so as to obtain the desired nearly scale invariant spectrum on CMB scales (García-Bellido and Ruiz Morales 2017). A very generic feature of such a potential is that although the inflaton starts in a slow-roll regime, it dynamically enters into an USR stage close to the inflection point for a short duration of e-folds that induces an enhancement in the spectrum. Nevertheless, it is possible to evade the USR regime in quasi-inflection point potentials (Ezquiaga et al. 2018). However, one must always be careful that this new feature in the potential does not affect the large-scale dynamics which is already strongly constrained by CMB and large-scale structure (LSS). These types of potentials arise naturally in models of Higgs inflation (Bezrukov and Shaposhnikov 2008; Ezquiaga et al. 2018), MSSM inflation (Allahverdi et al. 2006, 2007), accidental inflation (Linde and Westphal 2008), string inflation (Cicoli et al. 2018; Özsoy et al. 2018), α-attractor models (Dalianis et al. 2019; Iacconi et al. 2022; Kallosh and Linde 2022), punctuated inflation (Jain et al. 2009, 2010), non-canonical inflation (Kamenshchik et al. 2019; Lin et al. 2020; Papanikolaou et al. 2023a), as an effective description of multifield inflation (Geller et al. 2022) and in more general inflection point inflation (Hotchkiss et al. 2011). However, to produce sufficient

PBHs in these models, one crucial difference is that, rather than imposing the initial conditions on the inflaton evolution close to the inflection point, one must assume that the field starts in the slow-roll regime at larger values of the potential well above the inflection point, and then slow-rolls down towards the minimum of the potential, crossing the inflection point, typically 30 to 40 e-folds before the end of inflation. Such a dynamical evolution must ensure that large-scale dynamics are consistent with the CMB constraints, PBHs are produced at some intermediate smaller scales during the USR regime and inflation naturally ends when the field finally rolls down towards the true minimum of the potential. In this context, note that there has been an intense discussion recently on loop corrections induced on CMB scales by enhanced scalar perturbations on PBH scales (Kristiano and Yokoyama 2024a; Riotto 2023a, b; Kristiano and Yokoyama 2024b; Firouzjahi 2023; Firouzjahi and Riotto 2024; Franciolini et al. 2024a; Tasinato 2023; Cheng et al. 2024). Hints for significant one-loop contribution, to the point of undermining the consistency of such set-ups, have appeared in computations including a subset of vertices as derived from the interaction Hamiltonian. However, it has been recently shown that these effects disappear due to cancellations once all relevant interaction terms, at least at cubic order, are taken into account (Fumagalli 2023), and this subject will likely deserve further studies. Note also that enhanced fluctuations can truly lead, through loop effects, to an increase of power on (intermediate) larger scales due to infrared rescattering (Fumagalli et al. 2024), in single-field models and beyond, with potentially important consequences for the PBH population.

2.1.3 Example model: critical Higgs inflation

Critical Higgs Inflation (CHI) is probably among the best physically-motivated single-field models of inflation which can give rise to a quasi-inflection point (Ezquiaga et al. 2018) and a high plateau in the matter power spectrum. The action of the non-minimally coupled Higgs field ϕ is given by

$$S=\int \mathrm{d}^4x\sqrt{g}\left[\left(\frac{M_{\rm PI}^2}{2}+\frac{\xi(\phi)}{2}\phi^2\right)R-\frac{1}{2}(\partial\phi)^2-\frac{1}{4}\lambda(\phi)\phi^4\right] \tag{2}$$

where the running of Higgs couplings with the renormalization group scale μ can be parametrized as

$$\lambda(\phi) =\lambda_0+b_\lambda \ln^2(\phi/\mu), \tag{3}$$

$$\xi(\phi) =\xi_0+b_\xi \ln(\phi/\mu), \tag{4}$$

around the critical point $\phi=\mu$.

After standard metric and scalar field redefinitions,

$$g_{\mu\nu}\rightarrow\left(1+M_{\rm PI}^{-2}\xi(\phi)\phi^2\right)g_{\mu\nu}, \tag{5}$$

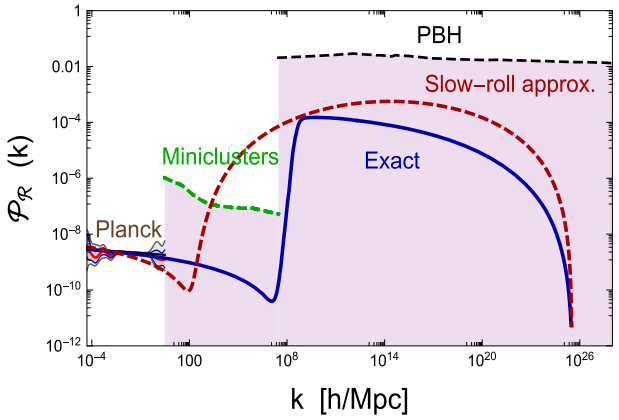

Fig. 3 Power spectrum $\mathcal{P}_{\mathcal{R}=\zeta}(k)$ for the single-field Critical Higgs Inflation model, with an inflection point at $N \approx 36$ satisfying the Planck 2018 constraints. Image adapted from García-Bellido and Ruiz Morales (2017) Image reproduced with permission

$$\phi \to \varphi = \int \mathrm{d}\phi \frac{\sqrt{1 + M_{\rm PI}^{-2}\xi(\phi)\phi^2\left(1 + 6\left(\xi(\phi) + \frac{1}{2}\phi\xi'(\phi)\right)^2\right)}}{1 + M_{\rm PI}^{-2}\xi(\phi)\phi^2}, \tag{6}$$

the effective inflationary potential becomes

$$V(x) = \frac{V_0\,(1 + a\,\ln^2 x)\,x^4}{\left(1 + c\,(1 + b\,\ln x)\,x^2\right)^2}\,, \tag{7}$$

with $V_0 = \lambda_0\mu^4/4$, $a = b_\lambda/\lambda_0$, $b = b_\xi/\xi_0$ and $c = \xi_0\,M_{\rm PI}^{-2}\mu^2$. The potential has a flat plateau at large values of the field $x = \phi/\mu$, see Fig. 2, where $V(x \gg x_{\rm c}) \simeq V_0\,\frac{a}{(bc)^2} = \frac{M_{\rm PI}^4}{4}\frac{b_\lambda}{b_\xi^2} \ll M_{\rm PI}^4$. The potential also has a short secondary plateau around the critical point, $\phi_{\rm c} = \mu$, where the inflaton-Higgs slows down and induces a large peak in the curvature power spectrum. This second plateau is induced by a quasi-inflection point at $x = x_{\rm c}$, where $V'(x_{\rm c}) \simeq 0$, $V''(x_{\rm c}) \simeq 0$. As a consequence, the number of e-folds has a sharp jump, ΔN, at that point, plus a slow rise towards larger field values, corresponding to CMB scales. This behavior is very similar to the one discussed in García-Bellido and Ruiz Morales (2017).

In order to have large PBH production and good agreement with the CMB constraints, the allowed range of CHI parameters can be found to be $\lambda_0 \approx (0.01 - 8) \times 10^{-7}$, $\xi_0 \approx (0.5 - 15)$, $x^2\mu^2 \approx (0.05 - 1.2)$, $b_\lambda \approx (0.008 - 4) \times 10^{-6}$ and $b_\xi \approx (1 - 18)$, for the USR phase to occur $N \in (30, 35)$ e-folds before the end of inflation. These values ensure the right amplitude and tilt of CMB fluctuations as measured by Planck (2018), and would also generate sufficiently large non-Gaussian tails of curvature fluctuations to produce PBH at the QCD epoch, corresponding to masses or order a solar mass, see Fig. 3. The question arises whether these values, corresponding to the model parameters at the critical scale μ,

are consistent with the values of the SM parameters at the EW scale. Given the latest values of the top quark mass $m_{\rm top}$ and strong coupling α_s (Sirunyan et al. 2020; Aad et al. 2019), the values of λ_0 and b_λ that we consider for the Higgs quartic coupling, are consistent, within 2σ, with the existence of a critical point $\lambda(\mu) \simeq \beta_\lambda(\mu) = 0$ around scales $\mu \simeq 10^{17} - 10^{18}$ GeV, where β_λ is the beta function of the RGE of the Higgs self-coupling in the SM.

Taking into account the running of both the Higgs self-coupling λ and the non-minimal coupling to gravity ξ, there are regions of parameter space allowed by the Standard Model for which the inflaton-Higgs potential acquires a second plateau at smaller scales, around the critical point. This plateau gives a super-slow-roll evolution of the Higgs, inducing a high peak in the curvature power spectrum which is very broad. When those fluctuations reenter the horizon during the radiation era, they collapse to form PBHs with masses in the range 0.1 to $100\,M_\odot$.

In single-field models with a near-inflection point, the inflaton slows down right before the end of inflation, creating a stronger backreaction and a quick growth in curvature fluctuations, giving rise to a significant increase in the power spectrum at scales much smaller than those probed by CMB and LSS observations. Since the spectral amplitude is essentially inversely proportional to the parameter ϵ_1, whose exact evolution can deviate significantly from the slow-roll approximation (García-Bellido and Ruiz Morales 2017), the power spectrum has to be calculated by integrating numerically the evolution of the inflaton field ϕ following the exact (beyond slow-roll) equations. In Fig. 3, we show a typical $\mathcal{P}(k)$ produced in quasi-inflection-point models like CHI (Ezquiaga et al. 2018). One can notice the difference between the exact power spectrum and that obtained in the slow-roll approximation. The power spectrum can be parametrized as a double step with different amplitudes and different tilts:

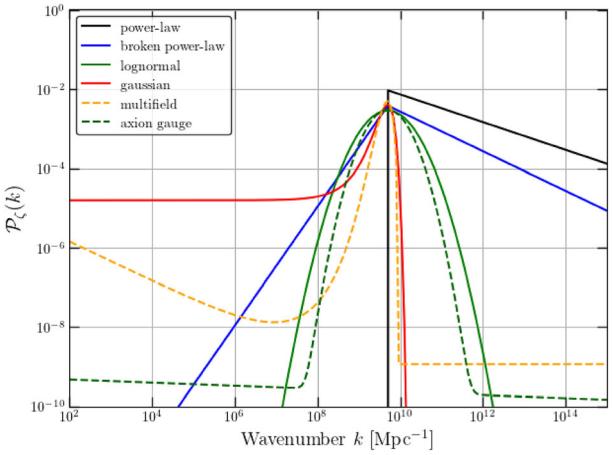

Fig. 4 Examples of primordial power spectra of curvature fluctuations, leading to (planetary-mass) PBH formation: power-law, broken power-law, Gaussian and log-normal models (solid lines), and particular examples of multifield and axion-gauge models (dashed lines). All amplitudes have been tuned to produce PBHs accounting for roughly 10% of all dark matter Image reproduced with permission

$$\mathcal{P}_\zeta(k) = \begin{cases} A_1 \left(\dfrac{k}{k_1}\right)^{n_{s1}-1} & \text{for } k < k_c \\ A_2 \left(\dfrac{k}{k_2}\right)^{n_{s2}-1} & \text{for } k > k_c \end{cases} \tag{8}$$

where A_i, n_{si}, k_i are two different amplitudes, spectral tilts and arbitrary pivot scales for the power spectrum, before and after the cut at k_c. It is also possible to introduce some small amount of running of the tilt. This power spectrum neglects quantum diffusion, which induces non-Gaussian contributions (Biagetti et al. 2018; Ezquiaga and García-Bellido 2018) and exponential tails (Ezquiaga et al. 2020), which can be responsible for a large probability of PBH formation even with a relatively small power spectrum amplitude, as will be discussed in subsequent sections. Figure 4 illustrates examples of additional common shapes for the curvature power spectrum utilised in several models discussed below.

2.1.4 Reverse engineering approach

In single-field inflationary models, the commonly adopted strategy is to start from some scalar potential that features an approximate stationary inflection point, as shown in Fig. 2; the latter is controlled by various free parameters, which are fine-tuned to guarantee the desired enhancement of the power spectrum of curvature perturbations (Inomata et al. 2017; García-Bellido and Ruiz Morales 2017; Ballesteros and Taoso 2018; Hertzberg and Yamada 2018; Kannike et al. 2017; Dalianis et al. 2019; Inomata et al. 2018; Cheong et al. 2021; Ballesteros et al. 2020c; Iacconi et al. 2022; Kawai and Kim 2021). Following Franciolini and Urbano (2022), a different, and much more powerful, approach can be entertained. In a reverse engineering procedure, the model building can be moved away from the scalar potential—that from this perspective is the output of the analysis instead of the starting point—and focused on the underlying inflationary dynamics (see Ragavendra et al. 2021; Tasinato 2021; Ng and Wu 2021; Karam et al. 2023 for a similar viewpoint).

The inflationary background dynamics can be captured by specifying a minimal set of inputs. Consider the Hubble parameters ϵ_1 and $\eta \equiv \epsilon_1 - \epsilon_2/2$, and the number of e-folds N, defined by $\mathrm{d}N = H\mathrm{d}t$. Franciolini and Urbano (2022) devised the following analytical *ansatz* for the time-evolution of η

$$\begin{aligned} 2\eta(N) = &\left[\eta_{\rm I} - \eta_{\rm II} + (\eta_{\rm II} - \eta_{\rm I}) \tanh\left(\frac{N - N_{\rm I}}{\delta N_{\rm I}}\right)\right] \\ &+ \left[\eta_{\rm II} + \eta_{\rm III} + (\eta_{\rm III} - \eta_{\rm II}) \tanh\left(\frac{N - N_{\rm II}}{\delta N_{\rm II}}\right)\right] \\ &+ \left[\eta_{\rm IV} - \eta_{\rm III} + (\eta_{\rm IV} - \eta_{\rm III}) \tanh\left(\frac{N - N_{\rm III}}{\delta N_{\rm III}}\right)\right]. \end{aligned} \tag{9}$$

The inflationary dynamics is therefore divided in different stages: (i) A first stage where $\eta_{\rm I}$ is constant and negative (necessarily taken to be small to reproduce the

conventional slow-roll dynamics) so that ϵ_1 increases relatively gently; (ii) A USR phase characterized by $\eta_{\rm II} > (3+\epsilon_1)/2 \simeq 3/2$, where negative friction makes the parameter ϵ_1 decrease abruptly (iii) An optional intermediate stage where ϵ_1 remains constant, achieved if $\eta_{\rm III} \simeq 0$, thus generating a second slow roll phase (i.e. an enhanced plateau in the curvature power spectrum; De Luca et al. 2021g; Franciolini and Urbano 2022); (iv) A final phase characterized by $\eta_{\rm IV} < 0$, that brings ϵ_1 back to $O(1)$ values for inflation to end. The parameters $\delta N_{\rm I,II,III}$ control the sharpness of the transitions.

As shown in Franciolini and Urbano (2022), Franciolini et al. (2022e), it is possible to choose the parameters controlling the ansatz of Eq. (9) in such a way that the power spectrum of curvature perturbations is compatible with CMB constraints at large scales as well as featuring an enhanced peak or plateau at scales beyond the FIRAS constraints (i.e. for $k \gtrsim 10^4/\text{Mpc}$), where a sizeable PBH abundance can be obtained, corresponding to the possible formation of masses smaller than $\mathcal{O}(10^4)M_\odot$.

Once the Hubble parameters are known, one can compute the inflationary potential by means of

$$\frac{V(N)}{V(N_{\rm ref})} = \exp\left\{-2\int_{N_{\rm ref}}^{N} dN' \left[\frac{\epsilon_1(3-\eta)}{3-\epsilon_1}\right]\right\}, \qquad \phi(N) = \phi(N_{\rm ref}) \pm \int_{N_{\rm ref}}^{N} dN' \sqrt{2\epsilon_1}\,, \tag{10}$$

where $N_{\rm ref}$ denotes an arbitrary reference e-fold time, and where in the second equation we consider the minus sign having in mind a large-field model in which the field value decreases as inflation proceeds. Combining $V(N)$ and $\phi(N)$, we reconstruct the profile $V(\phi)$ of the inflationary potential in field space (Byrnes et al. 2019). Equation (10) shows the convenience of modelling the inflationary dynamics directly at the level of η instead of $V(\phi)$. This is because the Hubble parameters enter in the exponent in the definition of $V(N)$, and thus allow for a much finer control on power spectral features when performing the reverse engineering procedure. This approach facilitates model building, even though it does not provide an interpretation of the reconstructed potential in terms of high-energy theories of inflation.

2.2 Multi-field inflationary models

As seen above, a common challenge of PBH formation within single-field inflationary models is keeping control over the two phases that lead respectively to the seeds for the CMB at large cosmic scales and for PBHs at smaller scales.

Multi-field inflationary scenarios can help separate and better control these two phases of perturbation generation, while also being very natural candidates from the UV perspective. Furthermore, violation of the standard slow-roll conditions can be efficiently realized in a context with more degrees of freedom (Clesse and García-Bellido 2015).

2.2.1 Hybrid inflation

In a setup with two scalar fields, the most studied scenario is perhaps *hybrid inflation* (Linde 1994; Copeland et al. 1994). In this class of models, inflation takes place along an almost flat valley in the direction of an initial slowly rolling scalar field, ϕ. Inflation ends with a waterfall instability when ϕ crosses a critical point, ϕ_c, due to the presence of a second field, ψ. The original hybrid potential can be written as

$$V(\phi,\psi) = \Lambda^4\left[\left(1 - \frac{\psi^2}{M^2} + \frac{\phi^2}{\mu^2} + 2\frac{\phi^2\psi^2}{\phi_c^2 M^2}\right)\right]. \tag{11}$$

The general shape of the hybrid potential is shown in Fig. 5.

When $\mu M \ll M_{\rm PI}^2$, the waterfall phase transition is nearly instantaneous and lasts less than one e-fold. The global minima of the potential are located at $\phi = 0$ and $\psi = \pm M$. Inflation can take place along the valley $\psi = 0$ with the effective potential

$$V(\phi,\psi) = \Lambda^4\left(1 + \frac{\phi^2}{\mu^2}\right) \tag{12}$$

that most often produces a *blue-tilted* power spectrum for the original potential (a *red-tilted* spectrum can nevertheless be obtained for some specific parameter values; Clesse and García-Bellido 2015). Other hybrid realisations, like F-term or D-term inflation, can produce other shapes for the effective potential, leading to a *red-tilted* spectrum, compatible with the Planck observations (see e.g. Braglia et al. 2023b, which realises this scenario via hybrid α-attractors models with scalar potentials with no tachyonic directions and, therefore, bounded from below). PBHs of tiny mass can be produced during a fast waterfall phase (García-Bellido et al. 1996), which would have evaporated today, eventually leading to the reheating of the Universe.

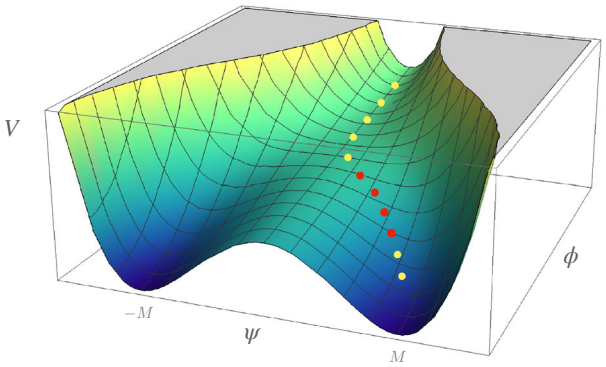

Fig. 5 Representation of a typical hybrid inflation potential, V, with a possible trajectory in two-field space (dotted line). CMB perturbations are created along the valley at $\psi = 0$, during a first phase of inflation. Curvature perturbations suitable for production of PBHs are generated in a second flat part of the potential (red dotted line), when the mass-squared of the field ψ changes sign Image reproduced with permission

In the other regime $\mu M \gg M_{\rm PI}^2$, the waterfall phase is slow, lasting $N \gg 60$ e-folds (Clesse 2011), and it is then crucial to consider the exact two-field dynamics to calculate the shape of the primordial power spectrum, which is however not compatible with Planck CMB measurements (Clesse et al. 2014).

Hybrid inflation becomes interesting for the production of massive PBHs in the transient regime, when $\mu M \sim M_{\rm PI}^2$, producing a significant but not too large number of e-folds, $10 \lesssim N \lesssim 40$. During the mild waterfall phase, the multi-field perturbation dynamics leads to a strong, exponential power spectrum enhancement (that can be sharper than the typical maximal $\propto k^4$ increase in single-field models; Byrnes et al. 2019; Cole et al. 2024) followed by a relatively sharp decrease, when going from large to small scales. The position and amplitude of the resulting broad peak is driven by a single combination of the hybrid potential parameters, $\Pi \equiv M\sqrt{\phi_{\rm c}\mu_1}/M_{\rm PI}^2$ where μ_1 comes from a linear expansion of the potential around the critical point $V \propto (\phi - \phi_{\rm c})/\mu_1$. Numerical calculations of the primordial power spectrum of curvature fluctuations using either the exact multi-field perturbation dynamics or the δN formalism (where the primordial curvature perturbations are identified with the variation of the number of e-folds over its mean, see Sect. 2.3.2 for more details), were first done in Clesse and García-Bellido (2015). The resulting power spectrum is well approximated by a log-normal in mass spectrum,

$$\mathcal{P}_\zeta(N_k) \approx P_{\rm p} \exp\left[-\frac{(N_k - N_{\rm p})^2}{2\sigma_{\rm p}^2}\right], \tag{13}$$

of maximal amplitude $P_{\rm p}$ and width $\sigma_{\rm p}$, where N_k and $N_{\rm p}$ denote the e-folds times associated to the Hubble exit of the scale k and of the scale p associated to the peak location in the power spectrum, respectively. Some examples of power spectra are shown in Fig. 6. Finally, let us emphasize that the exact amplitude of the power spectrum also depends on the quantum stochastic dynamics of the auxiliary field ψ close to the critical instability point. In principle, this should lead to slightly different power spectrum amplitudes in different regions of the Universe, and therefore different PBH abundances. A natural outcome of the hybrid inflation scenario would thus be that PBHs are formed in clusters whose mass and size depends on these quantum stochastic dynamics. This can be also somehow used to reduce the fine-tuning linked to the required power spectrum amplitude, since many realisations would have been generically produced within the Universe.

2.2.2 Turns in multi-field inflation

Embeddings of inflation in high energy physics motivate scenarios in which multiple scalar fields participate in the inflationary dynamics. An ubiquitous phenomenon in this context is the one of turns in field space, corresponding to a bending of the inflationary trajectory, or more accurately to its deviation from a geodesic of the field

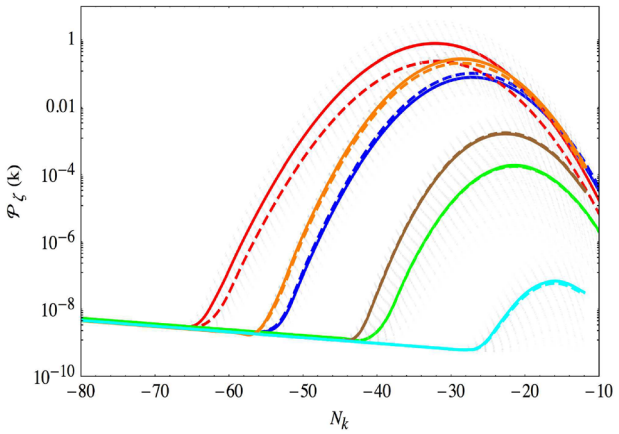

Fig. 6 Power spectrum of curvature perturbations for hybrid inflation parameters values $M = 0.1M_{\rm PI}$, $\mu_1 = 3 \times 10^5 M_{\rm PI}$ and $\phi_{\rm c} = 0.125M_{\rm PI}$ (red), $0.1M_{\rm PI}$ (blue), $0.075M_{\rm PI}$ (green), and $0.05M_{\rm PI}$ (cyan). Those parameters correspond respectively to $\Pi^2 = 375/300/225/150$. The power spectrum is degenerate for lower values of M, ϕ and larger values of μ_1, keeping the combination Π^2 constant. For larger values of $M, \phi_{\rm c}$ the degeneracy is broken: power spectra in orange and brown are obtained respectively for $M = \phi_{\rm c} = M_{\rm PI}$ and $\mu_1 = 300M_{\rm PI}/225M_{\rm PI}$. Dashed lines assume $\psi_c = \psi_0$ whereas solid lines are obtained after averaging over 200 power spectra obtained from initial conditions on ψ_c distributed according to a Gaussian of width ψ_0. The power spectra corresponding to these realizations are plotted in dashed light gray for illustration. The Λ parameter has been fixed so that the spectrum amplitude on CMB anisotropy scales is in agreement with Planck data. The parameter $\mu_2 = 10M_{\rm PI}$ so that the scalar spectral index on those scales is given by $n_{\rm s} = 0.96$. Image reproduced with permission from Clesse and García-Bellido (2015), copyright by APS Image reproduced with permission

space,[1] quantified by a dimensionless parameter $\eta_\perp(t)$ measuring the acceleration of the trajectory perpendicular to its direction (Groot Nibbelink and van Tent 2000, 2002). When such a turn is sufficiently strong, with $\eta_\perp \gtrsim 1$ (see Renaux-Petel 2022 for a short overview), it leads to a transient tachyonic instability of the scalar field fluctuations before Hubble crossing (Cremonini et al. 2011; Brown 2018; Garcia-Saenz et al. 2018), similar in essence to the one arising in axion gauge-field inflation (see Sect. 2.2.4). This gives rise to an exponential enhancement of the power spectrum on those scales, compared to the ones that cross the Hubble radius before and after the turn, and thus constitutes a natural mechanism to seed PBH formation (Palma et al. 2020; Fumagalli et al. 2023; Braglia et al. 2020; Iacconi et al. 2022). Interestingly, owing to its inherently multi-field origin, the growth rate of the power spectrum can overcome the bound deduced in single-field setups (Byrnes et al. 2019; Carrilho et al. 2019; Özsoy and Tasinato 2020; Cole et al. 2024), i.e., the peak of the power spectrum can be sharper. An important parameter is the duration of the turn in e-folds $\delta \equiv \delta N$, which leads to qualitatively different behaviours for broad ($\delta \gtrsim 1$) and sharp turns ($\delta \ll 1$). While broad turns lead to a featureless bump of the power spectrum, sharp turns lead to a localised peak of the envelope of the power

[1] In the context of string theory compactifications, it has recently been shown (Freigang et al. 2023) that deviations from geodesic trajectories must be negligible near the boundary of the moduli space. Large turns can therefore be engineered just in the moduli space bulk.

spectrum, modulated by order-one rapid oscillations, as described in simple cases by the analytical power spectrum (assuming a constant value of $\eta_\perp$ during the turn) (Palma et al. 2020; Fumagalli et al. 2021a)

$$\frac{\mathcal{P}_\zeta(k)}{\mathcal{P}_0} = \frac{e^{2\sqrt{(2-\kappa)\kappa}\,\eta_\perp \delta}}{2(2-\kappa)\kappa} \times \sin^2\left[e^{-\delta/2}\kappa\eta_\perp + \arctan\left(\frac{\kappa}{\sqrt{(2-\kappa)\kappa}}\right)\right]. \tag{14}$$

Here, $\mathcal{P}_0$ denotes the amplitude of the power spectrum in the absence of the transient instability, $\kappa = k/k_\mathrm{f}$ is the dimensionless wavenumber in units of the maximally enhanced one, with k_f the scale crossing the Hubble radius at the time of the sharp turn, and the formula is valid for $\kappa \leq 2$ (see Fumagalli et al. 2021a for generalisations). The oscillations there, which are to a very good approximation periodic in k, are characteristic of a sharp feature, and go hand in hand with a boosted power spectrum generated by an event localised in time (Fumagalli et al. 2021a). The mass function of PBHs is highly sensitive to the tail of the probability density function (PDF) of the smoothed density contrast, which is not yet known for the class of models described here. However, tentative results for the mass function indicate that the oscillatory patterns are washed out when assuming Gaussian statistics of the primordial curvature fluctuations (Fumagalli et al. 2023), and hence further investigation is required to assess the observational consequences for PBHs of the oscillatory features. What is known, however, is that the SGWB generated by scalar fluctuations at horizon re-entry does keep an imprint of the oscillations of the scalar power spectrum: they manifest as oscillations in the frequency profile of the SGWB, providing a robust probe of small-scale features that would be inaccessible otherwise (Fumagalli et al. 2021a, b; Braglia et al. 2021a; Witkowski et al. 2022; Fumagalli et al. 2022b).

If one uses the standard criterion that the power spectrum has to reach values $\mathcal{P}_\zeta \sim 10^{-2}$ to generate a substantial amount of PBHs, it is interesting that the required enhancement from the baseline value $\mathcal{P}_0 \sim 10^{-9}$ necessitates a total angle $\Delta\theta = \eta_\perp \delta$ swept by the trajectory during the turn exceeding the value π obtainable in flat field space, and hence requires the inflationary field space to be curved (Palma et al. 2020). Such large values of the power spectrum are not without consequences however, and considerations of backreaction and perturbative control are important to take into account to delineate the space of theoretically viable models (Fumagalli et al. 2021a). Indeed, the criterion for perturbative control parametrically depends on the large parameter $\eta_\perp$ in a way that imposes the bound $\eta_\perp^6 \mathcal{P}_\zeta \lesssim 1$ (or $\eta_\perp^4 \mathcal{P}_\zeta \lesssim 1$) for broad (Fumagalli et al. 2019; Bjorkmo et al. 2019) (or sharp) turns (Fumagalli et al. 2021a). Thus, an important open question is whether the inevitably present non-Gaussianities of the curvature fluctuations in these models, enhanced in flattened configurations (Garcia-Saenz and Renaux-Petel 2018; Fumagalli et al. 2019; Ferreira 2020), are such that a substantial amount of PBHs can be generated with a value of the power spectrum less than 10^{-2} while ensuring perturbative control.

2.2.3 Two-stage models

There are several concrete examples of PBH formation resulting from a turn in the field space during inflation that separates two stages of inflation. The first stage produces the primordial power spectrum on CMB scales while the second stage is responsible for the enhancement of power on smaller scales, leading to PBH formation. Oscillations are expected at the transition, as explained in the previous Sect. Pi et al. (2018) have proposed a model combining Starobinsky inflation with a scalaron field that becomes massive at the end of the first stage of inflation and a curvature field that plays the role of the inflaton in a second stage. Kawasaki et al. (2016) proposed a scenario with a second phase of double inflation in a supergravity framework. One should notice that non-Gaussianity is typically small in these models, since most of the field trajectories are effectively single-field. Other advantages of these models are that one does not especially need to tune the position of a peak in the power spectrum, since it can be nearly scale invariant, as generically predicted by slow-roll inflation, and that the transition between the two regimes can be very sharp. Due to the features at the transition in the power spectrum, such models can also produce multi-modal distributions of black holes, as proposed in Carr and Kuhnel (2019).

2.2.4 Axion-gauge scenario

PBHs can also arise in models in which rolling axions interact with gauge fields, enhancing primordial density perturbations (Linde et al. 2013; Bugaev and Klimai 2014; Domcke et al. 2017; García-Bellido et al. 2016, 2017; Özsoy and Lalak 2021; Özsoy 2021). In natural inflation (Freese et al. 1990; Adams et al. 1993), the couplings of the inflaton to matter respect a shift symmetry, $\phi \to \phi + \text{constant}$. Therefore, they do not provide by themselves quantum corrections to the inflaton potential (that arise from a breaking of the shift symmetry, as for instance from instanton effects), which can therefore be technically naturally small and flat. Also, UV-completed theories, such as string theory or supergravity models of inflation, contain a large number of pseudo-scalar particles that could be identified with the axion inflaton, or some other dynamically relevant axion. The shift-symmetric coupling between the axion and the gauge field is

$$\mathcal{L} \supset \frac{a}{f} F\tilde{F}, \tag{15}$$

where a is the pseudoscalar axion, F is the gauge field strength, $\tilde{F}$ its dual, and f is the axion decay constant. Shift-symmetry is satisfied due to the fact that $F\tilde{F}$ is a total derivative and the constant term becomes a topological invariant. This interaction amplifies one helicity of the vector field around horizon crossing. The amplified gauge quanta might affect the evolution of the axion field (Anber and Sorbo 2010) or, even if produced in a smaller amount, source scalar density perturbations (Barnaby et al. 2011) and parity violating tensor modes (Sorbo 2011). These effects are exponentially sensitive to the parameter $\xi \equiv \frac{\dot{a}}{2fH}$, and visible effects are obtained for

$f \simeq 10^{-2} M_{\rm Pl}$, namely for an axion decay constant parametrically equal to the string scale. On one hand, this enhances the possibility that models of string cosmology have a rich phenomenology. On the other hand, no effect is expected for models of a single axion inflaton, that are required to have a super-Planckian excursion, unless some specific mechanism allows excursions much greater than the scale of inflation, such is the case for monodromy (Silverstein and Westphal 2008) or for aligned axion inflation (Kim et al. 2005).

Scalar perturbations are produced via inverse decay $A + A \rightarrow a$ (where A denotes the gauge field), and therefore, they obey a non-Gaussian χ^2 distribution. The amplified gauge fields also produce GWs via an analogous $2 \rightarrow 1$ process. We note that these primordial GWs, which are produced during inflation, form a different stochastic GW background with respect to the secondary GWs that are sourced by density perturbations in the process of horizon re-entry in radiation or matter-dominated eras.

The power spectrum of density perturbations can be parametrized as (Namba et al. 2016; Peloso et al. 2016; García-Bellido et al. 2016)

$$\mathcal{P}_\zeta(k) = \mathcal{P}_{\rm vacuum}(k) + \mathcal{P}_{\rm sourced}(k) \,, \tag{16}$$

where $\mathcal{P}_{\rm vacuum} \simeq 2 \times 10^{-9} \, (k/k_{\rm cmb})^{n_{\rm s}-1}$ is the standard nearly scale invariant vacuum signal (with $k_{\rm cmb}$ being some pivot wavenumber at CMB scales). As already mentioned, the sourced signal is exponentially sensitive to the parameter $\xi \equiv \dot{a}/2fH$, and it is therefore highly sensitive to the speed of the axion, and, ultimately, to its potential. For axion inflation with a single monomial potential the signal is typically blue, and one simply needs to require that the production is sufficiently small so that no stable PBH is produced via this mechanism (Linde et al. 2013). This does not need to be the case for a more complicated potential, or in the case in which the axion is not identified with the inflaton (García-Bellido et al. 2016, 2017). In this second case, one can imagine a situation in which the axion rolls significantly only for a limited number of e-folds (Namba et al. 2016; Peloso et al. 2016) and the sourced spectrum can be described as a nearly log-normal bump, peaked at the scales that were exiting the horizon while a was rolling. The infra-red part of the spectrum scales as $\mathcal{P} \propto k^3$ due to causality, while, close to the peak, the spectrum is well parametrized by (Namba et al. 2016)

$$\mathcal{P}_{\rm sourced}(k) = \mathcal{A}(\xi_*, \mathcal{W}) \exp\left[-\frac{\ln^2(k/k_*)}{2\sigma^2(\xi_*, \mathcal{W})} \right] \,, \tag{17}$$

where the amplitude $\mathcal{A}$, the central position k_*, and the width σ of the peak are functions of the maximum value of the particle production parameter ξ and of the amount of e-folds $\mathcal{W}$ during which the axion is significantly rolling. An analogous parametrization also holds for the amount of sourced GWs (Namba et al. 2016).

The sourced scalar perturbations are highly non-Gaussian (Barnaby et al. 2011). For a nearly scale-invariant signal (as is the case if the axion is the inflaton), their bispectrum has a shape which is very close to the equilateral one. For the case of short-duration production leading to Eq. (17), the bispectrum is a maximum when the

magnitude of the three momenta is parametrically equal to k_*, and its scale-dependence can also be described accurately via a log-normal shape (Namba et al. 2016). The fact that the sourced scalar perturbations obey a χ^2 statistics makes PBH production much more significant compared to Gaussian perturbations with the same power. Therefore, an equal amount of PBHs is produced with a much smaller power spectrum than in the Gaussian case. This results in a significantly smaller amount of stochastic GWs produced at second order by the scalar perturbations, with a different prospect for detection at LISA and PTA-SKA, see for example Fig. 7. This is discussed in more detail in Sect. 5.1.

2.2.5 False-vacuum models

It is also possible to form PBHs in both single and multi-field scenarios if some spatial regions end up in a false-vacuum. These regions can collapse into black holes before the field can pass the potential barrier through quantum tunneling and evolve towards the true vacuum. Several examples have been proposed.

For instance, the Higgs field is suspected to be metastable. If it is a spectator field during inflation, some regions may have ended in this region of the potential, thereby leading to the formation of black holes (Passaglia et al. 2020). Nevertheless, their abundance cannot be significant enough to contribute to the dark matter. Another possibility is a tiny step in the inflaton potential that can basically be overcome by most of field trajectories, but not all (Cai et al. 2022b). This can radically change the

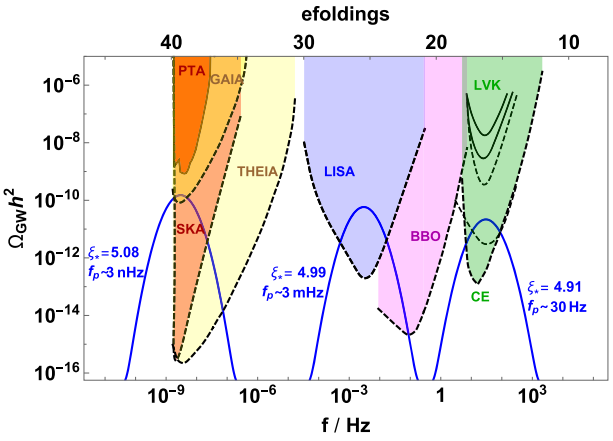

Fig. 7 The stochastic GWs produced by axion inflation at four main scales of interferometers for which we show the approximate sensitivities, nHz (PTAs and SKA), μHz (Gaia and Theia), mHz (LISA and BBO) and Hz (LVK, Einstein Telescope, and Cosmic Explorer). The enhanced density perturbations may produce PBHs which are a significant fraction of dark matter for $1-100\,M_\odot$ and the totality in the 10^{-14}–$10^{-11}\,M_\odot$ mass range and, remarkably, the enhanced perturbations leave inevitable GW backgrounds at the most sensitive regimes of GW detectors: for the first range of BHs this corresponds to PTA frequencies (and possibly future SKA) and LISA frequencies for the second range. The PBHs formed from fluctuations peaking at Hz scales will be so light that they are expected to be part of thermal history through Hawking radiation. The figure is updated (with slight modifications) from García-Bellido et al. (2017), Ünal (2019), García-Bellido et al. (2021b) Image reproduced with permission

tail of the Gaussian fluctuations, even if the conventional non-linearity parameters ($f_{\rm NL}, g_{\rm NL}$,...) remain small. The regions with large curvature fluctuations later form PBHs.

It has also been proposed that a light spectator field during inflation, having an asymmetric polynomial potential, experiences stochastic fluctuations that displace the field from the global minimum of its potential and populate a false vacuum state (Maeso et al. 2022). Lattice simulations have been used to show how when the Hubble radius reaches the false-vacuum bubble size, the potential energy is transferred to the kinetic and gradient energies of the bubble wall, such that it begins to contract and possibly collapse into a black hole. Finally, multi-field realisations have been proposed, for instance in Garriga et al. (2016), Deng and Vilenkin (2017).

2.3 Non-Gaussian models

2.3.1 Motivations

In Sect. 2.1, we discussed how PBHs could be generated in single-field models due to an enhancement of the power spectrum caused, for example, by a second plateau in the potential. However, as we will discuss in more detail in Sect. 3, what really matters to determine the PBH formation is the full profile of the PDF of the primordial curvature perturbations, in particular the probability to be above a given threshold. This implies that PBH abundance is largely controlled by the tails of the PDF, which at the same time are highly sensitive to any non-Gaussian corrections.

Non-Gaussian corrections can either enhance or suppress the production of PBHs depending on their effect on the tail of the PDF. One way of accounting for these effects is to compute the different statistical moments of the distribution. Gaussian profiles are fully characterized by the second moment (the power spectrum), while general PDFs can have contributions from any of the higher moments. For illustrative purposes, we plot in Fig. 8 the effect of the third and fourth moment as determined by the skewness and kurtosis, respectively. As it can be clearly seen, a positive kurtosis has a large impact in the tail of the PDF. Interestingly, one can analytically compute the effect of non-zero higher order moments in the abundance of PBHs (Franciolini et al. 2018; Matsubara and Sasaki 2022).

Non-Gaussian corrections are known to be relevant in multi-field models of inflation. For instance, models of axion inflation in which the gauge field sources the curvature perturbations (García-Bellido et al. 2016) display χ^2 statistics for the curvature perturbation. This has implications both for the PBH abundance and for the GW signature, as studied in detail in García-Bellido et al. (2017). In particular, a strong increase of the PBH abundance associated with a greater tail of the PDF does not correspond to a strong increase of the associated GW production. Therefore, for equal PBH abundance, a smaller GW signal is produced with respect to the Gaussian case.

Moreover, these non-Gaussian corrections can also enhance the abundance of PBHs in single-field models due to the dynamics of the ultra-slow roll phase (Biagetti et al. 2021; Cai et al. 2022a) and the effect of quantum diffusion beyond slow-

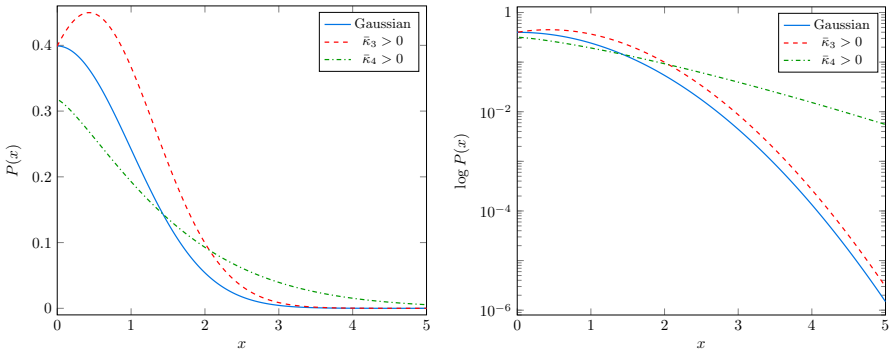

Fig. 8 Illustration of the effect of a positive skewness, $\bar{\kappa}_3$, and a positive (excess) kurtosis, $\bar{\kappa}_4$, for the probability density function $P(x)$ (left) and its logarithm (right) in comparison with a Gaussian distribution ($\bar{\kappa}_{n>2} = 0$). The dominant effect in the tail is given by a positive kurtosis. Image reproduced with permission from Ezquiaga and García-Bellido (2018), copyright by IOP and SISSA Image reproduced with permission

roll (Firouzjahi et al. 2019; Biagetti et al. 2018; Ezquiaga and García-Bellido 2018; Pattison et al. 2021).[2] In fact, in general terms, quantum diffusion introduces an exponential tail in the PDF of curvature perturbations (Pattison et al. 2017; Ezquiaga et al. 2020). For this reason, we discuss next the effect of quantum diffusion in the production of PBHs.

2.3.2 Quantum diffusion

Primordial curvature perturbations are expected to be well-described by a quasi-Gaussian distribution when they are small and close to the maximum of their probability distribution. This can be modelled using conventional cosmological perturbation theory where the free field fluctuations during inflation describe a Gaussian distribution and higher-order interactions lead to non-Gaussian corrections. However, PBHs result from the collapse of large density perturbations, which may be far from the peak of the distribution. In this regime, we require a non-perturbative approach, such as the stochastic-δN formalism (Enqvist et al. 2008; Fujita et al. 2013; Vennin and Starobinsky 2015).

Stochastic inflation (Starobinsky 1982) splits the inflaton field into small-scale quantum fluctuations and a large-scale effectively classical field above a coarse-graining scale (typically around the Hubble length). The large-scale field follows the non-linear evolution of a (locally) homogeneous and isotropic cosmology (Salopek and Bond 1990; Wands et al. 2000; Rigopoulos and Shellard 2003), except that small-scale modes are constantly swept up from the quantum vacuum state, crossing into the coarse-grained field, leading to quantum diffusion $\langle \Delta\varphi^2 \rangle \approx (H/2\pi)^2$ per Hubble volume per Hubble time. In regimes where PBHs are formed, the inflaton must undergo large quantum fluctuations (for instance as the result of travelling

[2] A violation of slow-roll is necessary for non-Gaussian effects to be sufficiently large to change the PBH abundance in single-field models (Passaglia et al. 2019).

through a very flat potential), which implies that stochastic corrections are important and must be taken into account (Pattison et al. 2017; Ezquiaga and García-Bellido 2018; Biagetti et al. 2018; Ezquiaga et al. 2020).

In order to derive the predicted abundance of PBHs in stochastic inflation, we make use of the δN formalism (Starobinsky 1982, 1985; Sasaki and Stewart 1996; Wands et al. 2000; Lyth et al. 2005), in which the primordial curvature perturbation is identified with the perturbation in the number of e-folds $N = \int H \, \mathrm{d}t$ with respect to the average, $\zeta = \mathcal{N} - \langle \mathcal{N} \rangle$ (where $\mathcal{N}$ denotes the duration of inflation starting from an initial field configuration, measured in number of e-folds N). One thus has to extract the distribution $P_\phi(\mathcal{N})$ of the number of e-folds of expansion $\mathcal{N}$ from a given inflaton field value ϕ to the end of inflation. This is the program of the stochastic δN formalism, in which it can be shown (Vennin and Starobinsky 2015; Pattison et al. 2017; Ezquiaga et al. 2020; Ando and Vennin 2021) that the Fokker–Planck equation driving the stochastic evolution of the coarse-grained field with respect to the integrated expansion during inflation, $\partial P_N(\phi)/\partial N = \mathcal{L}_{\mathrm{FP}}(\phi) \cdot P_N(\phi)$, can be recast in terms of the adjoint Fokker–Planck operator acting on the duration distribution $P_\phi(\mathcal{N})$, such that $\partial P_\phi(\mathcal{N})/\partial \mathcal{N} = \mathcal{L}^\dagger_{\mathrm{FP}}(\phi) \cdot P_\phi(\mathcal{N})$.

By solving this equation in different setups, one can show that quantum diffusion leads unavoidably to non-Gaussian tails (Pattison et al. 2017; Ezquiaga et al. 2020). In particular, if the classical evolution gives a finite number of e-folds N_{c} from a given field value to the end of inflation, then the large-$\mathcal{N}$ limit (where $\mathcal{N} \gg N_{\mathrm{c}}$) is inevitably dominated by quantum diffusion since it requires many quantum kicks to evade the classical drift towards the end of inflation. Quite generally, the probability distribution approaches an exponential tail, $P_\phi(\mathcal{N}) = \sum_n a_n e^{-\Lambda_n \mathcal{N}} \propto e^{-\Lambda_0 \mathcal{N}}$ as $\mathcal{N} \to \infty$ (Pattison et al. 2017; Ezquiaga et al. 2020; Jackson et al. 2022), which cannot be described by a quasi-Gaussian distribution (see Fig. 9). Thus predictions for the abundance of PBHs, which will be described by the integrated probability distribution function above a given threshold, may differ by several orders of magnitude from results obtained assuming a Gaussian distribution (Pattison et al. 2017; Ezquiaga et al. 2020; Biagetti et al. 2021; Kitajima et al. 2021; De Luca and Riotto 2022; Gow et al. 2023).

Let us also stress that these exponential tails cannot be properly described by usual, perturbative parametrisations of non-Gaussian statistics (such as those based on computing the few first moments of the distribution and the non-linearity parameters f_{NL}, g_{NL}, etc.), which can only account for polynomial modulations of Gaussian tails. A non-perturbative approach, such as the one presented here, is therefore necessary.

It is also worth mentioning that the details of the tail (such as the value of a_0 and Λ_0) are determined by the specifics of the inflationary model under consideration. For instance, in the simplest setup where inflation is realised with a single scalar field, if the potential energy V is constant across a field region of size $\Delta\phi$, then (Pattison et al. 2017) $\Lambda_0 = V/(96 M_{\mathrm{Pl}}^2 \Delta\phi^2)$ and $\Lambda_n = (2n+1)^2 \Lambda_0$. Wider "quantum wells" (i.e. larger values of $\Delta\phi$) thus lead to smaller Λ_0 and to wider tails. This result is valid if the initial velocity of the inflaton into the quantum well is vanishing. Otherwise, a transient period of "ultra slow roll" takes place until the inflaton relaxes to the slow-

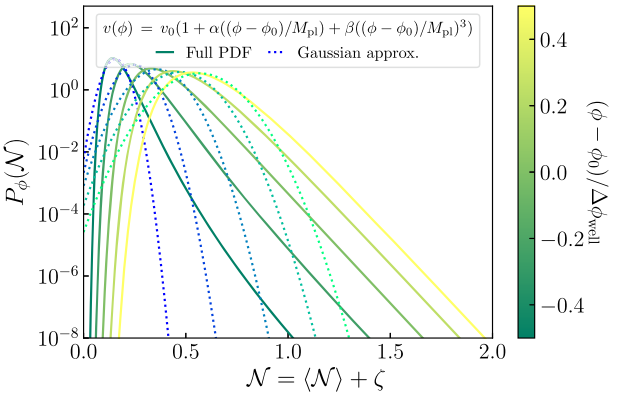

Fig. 9 Probability density functions of the curvature perturbations generated by an inflection-point inflationary potential (see inset). Solid lines correspond to the full distribution functions computed by mean of the stochastic-δN formalism, where different colours correspond to different locations in the potential $v(\phi)$ where the scale under consideration emerges from the Hubble radius and where $\Delta\phi_{\rm well}$ denotes the field range for which stochastic effects dominate over the classical dynamics. The dotted lines correspond to the standard result, which provides a good Gaussian approximation for the maximum of the distribution but that however fails to describe the exponential tails, where PBHs are nonetheless produced. Image reproduced with permission from Ezquiaga et al. (2020), copyright by IOP and SISSA Image reproduced with permission

roll attractor, and on top of the eigenvalues Λ_n given above, a second set of decay rates $\Lambda'_n = \Lambda_n + 3$ also arises (Pattison et al. 2021). When the initial velocity is large compared to the velocity that would be required to cross the well classically, the amplitudes a'_n associated with those eigenvalues are larger than those for the rates Λ_n, hence the tails are more suppressed. Another way to suppress the tails is to add a tilt in the inflationary potential, $V = 24\pi^2 M_{\rm PI}^4 v_0(1 + \alpha\phi/M_{\rm PI})$, for which the decay rates are all shifted by a constant value (Ezquiaga et al. 2020), i.e. $\Lambda'_n = \Lambda_n + \alpha^2/(4v_0)$. Unless α^2 is fine tuned to values less than the potential energy in Planckian units, the exponential tails are heavily suppressed. As a last example, let us mention the case where the potential features an inflection point, close to which one can approximate $V = 24\pi^2 M_{\rm PI}^4 v_0[1 + \beta(\phi/M_{\rm PI})^3]$. In such models, if slow roll is not violated when approaching the inflection point (which depends on the details of the inflationary potential away from that point), one finds (Ezquiaga et al. 2020) $\Lambda_n = (3/2)^{2/3}\pi^2(v_0\alpha)^{1/3}(n + 1/2)^2$, such that primordial black holes are always overproduced.

These examples show that the abundance of primordial black holes is ultimately related to the details of the inflationary potential where quantum diffusion plays an important role. PBHs would thus provide access to regions of the inflationary potential that can otherwise not be probed with other cosmological measurements such as the cosmic microwave background.

2.3.3 Stochastic spectator field

Another recent scenario (Carr et al. 2021a) takes the advantage of the dynamics of a stochastic spectator field to produce PBHs, while the primordial power spectrum

remains at the CMB level almost everywhere in our Universe, except in subdominant regions where PBHs can form. If PBHs are linked to the generation of the baryon asymmetry of the Universe, thereby connecting (1) The PBHs and baryon abundance, (2) The baryon-to-photon ratio to the PBH density at the time of their formation, the stochastic and quantum nature of the spectator field fluctuations allows one to invoke an anthropic selection mechanism to resolve the long-standing parameter fine-tuning issues related to PBH formation (García-Bellido et al. 2021a; Carr et al. 2021a; García-Bellido 2019).

In this scenario, the stochastic spectator field, denoted ψ, experiences quantum fluctuations during inflation that lead it to explore a wide range of the potential, including its slow-roll part, in different Hubble patches. But the field does not have any impact on the inflationary dynamics, thus being a *spectator* field. Because the number of patches is huge, there necessarily exist some in which the spectator field ψ, at the time of Hubble exit, has the required mean value for subsequent quantum fluctuations (but sub-Hubble at that time) to later induce large curvature fluctuations. Our observable Universe would correspond to one of these patches.

After inflation, the spectator field and its fluctuations within these patches remain frozen during the radiation era until its potential energy starts to dominate the density of the Universe, well after inflation but also possibly well before the time of PBH formation. At this point, in the regions where the field is in the slow-roll part of the potential, a very short second inflationary phase (for at most a few e-folds) takes place, whereas in the rest of the patch the field quickly rolls down its potential without inflating. Such an extra expansion corresponds to the production of local non-linear curvature fluctuations that are still super-horizon at that time. Only later they re-enter the horizon and collapse into PBHs. But in the rest of the Universe the curvature fluctuations are statistically Gaussian and behave as expected in standard slow-roll inflation, unaffected by the spectator field.

The probability to form a PBH in a given region (that can be connected to the function β introduced in the next section) has been calculated as (Carr et al. 2021a)

$$P_{\rm PBH} = \sqrt{\frac{2}{\pi}} \frac{\Delta\psi^{\rm sr}}{\sqrt{H_N^2/4\pi^2 + \langle\delta\psi^2\rangle_{N-1}}} \times \exp\left[-\frac{\langle\psi\rangle^2}{2(H_N^2/4\pi^2 + \langle\delta\psi^2\rangle_{N-1})}\right], \qquad (18)$$

where $\Delta\psi^{\rm sr}$ is the size of the slow-roll region where the field can induce $\mathcal{O}(1)$ curvature fluctuations. The subscript N is used to indicate that a quantity is evaluated at the e-fold time at which the scale exited the horizon during inflation. It can be noticed that the mathematical form of $P_{\rm PBH}$ is quite similar to the one of β (see next section) in more standard models of Gaussian inflationary perturbations. As a consequence, the shape of the PBH mass function is also very similar and driven by the evolution of H during inflation. There is also no need to precisely fix the potential parameters in this model, the only condition being that the potential is of plateau or small-field type and that it can dominate the density of the Universe prior the QCD epoch (if one is interested to get stellar-mass or heavier PBHs). More precise calculations of the probability distribution of curvature fluctuations and some embedding in high-energy frameworks, including with the Brought–Englert–Higgs field,

were recently presented and discussed in Stamou and Clesse (2024a), Stamou and Clesse (2024b).

2.4 Curvaton

A different possibility to generate PBHs, while keeping the generation mechanisms for curvature perturbations at different scales decoupled, is represented by a simple modification of the original *curvaton scenario* (in the original curvaton model (Lyth and Wands 2002; Moroi and Takahashi 2001), one field, the inflaton, is responsible only for sustaining the inflationary background evolution while the other field, the curvaton, produces the primordial curvature perturbations). In this setup with two fields, the primordial curvature perturbations on CMB scales are produced by the inflaton, which acts very similarly to the standard single-field scenario, while the curvaton field becomes responsible for perturbations on smaller scales and thus formation of PBHs.

The power spectrum of curvature perturbations will be given as the sum of the contributions of the inflaton and of the curvaton

$$\mathcal{P}(k) = \mathcal{P}_{\rm infl}(k) + \mathcal{P}_{\rm curv}(k)\,. \tag{19}$$

where $\mathcal{P}_{\rm curv}(k)$ can be described by a lognormal function such as in Eq. (17).

At large scales (reasonably $k \lesssim 1\text{Mpc}^{-1}$), the first term will be dominating, with its magnitude being determined by CMB normalization, that is $\mathcal{P}_{\rm infl}(k) \simeq 2 \times 10^{-9}$. Moving to smaller scales (larger k), the second contribution, given by the curvaton field, increases and becomes dominant.

So, as long as the curvature perturbation on large cosmological scales is dominated by inflaton fluctuations with an almost scale-invariant spectrum, the curvaton field is not required to be light during inflation and its fluctuations may have a steep blue spectrum. Curvaton fluctuations could then give the dominant contribution to the primordial density perturbations on small scales after the curvaton decays. The curvaton may have a steep blue spectrum either due to interactions with the inflaton or other fields evolving during inflation (Yokoyama 1997), a non-trivial kinetic term (Pi and Sasaki 2023) or in an axion-like model, where the curvaton is identified with the phase of a complex field whose modulus decreases rapidly during inflation (Kawasaki et al. 2013).

An important characteristic of any curvaton model is that the fluctuations originate from non-adiabatic field fluctuations during inflation, a fact which gives rise to a non-Gaussian distribution in the primordial curvature perturbations, including a finite non-Gaussianity in the squeezed limit. Although this local-type non-Gaussianity is typically small ($f_{\rm NL} \sim 1$), it can nonetheless have a significant effect on the abundance of PBHs, as discussed in Sect. 2.3.

2.5 Preheating

Another way through which one can produce PBHs is the preheating instability. During the preheating period after inflation, when the inflaton oscillates coherently at

its ground state and decays to other degrees of freedom, it is widely argued that resonant amplification of quantum field fluctuations, responsible for particle production, take place (Kofman et al. 1994, 1997). These amplified quantum fluctuations should be accompanied by a resonant amplification of the scalar metric fluctuations (usually quoted as metric preheating, see Finelli and Brandenberger 1999; Bassett et al. 1999b; Jedamzik and Sigl 2000; Bassett and Viniegra 2000), responsible for gravitational fluctuations in the curvature, since the two are coupled through Einstein's equations. One then expects that the amplified metric perturbations give rise to large curvature/matter perturbations, which in their turn collapse and form PBHs.

Historically, PBHs emanating from the preheating instability were speculated in the context of multi-field inflation and in particular in the context of two-field chaotic inflation (Bassett et al. 1999a; Green and Malik 2001; Bassett and Tsujikawa 2001; Suyama et al. 2005; and more recently in Torres-Lomas and Urena-LAlpez 2013; Torres-Lomas et al. 2014), since in this case the parametric amplification of entropy (isocurvature) fluctuations can source the parametric amplification of the adiabatic (curvature) fluctuations in the regime of broad resonance. Thus, these amplified curvature fluctuations could break the scale-invariance of the primordial power spectrum and give birth to PBHs through non-linear gravitational fluctuations inducing large density contrasts (Kou et al. 2021; Joana 2022).

It is predicted as well (Jedamzik et al. 2010; see also Easther et al. 2011) that in the context of single-field inflation, there is a pronounced resonant instability structure in the narrow regime where amplified metric perturbations can induce the production of PBHs as recently studied in Martin et al. (2020b), Auclair and Vennin (2021). At this point, one should point out that the narrow resonant structure of metric preheating was shown in Martin et al. (2020a) to be immune to the decay of the inflaton into a radiation fluid, ensuring in this way the transition to the Hot Big Bang phase of the Universe.

The case of metric preheating Most of the studies in which PBHs are produced during preheating treat them in the context of multi-field and especially in the context of two-field inflation. This makes it difficult to predict in an analytic way the matter power spectrum responsible for the PBH formation, which is constructed consequently numerically. On the contrary, in the context of single-field inflation, one can in principle extract in a direct way the matter power spectrum responsible for the PBH production. In what follows we emphasize on a specific scenario studied in Martin et al. (2020b), Auclair and Vennin (2021), in which PBHs are produced during the preheating phase due to the emergence of a resonant instability structure concerning the equation of motion of the scalar metric perturbations that are enhanced on small scales (metric preheating), which exit the Hubble radius close to the end of inflation. Specifically, the modes concerned satisfy the relation

$$aH < k < a\sqrt{3Hm}, \tag{20}$$

where k is the comoving scale concerned, a is the scale factor, H is the Hubble parameter and m is the mass parameter of the inflationary potential. For these modes, as shown in Martin et al. (2020b), the density contrast scales linearly with the scale

factor, i.e. $\delta_k \sim a$, manifesting in this way an effective "dust" behavior during the instability phase in which PBHs can be easily produced.

Considering only the modes entering the instability band from above, namely the left hand side of the inequality (20), the matter power spectrum responsible for the PBH formation at the end of the preheating instability phase can be written analytically as (Martin et al. 2020b)

$$\mathcal{P}_\delta\left(t_\Gamma, \frac{k}{k_{\rm end}}\right) = \left(\frac{k}{k_{\rm end}}\right)^4 \left(\frac{\rho_{\rm inf}}{\rho_\Gamma}\right)^{2/3} \left(\frac{6}{5}\right)^2 \mathcal{P}_{\zeta,{\rm end}}\left(\frac{k}{k_{\rm end}}\right), \tag{21}$$

where $k_{\rm end}$ is the comoving scale exiting the Hubble radius at the end of inflation, $\rho_{\rm inf}$ is the energy scale at the end of inflation, ρ_Γ is the energy scale at the end of the preheating instability phase and $\mathcal{P}_{\zeta,{\rm end}}\left(\frac{k}{k_{\rm end}}\right)$ is the curvature power spectrum at the end of inflation which in the slow-roll approximation reads as (Schwarz et al. 2001; Gong and Stewart 2001)

$$\mathcal{P}_{\zeta,{\rm end}}\left(\frac{k}{k_{\rm end}}\right) = \frac{H_*^2(k)}{8\pi^2 M_{\rm PI}^2 \epsilon_{1*}(k)} \left[1 + \left(\frac{k}{k_{\rm end}}\right)^2\right] \left[1 - 2(C+1)\epsilon_{1*}(k) - C\epsilon_{2*}(k)\right] \text{ for } k < k_{\rm end}. \tag{22}$$

The functions $H_*(k)$, $\epsilon_{1*}(k)$ and $\epsilon_{2*}(k)$ denote respectively the values of H, ϵ_1 and ϵ_2 at the time when the mode k exits the Hubble radius during inflation. The parameter $C \simeq -0.7296$ is a numerical constant. It is important to mention here that Eq. (22) is the curvature power spectrum at NLO within the slow-roll approximation in contrast with Eq. (1) which gives $\mathcal{P}_\zeta(k)$ at leading-order (LO). This is why we obtain the extra $1 + \left(\frac{k}{k_{\rm end}}\right)^2$ term, which captures the first NLO correction coming from the decaying mode of ζ and is actually significant for modes k close to $k_{\rm end}$ as the ones considered here. Note also that Eq. (1) is expanded around a pivot scale k_* whereas Eq. (22) is valid for all values of k within the slow-roll approximation.

The relevant range of the density contrast at the end of the preheating phase is

$$\left(\frac{\rho_{\rm inf}}{\rho_\Gamma}\right)^{1/3} \left(\frac{k}{k_{\rm end}}\right)^2 \left(\frac{3\pi}{2}\right)^{2/3} \left[\left(\frac{k}{k_{\rm end}}\right)^3 \sqrt{\frac{\rho_{\rm inf}}{\rho_\Gamma}} - 1\right]^{-2/3} < \delta_k(t_\Gamma) < 1, \tag{23}$$

while the relevant parameter space $(\rho_\Gamma, \rho_{\rm inf})$ so that we do not have PBH overproduction during preheating reads as

$$\frac{\rho_\Gamma}{M_{\rm PI}^4} < \frac{4}{125\sqrt{3}\pi^5} \left(\frac{\rho_{\rm inf}}{M_{\rm PI}^4}\right)^{5/2} \tag{24}$$

Below, in Fig. 10 we see the behavior of $\mathcal{P}_\delta\left(t_\Gamma, \frac{k}{k_{\rm end}}\right)$ [see Eq. (21)] by fixing $\rho_{\rm inf}^{1/4} = 10^{14}$ GeV and $\rho_\Gamma^{1/4} = 10^7$ GeV. At this point, it is important to stress out that exactly at $k = k_{\rm end}$, Eq. (22) is not trustful since there the slow-roll approximation breaks down.

The corresponding mass of the PBHs produced is related to the mass inside the Hubble radius at the time when a scale k re-enters the horizon, namely

$$m_{\rm PBH} = \gamma M_{\rm H} = \gamma \frac{\left(3M_{\rm pl}^2\right)^{3/2}}{\sqrt{\rho_{\rm inf}}} \left(\frac{k}{k_{\rm end}}\right)^{-3}, \tag{25}$$

where γ is an efficiency parameter of order one depending on the details of the gravitational collapse. Here, it is important to notice that in Eq. (25), one clearly sees the dependence of the PBH mass on the energy scale at the end of inflation and as a consequence on the underlying inflationary model. We need to stress here that Eq. (25) gives the PBH mass as a function of the comoving scale k for PBHs forming during preheating, when the Universe behaves effectively as pressureless dust. This gives rise to a k scaling of the PBH mass of the form of k^{-3} in contrast with the k^{-2} scaling valid for a PBH forming during a radiation-dominated era [See the discussion in Sect. 3].

Regarding the characteristic PBH mass produced during preheating one can choose $k/k_{\rm end} = 0.1$, and using a relative high energy scale at the end of inflation, $\rho_{\rm inf}^{1/4} = 10^{14}$ GeV, from Eq. (25) one obtains $m_{\rm PBH} \simeq 10^{-27} M_{\odot}$. This mass, around which the matter power spectrum peaks, is very small compared to the mass range LISA can detect through the GW portal of PBH mergers. However, as pointed out recently in Auclair and Vennin (2021), in which the PBH mass function is computed more accurately with the use of the excursion-set formalism, the mass of PBHs produced from the metric preheating instability, at which the PBH mass function peaks, is higher than the PBH mass quoted above and can be as high as the solar mass, lying in this way within the mass range probed by LISA.

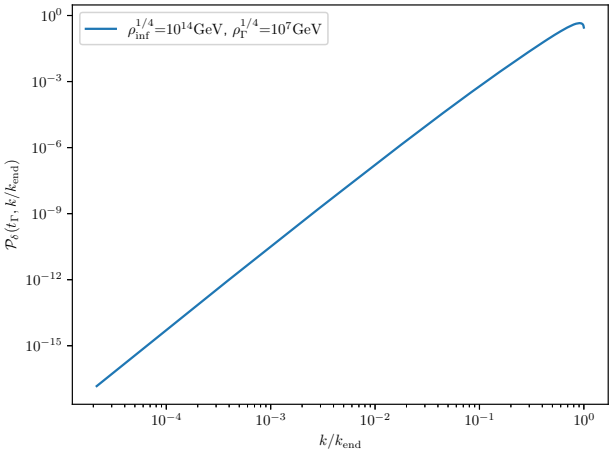

Fig. 10 The matter power spectrum at the end of the preheating instability phase. The energy scales at the end of inflation and at the end of the preheating instability phase are fixed as $\rho_{\rm inf}^{1/4} = 10^{14}$GeV and $\rho_{\rm r}^{1/4} = 10^{7}$GeV Image reproduced with permission

At this point, one should also stress that ultralight PBHs, such as the ones produced from the preheating instability, can be potentially detected by LISA through the stochastic background of GWs induced at second order from PBH isocurvature perturbations, as argued in Papanikolaou et al. (2021). For these GWs, the peak frequency could lie within the LISA band despite the smallness of the PBH mass.

2.6 Early matter era

An early prolonged period of matter domination – after the end of inflation – could arise due to the domination of moduli fields which are a natural prediction of any supergravity or superstring-inspired theory of the early Universe. Since the curvature threshold for the PBH collapse depends on the equation of state of the Universe, it might be easier to obtain the same abundance of PBH during the moduli dominated epoch from a peak in the inflationary power spectrum less strong than the typical $O(10^{-2})$ required in the standard scenario of radiation domination. Several mechanisms have been proposed to lead to such a production during an early matter dominated era, see e.g. Khlopov and Polnarev (1980), Khlopov et al. (1985), Green et al. (1997), Nayak and Singh (2012), Harada et al. (2016), Carr et al. (2017, 2018), Kokubu et al. (2018), Ballesteros et al. (2020b), de Jong et al. (2022), De Luca et al. (2022a). In such scenarios, the mass and fraction of PBHs produced from a given inflationary potential depend on whether the moduli dominated epoch is immediate or delayed after the end of inflation. Recently, it has also been pointed out that even if PBHs are formed during radiation domination, the presence of a reheating epoch can still crucially affect the PBH abundance (Cai et al. 2018; Bhaumik and Jain 2020).

In models of inflation based on moduli stabilisation in string theory compactifications, for example, the inflaton may be identified with a modulus field which is only gravitationally coupled to the visible sector, leading to a slow-reheating phase, where the inflaton decay is via Planck-suppressed operators, and hence a prolonged duration of matter-domination after inflation (Green et al. 1997; Ballesteros et al. 2020b). Ballesteros et al. (2020b) finds that PBH formation is most effective for reheating temperatures $\lesssim 10^6$ GeV, in which case PBHs can form a significant fraction of the dark matter density today when primordial curvature fluctuations from inflation are of order 10^{-4} in a matter-dominated era, rather than $\sim 10^{-2}$ usually required in a radiation-dominated era.

2.7 Phase transitions

The formation and abundance of PBHs can also be affected by phase transitions in the early Universe. During the radiation era, the formation of PBHs may be facilitated if pre-existing super-horizon density fluctuations enter the cosmological horizon during a first order phase transition which proceeds in approximate equilibrium (Khlopov et al. 1985; Jedamzik and Niemeyer 1999). During this phase transition the speed of sound tends to zero and the pressure response of the fluid

vanishes and does not counter-balance the gravitational collapse of horizon-sized primordial over-densities. Detailed numerical simulations using general-relativistic hydrodynamics show that the overdensity threshold required for PBH formation by fluctuations that enter the cosmological horizon around the phase transition is smaller than the ordinary value for PBH formation during the radiation epoch. This would produce an increase in the PBH mass spectrum around the corresponding horizon mass in which the phase transition occurs.

It has been argued that the QCD phase transition could produce an enhancement of the population of PBH's around $1M_{\odot}$ (Jedamzik 1997), but lattice QCD calculations have shown that the QCD phase transition in the Standard Model is not first order but a continuous cross-over (Bhattacharya et al. 2014). Nevertheless, it is possible to collapse a significant amount of PBHs at the QCD transition if there are large fluctuations and radiation pressure drops as the relativistic quark and gluon degrees of freedom disappear from the plasma (Byrnes et al. 2018; Carr et al. 2021b; Jedamzik 2021).

Alternative scenarios have been proposed, where the dynamics of the QCD phase transition incorporates extra degrees of freedom, like lepton number violation (Bödeker et al. 2021) and solitosynthesis (García-Bellido et al. 2021b). In other models, the QCD transition could be first order if the number of light quarks were larger than three at the confinement. Models in which the dynamics of a light scalar field have been tailored to suppress quark masses before the QCD transition, while recovering the measured values after the transition, have been developed in Davoudiasl (2019).

Another possibility is that the collision of bubbles formed during a first order phase transition in the early Universe could create either remnant regions dominated by the false vacuum or a sufficiently large local concentration of the energy stored in the walls, or even other more complex processes, to cause gravitational collapse and the formation of a primordial black hole (Hawking et al. 1982; Liu et al. 2022; Jung and Okui 2021; Baker et al. 2021b; Flores et al. 2024; Lewicki et al. 2023). This process could be affected by spatial clustering properties of bubble generated in high-energy phase transitions (Pirvu et al. 2022; De Luca et al. 2021e). Recent models (Baker et al. 2021c) consider the possibility that there may be particles whose mass increases significantly during the phase transition, suppressing the transmission of the corresponding particles through the advancing bubble walls. This effect can build a sufficiently large overdensity in front of the walls that collapse into a primordial black hole. The primordial black hole density and mass distribution depend on the model parameters. Other models (Kawana and Xie 2022) consider fermion species that gain big masses in the true vacuum, so that the corresponding particles get trapped in the false vacuum as they do not have sufficient energy to penetrate the bubble wall. After the first order phase transition, the fermions are compressed into the false vacuum remnants to form Fermi-balls that finally collapse to PBH due to the Yukawa attractive force.

Higher-order phase transitions periods in the early Universe may also lead to the formation of PBHs. For example, domain walls can be generated during a non-equilibrium second order phase transition in the vacuum state of a scalar field with a flat direction during inflation (Rubin et al. 2000). The background de Sitter

fluctuations of such an effectively massless scalar field could provide non-equilibrium redefinition of correlation length and give rise to the islands of one vacuum in the sea of another one. After the phase transition takes place in the Friedman–Robertson–Walker (FRW) epoch, the two vacua are separated by a wall. Some of these closed and sufficiently large walls could accumulate enough energy to collapse and form a massive black hole. The mass spectrum of the PBHs which can be created in such a way depends on the details of the potential of the scalar field that has the flat direction during inflation and triggers the phase transition.

2.8 Domain walls and cosmic strings

Topological defects in the early Universe may also lead to the production of PBHs. Hawking (1989) was the first to show that PBHs could form from the collapse of cosmic string loops. He argued that loops that collapse by a factor $(G\mu)^{-1}$, where μ is the mass per unit length of the strings, will inevitably collapse to form black holes. PBH production can be used to place bounds on the cosmic string network (Hawking 1990; Polnarev and Zembowicz 1991; Caldwell and Gates 1993; Garriga and Sakellariadou 1993; Caldwell and Casper 1996; MacGibbon et al. 1998; Helfer et al. 2019; James-Turner et al. 2020) or cosmic strings nucleated during inflation (Garriga and Vilenkin 1993). More recently it has been argued that cosmic string cusps can collapse gravitationally into PBHs with a mass function that could extend up to stellar-masses (Jenkins and Sakellariadou 2020), although this claim has been disputed in Blanco-Pillado et al. (2021a).

Moreover, domain walls, which arise in theories with a broken discrete symmetry, can also form PBHs when such domain walls are smaller than a critical radius fall within the cosmological horizon and collapse due to their own tension (Ferrer et al. 2019) or are produced by tunnelling during inflation (Liu et al. 2020). In such scenarios, the mass function of PBHs in general has a spikelike structure. Moreover, in QCD axion models, PBHs can form either by the collapse of long-lived string-domain wall networks or from the collapse of closed domain walls (Ferrer et al. 2019; Ge 2020). The mass and abundance of PBHs formed in these scenarios crucially depends on the QCD axion mass. However, interestingly, various observational constraints on the PBH abundance in turn limit the QCD axion parameter space.

2.9 Primordial magnetic fields

Primordial magnetic fields generated in the early Universe are considered one of the feasible candidates to provide the required seeds for the observed large-scale intergalactic magnetic fields. In addition, such primordial fields also generally induce an anisotropic stress that can act as a source for the evolution of the super-horizon curvature perturbations, leading to the formation of PBHs with a broad possible range of masses. Since a large abundance of PBHs requires a large amplitude of density perturbations, the strength of these primordial magnetic fields on small scales should also be large enough for this mechanism to work (Saga et al. 2020). Based on

this idea, strong constraints on the amplitude of primordial magnetic fields have been established, a few hundreds nano-Gauss on scales in the wave-number range $10^2\,\mathrm{Mpc}^{-1} \leq k \leq 10^{18}\,\mathrm{Mpc}^{-1}$.

Alternatively, it has been proposed that PBHs can act as seeds of cosmic magnetic fields due to their accretion disks, either due to a *Biermann battery* (Safarzadeh et al. 2018; Papanikolaou and Gourgouliatos 2023b) mechanism or more exotic mechanisms such as monopoles (Maldacena 2021; Araya et al. 2021) or Kerr–Newman PBHs (Hooper et al. 2023). In particular, in Papanikolaou and Gourgouliatos (2023b) it was shown that locally isothermal disks around supermassive PBHs with masses $M > 10^{10} M_{\odot}$, can generate a seed primordial magnetic field of the order of 10^{-30}g, which can be later amplified by various dynamo/instability processes and provide the seed for the present day magnetic field in intergalactic scales. Interestingly enough, this population of magnetised supermassive PBHs can induce a stochastic GW background which can be used to set tight constraints on the supermassive PBH abundances (see Papanikolaou and Gourgouliatos 2023a for more details).

2.10 Summary

In this section, we have explored multiple mechanisms described in the literature for generating primordial black holes, from gravitational collapse of primordial fluctuations and inflation to preheating, phase transitions, collisions of bubble walls and cosmic strings. Each of these mechanisms has its own mass spectrum and individual characteristics, which makes it possible to differentiate between them. The most developed one is that of primordial fluctuations, where specific models exist that can be put to test by present and future observations. Other mechanisms have also been explored and predictive models exist, but are not yet sufficiently developed to compare with observations. But we also emphasized the possible role of non-Gaussian tails in the distribution of curvature fluctuations, which arise in models with an ultra-slow-roll phase of inflation or in models with a stochastic spectator field. This is an interesting, recent and active research area since this could soften or even resolve the fine-tuning issues, which have recently been quantified in Cole et al. (2023b), associated to the formation of PBHs with significant abundances. In the next Sections, we will explore the dynamics of gravitational collapse and how it depends on the thermal history of the Universe, with its impact on the PBH mass function, their spin distribution and merging rates.

3 PBH formation, mass function and clustering

In this section we will concentrate on the concrete PBH formation mechanism based on gravitational collapse of large density or curvature fluctuations, and derive expressions for the mass function and clustering of PBH formed this way.

3.1 From curvature perturbations to density contrast

PBHs form after cosmological perturbations re-enter the cosmological horizon. Assuming spherical symmetry on superhorizon scales, the local region of the Universe describing such perturbations has the following asymptotic form of the metric

$$\mathrm{d}s^2 = -\mathrm{d}t^2 + a^2(t)\left[\frac{\mathrm{d}r^2}{1-K(r)r^2} + r^2\mathrm{d}\Omega^2\right] = -\mathrm{d}t^2 + a^2(t)e^{2\zeta(\hat{r})}\left[\mathrm{d}\hat{r}^2 + \hat{r}^2\mathrm{d}\Omega^2\right], \tag{26}$$

where $a(t)$ is the scale factor, while $K(r)$ and $\zeta(\hat{r})$ are the conserved comoving curvature perturbations, defined on a super-Hubble scale, converging to zero at infinity where the universe is taken to be unperturbed and spatially flat. The equivalence between the radial and the angular parts of these two forms of the metric gives

$$\begin{cases} r = \hat{r}e^{\zeta(\hat{r})}\,, \\ \dfrac{\mathrm{d}r}{\sqrt{1-K(r)r^2}} = e^{\zeta(\hat{r})}\mathrm{d}\hat{r} \end{cases} \tag{27}$$

and the difference between the two Lagrangian coordinates r and $\hat{r}$ is related to the parametrisation of the comoving coordinate, fixed by the curvature perturbation chosen in the metric (i.e. $K(r)$ or $\zeta(\hat{r})$). From a geometrical point of view, the coordinate $\hat{r}$ considers the perturbed region as a local FLRW separated universe with the curvature perturbation $\zeta(\hat{r})$ modifying the local expansion, while the curvature profile $K(r)$ is defined with respect to the background FLRW solution ($K = 0$) and measures more directly the spatial geometry of space-time.

On superhorizon scales, where the curvature profile is time independent, these two are related as

$$K(r)r^2 = -\hat{r}\zeta'(\hat{r})[2 + \hat{r}\zeta'(\hat{r})]\,. \tag{28}$$

In this regime, we can use the gradient expansion approach (Shibata and Sasaki 1999; Tomita 1975; Salopek and Bond 1990; Polnarev and Musco 2007), based on expanding the time dependent variables, like energy density and velocity profiles, as power series of a small parameter $\epsilon \ll 1$ up to the first non zero order, where ϵ is conveniently identified with the ratio between the Hubble radius and the length scale of the perturbation. Although this approach reproduces the time evolution of the linear perturbation theory, it also allows having non linear curvature perturbations if the spacetime is sufficiently smooth on the scale of the perturbation (see Lyth et al. 2005). This is equivalent to saying that in this regime pressure gradients are negligible, not playing an important role in the perturbation evolution, which grows with the Universe expansion in a self similar way.

In this approximation, the energy density profile can be written as[3] (Yoo et al. 2018; Musco 2019)

$$\frac{\delta\rho}{\rho_{\rm b}} \equiv \frac{\rho(r,t)-\rho_{\rm b}(t)}{\rho_{\rm b}(t)} = \frac{1}{a^2H^2}\frac{3(1+w)}{5+3w}\frac{[K(r)\,r^3]'}{3r^2} = -\frac{1}{a^2H^2}\frac{4(1+w)}{5+3w}e^{-5\zeta(\hat{r})/2}\nabla^2 e^{\zeta(\hat{r})/2}, \tag{29}$$

where $H(t)=\dot{a}(t)/a(t)$ is the Hubble parameter. The parameter w is the coefficient of the equation of state $p=w\rho_{\rm b}$, relating the total (isotropic) pressure p to the total background energy density $\rho_{\rm b}$.

In the linear regime of curvature perturbations, when $\zeta \ll 1$, this expression can be written as

$$\frac{\delta\rho}{\rho_{\rm b}} \simeq -\frac{1}{a^2H^2}\frac{2(1+w)}{5+3w}\nabla^2\zeta(\hat{r}) = -\frac{k^2}{a^2H^2}\frac{2(1+w)}{5+3w}\zeta_k\,, \tag{30}$$

where the second equality is obtained from the Fourier transformation $\nabla^2\zeta = k^2\zeta_k$, showing that in the linear regime there is a simple one to one mapping between the real space, where the perturbations collapses, and the Fourier space where the power spectrum of cosmological perturbations is defined. If the curvature perturbation ζ is a Gaussian variable, the density contrast $\delta\rho/\rho_{\rm b}$ has also a Gaussian distribution within the linear regime described by Eq. (30). However, because the amplitude of the threshold $\delta_{\rm c}$ for PBHs is non linear, the linear regime does not give an accurate description of the statistics of the density contrast, and the mapping between the Fourier space and the real space requires a more elaborate approach. As we will see later, this allows to compute the threshold $\delta_{\rm c}$ from the shape of the power spectrum $\mathcal{P}_\zeta$.

For this reason, the definition of the threshold in terms of $\zeta_{\rm c}$ computed from the linear approximation given by Eq. (30), does not give an accurate description and should be dropped in favour of $\delta_{\rm c}$ which is clearly defined in the following section. We anticipate that the nonlinear relation between the density contrast and the comoving curvature perturbations causes the former to obey non-Gaussian statistics, even in absence of primordial non-Gaussianity. Computations based on peak theory and on threshold statistics show that this unavoidable non-Gaussianity makes the production of PBHs more difficult. In case of a peaked power spectrum, this effect is compensated by an increase of the amplitude by an order 2–3 factor (De Luca et al. 2019c; Young et al. 2019).

3.2 Perturbation amplitude

To define the amplitude of a cosmological perturbation, it is useful to introduce the compaction function (Shibata and Sasaki 1999; Musco 2019), defined as

[3] $K'(r)$ denotes differentiation with respect to r while $\zeta'(\hat{r})$ and $\nabla^2\zeta(\hat{r})$ denote differentiation with respect to $\hat{r}$.

$$\mathcal{C} \equiv 2\frac{\delta M(r,t)}{R(r,t)}\,, \tag{31}$$

where $R(r,\,t)$ is the areal radius and $\delta M(r,t)$ is the difference between the Misner–Sharp mass within a sphere of radius $R(r,\,t)$, and the background mass $M_{\rm b}(r,t) = 4\pi\rho_{\rm b}(r,t)R^3(r,t)/3$ within the same areal radius but calculated with respect to a spatially flat FLRW metric. In the superhorizon regime (i.e. $\epsilon \ll 1$) the compaction function is time independent, and directly related to the curvature profile as

$$\mathcal{C}(r) = \frac{3(1+w)}{5+3w}K(r)r^2, \tag{32}$$

where this expression can be written in terms of $\zeta(\hat{r})$ using Eq. (28).

The comoving length scale of the perturbation can be conveniently identified with the distance where the compaction function reaches its peak (which is a maximum for a positive perturbation and a minimum for a negative one) when $r = r_{\rm m}$ (Musco 2019)(i.e. $\mathcal{C}'(r_{\rm m}) = 0$), characterized by a constraint relation in terms of the curvature profile

$$K(r_{\rm m}) + \frac{r_{\rm m}}{2}K'(r_{\rm m}) = 0, \quad \text{or} \quad \zeta'(\hat{r}_{\rm m}) + \hat{r}_{\rm m}\zeta''(\hat{r}_{\rm m}) = 0. \tag{33}$$

Given the curvature profile, the parameter ϵ of the gradient expansion is therefore defined as

$$\epsilon \equiv \frac{R_{\rm H}(t)}{R_{\rm b}(r_{\rm m},t)} = \frac{1}{aHr_{\rm m}} = \frac{1}{aH\hat{r}_{\rm m}e^{\zeta(\hat{r}_{\rm m})}}\,, \tag{34}$$

where $R_{\rm H} = 1/H$ is the cosmological horizon and $R_{\rm b}(r,t) = a(t)r$ is the background component of the areal radius. With these definitions, the expression written in Eq. (29) is valid with good accuracy for $\epsilon \ll 1$.

According to this, we can now consistently define the perturbation amplitude as being the mass excess of the energy density within the scale $r_{\rm m}$ when $\epsilon = 1$ ($aHr_{\rm m} = 1$). This corresponds to defining the horizon crossing time $t_{\rm H}$ with a linear extrapolation from the superhorizon regime. Although this is not very accurate, it provides a well defined criterion to measure and compare consistently the amplitude of different perturbations, understanding how the threshold is varying with respect to the initial curvature profiles.

The amplitude of the perturbation measured at $t_{\rm H}$, which we refer to as $\delta_{\rm m} \equiv \delta(r_{\rm m}, t_{\rm H})$, is given by the excess of mass averaged over a spherical volume of radius $R_{\rm m}$, defined as

$$\delta_{\rm m} = \frac{4\pi}{V_{R_{\rm m}}}\int_0^{R_{\rm m}}\frac{\delta\rho}{\rho_{\rm b}}\,R^2{\rm d}R \;= \frac{3}{r_{\rm m}^3}\int_0^{r_{\rm m}}\frac{\delta\rho}{\rho_{\rm b}}\,r^2{\rm d}r\,, \tag{35}$$

where $V_{R_{\rm m}} = 4\pi R_{\rm m}^3/3$. The second equality is obtained by neglecting the higher order terms in ϵ, approximating $R_{\rm m} \simeq a(t)r_{\rm m}$, which allows to simply integrate over the comoving volume of radius $r_{\rm m}$. Inserting the expression for $\delta\rho/\rho_{\rm b}$ given by

Eq. (29) into Eq. (35), one obtains $\delta_{\rm m} = \mathcal{C}(r_{\rm m})$, and with simple calculation seen in Musco (2019), one obtains the fundamental relation

$$\delta_{\rm m} = 3\frac{\delta\rho}{\rho_{\rm b}}(r_{\rm m}, t_{\rm H}), \tag{36}$$

showing that at $r_{\rm m}$ the perturbation amplitude is not affected by the location where this is measured.

3.3 Threshold for PBH formation

PBHs form when the perturbation amplitude $\delta_{\rm m} > \delta_{\rm c}$, where the value of the threshold $\delta_{\rm c}$ depends on the shape of the energy density profile and the equation of state. For a radiation-dominated Universe ($p = \frac{1}{3}\rho$), it has been found that $2/5 \leq \delta_{\rm c} \leq 2/3$, with the shape of the cosmological perturbation simply characterised by one dimensionless parameter corresponding to the width of the peak of the compaction function (Musco 2019; Escrivà et al. 2020)

$$\alpha = -\frac{\mathcal{C}''(r_{\rm m})r_{\rm m}^2}{4\mathcal{C}(r_{\rm m})}\,. \tag{37}$$

The shape of the energy density contrast becomes peaked for $\alpha < 1$ corresponding to a broad profile of the compaction function, whereas the shape of the compaction function C is more peaked for values of $\alpha > 1$, corresponding to broad profiles of the energy density contrast (Musco et al. 2021). See e.g. Fig. 2.1 of Franciolini (2021) for a graphical representation of this scaling. This allows to compute the threshold $\delta_{\rm c}$ as a function of the shape parameter α, with an analytic expression up to a few percent precision (Escrivà et al. 2020)

$$\delta_{\rm c} \simeq \frac{4}{15} e^{-\frac{1}{\alpha}} \frac{\alpha^{1-\frac{5}{2\alpha}}}{\Gamma\left(\frac{5}{2\alpha}\right) - \Gamma\left(\frac{5}{2\alpha}, \frac{1}{\alpha}\right)}, \tag{38}$$

where Γ identifies the special Gamma-functions. This is consistent with the numerical analysis made in Musco (2019), where it was shown that the effects on the threshold of additional parameters are negligible, because the collapse in spherical symmetry is basically characterized by the configuration of the region within the forming apparent horizon ($r \leq r_{\rm m}$), whose initial configuration is fully described by the shape parameter α.

The mass of a PBH is determined by the amplitude δ of the perturbation with respect to the corresponding threshold $\delta_{\rm c}$, according to the scaling law of critical collapse

$$m_{\rm PBH} = \mathcal{K}(\delta - \delta_{\rm c})^{\eta} M_{\rm H} \tag{39}$$

where the critical exponent η depends only on the equation of state ($\eta \simeq 0.36$ for a radiation-dominated Universe), while $\mathcal{K}$, as for $\delta_{\rm c}$, depends on the initial configuration of the energy density profile, roughly varying between 1 and 10. For the standard scenario of a radiation-dominated Universe, expression (39) describes the

mass with good accuracy when $(\delta - \delta_c) \lesssim 10^{-2}$, corresponding to $m_{\rm PBH} \simeq \gamma M_{\rm H}$, where γ, varying roughly between 0.1 and 1, is an efficiency parameter encapsulating the details of the gravitational collapse.

Although non linear cosmological density perturbations are described by a non Gaussian random field, when the Universe is still radiation-dominated one can compute the threshold δ_c from the shape of the Gaussian inflationary power spectrum following a simple prescription. The algorithm, divided into a few simple steps, accounts for both the non linear effects associated with the relation between the Gaussian curvature perturbation and the density contrast as well as for those arising at horizon crossing. While a more refined description of the various steps will be found in Musco et al. (2021), we give here a synthetic overview of the prescription one needs to follow.

1. *The power spectrum of the curvature perturbation*: take the primordial power spectrum $\mathcal{P}_\zeta$ of the Gaussian curvature perturbation and compute, on superhorizon scales, its convolution with the transfer function $T(k, \eta)$

$$P_\zeta(k, \eta) = \frac{2\pi^2}{k^3} \mathcal{P}_\zeta(k) T^2(k, \eta). \tag{40}$$

2. *The comoving length scale* $\hat{r}_{\rm m}$ of the perturbation is related to the characteristic scale k_* of the power spectrum P_ζ. Compute the value of $k_* \hat{r}_{\rm m}$ by solving the following integral equation

$$\int {\rm d}k k^2 \left[(k^2 \hat{r}_{\rm m}^2 - 1) \frac{\sin(k\hat{r}_{\rm m})}{k\hat{r}_{\rm m}} + \cos(k\hat{r}_{\rm m}) \right] P_\zeta(k, \eta) = 0\,. \tag{41}$$

3. *The shape parameter:* compute the corresponding shape parameter α of the collapsing perturbation, including the correction from the non linear effects, by solving the following equation

$$F(\alpha)[1 + F(\alpha)]\alpha = 2\alpha_G \tag{42}$$

with

$$\begin{aligned} \alpha_G &= -\frac{1}{4}\left[1 + \hat{r}_{\rm m} \frac{\int {\rm d}k k^4 \cos(k\hat{r}_{\rm m}) P_\zeta(k, \eta)}{\int {\rm d}k k^3 \sin(k\hat{r}_{\rm m}) P_\zeta(k, \eta)} \right], \\ F(\alpha) &= \sqrt{1 - \frac{2}{5} e^{-\frac{1}{\alpha}} \frac{\alpha^{1-\frac{5}{2\alpha}}}{\Gamma\left(\frac{5}{2\alpha}\right) - \Gamma\left(\frac{5}{2\alpha}, \frac{1}{\alpha}\right)}}\,. \end{aligned} \tag{43}$$

A numerical fit of the shape parameter α as a function of α_G, which represents the solution of Eq. (42) with a percent accuracy, is given by (Franciolini 2021)

$$\alpha \simeq \begin{cases} 1.758\, \alpha_G^{2.335} + 1.912\, \alpha_G & 0.1 \lesssim \alpha \lesssim 4.5, \\ 4\, \alpha_G^2 + 3.930\, \alpha_G & \alpha \gtrsim 8. \end{cases} \tag{44}$$

In the intermediate region where $4.5 < \alpha < 8$, no simple power law fit with a percent accuracy was found, and one needs to solve Eq. (42) numerically.

4. *The threshold* δ_c: compute the threshold as function of α, fitting the numerical simulations.

   - At *superhorizon scales* making a linear extrapolation at horizon crossing ($aHr_m = 1$).

$$\delta_c \simeq \begin{cases} \alpha^{0.047} - 0.50 & 0.1 \lesssim \alpha \lesssim 7 \\ \alpha^{0.035} - 0.475 & 7 \lesssim \alpha \lesssim 13 \\ \alpha^{0.026} - 0.45 & 13 \lesssim \alpha \lesssim 30 \end{cases} \tag{45}$$

   - At *horizon crossing* taking into account also the non linear effects.

$$\delta_c \simeq \begin{cases} \alpha^{0.125} - 0.05 & 0.1 \lesssim \alpha \lesssim 3 \\ \alpha^{0.06} + 0.025 & 3 \lesssim \alpha \lesssim 8 \\ 1.15 & \alpha \gtrsim 8 \end{cases} \tag{46}$$

This prescription is using the fact that, if $\mathcal{P}_\zeta$ follows a Gaussian distribution, $\Phi_L \equiv -\hat{r}\zeta'(\hat{r})$ is also a Gaussian variable, and one can write δ_m as

$$\delta_c = \frac{4}{3}\Phi_{c,L}\left(1 - \frac{1}{2}\Phi_{c,L}\right) \tag{47}$$

where $\Phi_{m,L} = \Phi_L(\hat{r}_m)$, and Φ is such that $0.37 \lesssim \Phi_{c,L} \leq 1$.

In Fig. 11, we show the threshold density contrast as a function of the shape parameter (left panel). Also, in the right panel, we report the critical collapse parameter $\mathcal{K}$ defined in Eq. (39). We recall that the critical collapse exponent η is independent from the shape of the collapsing overdensity peak (i.e. independent from α) and it is fixed to be $\eta = 0.358$ in a perfect radiation fluid. In the following, we will discuss how these parameters are modified when thermal effects during the evolution of the universe, causing a significant departure from the perfect radiation fluid approximation.

Before concluding this Section, we mention two relevant points. First, it has been recently observed that corrections from the non-linear radiation transfer function and the determination of the true physical horizon crossing tend to decrease the PBH abundance (De Luca et al. 2023b). Secondly, a recent study (Musco and Papanikolaou 2022) investigated the formation of PBHs with an anisotropic relativistic perfect fluid, using a covariant form of the EoS in terms of pressure and energy density gradients. This indicates that the value of the threshold δ_c is increasing with the amplitude of the anisotropy, if this is not large, while further studies are necessary for a nonlinear modification of the EoS.

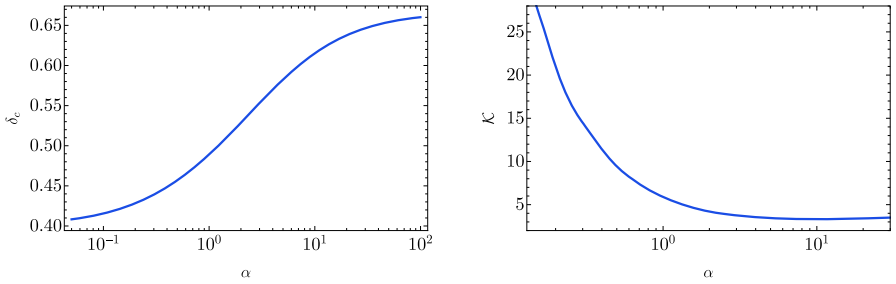

Fig. 11 Threshold δ_c and critical collapse parameter $\mathcal{K}$ as a function of the shape parameter α, assuming a universe dominate by perfect radiation (i.e. $w = 1/3$). Figure adapted from Musco et al. (2021) Image reproduced with permission

3.4 Gravitational collapse of primordial curvature perturbations – standard formalism

Although PBHs can be generated by many different mechanisms, we will focus here on the collapse of cosmological perturbations. In this case, the fraction $\beta_{\rm f}$ of PBHs formed in the early Universe is determined by the probability that a given primordial curvature fluctuation ζ, characterized by an amplitude δ of the density contrast, is above a certain threshold $\delta_{\rm c}$. The fraction of PBHs at formation is then usually given by

$$\beta_{\rm f}(m_{\rm PBH}) = \int_{\delta_{\rm c}}^{\infty} P(m_{\rm PBH}, \delta) {\rm d}\delta \,, \tag{48}$$

and the abundance of PBHs is sensitive to the PDF $P(m_{\rm PBH}, \delta)$ as to the value of the threshold $\delta_{\rm c}$. In particular, the PDF is characterized by the physics in the early Universe while the threshold $\delta_{\rm c}$ depends on the conditions at the time of formation. In particular, $\delta_{\rm c}$ has been actively studied in the past years (Musco et al. 2005; Polnarev and Musco 2007; Kopp et al. 2011; Harada et al. 2013; Young et al. 2014), with recent analysis on the dependence of the threshold on the shape of the power spectrum (Yoo et al. 2018; Germani and Musco 2019; Musco 2019), on the non-linear relation between the curvature perturbations and the density contrast (Young et al. 2019; De Luca et al. 2019c) as well as on the equation of state (EoS) (Harada et al. 2013; Escrivà et al. 2021; Papanikolaou 2022b) with a particular focus on the QCD phase transition (Jedamzik 1997; Byrnes et al. 2018).

Note also that in Eq. (48), we have expressed the PDF in terms of the mass $m_{\rm PBH}$ of the PBHs formed instead of the number of e-folds because in first approximation the mass of PBHs is related to the size of the causal horizon collapsing, depending on the time of formation (See Eq. 39).

Given the fraction of PBHs $\beta_{\rm f}(M)$, one can compute the contribution of PBHs to the energy density of the Universe and determine the fraction of DM they represent today. In this sense it is convenient to compute this quantity at the time of matter-radiation equality

$$\Omega_{\rm PBH}^{\rm eq} = \int_{M\,ev}^{M_{\rm eq}} \beta_{\rm eq}(m_{\rm PBH}) {\rm d}\ln m_{\rm PBH} \tag{49}$$

where $M_{\rm ev}$ is the lower bound due to Hawking evaporation, i.e. PBHs with $M < M_{\rm ev}$ would already been evaporated by now. We assume that the fraction of PBH at the time of matter-radiation equality has grown because of the cosmic expansion followed after the time of formation, which gives

$$\beta_{\rm eq}(m_{\rm PBH}) = e^{(N_{\rm eq}-N_{\rm f})}\beta_{\rm f}(m_{\rm PBH})\,. \tag{50}$$

Large curvature fluctuations can be produced by very different means in the early Universe. If the curvature perturbations were Gaussian, then the PDF would be described only by its variance σ^2 and the fraction of PBHs measured at the time of formation is usually computed as

$$\beta_{\rm f}(m_{\rm PBH}) = 2\int_{\delta_{\rm c}}^{\infty} \frac{1}{\sqrt{2\pi\sigma}} e^{-\frac{\delta^2}{2\sigma^2}} {\rm d}\delta = 1 - {\rm erf}\left(\frac{\delta_{\rm c}}{\sqrt{2}\sigma}\right) = {\rm erfc}\left(\frac{\delta_{\rm c}}{\sqrt{2}\sigma}\right), \tag{51}$$

where the factor 2 outside the integral is sometimes introduced when the abundance is computed using the excursion set method (see, e.g., Moradinezhad Dizgah et al. 2019; De Luca et al. 2020f). This expression, however, does not take into account that when δ is larger then a certain value $\delta_{\rm max}$ (originally estimated $\delta_{\rm max} \sim 1$ by Carr 1975), the perturbation forms a separate closed universe, topologically disconnected. A more accurate version can nevertheless be obtained re-normalizing the previous expression as

$$\beta_{\rm f}(m_{\rm PBH}) = \frac{\displaystyle\int_{\delta_{\rm c}}^{\delta_{\rm max}} \frac{1}{\sqrt{2\pi\sigma^2}} e^{-\frac{\delta^2}{2\sigma^2}} {\rm d}\delta}{\displaystyle\int_{0}^{\delta_{\rm max}} \frac{1}{\sqrt{2\pi\sigma^2}} e^{-\frac{\delta^2}{2\sigma^2}} {\rm d}\delta} = 1 - \frac{{\rm erf}\left(\frac{\delta_{\rm c}}{\sqrt{2}\,\sigma}\right)}{{\rm erf}\left(\frac{\delta_{\rm max}}{\sqrt{2}\,\sigma}\right)} = \frac{{\rm erfc}\left(\frac{\delta_{\rm c}}{\sqrt{2}\sigma}\right) - {\rm erfc}\left(\frac{\delta_{\rm max}}{\sqrt{2}\sigma}\right)}{1 - {\rm erfc}\left(\frac{\delta_{\rm max}}{\sqrt{2}\sigma}\right)}\,. \tag{52}$$

PBHs are produced through the tail of the PDF, ie. the area left under the PDF curve where δ is larger than the critical threshold $\delta_{\rm c}$. Therefore, PBH abundance is exponentially sensitive to the threshold and the statistical properties of the primordial perturbations. Even tiny modifications in the tail of the distribution can change the PBH abundance by many orders of magnitude.

The variance of the field of density perturbations σ, according to the Gaussian distribution of δ, consistent with the linear approximation of the relation between the energy density contrast and the curvature perturbation (see next subsection), is given by

$$\sigma^2 = \langle\delta^2\rangle = \int_0^{\infty} \frac{{\rm d}k}{k} \mathcal{P}_\delta(k,r) = \frac{16}{81}\int_0^{\infty} \frac{{\rm d}k}{k} (kr)^4 \tilde{W}^2(k,r) T^2(k,r) \mathcal{P}_\zeta(k)\,, \tag{53}$$

where $\mathcal{P}_\delta(k,r)$ and $\mathcal{P}_\zeta(k)$ are the density and the curvature power spectra, while

$\tilde{W}(k,r)$ is the Fourier transform of the top-hat smoothing function and $T(k, r)$ is the linear transfer function

$$\tilde{W}(k,r) = 3\left[\frac{\sin(kr) - kr\cos(kr)}{(kr)^3}\right] \tag{54}$$

$$T(k,r) = 3\left[\frac{\sin\left(\frac{kr}{\sqrt{3}}\right) - \frac{kr}{\sqrt{3}}\cos\left(\frac{kr}{\sqrt{3}}\right)}{\left(\frac{kr}{\sqrt{3}}\right)^3}\right]. \tag{55}$$

The quantities δ_c and σ, giving the critical threshold $\nu_c \equiv \delta_c/\sigma$, are typically computed at super horizon scale, when the curvature perturbation ζ for adiabatic perturbations is time independent, making a linear extrapolation at horizon crossing time, which is approximately the time when PBHs are formed (we will discuss this later in more details). All this shows that a larger amplitude of the power spectrum, combined with a shape decreasing the corresponding value of ν_c, could increase significantly the fraction of PBHs because the abundance of PBHs is exponentially sensitive to the value of δ_c.

The linear transfer function[4] ensures that the variance would always converge, because the window function by itself, chosen consistently with the top-hat window function in real space used in the definition of δ_c, does not guarantee convergence if the power spectrum considered is sufficiently broad. An alternative approach is to use a Gaussian window function, which provides always convergence of the variance, but this is contaminating the value of δ_c, introducing an error in the final computation of the abundance (Young 2019).

3.5 The inevitable non-Gaussianity of the primordial black hole abundance

The non-linear relation between the curvature perturbation and the density contrast in (29) induces an inescapable non-Gaussianity of the density contrast, even assuming a Gaussian primordial initial condition (Musco 2019; Young et al. 2019; De Luca et al. 2019c). This can be captured in the non-linear expression (Young et al. 2019)

$$\delta_m = \delta_l - \frac{3}{8}\delta_l^2, \qquad \delta_l = -\frac{4}{3}r_m\zeta'(r_m). \tag{56}$$

It highlights two key points. First of all, the probability of forming PBHs does not depend on the comoving curvature perturbation itself ζ, but on its derivative ζ'. This is expected, given that on superhorizon scales one can always add or subtract to the comoving curvature perturbation a constant by a coordinate transformation and this may not influence any physical result. Secondly, thanks to the conservation of the probability

[4] De Luca et al. (2023b) has recently investigated the role of non-linear corrections, coming from the non-linear radiation transfer function and the determination of the true physical horizon crossing, on the PBH abundance, showing that, while the critical threshold is larger than what routinely assumed, the variance is unlikely to be changed with respect to the linear one.

$$P(\delta_{\rm l}) = P[\delta_{\rm m}(\delta_{\rm l})]\left|\frac{{\rm d}\delta_{\rm m}}{{\rm d}\delta_{\rm l}}\right|, \tag{57}$$

one can compute the abundance of PBHs simply using the Gaussian probability of $\delta_{\rm l}$, integrating it from the critical amplitude for $\delta_{\rm l}$

$$\delta_{\rm l,c} = \frac{4}{3}\left(1 - \sqrt{1 - \frac{3}{2}\delta_{\rm c}}\right), \tag{58}$$

in terms of the critical amplitude $\delta_{\rm c}$.

3.6 Collapse of some initial non-Gaussian perturbations

It has been observed that nearly all models discussed in Sect. 2 generate a considerable amount of primordial non-Gaussianity. We briefly summarize the β function in case of large local non-Gaussianity, which turns the PDF into a χ^2 distribution, explicitly $\delta_{\chi^2} = G^2 - \langle G^2\rangle$; and also in case of large cubic interactions, which turn the PDF into a cubic-Gaussian distribution, explicitly $\delta_{G^3} = G^3$, with G a field obeying Gaussian statistics (Lyth 2012; Linde et al. 2013; Young and Byrnes 2013; Bugaev and Klimai 2014).

$$\begin{aligned}
\beta_{{\rm f},\,\chi^2}(m_{\rm PBH}) =& {\rm erfc}\left(\sqrt{\frac{1}{2} + \frac{\delta_{\rm c}}{\sqrt{2}\sigma}}\right), \\
\beta_{{\rm f},\,G^3}(m_{\rm PBH}) =& {\rm erfc}\left(\left(\frac{\delta_{\rm c}}{\sqrt{\frac{8}{15}}\sigma}\right)^{1/3}\right).
\end{aligned} \tag{59}$$

We also note that the threshold density $\delta_{\rm c}$ depends slightly on the non-Gaussianity (Kehagias et al. 2019; Kitajima et al. 2021; Escrivà et al. 2022).

3.7 Non-perturbative abundance from non-Gaussian perturbations

Ferrante et al. (2023b) and Gow et al. (2023) addressed the problem of computing the impact of a general form of local primordial NG on PBH abundance beyond the perturbative approach. In particular, let us focus on the functional form

$$\zeta(\vec{x}) = F(\zeta_G(\vec{x}))\,, \tag{60}$$

where F is a generic non-linear function of the Gaussian component ζ_G. There is a large number of relevant cases in the literature of PBH formation where the NGs can be modelled as in Eq. (60). We summarize few relevant examples in Table 1 (adapted from Ferrante et al. 2023b).

It is important to stress here that going beyond the perturbative approach becomes a necessity at least when dealing with broad spectra of curvature perturbations. This is because, as shown in Ferrante et al. (2023b), in these cases the probability

distribution function of ζ_G is evaluated beyond the radius of convergence of the series expansion, leading to inaccurate results if the series is truncated at finite order. Notice that in non-attractor models the sign of non-Gaussianity is always positive (Firouzjahi and Riotto 2023), thus enhancing the PBH abundance.

Using the relation between the curvature perturbation and the compaction function in the gradient expansion (29), it is possible write

$$\mathcal{C}(r) = -2\Phi\, r\,\zeta'(r)\left[1+\frac{r}{2}\zeta'(r)\right] = \mathcal{C}_1(r) - \frac{1}{4\Phi}\mathcal{C}_1(r)^2\,, \qquad \mathcal{C}_1(r) \equiv -2\Phi\, r\,\zeta'(r)\,, \tag{61}$$

where $\mathcal{C}_1(r)$ defines the so-called linear component of the compaction function and we introduced the prefactor Φ that accounts for potential thermal effects (see more in depth discussion below Eq. (70)). Substituting in the previous expression the relation $\zeta = F(\zeta_G)$ (see Eq. (60)), one obtains that the linear component of the compaction function takes the form

$$\mathcal{C}_1(r) = -2\Phi\, r\,\zeta_G'(r)\,\frac{dF}{d\zeta_G} = \mathcal{C}_G(r)\,\frac{dF}{d\zeta_G} \tag{62}$$

with $\mathcal{C}_G(r) \equiv -2\Phi\, r\,\zeta_G'(r)$. Consequently, the compaction function reads

$$\mathcal{C}(r) = \mathcal{C}_G(r)\,\frac{dF}{d\zeta_G} - \frac{1}{4\Phi}\mathcal{C}_G^2(r)\left(\frac{dF}{d\zeta_G}\right)^2. \tag{63}$$

Crucially, $\mathcal{C}(r)$ depends on both the Gaussian linear component $\mathcal{C}_G$ and the Gaussian curvature perturbation ζ_G. Both these random variables are Gaussian; ζ_G is Gaussian by definition while $\mathcal{C}_G$ is defined by means of the derivative of the Gaussian variable ζ_G.

Adopting threshold statistics on the compaction function, one can express the non-Gaussian mass fraction as an integration of the joined PDF in the domain which results in over-threshold perturbations, i.e.

Table 1 Some examples of PBH formation scenarios characterised by local non-Gaussianity of the form defined in Eq. (60). The function $X(r_{\rm dec}, \zeta_G)$ given in the second row is defined in (Sasaki et al. 2006)

Power-series expansion (Bugaev and Klimai 2013; Nakama et al. 2017; Byrnes et al. 2012; Young and Byrnes 2013; Yoo et al. 2018; Kawasaki and Nakatsuka 2019; Yoo et al. 2019; Riccardi et al. 2021; Taoso and Urbano 2021; Meng et al. 2022; Escrivà et al. 2022)	$\zeta = \zeta_G + \frac{3}{5}f_{NL}\zeta_G^2 + \frac{9}{25}g_{\rm NL}\zeta_G^3 + \dots$
Curvaton (Sasaki et al. 2006; Pi and Sasaki 2023)	$\zeta = \log[X(r_{\rm dec}, \zeta_G)]$
USR (Atal et al. 2019)	$\zeta = -\left(\frac{6}{5}f_{NL}\right)^{-1}\log\left(1-\frac{6}{5}f_{NL}\zeta_G\right)$
USR with an upward step (Cai et al. 2022a)	$\zeta = -\frac{2}{\lvert h\rvert}\left[\sqrt{1-\lvert h\rvert\zeta_G}-1\right]$

$$\beta_{\rm NG} = \int_{\mathcal{D}} \mathcal{K}(\mathcal{C} - \mathcal{C}_{\rm th})^{\gamma} \mathrm{P}_G(\mathcal{C}_G, \zeta_G) \mathrm{d}\mathcal{C}_G \mathrm{d}\zeta_G \,, \tag{64}$$

$$\mathcal{D} = \{\mathcal{C}_G,\, \zeta_G \in \mathbb{R} \,:\, \mathcal{C}(\mathcal{C}_G, \zeta_G) > \mathcal{C}_{\rm th} \,\wedge\, \mathcal{C}_1(\mathcal{C}_G, \zeta_G) < 2\Phi\} \,, \tag{65}$$

where the multivariate normal distribution of $(\mathcal{C}_G, \zeta_G)$ can be written as

$$\mathrm{P}_G(\mathcal{C}_G, \zeta_G) = \frac{1}{(2\pi)\sigma_c \sigma_r \sqrt{1-\gamma_{cr}^2}} \exp\left(-\frac{\zeta_G^2}{2\sigma_r^2}\right) \exp\left[-\frac{1}{2(1-\gamma_{cr}^2)}\left(\frac{\mathcal{C}_G}{\sigma_c} - \frac{\gamma_{cr}\zeta_G}{\sigma_r}\right)^2\right] . \tag{66}$$

To shorten the notation, we have followed Young (2022) and defined the element of the covariance matrix as

$$\langle \mathcal{C}_G \mathcal{C}_G \rangle = \sigma_c^2 = \frac{4\Phi^2}{9} \int_0^{\infty} \frac{dk}{k} (k r_m)^4 \tilde{W}^2(k, r_m) T^2(k, r_m) P_{\zeta}(k) \,, \tag{67}$$

$$\langle \mathcal{C}_G \zeta_{\rm G} \rangle = \sigma_{cr}^2 = \frac{2\Phi}{3} \int_0^{\infty} \frac{dk}{k} (k r_m)^2 \tilde{W}(k, r_m) W_s(k, r_m) T^2(k, r_m) P_{\zeta}(k) \,, \tag{68}$$

$$\langle \zeta_{\rm G} \zeta_{\rm G} \rangle = \sigma_r^2 = \int_0^{\infty} \frac{dk}{k} W_s^2(k, r_m) T^2(k, r_m) P_{\zeta}(k) \,, \tag{69}$$

where $W_s(k, r) = \sin(kr)/kr$, $\tilde{W}(k, R)$ and $T(k, \tau)$ are given in Eqs. (55) and (54), while $\gamma_{cr} \equiv \sigma_{cr}^2/\sigma_c \sigma_r$.

3.8 Thermal history

3.8.1 The equation of state and the number of relativistic degrees of freedom

The reheating at the end of inflation should have filled the Universe with radiation. In the absence of extensions beyond the Standard Model (SM) of particle physics, the Universe remains dominated by relativistic particles with an energy density decreasing as the fourth power of the temperature as the Universe expands and cools down. The number of relativistic degrees of freedom remains constant ($g_* = 106.75$) until around 200 GeV, when the temperature of the Universe falls to the mass thresholds of SM particles.

As shown in Fig. 12 (left panel), the first particle to become non-relativistic is the top quark at $T \simeq m_{\rm t} = 172$ GeV, followed by the Higgs boson at 125 GeV, and the Z and W bosons at 92 and 81 GeV, respectively. These particles become non-relativistic at nearly the same time and this induces a significant drop in the number of relativistic degrees of freedom down to $g_* = 86.75$. There are further changes at the b and c quark and τ-lepton thresholds but these are too small to appear in Fig. 12. Thereafter, g_* remains approximately constant until the QCD transition at around 200 MeV, when protons and neutrons condense out of the free light quarks and gluons. The number of relativistic degrees of freedom then falls abruptly to

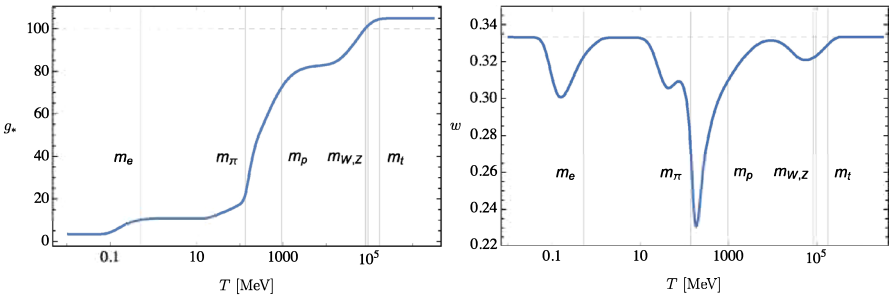

Fig. 12 Relativistic degrees of freedom g_* (*Left panel*) and equation-of-state parameter w (*Right panel*), both as a function of temperature T (in MeV). The grey vertical lines correspond to the masses of the electron, pion, proton/neutron, W, Z bosons and top quark, respectively. The grey dashed horizontal lines indicate values of $g_* = 100$ and $w = 1/3$, respectively Image reproduced with permission

$g_* = 17.25$. A little later the pions become non-relativistic and then the muons, giving $g_* = 10.75$. After that, g_* remains constant until e^+e^- annihilation and neutrino decoupling at around 1 MeV, when it finally drops to $g_* = 3.36$.

Whenever the number of relativistic degrees of freedom suddenly drops, it changes the effective equation of state parameter w. As shown in Fig. 12 (right panel), there are thus three main periods in the thermal history of the Universe when w decreases. After each period, w resumes its relativistic value of 1/3 but each sudden drop modifies the probability of gravitational collapse of any large curvature fluctuations present at that time.

3.8.2 Thermal effects on PBH formation and abundance

Because the threshold δ_c is a measure of the pressure gradients working against the gravitational collapse, it depends on the equation-of-state, and since the PBH abundance depends exponentially on the value of the threshold, the thermal history should have left imprints in the PBH mass distribution. In particular, assuming a nearly scale-invariant primordial power spectrum, one finds that the PBH mass distribution is broad with features in the form of a high peak at the solar-mass scale, a bump around $30M_\odot$, which would have implications for LVK observations, as well as one bump at planetary-masses from the electroweak scale and a final one for intermediate-mass PBHs (Byrnes et al. 2018; Carr et al. 2021b).

In order to gain an intuition on the relevance of these effects for on the mass distribution derived from (nearly) scale invariant power spectra, we show in Fig. 13 two representative models of PBH formation from power spectra with spectral index $n_s = 0.97$ and $n_s = 1$. These models are later used in this review for computing the PBH merger rates and SGWB. However, to obtain Fig. 13 the effects of the variation of the equation-of-state and of the pressure gradients *during* the PBH formation process, discussed later, were neglected.

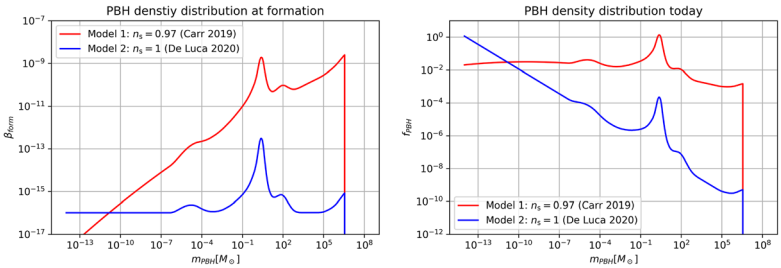

Fig. 13 PBH density fraction at formation β^{form} (left panel) and the corresponding PBH mass function f_{PBH} today (right panel), neglecting the effects of PBH growth by accretion and hierarchical mergers, for two models with a power-law primordial power spectrum and including the effects of thermal history: Model 1 from Carr et al. (2021b), Clesse and García-Bellido (2022) with spectral index $n_{\text{s}} = 0.97$; Model 2 from De Luca et al. (2021g), Byrnes et al. (2018) with $n_{\text{s}} = 1$. and a cut-off mass of $10^{-14}\,M_{\odot}$. The transition between the large-scale and small-scale power spectrum is fixed at $k = 10^3\,\text{Mpc}^{-1}$. The power spectrum amplitude is normalized such that both models produce an integrated PBH fraction $f_{\text{PBH}} = 1$, i.e. PBH constitute the totality of Dark Matter. A value of $\gamma = 0.8$ (ratio between the PBH mass and the Hubble horizon mass at formation) was assumed. Image reproduced with permission from Auclair et al. (2023), copyright by the author(s) Image reproduced with permission

More recently, new numerical simulations of PBH formation at the QCD epoch have been performed (Escrivà et al. 2023; Musco et al. 2024), including the time and radial variations of the equation of state. These modify significantly the PBH mass function characterised by a lower but broader QCD-induced peak. The physical reason of this broadening is the time duration of the formation process, during which the changes in the equation-of-state favor the collapse. As a result, the threshold and the resulting PBH mass distribution do not only depend on the fluctuation mass at horizon crossing, but also on the precise evolution of the equation of state, as well as the details of the curvature fluctuation profile.

The thermal history, affecting the equation of state of the fluid dominating the energy density at the time of PBH collapse, impacts many aspects of the PBH formation. Following Franciolini et al. (2022e), Musco et al. (2024), here we discuss how the threshold is varying according to the equation of state, focusing on the modification of the relation between the density contrast and the curvature perturbation when the equation of state is varying with time. This has an impact also on the PBH masses with a modified scaling behaviour of the critical collapse.

When the equation-of-state is not constant, Eq. (29) is modulated by an overall factor $\Phi(t)$, which we can define in the long wavelength approximation as (Franciolini et al. 2022e)

$$\frac{\delta\rho}{\rho_b}(r,t) = -\frac{4}{3}\Phi\left(\frac{1}{aH}\right)^2 e^{-5\zeta(r)/2}\nabla^2 e^{\zeta(r)/2}. \tag{70}$$

$\Phi(t)$ can be computed by solving the equation (Polnarev and Musco 2007)

$$\frac{1}{H}\frac{\mathrm{d}\Phi(t)}{\mathrm{d}t}+\frac{5+3w(t)}{2}\Phi(t)-\frac{3}{2}(1+w(t))=0 \tag{71}$$

integrated from past infinity to the time when the amplitude of the perturbation is computed. Assuming the standard models of the very early Universe, the initial condition for Eq. (71) is derived assuming a radiation dominated medium, with an equation-of-state $p=w\rho$ and $w=1/3$. When a constant $w(t)=\bar{w}$ characterises the fluid dominating the energy budget of the Universe, we have $\mathrm{d}\Phi(t)/\mathrm{d}t=0$ and one obtains

$$\bar{\Phi}=\frac{3(1+\bar{w})}{(5+3\bar{w})}, \tag{72}$$

yielding $\bar{\Phi}=2/3$ for a radiation fluid with $\bar{w}=1/3$. Such a prefactor is standardly reported in Eq. (29). The behavior of Φ across the QCD phase transition, obtained by solving Eq. (71), differs from the average $\bar{\Phi}$, particularly in the region where w and c_s^2 are quickly varying with respect to M_H (left panel of Fig. 14). The resulting evolution of Φ as a function of horizon crossing mass is shown in the middle panel of Fig. 14.

Overall, the QCD phase transition introduces an additional degree of freedom into the problem, which is the characteristic scale of the horizon crossing of the cosmological perturbation. In Fig. 15, obtained from the computations done in Musco et al. (2024), we summarise the modified behaviour of the threshold δ_{c} for different values of the shape parameter α defined in (37). The different lines with a color varying between red, for smaller values of α and blue, for larger values, shows as the threshold is varying during the QCD epoch, as function of the cosmological horizon mass M_H. This is in agreement with the results obtained in Escrivà et al. (2023), apart from a few percent difference due to the different set up of the initial conditions.

Musco et al. (2024) have computed also the modified critical scaling behaviour defined in Eq. (39), which is modified as

$$m_{\mathrm{PBH}}=\mathcal{K}(M_H)[\delta-\delta_{\mathrm{c}}(M_H)]^{\gamma(M_H)}M_{\mathrm{H}}, \tag{73}$$

where $\delta_c(M_H)$, $\gamma(M_H)$ and $\mathcal{K}(M_H)$ are fitted to numerical simulations performed in Musco et al. (2024) as a function of M_H, i.e. when the perturbation is crossing the cosmological horizon, defined as

$$M_H\simeq 17M_\odot\left(\frac{g_*}{10.75}\right)^{-1/6}\left(\frac{k/\kappa}{10^6\mathrm{Mpc}^{-1}}\right)^{-2}, \tag{74}$$

where g_* is the number of degrees of freedom of relativistic particles and $\kappa\equiv r_m k$ relates the spectral wavenumber with the horizon crossing size of perturbations as derived in Sec. 3.3. The different lines shown in Fig. 16 with a color varying between red, for smaller values of M_H, and blue for larger values, shows how the scaling law is modified by the characteristic scale of the problem. Notice that an exact power-law critical behaviour is only obtained close enough to the density threshold

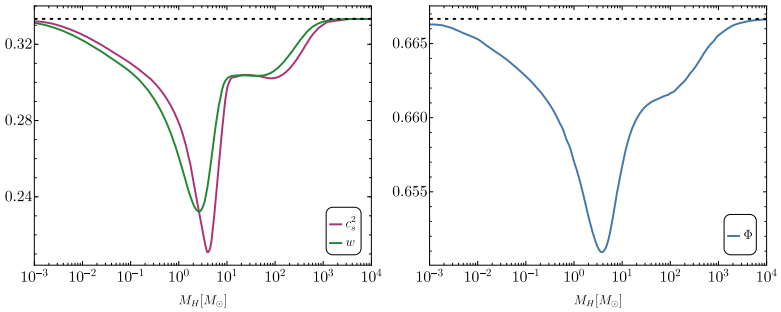

Fig. 14 Left panel: the equation-of-state parameter $w = p/\rho$ (red) and squared speed of sound (blue) as functions of the cosmological horizon mass M_H. Right panel: Evolution of the equation-of-state dependent parameter Φ, relating the density contrast to the curvature perturbation as functions of the cosmological horizon mass M_H. Image reproduced with permission from Franciolini et al. (2022e), copyright by APS Image reproduced with permission

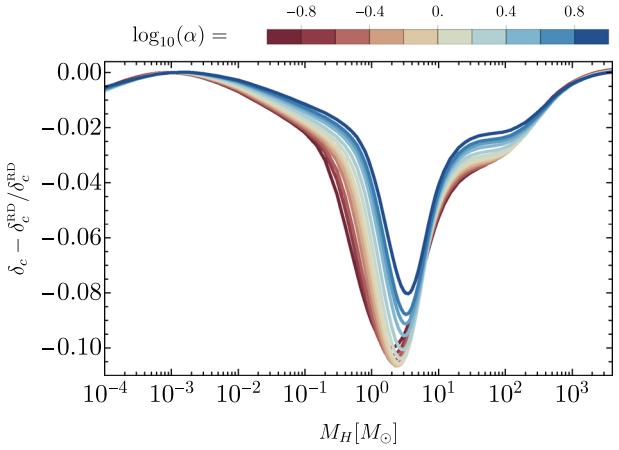

Fig. 15 Relative variation of the threshold compared to what is obtained assuming perfect radiation as a function of the horizon crossing time (parametrised here with M_H) induced by the QCD thermal effects. The color code indicates the different values of $\log_{10}(\alpha)$ as indicated by the bar on top of the frame. Figure adapted from Musco et al. (2024) Image reproduced with permission

$(\delta - \delta_c \lesssim 10^{-5})$, where the PBH masses are significantly smaller than the cosmological horizon mass, not able to affect significantly the collapse, while for larger values the equation-of-state during the QCD epoch induces further modifications. Franciolini et al. (2022e) fit the relation between the PBH and horizon mass using the power-law template (73) in the range of δ which most contributes to the abundance, i.e. $(\delta - \delta_c) \in [10^{-5}, 2 \times 10^{-2}]$, and finds that deviations from the functional form used in Eq. (73) would only induce a small correction which we can neglect. The resulting values of $\mathcal{K}(M_H)$ and $\gamma(M_H)$ used here are shown in the right plot of Fig. 16. For reference, we also show the critical collapse during the radiation dominated epoch of the early Universe, indicated with a black dashed line. A general

trend is observed: for $M_H \lesssim 3M_\odot$, there is a tendency to generate heavier PBHs, while the opposite is found when $M_H \gtrsim 3M_\odot$. This can be seen in the left panel of Fig. 16, where orange (light blue) lines fall above (below) the dashed black line indicating the result for a radiation perfect fluid.

In order to compute the full mass distribution, including both the thermal effects as well as non-linearities (56), it is convenient to invert the relation between horizon and PBH mass through the critical collapse relation (73), focusing only on the so called type-I branch for which $\delta_l < \Phi$, see Musco et al. (2021) for more details, as

$$\delta_l = 2\Phi\left(1-\sqrt{\Lambda}\right), \qquad \text{where} \qquad \Lambda = 1 - \frac{\delta_c}{\Phi} - \frac{1}{\Phi}\left(\frac{m_{\rm PBH}}{\mathcal{K} M_H}\right)^{1/\gamma}. \tag{75}$$

Finally, one can arrive at a compact expression for the computation of the mass distribution which is

$$\psi(m_{\rm PBH}) \equiv \frac{1}{\Omega_{\rm PBH}}\frac{{\rm d}\Omega_{\rm PBH}}{{\rm d}m_{\rm PBH}} = \frac{8}{3\pi\,\Omega_{\rm PBH} m_{\rm PBH}} \int \frac{{\rm d}M_H}{M_H}\left(\frac{M_{\rm eq}}{M_H}\right)^{1/2}\left(\frac{\sigma_1}{aH\sigma_0}\right)^3 \times \frac{\Phi^3 \mathcal{K}}{\gamma \sigma_0^4}\left(\frac{m_{\rm PBH}}{\mathcal{K} M_H}\right)^{\frac{1+\gamma}{\gamma}} \frac{\left(1-\sqrt{\Lambda}\right)^3}{\Lambda^{1/2}} \exp\left[-\frac{2\Phi^2}{\sigma_0^2}\left(1-\sqrt{\Lambda}\right)^2\right], \tag{76}$$

and the integration range of M_H is subject to the condition $\Lambda > 0$ (because we require $\delta > \delta_c$). An extension of this formula that includes both thermal effects and non-Gaussianities of ζ, as discussed in Sect. 3.7, is presented in Ferrante et al. (2023b). The quantities $\mathcal{K}(M_H)$, $\gamma(M_H)$, $\Phi(M_H)$, $\delta_c(M_H)$, and $\sigma_i(M_H)$ are left within the integration over the horizon mass scale, as they all explicitly depend on M_H when thermal effects are included. The variances can be computed integrating the curvature power spectrum as

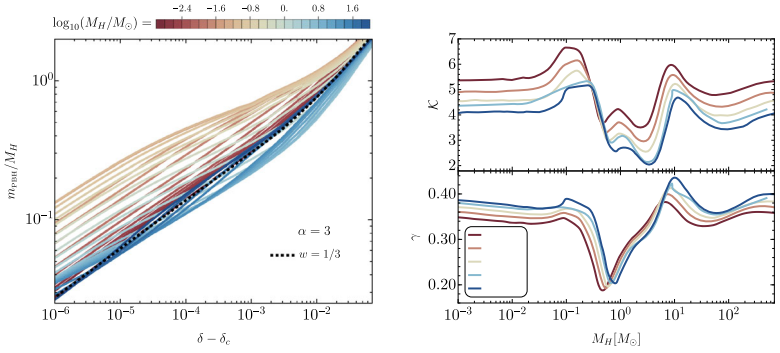

Fig. 16 Left panel: PBH mass $m_{\rm PBH}$ plotted as a function of $\delta - \delta_c$ computed at the cosmological horizon crossing (see Musco et al. 2024 for more details). The behavior for a radiation dominated medium is plotted with a black dashed line. Right panel: The values of the power law coefficients in Eq. (73) found by fitting the results of numerical simulations shown in the left panel. Image adapted from Franciolini et al. (2022e) Image reproduced with permission

$$\sigma_i^2(r_m) = \frac{4}{9}\Phi^2 \int_0^\infty \frac{\mathrm{d}k}{k} (kr_m)^4 \tilde{W}^2(k, r_m) T^2(k, r_m) k^{2i} \mathcal{P}_\zeta(k), \tag{77}$$

where $i = 0, 1$ and the window and transfer functions are defined in Eqs. (54) and (55), respectively. If a nearly scale invariant spectrum of curvature perturbations is assumed, the smoothing scale r_m is related with power spectral modes as $r_m k \equiv \kappa = 4.49$, as discussed in Sect. 3.3. This relation is strictly valid for a shape parameter $\alpha = 3$ (Musco et al. 2021). Notice that in the low mass limit, that is when we consider masses much below the smallest M_H, one can find that the mass distribution (76) scales as

$$\psi(m_{\rm PBH}) \propto \left(m_{\rm PBH}\right)^{1/\gamma}, \tag{78}$$

where $1/\gamma \simeq 2.8$ if one assumes the energy density of the Universe behaving as a relativistic fluid with $w = 1/3$, which gives $\gamma \approx 0.36$ (Niemeyer and Jedamzik 1998).

We conclude this section with a note of caution. While it is true that the QCD era produces a natural boost of formation around the solar mass, the physics of collapse alone is not predictive. This is because all the model dependence is retained in the spectrum and in the statistics of curvature perturbations. Without strong assumptions on the tilt and running of the spectrum, for instance, no prediction on the height of the QCD peak at the solar mass compared to other scales can be obtained. This is reflected in Fig. 17, where different mass distributions are derived, assuming a power-law curvature power spectrum with varying tilt n_s (not necessarily related to the one at large CMB scales). The different ways one can introduce the curvature or density profiles can explain some of the differences observed between Musco et al. (2024) and Escrivà et al. (2023), as well as the still low degree of accuracy to which we know the evolution of the equation-of-state from QCD lattice simulations. Overall, the PBH formation remains an intrinsically non-linear and fully relativistic process, which makes the physics quite complex, as the recent developments have shown. The improvement of our understanding of PBH formation has been very important and will probably be pushed further ahead in the next years, with significant implications for the PBH mass distribution expected in the various proposed models.

3.9 Evolution of the mass function through accretion

The primordial PBH mass function would be preserved up to the present epoch unless phenomena affecting the PBH masses modify it during the cosmological history. In particular, it was shown that PBH mass accretion may be relevant for the PBH evolution (De Luca et al. 2020e). In this Subsection and in the following, we will describe the impact on the mass and spin of PBHs by a phase of accretion (see De Luca and Bellomo 2023 for a recent review).

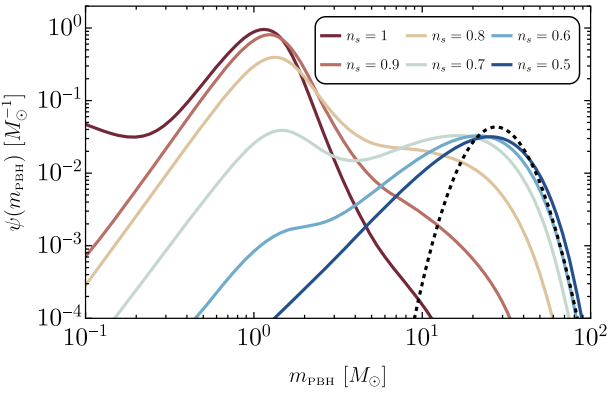

Fig. 17 Mass function obtained with a few choices of the curvature power spectrum. This plot assumes $f_{\rm PBH} = 10^{-3}$, the minimum horizon mass to be $\lesssim 10^{-2.5} M_\odot$, the largest mass $M_H^{\rm max} = 10^{2.8} M_\odot$ and a variable tilt n_s. The black dashed line reports the lognormal mass distribution found as the best fit in the analysis of Franciolini et al. (2022a). Image reproduced with permission from Franciolini et al. (2022e), copyright by APS Image reproduced with permission

3.9.1 Accretion onto isolated PBHs

PBHs can accrete mass if particles from the surrounding environment fall into the gravitational potential well generated by the compact object and eventually get eaten by the PBH. It can be shown that the strongest impact on the PBH mass is coming from baryonic accretion. In case PBHs are not accounting for the entirety of the DM, there exists an additional DM fluid in the Universe. Such a secondary DM component however would only act as a catalyst of baryonic accretion while it marginally contributes to the PBH mass growth (Ricotti et al. 2008).

During the cosmological history, one can model the mass variation using the Bondi–Hoyle accretion rate (Bondi 1952; Hoyle and Lyttleton 1939, 1940a, b; Ricotti 2007; Ricotti et al. 2008)

$$\dot{m}_{\rm PBH} = 4\pi\lambda m_{\rm p} n_{\rm gas} v_{\rm eff}^{-3} m_{\rm PBH}^2, \tag{79}$$

where the PBH effective velocity $v_{\rm eff} = \sqrt{v_{\rm rel}^2 + c_{\rm s}^2}$ is given in terms of the relative velocity $v_{\rm rel}$ with respect to the surrounding gas of hydrogen with mass $m_{\rm p}$, sound speed $c_{\rm s}$ and number density $n_{\rm gas}$. We denote with the Bondi radius $r_{\rm b}$ the region of space under the influence of the PBH potential well which is also determining the characteristic scale of the gas cloud accreting onto the PBHs. The parameter λ, whose explicit expression is summarized for example in Appendix B of De Luca et al. (2020e), takes into account the effects of gas viscosity, Hubble expansion and the coupling of the CMB radiation to the gas through Compton scattering (Ricotti 2007). Notice that the aforementioned treatment is based on newtonian mechanics, and general-relativistic effects may lead to a significant increase in the mass accretion rate, depending on the specific environmental settings, see for example Cruz-Osorio and Rezzolla (2020), Cruz-Osorio et al. (2021).

The presence of observational constraints for PBHs with masses larger than $\mathcal{O}(M_\odot)$ suggest that they can comprise only a fraction of the DM in the Universe, and therefore an additional DM halo has to be considered when modelling gas accretion (Mack et al. 2007; Adamek et al. 2019). The presence of a DM halo catalyses the accretion of gas onto the PBHs, with a halo characteristic size and mass which grows with time as (Ricotti et al. 2008)

$$r_{\rm halo} = 0.019\,{\rm pc}\left(\frac{M_{\rm halo}}{M_\odot}\right)^{1/3}\left(\frac{1+z}{1000}\right)^{-1}, \qquad M_{\rm halo} = 3m_{\rm PBH}\left(\frac{1+z}{1000}\right)^{-1} \tag{80}$$

and enhances the accretion rate (Ricotti 2007). In the limit in which the characteristic halo radius is smaller than the PBH Bondi radius, accretion occurs onto a PBH with effective point mass $M_{\rm halo}$, while for comparable sizes or in the opposite limit, the proper contribution is captured by corrections to the accretion parameter λ, see Appendix B of De Luca et al. (2020e) and references therein for additional details.

For PBHs with masses larger than $\mathcal{O}(10)M_\odot$, accretion can reach super-Eddington values before the reionization epoch and play an important role in both the mass and spin evolution of PBHs (see Ricotti 2007; De Luca et al. 2020e). The increase of the PBH masses due to accretion also affects their mass distribution function in a non-linear fashion (García-Bellido 2018; De Luca et al. 2019a). Indeed, for an initial mass function $\psi(m^{\rm I}_{\rm PBH}, z_{\rm I})$ at formation redshift $z_{\rm I}$, its evolution is governed by the identity (De Luca et al. 2020e, c)

$$\psi(m_{\rm PBH}(m^{\rm I}_{\rm PBH}, z), z)\,{\rm d}m_{\rm PBH} = \psi(m^{\rm I}_{\rm PBH}, z_{\rm I})\,{\rm d}m^{\rm I}_{\rm PBH}, \tag{81}$$

where $m_{\rm PBH}(m^{\rm I}_{\rm PBH}, z)$ is the final mass at redshift z for a PBH with mass $m^{\rm I}_{\rm PBH}$ at redshift $z_{\rm I}$. The main effect of accretion on the mass distribution is to make the latter broader at high masses, producing a high-mass tail that can be orders of magnitude above its corresponding value at formation (De Luca et al. 2020c).

Accretion may be also particularly relevant for the formation of SMBHs with masses $m_{\rm BH} \gtrsim 10^9 M_\odot$, from PBHs lighter than $10^4 M_\odot$ formed at high redshift (Serpico et al. 2020). In particular, assuming Gaussian initial conditions and PBH abundance $f_{\rm PBH} \lesssim 10^{-9}$ in order to be compatible with the strong observational constraints by CMB spectral distortions (Kohri et al. 2014; Carr and Silk 2018; Nakama et al. 2018; Ünal et al. 2021), epochs of Eddington accretion onto PBHs with masses $\sim 200 M_\odot$ may be responsible for the formation of SMBHs at redshift $z \gtrsim 6$ (Serpico et al. 2020), whose merging will possibly be detected by LISA.

At the onset of structure formation and reionization epoch, the increase of the PBH characteristic velocities and the gas speed of sound reduce the accretion efficiency (Ali-Haïmoud et al. 2017; Hasinger 2020; Hütsi et al. 2019). One can adopt an agnostic view and consider a cut-off redshift $z_{\rm cut-off}$ below which accretion is negligible (De Luca et al. 2020e, d). Its value is relatively unconstrained due to the large uncertainties in modelling accretion at relatively small redshift, such as X-ray pre-heating (Oh and Haiman 2003), details of the structure formation and feedback effects (Park and Ricotti 2011, 2012, 2013). In particular, the emission of X-rays from accreting PBHs may heat the plasma locally (local type) or produce Strömgren

spheres of ionised H-II which may impact the gas sound speed and thus the PBH accretion rate (global type) (Ricotti et al. 2008; Ali-Haïmoud and Kamionkowski 2017), while the generation of outflows may reduce the accretion efficiency depending on the outflow's velocity and direction (mechanical type) (Bosch-Ramon and Bellomo 2020). Similarly, the nonspherical nature of the accretion flow could impact on the efficiency of the process. These effects make the full accretion process more complicated, and dedicated works beyond the Bondi-Hoyle formalism are needed to draw firmer conclusions on its final impact onto PBHs.

3.9.2 Accretion onto PBH binaries

When accretion occurs onto binary PBHs, one has to take into account both global accretion processes (i.e., of the binary as a whole) and local accretion processes (i.e., onto the individual components of the binary). In particular, as the typical binary separation is smaller than the binary Bondi radius, the infall of gas is driven by the total mass $M_{\rm tot}$ of the binary system. In this configuration, both PBHs experience accretion from the gas with an enhanced density, and their individual accretion rates are modulated by their masses and orbital velocities (De Luca et al. 2020d)

$$\dot{m}_1 = \dot{M}_{\rm tot}\frac{1}{\sqrt{2(1+q)}}, \qquad \dot{m}_2 = \dot{M}_{\rm tot}\frac{\sqrt{q}}{\sqrt{2(1+q)}} \tag{82}$$

where the accretion rate $\dot{M}_{\rm tot}$ is computed using Eq. (79) adopting the binary system parameters. For binary systems, one always finds that the relative accretion rate for the secondary component is larger than the one for the primary component, resulting in a growth of the mass ratio of the binary towards unity according to the equation (De Luca et al. 2020d)

$$\dot{q} = q\left(\frac{\dot{m}_2}{m_2} - \frac{\dot{m}_1}{m_1}\right) > 0. \tag{83}$$

3.10 Spin distribution

In this subsection, we discuss the theoretical expectation for the PBH initial spin and how it evolves when accretion is effective.

The collapse of density perturbations generating a PBH is expected to be a rare event due to the fact that their cosmological abundance cannot exceed that of the DM, and applying the peak theory formalism one finds that the high (and rare) peaks in the density contrast giving rise to PBHs are primarily spherical (Bardeen et al. 1986). At first order in perturbation theory, however, small asymmetries introduce torques induced by the surrounding matter perturbations, which are ultimately responsible for the generation of a small angular momentum before collapse. The small time of collapse makes however the action of these torques limited in time. At formation, the mean PBH dimensionless Kerr parameter $\chi \equiv J/m_{\rm PBH}^2$ is estimated to be (De Luca et al. 2019a)

$$\chi_{\rm i} \sim 10^{-2}\sqrt{1-\gamma_{\rm PS}^2}, \tag{84}$$

in terms of the power spectrum shape parameter $\gamma_{\rm PS}$, defined as the ratio between the cross and auto-correlations of the density contrast and its spatial derivatives (close to unity for very narrow power spectra). The initial PBH spin is therefore expected to be below the percent level (see also Mirbabayi et al. 2020; Harada et al. 2021).[5] The distribution of the dimensionless Kerr parameter at formation takes the form as found in (De Luca et al. 2019a)

$$P(\chi_{\rm i})\mathrm{d}\chi_{\rm i} = u\exp\left[-2.37 - 4.12\,\ln(u\chi_{\rm i}) - 1.53\,\ln^2(u\chi_{\rm i}) - 0.13\,\ln^3(u\chi_{\rm i})\right]\mathrm{d}\chi_{\rm i}, \tag{85}$$

where for simplicity we defined

$$u \equiv \left(\frac{5}{2^{7/2}}\frac{\gamma_{\rm PS}^6 \nu}{\sigma_\delta\sqrt{1-\gamma_{\rm PS}^2}}\right), \tag{86}$$

in terms of the rescaled critical peak amplitude $\nu \equiv \delta_{\rm c}/\sigma_\delta$ and the density contrast variance σ_δ.

The initial PBH spin will be retained until the time of merger unless an efficient phase of accretion underwent during the PBH cosmological evolution. Indeed, since the accretion rate and the geometry of the accretion flow are intertwined, for accretion rates slightly above the super-Eddington limit, the angular momentum carried by the infalling accreting gas may lead to the formation of a geometrically thin accretion disk along the equatorial plane of the PBH (Shakura and Sunyaev 1973; Novikov and Thorne 1973; Ricotti et al. 2008).[6] Apart from efficient accretion, the formation of a disk happens if the typical gas velocity is larger than the Keplerian velocity near the PBH, which translates into a condition on the minimum PBH mass (De Luca et al. 2020e)

$$m_{\rm PBH} \gtrsim 6\cdot 10^2 M_\odot\, D^{1.17}\xi^{4.33}(z)\frac{(1+z/1000)^{3.35}}{\left[1+0.031(1+z/1000)^{-1.72}\right]^{0.68}}, \tag{87}$$

in terms of the constant factor $D \sim \mathcal{O}(1-10)$, which takes into account relativistic effects, and the parameter $\xi(z) = \max[1, \langle v_{\rm eff}\rangle/c_{\rm s}]$, which describes the effect of the PBH motion with respect to the gas.

In such a configuration, mass accretion is accompanied by an increase of the PBH spin perpendicularly to the disk plane, whose growth rate can be described following a geodesic model for circular disk motion as (Bardeen et al. 1972; De Luca et al.

[5] The formation of PBHs in non-standard scenarios, like during an early matter-dominated epoch following inflation (Harada et al. 2017) or from the collapse of Q-balls (Cotner and Kusenko 2017), may lead to higher values of the initial spin.

[6] For accretion rates slightly smaller than the Eddington limit, accretion is non-spherical and an advection-dominated accretion flow (ADAF) may form (Narayan and Yi 1995). In the opposite case, the accretion luminosity might be so strong that the disk "puffs up" and becomes thicker, resulting in less efficient angular momentum transfer.

2020e) (see also Bardeen et al. 1972; Thorne 1974; Brito et al. 2015; Volonteri et al. 2005)

$$\dot{\chi} = (\mathcal{F}(\chi) - 2\chi)\frac{\dot{m}_{\rm PBH}}{m_{\rm PBH}}, \tag{88}$$

in terms of the combination $\mathcal{F}(\chi) \equiv L(m_{\rm PBH}, J)/m_{\rm PBH}E(m_{\rm PBH}, J)$, which is a function of the energy and angular momentum per unit mass (Bardeen et al. 1972)

$$E(m_{\rm PBH}, J) = \sqrt{1 - 2\frac{m_{\rm PBH}}{3r_{\rm ISCO}}} \quad \text{and} \quad L(m_{\rm PBH}, J) = \frac{2m_{\rm PBH}}{3\sqrt{3}}\left(1 + 2\sqrt{3\frac{r_{\rm ISCO}}{m_{\rm PBH}} - 2}\right), \tag{89}$$

depending on the ISCO radius

$$r_{\rm ISCO}(m_{\rm PBH}, J) = m_{\rm PBH}\left[3 + Z_2 - \sqrt{(3 - Z_1)(3 + Z_1 + 2Z_2)}\right], \tag{90}$$

with $Z_1 = 1 + (1-\chi^2)^{1/3}\left[(1+\chi)^{1/3} + (1-\chi)^{1/3}\right]$ and $Z_2 = \sqrt{3\chi^2 + Z_1^2}$. The spin evolution continues within the relevant accretion timescale until it reaches the extremal limit $\chi_{\rm max} = 0.998$ dictated by radiation effects (Thorne 1974). An analytical fit of the spin as a function of mass induced by accretion onto PBH binaries can be found in Franciolini et al. (2022b). This fit is based on the accretion model presented in De Luca et al. (2020e, 2020d) which is valid in the mass range currently observed by LVKC experiment. Detailed modelling of accretion on PBH with masses above around $\mathcal{O}(10^2)M_\odot$, particularly relevant for PBH mergers observable by LISA, is still lacking in the literature, due to the difficulty in modelling accretion with the inclusion of feedback effects at such large masses.

If instead accretion occurs onto a PBH binary, the fact that total mass of the binary drives accretion leads to a much more efficient angular momentum transfer on each PBH (De Luca et al. 2020d, e). In this case, the accretion onto the binary components is never spherical and disks can form easier around the PBHs. Moreover, since the lighter component of the binary experiences a stronger accretion rate, this results into a higher spin with respect to the one of the primary and heavier component (De Luca et al. 2020d).

An important parameter measurable through GW observations is the effective spin

$$\chi_{\rm eff} \equiv \frac{\chi_1 \cos\alpha_1 + q\chi_2 \cos\alpha_2}{1+q}, \tag{91}$$

which is a function of the mass ratio q, of both BH spin magnitudes χ_j ($j = 1, 2$), and of their orientation with respect to the orbital angular momentum, parametrized by the tilt angles α_j. In Fig. 18, we show the expected distribution of $\chi_{\rm eff}$ by averaging over the spin angles, as a function of PBH masses in binaries for various choices of $z_{\rm cut-off}$.

An alternative scenario for inducing spin on PBH occurs in the context of dense PBH clusters, where close hyperbolic encounters (García-Bellido and Nesseris 2017, 2018) may spin up both black holes (Nelson et al. 2019; Jaraba and García-Bellido 2021) due to the fundamental frame-dragging effect of general relativity, analogous to magnetic induction in electromagnetism, in this case due to a current of

matter as one black hole scatters off another. In the case of highly asymmetric binaries with large mass ratios, the induced spin can reach up to $\chi \simeq 0.8$ for the most massive one (Jaraba and García-Bellido 2021). Nevertheless, the distribution of spins of PBH in dense clusters is still characterized by a Gaussian around zero-spin with a width of order $\sigma \simeq 0.2$ (García-Bellido et al. 2021c).

3.11 Comments on the clustering from Poisson initial conditions

In the absence of non-Gaussian initial conditions, PBHs are Poisson distributed, as shown in Desjacques and Riotto (2018). In such a case, the PBH clustering evolution has been studied with a cosmological N-body simulations in Inman and Ali-Haïmoud (2019) up to redshift of $\mathcal{O}(10^2)$ and confirmed analytically in De Luca et al. (2020a) assuming a monochromatic PBH mass distribution. In this Subsection we briefly summarise the main conclusions.

To characterize the PBH two-point correlation function as a function of the comoving separation $x = |\vec{x}|$, we introduce the overdensity of discrete PBH centers at position $\vec{x}_i$ with respect to the total background DM energy density,

$$\frac{\delta\rho_{\rm PBH}(\vec{x},z)}{f_{\rm PBH}\overline{\rho}_{\rm DM}} = \frac{1}{\bar{n}_{\rm PBH}}\sum_i \delta_{\rm d}(\vec{x}-\vec{x}_i(z)) - 1, \tag{92}$$

where $\delta_{\rm d}(\vec{x})$ is the three-dimensional Dirac distribution, and

$$\bar{n}_{\rm PBH} \simeq 3.2 f_{\rm PBH}\left(\frac{20\,M_\odot/h}{m_{\rm PBH}}\right)(h/{\rm kpc})^3 \tag{93}$$

is the average number density of PBHs per comoving volume. Here, i runs over the positions of PBHs. The two-point correlation function of this discrete point process takes the general form

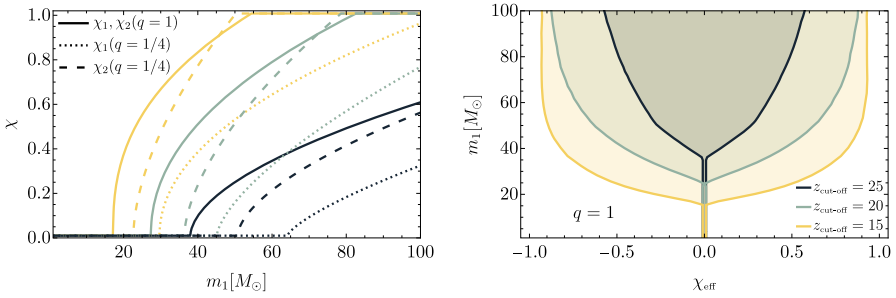

Fig. 18 Left: Predicted primary (χ_1) and secondary (χ_2) spins as a function of primary mass m_1 and mass ratio q for various values of $z_{\rm cut-off}$ (indicated by colors specified in the right panel). Right: Predicted distribution of $\chi_{\rm eff}$ as a function of PBH mass m_1 (assuming equal mass binaries) for three choices of $z_{\rm cut-off}$. Image reproduced with permission from Franciolini et al. (2022b), copyright by APS Image reproduced with permission

$$< \frac{\delta\rho_{\rm PBH}(\vec{x},z)}{\overline{\rho}_{\rm DM}} \frac{\delta\rho_{\rm PBH}(0,z)}{\overline{\rho}_{\rm DM}} > = \frac{f_{\rm PBH}^2}{\bar{n}_{\rm PBH}} \delta_{\rm d}(\vec{x}) + \xi(x,z). \tag{94}$$

This expression emphasizes that $\xi(x,z)$ is the so-called reduced PBH correlation function and, thus, is distinct from the additive Poisson noise proportional to the Dirac delta. As mentioned before, initially the reduced correlation function is negligible. The corresponding PBH power spectrum

$$\Delta^2(k,z) = \frac{k^3}{2\pi^2} \int {\rm d}^3x\, e^{i\vec{k}\cdot\vec{x}} < \frac{\delta\rho_{\rm PBH}(\vec{x},z)}{\overline{\rho}_{\rm DM}} \frac{\delta\rho_{\rm PBH}(0,z)}{\overline{\rho}_{\rm DM}} >, \tag{95}$$

is conveniently defined relative to the total cold dark matter average density.

After a linear growth, the PBH power spectrum enters in the so called "Quasi-Linear" regime during which

$$\Delta^2_{\rm QL}(k) \simeq 0.04 f_{\rm PBH}^{3/4} \left(\frac{20\, M_\odot/h}{m_{\rm PBH}}\right)^{-3/4} \left[1 + 26 f_{\rm PBH} \left(\frac{100}{1+z}\right)\right]^{3/2} \left(\frac{k}{h/{\rm kpc}}\right)^{9/4}. \tag{96}$$

When the power spectrum becomes larger than around 200, it enters in the "Non-Linear" regime during which

$$\Delta^2_{\rm NL}(k) \simeq 0.2 f_{\rm PBH}^{3/5} \left(\frac{m_{\rm PBH}}{20 M_\odot/h}\right)^{3/5} \left[1 + 26 f_{\rm PBH} \left(\frac{100}{1+z}\right)\right]^{6/5} \left(\frac{k}{h/{\rm kpc}}\right)^{9/5}. \tag{97}$$

PBHs form halos whose mass distribution may be described by the Press–Schechter theory (Press and Schechter 1974) with an initial Poisson power spectrum. The resulting number density of PBH halos with mass between M and $(M + {\rm d}M)$ reads

$$\frac{{\rm d}n(M,z)}{dM} = \frac{\overline{\rho}_{\rm PBH}}{\sqrt{\pi}} \left(\frac{M}{M_*(z)}\right)^{1/2} \frac{e^{-M/M_*(z)}}{M^2}, \tag{98}$$

where $\overline{\rho}_{\rm PBH}$ is the average PBH energy density and (Hütsi et al. 2019)

$$M_*(z) = N_*(z) \cdot m_{\rm PBH} \simeq f_{\rm PBH}^2 \left(\frac{2600}{1+z}\right)^2 m_{\rm PBH} \tag{99}$$

is the typical mass of halos collapsing at redshift z. This prediction agrees with the results of cosmological N-body simulations, as shown in Fig. 19.

If we restrict ourselves to small scales, both members of a PBH pair are almost certainly drawn from the same PBH halo. In this limit, if the PBH density profile is $\rho_{\rm PBH}(x) \sim x^{-\epsilon_{\rm PBH}}$, then the two-point correlation function must behaves like $\sim x^{-2\epsilon_{\rm PBH}+3}$ (Peebles 1974; McClelland and Silk 1977) as it is proportional to the square density profile. Imposing $(-2\epsilon_{\rm PBH} + 3) = -9/5$, we infer that the PBH density profile should satisfy

$$\rho_{\rm PBH}(x) \sim x^{-12/5}, \tag{100}$$

which is confirmed by numerical simulations presented in Raidal et al. (2019). Notice that since clustering is hierarchical, each halo has a certain survival time and, therefore, a given probability to be absorbed by a bigger halo formed at a later redshift. As shown in De Luca et al. (2020a) the evaporation time (due to dynamical relaxation) of PBH halos is typically larger than their survival time, which implies that PBH halos are stable against evaporation. We will discuss later on the impact of clustering on the merger rate of PBH binaries.

3.12 Summary

In this section, we did not only review the standard formalism to compute the PBH mass function from the curvature or density power spectrum, but also the most recent developments on the computation of the critical overdensity threshold and of the relation between curvature and density fluctuations, which depend on the perturbation statistics (Gaussian, non-Gaussian), the primordial power spectrum and the evolution of the equation-of-state through different phases like the QCD transition. The impact of these effects is important on the PBH abundance and mass function. Even if it is possible to rescale the power spectrum amplitude in order to obtain the required PBH abundance when one only focuses on a single observable, this is not the case anymore when one tries to correlate multiple observations (e.g. PBH abundance and induced GWs, as discussed in the following sections). In particular, the effects of the QCD transition may have greatly imprinted on the mass function for stellar-mass PBHs with direct consequences for GW observations that will be discussed in the next Sections. We also went beyond the common assumption that the

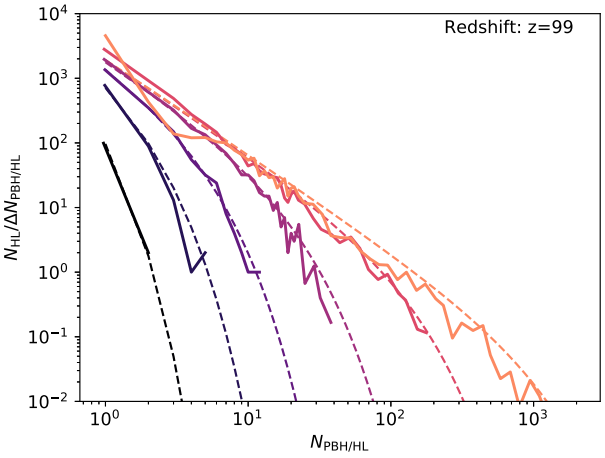

Fig. 19 The abundance of halos $N_{\rm HL}$ containing a given number of PBHs, $N_{\rm PBH/HL}$, i.e. halo mass function. Solid lines report the results of the N-body simulations while dashed lines are indicates the theoretical prediction assuming Poisson statistics. Image reproduced with permission from Inman and Ali-Haïmoud (2019), copyright by APS Image reproduced with permission

PBH mass and spin distributions do not change much with time, by considering effects of accretion on isolated PBHs and PBH binaries. Finally we emphasized the importance of the inevitable clustering of PBHs due to their inevitable Poisson fluctuations.

4 PBH merging and encounter rates

In this section, we calculate the expected PBH merging rates and their evolution with redshift for two different binary formation channels: before matter-radiation equality and due to tidal capture in clusters. For this purpose, we use a general mass distribution $f(m_{\rm PBH})$ that must be specified by the underlying theoretical model and assumptions about PBH formation, as explained in the previous sections. For the two channels, we also discuss some effects linked to PBH clustering induced by the inevitable Poisson fluctuations in their spatial distribution. This can cause a merging rate suppression for early binaries due to their tidal disruption by early-forming clusters and a merger rate boost for late-binaries due to an enhanced clustering compared to common halo mass functions in Λ-CDM cosmology. We also review the expected rates of disrupted binaries. Finally, we study the rate of hyperbolic encounters in PBH clusters that can induce GW bursts, possibly observable in Earth-based and space-based detectors.

4.1 Early binaries

4.1.1 General rate formula

PBH binaries may have formed in the early Universe before matter-radiation equality. Because of their random spatial distribution at formation, two PBHs can form sufficiently close to each other for their dynamics to decouple from the Universe expansion. They form a binary instead of directly merging, because of the gravitational influence of one or several PBHs nearby. Possibly, the binary is sufficiently stable and it takes of the order of the age of the Universe for the two black holes to merge.

Under the hypothesis that there is no local non-Gaussianity cross-correlating large and small scales, PBHs do not form in clusters, but follow a Poissonian distribution (Desjacques and Riotto 2018; Ali-Haïmoud 2018; Ballesteros et al. 2018; Moradinezhad Dizgah et al. 2019; Inman and Ali-Haïmoud 2019). The merging rates (per unit logarithmic mass of the two binary components) of such early binaries (denoted EB) at a time t were first estimated in (Ioka et al. 1998) and are given by (Sasaki et al. 2016; Ali-Haïmoud et al. 2017; Kocsis et al. 2018; Raidal et al. 2019; De Luca et al. 2020d; Hütsi et al. 2021c)

$$R_{\rm EB} = \frac{1.6\times10^6}{\rm Gpc^3\,yr}\times f_{\rm sup}(m_1,m_2,f_{\rm PBH}) f_{\rm PBH}^{53/37} f(m_1) f(m_2) \times \left(\frac{t}{t_0}\right)^{-34/37}\left(\frac{m_1+m_2}{M_\odot}\right)^{-32/37}\left[\frac{m_1 m_2}{(m_1+m_2)^2}\right]^{-34/37}, \quad (101)$$

where m_1 and m_2 are the two black hole masses and t_0 is the age of the Universe. Compared to the predictions of (Sasaki et al. 2016), one has to include a suppression factor $f_{\rm sup}$ to take into account several physical effects that have been initially neglected but were revealed by N-body simulations of (Raidal et al. 2019).

Some analytical prescriptions have been proposed, e.g. in (Raidal et al. 2019; Hütsi et al. 2021c), to calculate the suppression factor $f_{\rm sup}(f_{\rm PBH}, m_1, m_2)$. It can be written as the product of $S_1(f_{\rm PBH}, m_1, m_2)$ and $S_2(f_{\rm PBH})$ that take into account the rate suppression due to nearby PBHs or matter fluctuations and PBH clusters seeded by Poisson fluctuations, respectively. These analytical prescriptions have been compared with N-body simulations, but only in the case of monochromatic and log-normal PBH mass distributions. Therefore, one must be cautious when applying them to broad mass functions, even if they exhibit a peak, like the one from the QCD transition.

4.1.2 Suppression from close PBHs and matter inhomogeneities

The first suppression factor we consider (S_1) takes into account the binary disruption by either matter fluctuations, with a (rescaled) variance $\sigma_{\rm m}^2$, usually around 0.005, or by the number $\bar{N}$ of PBHs within a sphere centered on the binary of radius corresponding to the maximum comoving distance at which a nearby PBH would fall onto the binary to disrupt it, before matter-radiation equality. An analytical prescription for S_1 has been proposed in (Raidal et al. 2019; Hütsi et al. 2021c), and is given by

$$S_1 \approx 1.42\left[\frac{(\langle m_{\rm PBH}^2\rangle/\langle m_{\rm PBH}\rangle^2)}{\bar{N}+C}+\frac{\sigma_{\rm m}^2}{f_{\rm PBH}^2}\right]^{-21/74} {\rm E}^{-\bar{N}}, \quad (102)$$

with

$$\bar{N} = \frac{m_1+m_2}{\langle m_{\rm PBH}\rangle}\frac{f_{\rm PBH}}{f_{\rm PBH}+\sigma_M}. \quad (103)$$

Note that in Eqs. (102) and (103), the mean PBH mass and their variance are calculated from the mass function through

$$\langle m_{\rm PBH}\rangle = \frac{\int m_{\rm PBH}{\rm d}n_{\rm PBH}}{n_{\rm PBH}} = \left[\int \frac{f(m_{\rm PBH})}{m_{\rm PBH}}{\rm d}\ln m_{\rm PBH}\right]^{-1} \quad (104)$$

$$\langle m_{\rm PBH}^2\rangle = \frac{\int m_{\rm PBH}^2 {\rm d}n_{\rm PBH}}{n_{\rm PBH}} = \frac{\int m_{\rm PBH} f(m_{\rm PBH}) {\rm d}\ln m_{\rm PBH}}{\int \frac{f(m_{\rm PBH})}{m_{\rm PBH}} {\rm d}\ln m_{\rm PBH}} \tag{105}$$

where $n_{\rm PBH}$ denotes the total PBH number density. The function C encodes the transition between small and large $\bar{N}$ limits. A good approximation is given by (Hütsi et al. 2021c)

$$C \simeq \frac{f_{\rm PBH}^2 \langle m_{\rm PBH}^2\rangle}{\sigma_{\rm m}^2 \langle m_{\rm PBH}\rangle^2} \times \left\{ \left[\frac{\Gamma(29/37)}{\sqrt{\pi}} U\left(\frac{21}{74}, \frac{1}{2}, \frac{5 f_{\rm PBH}^2}{6\sigma_{\rm m}^2}\right)\right]^{-74/21} - 1 \right\}^{-1}, \tag{106}$$

where Γ is the Euler function and U is the confluent hypergeometric function.

The value of S_1 as a function of $f_{\rm PBH}$ has been represented in Fig. 20 for different cases. Assuming $\bar{N} = 2$, as expected for a close-to-monochromatic distribution, the value of S_1 ranges from 10^{-2} when $f_{\rm PBH} \simeq 10^{-3}$ to 0.1 when $f_{\rm PBH} \simeq 1$. In particular, one can also obtain a maximum value $S_1^{\rm max}$ that is independent of the mass distribution when $\bar{N} \to 0$. This maximal value is around unity for $f_{\rm PBH} \gtrsim 0.1$ and goes down to 10^{-1} for lower values. In this limit, one recovers the results from Chen and Huang (2018), Ali-Haïmoud et al. (2017) that only take into account the effect of matter inhomogeneities.

Finally, we would like to comment on the calculation of S_1 using different definitions of the PBH mass function, which in particular modify the way to compute $\langle m\rangle$ and $\langle m^2\rangle$ depending on whether the mass distribution is defined with respect to the PBH number density n or the PBH density ρ, or if the normalisation changes. The possible definitions, the way they are related, and the corresponding calculation rules are summarized in Table 2 from Escrivà et al. (2023). It is important to do these calculations carefully because they can significantly impact the resulting rates, and because some inconsistencies were found in the literature. As pointed out in Escrivà

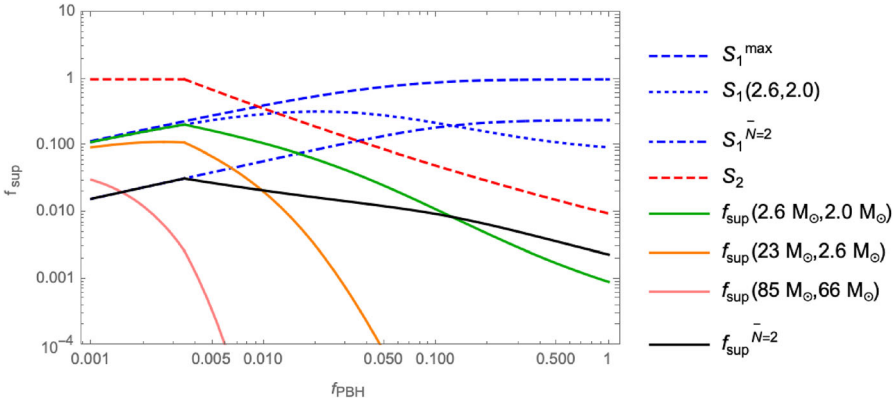

Fig. 20 Suppression factor $f_{\rm sup}$ and its possible contributions S_1 and S_2 in different cases, in terms of the PBH abundance. When PBH masses are specified, it assumes a PBH mass function from a nearly-scale invariant primordial power spectrum of curvature fluctuations and including QCD-induced features. Image

et al. (2023), there was a conversion factor $m/\langle m\rangle$ not considered in Franciolini et al. (2022e) which led to an inconsistency with Hütsi et al. (2021c) which uses exactly the same definition and normalization of the PBH mass distribution, but a different merger rate formula. There was also a typo in the Eq. (A4) of Clesse and García-Bellido (2022) that has an incorrect mass dependence even if the correct formula was used for the calculations and paper figures.

Following these rules for an extended mass function, one gets that the abundance of light PBHs can strongly impact $\langle m\rangle$ and the resulting values of $\bar{N}$ that typically increases. In turn, S_1 and the resulting value of $f_{\rm sup}$ can be strongly suppressed due to the exponential dependence in $\bar{N}$, and their exact value is dependent on the chosen lower mass cut for the PBH mass distribution. Physically, this suppression comes from the numerous light black holes, reducing the value of the average black hole mass, at proximity of the binary that are considered as being able to disrupt it when one uses the presented conservative approach. Such an issue was pointed out in Gow et al. (2020), Clesse and García-Bellido (2022), Escrivà et al. (2023) and suggests that the rates of early binaries should probably be revised in the case of a very broad mass distribution. In absence of a clear solution, the approach of Clesse and García-Bellido (2022), Escrivà et al. (2023) was to consider the limit obtained for a monochromatic mass function, motivated by the QCD-induced peak, and assume that $\bar{N}\approx 2$. In Franciolini et al. (2022e), which used another averaging procedure, there was a strong dependence on the high-mass PBH distribution and a high-mass cut-off was introduced that may naturally arise from the transition in the primordial power spectrum. The different approaches however lead to different merger rates and different possible interpretations of the LIGO/Virgo observations, as well as different limits on the possible PBH abundance.

Table 2 Different definitions of the normalized PBH mass distribution proposed in various references with their conversion, their normalisation rule and the corresponding $\langle m\rangle$ and $\langle m^2\rangle$

Escrivà et al. (2023) Clesse and García-Bellido (2022)* Bagui and Clesse (2022)	Raidal et al. (2019) Franciolini et al. (2022e)* Hall et al. (2020)	Hütsi et al. (2021c)	Kocsis et al. (2018)
$f\equiv\frac{1}{\rho_{\rm PBH}}\frac{{\rm d}\rho_{\rm PBH}}{{\rm d}\ln m}$	$\psi_1\equiv\frac{1}{\rho_{\rm PBH}}\frac{{\rm d}\rho_{\rm PBH}}{{\rm d}m}$	$\psi_2\equiv\frac{1}{n_{\rm PBH}}\frac{{\rm d}n_{\rm PBH}}{{\rm d}\ln m}$	$\psi_3\equiv\frac{1}{n_{\rm PBH}}\frac{{\rm d}n_{\rm PBH}}{{\rm d}m}$
$f=m\psi_1$	$\psi_1=f/m$	$\psi_2=f\langle m\rangle/m$	$\psi_3=\langle m\rangle f/m^2$
$=m\psi_2/\langle m\rangle$	$=\psi_2/\langle m\rangle$	$=\langle m\rangle\psi_1$	$=\langle m\rangle\psi_1/m$
$=m^2\psi_3/\langle m\rangle$	$=m\psi_3/\langle m\rangle$	$=m\psi_3$	$=\psi_2/m$
$\int f{\rm d}\ln m=1$	$\int\psi_1{\rm d}m=1$	$\int\psi_2{\rm d}\ln m=1$	$\int\psi_3{\rm d}m=1$
$\langle m\rangle=\left(\int\frac{f}{m}{\rm d}\ln m\right)^{-1}$	$\left(\int\frac{\psi_1}{m}{\rm d}m\right)^{-1}$	$\int m\psi_2{\rm d}\ln m$	$\int m\psi_3{\rm d}m$
$\langle m^2\rangle=\langle m\rangle\int mf{\rm d}\ln m$	$\langle m\rangle\int m\psi_1{\rm d}m$	$\int m^2\psi_2{\rm d}\ln m$	$\int m^2\psi_3{\rm d}m$

The asterisk denotes the references in which an inconsistency has been found (see details in the text). In this review, we considered both f and $\psi_1\equiv\psi$ with our notations. Table adapted from Escrivà et al. (2023)

4.1.3 Suppression from early Poisson-induced clustering

The second factor $S_2(f_{\rm PBH})$ accounts for the effect of binary disruption in PBH clusters that rapidly form after PBH formation if their abundance is large enough (Inman and Ali-Haïmoud 2019), due to their initial Poisson fluctuations. The interaction of binaries with other PBHs in early-Universe clusters typically induces a modification of their semi-major axis and eccentricity, which leads to longer merger timescales and a suppression of the merger rate (Trashorras et al. 2021; Jedamzik 2020, 2021). In order to have a conservative estimate of the merger rate, Vaskonen and Veermäe (2020) (and De Luca et al. 2020a includes an analytical modelling of clustering evolution) computed the fraction of binaries which never enter in dense enough environments. This fraction S_2 today can be approximated by (Hütsi et al. 2021c)

$$S_2 \approx \min\left(1, 9.6\times10^{-3} f_{\rm PBH}^{-0.65} {\rm E}^{0.03\ln^2 f_{\rm PBH}}\right). \tag{107}$$

The value of S_2 as a function of $f_{\rm PBH}$ has been represented and compared to S_1 and the resulting total suppression factor $f_{\rm sup}$ in Fig. 20. When it is considered at a time t, a good approximation is to replace $f_{\rm PBH}$ by $f_{\rm PBH}[t(z)/t_0]^{0.44}$, valid for $z \leq 100$ (Hütsi et al. 2021c).

4.1.4 Merging rates of perturbed binaries

Numerical studies find that binaries are likely to be perturbed, i.e. early binaries whose semi major axis and eccentricity are modified but remain bound after the interactions with surrounding perturbers after their formation. This can happen in two ways: (1) The initial configuration contains a third PBH close to the initial PBH pair that will very likely collide with the forming binary; (2) Binaries are absorbed by dense PBH clusters that form early in the history of the Universe. A conservative calculation of the possible merging rates of PBH binaries that have been disrupted in early-forming halos has been proposed in (Vaskonen and Veermäe 2020). Moreover, let us note that estimates indicate that most PBH binaries are not perturbed in typical DM halos larger than 10 PBHs, and that nearly all initial binaries might be disrupted within the age of the Universe, since the fraction of disrupted binaries is relatively high at $z = 1100$ when $f_{\rm PBH} \gtrsim 0.1$.

For a monochromatic mass function, the merger rate of perturbed binaries at time t is given by (Vaskonen and Veermäe 2020)

$$R_{\rm p}(t) \propto f_{\rm PBH}^{\frac{144\gamma}{259}+\frac{47}{37}} t^{\frac{\gamma}{\gamma}-1} m_{\rm PBH}^{\frac{5\gamma-32}{37}}, \tag{108}$$

where $\gamma \in [1,2]$, based on the angular momentum distribution for perturbed binaries in the early Universe. The main result of this analysis is that the rate of perturbed binaries can exceed the rate of the unperturbed ones discussed in the previous section, when $f_{\rm PBH} \gtrsim 0.1$. However, when $f_{\rm PBH} \lesssim 0.02$, the rate of perturbed binaries should be subdominant, at least for peaked mass functions. But it is still unclear how this formula and results are generalized to any broad PBH mass distribution.

4.1.5 Link with observations of compact binary coalescences

In Fig. 20, we represented the values of S_1, S_2 and the resulting suppression factor $f_{\rm sup}$ as a function of $f_{\rm PBH}$ for the choice of the broad mass function of Clesse and García-Bellido (2022), at the mean masses of the exceptional GW events GW190425, GW190814 and GW190521.[7] We also calculated $S_1^{\rm max}$ in the limit $\bar{N} \ll \min(C, 1)$ that is independent of the two binary component masses.

For an arbitrary broad mass distribution, one critical difference with respect to a monochromatic or a relatively sharp log-normal mass function comes from the large number density of tiny black holes, implying that $\langle m_{\rm PBH}\rangle \ll M_\odot$ and $\langle m_{\rm PBH}^2\rangle/\langle m_{\rm PBH}\rangle^2 \ll 1$. This implies that generically $\bar{N} \gg 1$. If the analytical prescription is strictly applied, this leads to a huge exponential suppression of the EB merging. However, this rate suppression is very likely overestimated because PBHs that are much lighter than the binary components are probably not able to bring enough energy to the system in order to disrupt it.

Instead, it is probably more realistic to consider only the disruption by nearby PBHs whose mass is similar to the mean of the binary component masses. By doing so, one gets $\langle m_{\rm PBH}\rangle \sim (m_1 + m_2)/2$ and $\langle m_{\rm PBH}^2\rangle/\langle m_{\rm PBH}\rangle^2 \sim 1$. In such a case, one gets $\bar{N} \approx 2$ (just as in the monochromatic case) and the suppression factor obtained when $f_{\rm PBH} \simeq 1$ becomes independent of the mass, slightly below $S_2^{\rm max}$, depending on the exact value of $\bar{N}$. Different values of $\bar{N}$ (but still of the same order) typically lead $f_{\rm sup}$ to be of order $S_2^{\rm max} \times \mathcal{O}(0.1-1)$. In particular, for $\bar{N} = 2$ and $f_{\rm PBH} = 1$, one gets $f_{\rm sup} \simeq 0.002$. We have chosen this value to compute the EB merging rate for two typical mass functions impacted by the thermal history. They are represented on Fig. 21. One can see that these merging rates can in principle accommodate some of the LIGO/Virgo GW events and are significantly enhanced when the binary includes a PBH from the QCD peak.

4.1.6 Limitations

Even if the merging rates given by Eq. (101) are consistent with N-body simulations for monochromatic and log-normal mass functions in the stellar-mass range, there are still a series of uncertainties that could limit the applicability of this formalism. Hereafter we list some of these possible limitations.

1. So far, no N-body simulations have been performed on PBH models that include thermal features, whereas it is proven that they have an important impact for stellar-mass PBHs. In general, broad-mass functions could see also deviations from those estimations, in particular for binaries with very low mass ratios.
2. Eq. (101) including the effect described in Eq. (108) should be improved by more appropriate calculation of the distribution of the binary parameters as

[7] We note that the parameter estimation of GW events characterised by a small signal-to-noise ratio at the LVKC detectors may still be sensitive to the priors assumed in the analysis (see e.g. Vitale et al. 2017). Therefore, the interpretation of some events may change if PBH motivated priors are assumed (Bhagwat et al. 2021), in particular when focusing on the binary mass ratio and effective spin.

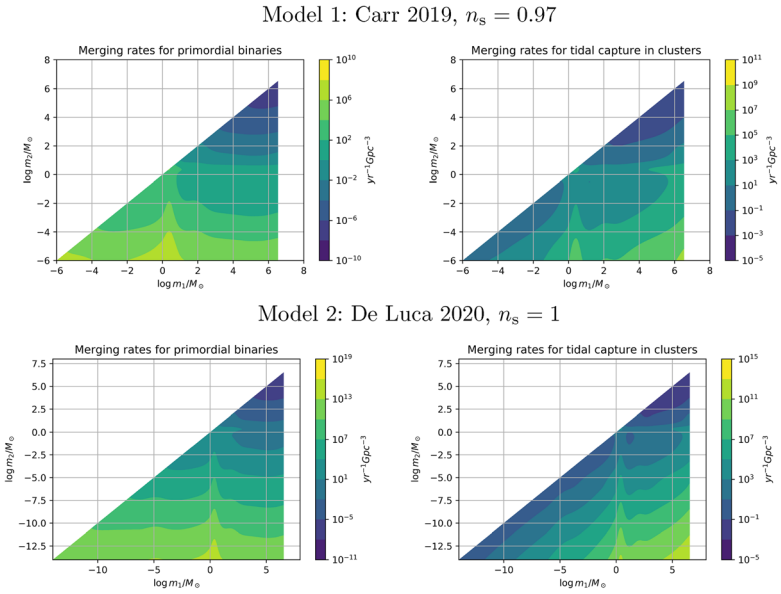

Fig. 21 Expected differential merging rates $\mathrm{d}R/\mathrm{d}\ln m_1 \mathrm{d}\ln m_2$ of PBH of masses m_1 and m_2, for the two mass models represented on Fig. 13 (top panels: Model 1, bottom panels: Model 2), for the two considered binary formation channel: primordial binaries (see Eq. (101)) on the left panels, and tidal capture in halos (see Eq. (109)) on the right panels. Image reproduced with permission from Auclair et al. (2023), copyright by the author(s) Image reproduced with permission

interactions have occurred, encoded in the parameter γ (Vaskonen and Veermäe 2020). Analytical prescriptions for non-equal mass binaries should also be further developed and checked.

3. The fraction of PBH binaries that are disrupted as a function of the mass of an infalling PBH is uncertain. This question is particularly relevant for binaries with strong differences in mass components, and for broad mass functions with lots of small PBHs that would dominate the calculation of $\bar{N}$, without being massive enough to disrupt a massive binary. The same question arises in the case of sub-dominant intermediate-mass binaries that would hardly be disrupted by a dominant population of stellar-mass or asteroid-mass PBHs.
4. The effect of heavy PBHs in the tail of a broad mass distribution would be to seed PBH clusters, an effect that would be superimposed to the Poisson clustering, but that has been neglected so far in merging rate computations.
5. Slightly different results and another possible dependence in f_{PBH} have been obtained in Kocsis et al. (2018) using analytical methods.
6. The suppression due to PBH clusters depends on the exact clustering history, on the cluster relaxation time, on the evaporation as well as on internal dynamics (see e.g. De Luca et al. 2020a).

7. PBH clustering at formation may either boost or suppress the merger rates of early binaries, but this effect is very model dependent and still debated (see e.g. Raidal et al. 2017; Young and Byrnes 2020; De Luca et al. 2021d for different models and conclusions).
8. Dark matter spikes around PBHs should affect the merging time of PBH binaries and enhance their merger rates, which typically leads to more stringent limits on their abundance inferred from GW observations (Kavanagh et al. 2018; Pilipenko et al. 2022; Jangra et al. 2023). Nevertheless the whole process might be more complicated with various possible regimes and dynamics, boosting or suppressing the merger rates and leading to model-dependent results, as noticed in Jangra et al. (2023).
9. It has recently been claimed in Boehm et al. (2021) that subtle general relativistic effects may highly suppress this PBH binary formation channel, but this result has been disputed in De Luca et al. (2020a), Hütsi et al. (2021a, 2021b). This problem is related to the question of which metric is physically relevant to describe the PBH environment (Takhurta metric, generalized Mc-Vittie, other).

In general, one should not forget that early binaries can be impacted by their environment during the whole cosmic history, and this environment has a complex evolution, influenced by the clustering after matter-radiation equality, accretion, dynamical heating, etc. Therefore one should be cautious and strong claims relying on these merging rates are probably still premature. Nevertheless, Eq. (101) likely gives good estimations for some models, at least in some regimes. To that end, they are relevant for estimating not only the merging rates but also the resulting SGWB background, based on our current (but rapidly evolving) knowledge.

4.2 Late binaries

4.2.1 General formula

The second binary formation channel is through dynamical capture in dense environments. We will give a particular emphasis to the case in which PBHs comprise the totality of the dark matter in the universe and investigate the dynamical formation in dense PBH halos. As any other DM candidate, PBHs are expected to form halos during the cosmic history. The clustering properties typically determine the overall merging rate. For a generic PBH mass function $f(m_{\rm PBH})$, an effective formula has been proposed (Carr et al. 2021b),

$$R_{\rm LB} \approx R_{\rm clust} f_{\rm PBH}^2 f(m_1) f(m_2) \frac{(m_1+m_2)^{10/7}}{(m_1 m_2)^{5/7}} {\rm yr}^{-1}{\rm Gpc}^{-3}, \tag{109}$$

where $R_{\rm clust}$ is a scaling factor that depends on the PBH clustering properties and velocity distribution. This formula comes from the two-body capture in a cluster and assumes that the time it takes for the binary to merge is much shorter than cosmological times.

Hereafter, we present the estimation for $R_{\rm clust}$ in the case of Poisson clustering. We then discuss the implications in the context of the present LIGO/Virgo observations. Finally, we present the possible limitations of these approaches and how different models could lead to different merging rates.

Poisson clustering introduces a natural clustering scale, leading to $R_{\rm clust}$ in the range between 10^2 and 10^3 for solar-mass PBHs and $f_{\rm PBH} \simeq 1$ (De Luca et al. 2020a). Other clustering scenarios (e.g. clusters at formation) could induce even larger values of $R_{\rm clust}$, fixed by the model as well as the evolution of these clusters (dynamical heating, mergers, etc.) through the cosmic history.

In general, one can consider a simplified picture where the PBH halo density is described by the local density contrast $\delta_{\rm loc}$. The number density of PBHs can be given as $n(m_{\rm PBH}) \equiv \delta_{\rm loc}\overline{\rho}_{\rm DM}/m_{\rm PBH}$, with the mean dark matter cosmological energy density $\overline{\rho}_{\rm DM} = \Omega_{\rm DM}\rho_{\rm c}$, where $\Omega_{\rm DM} \simeq 0.25$ is the density parameter for dark matter. In this case, $R_{\rm clust}$ was estimated as (Clesse and García-Bellido 2017a; García-Bellido et al. 2022)

$$R_{\rm clust} \approx 3.6h^4 \left(\frac{\Omega_{\rm DM}}{0.25}\right)^2 \left(\frac{\delta_{\rm loc}}{10^8}\right) \left(\frac{v_0}{10\,{\rm km/s}}\right)^{-11/7}, \tag{110}$$

where v_0 is the velocity of PBHs and h is the Hubble parameter today in units of $H_0 = 100\,h\,{\rm km/s/Mpc}$. If one assumes $v \sim O(1-10){\rm km/s}$ and local densities $\delta_{\rm loc} \sim 10^8$ typical to the ones of ultra-faint-dwarf galaxies, as one may also expect for Poisson clusters of size around $\sim 10 - 100{\rm p}c$, one typically get $R_{\rm clust} \sim 10^2 - 10^3$. This provides an effective formula but in realistic scenarios, several effects could impact the exact value of $R_{\rm clust}$ such as the dynamical heating, merger and disruption history of PBH clusters, how extended is the PBH mass function leading to different efficiencies of the Poisson clustering effect, the radial distribution of PBHs inside a cluster and their possible mass segregation for extended mass functions.

4.2.2 Merging rates of binaries induced by three-body interactions

PBH binary formation is also expected to take place in the Poisson induced PBH small scale structure at high redshift. After the matter-radiation equality, the seeding effect of Poisson fluctuations in the PBH distribution give rise to the formation of small scale clusters (see Inman and Ali-Haïmoud 2019 for a N-body simulation and De Luca et al. 2020a for an analytical treatment). In this clusters, three-body interactions may efficiently produce binaries which can then merge in a time-scale comparable to the age of the Universe and be visible with present day GW experiments (Franciolini et al. 2022c) (at odds with mergers induced by GW capture which merge promptly). In this sense, this formation mechanism is similar to the one taking place in the early Universe out of binary directly decoupling from the Hubble flow.

The rate density for three bodies to interact and form PBH binaries can be expressed as (Rodriguez et al. 2022)

$$\gamma_{3b}(\eta \geq \eta_{\rm min}) = \frac{3^{9/2}\pi^{13/2}}{2^{25/2}}\eta_{\rm min}^{-\frac{11}{2}}(1+2\eta_{\rm min})(1+3\eta_{\rm min}) \times \frac{n_{\rm PBH}^3 (Gm_{\rm PBH})^5}{\sigma_v^9} \simeq 3.8\times 10^{-2}{\rm Gyr}^{-1}{\rm pc}^{-3}\left(\frac{n_{\rm PBH}}{{\rm pc}^{-3}}\right)^3\left(\frac{m_{\rm PBH}}{30M_\odot}\right)^5\left(\frac{\sigma_v}{\rm km/s}\right)^{-9}, \quad (111)$$

where $n_{\rm PBH}$ is the number density of PBHs. We also defined the hardness ratio $\eta = Gm_{\rm PBH}/a\sigma_v^2$ as the binding energy of a binary with size a normalized to the average cluster kinetic energy, where σ_v is the PBH velocity dispersion within the clusters. Also, in order to require the efficiency of binary formation to be close to unity and PBH binaries resulting from this channel to be in the region of parameter space where binaries are hard, one should set $\eta_{\rm min} = 5$ as used in the literature (see e. g. Morscher et al. 2015; Rodriguez et al. 2022).

One can compute the merger rate density of binaries produced by 3-body interactions by integrating the binary formation rate over the PBH cluster distribution throughout the evolution of Universe and by multiplying by the fraction of binaries merging within the remaining time window (see Franciolini and Pani 2022 for more details). Depending on the assumed cluster core size and eccentricity distribution $e \equiv \sqrt{1-j^2}$ for the 3-body induced binaries (Ambartsumian 1937; Heggie 1975; Stone and Leigh 2019; Raidal et al. 2019; Vaskonen and Veermäe 2020) (i.e. $f(j) \simeq j^\gamma$ with $\gamma = 1$ for thermal or $\gamma = 0$ for super-thermal), this channel was found to give at least a contribution comparable to the one from dynamical capture discussed in the following section (Franciolini and Pani 2022).

One can also estimate how this contribution scales with the PBH abundance. Following Franciolini and Pani (2022), this was estimated to be $R^{\rm 3b} \propto f_{\rm PBH}^{2+(1+\gamma)/2}$, showing this channel may only be relevant, compared to the EB contribution, in case of large values of the PBH abundance $f_{\rm PBH}$.

4.2.3 Link with observations of compact binary coalescences

If PBHs significantly contribute to the dark matter, late binaries merging rates are enhanced around $30-100M_\odot$, where most compact binary mergers have been observed. Assuming Poisson clustering and $R_{\rm clust} = 450$, the corresponding merging rates for the PBH mass function of Fig. 13 that includes thermal features have been represented on Fig. 21. Typically one can obtain the LIGO/Virgo rates in this range with values of $f_{\rm PBH}^2 \times f(m_{\rm PBH})^2 \sim 10^{-3}$. At the solar-mass scale, the rates for early and late binaries compete at a similar level and it is possible to get the LIGO/Virgo rates inferred for the latest events observed. These are canonically interpreted as neutron star binary mergers, even though the absence of the observation of tidal effects may allow for a primordial interpretation, with the exception of GW170817 for which the electromagnetic counterpart has also been observed.

4.2.4 Limitations

For realistic, extended mass functions, a series of effects can either boost or suppress the merging rate of late binaries and make it a rather complex and model-dependent process, subject to large uncertainties (see e.g. Chisholm 2006, 2011; Ali-Haïmoud 2018; De Luca et al. 2020a; Inman and Ali-Haïmoud 2019; Clesse and García-Bellido 2022, 2017b; Moradinezhad Dizgah et al. 2019; Belotsky et al. 2014; Young and Byrnes 2020; De Luca et al. 2021f; Padilla et al. 2021; Suyama and Yokoyama 2019; Ballesteros et al. 2018 for studies on PBH clustering). Some of these limitations or effects are listed below:

1. The Poisson clustering is modified by the mass function and could be dominated by other mass scales than the dominant PBH masses. Therefore, one in principle needs to consider the whole mass spectrum in order to derive the importance of Poisson clustering.
2. The mass function also impacts the process of dynamical heating and dilution of sub-halos inside larger halos, which is essential to derive the natural clustering scale and the $R_{\rm clust}$ parameter.
3. Poisson clustering should induce a broad range of cluster masses, evolving and interacting with each others in possibly complex ways through dynamical heating, dilution, collisions, tidal disruptions, etc, resulting in possibly complex time dependence and various possible PBH local environments.
4. The existence of intermediate-mass and supermassive PBHs leads to a seed effect that should also impact the clustering properties.
5. Clustering at formation, obtained e.g. for non-Gaussian models (Atal et al. 2020), also have an uncertain impact.
6. For extended mass function, the role of mass segregation in a cluster should be considered. In average, more massive PBHs falling at the center should have a higher local density than lighter PBHs, leading to an additional mass dependence in the merger rates that was not considered so far in most analysis.

4.3 Hyperbolic encounters

In the scenario of *clustered* PBH of Clesse and García-Bellido (2015), it is expected that a large fraction of BH encounters will not end up producing bound systems, which would then inspiral, but rather produce a single scattering event, via an hyperbolic encounter. This could happen, e.g. if the relative velocity or relative distance of the two PBHs is high enough that capture is not possible. The emission of GWs in close encounters of compact bodies has been studied in Kocsis et al. (2006), O'Leary et al. (2009), Capozziello et al. (2008), De Vittori et al. (2012), García-Bellido and Nesseris (2017, 2018), Gröbner et al. (2020), Mukherjee et al. (2021). These events generate *bursts* of gravitational waves, which can be sufficiently bright to be detected at distances up to several Gpc. For clustered PBHs, the waveform and characteristic parameters of the GW emission in hyperbolic encounters are different to those of the inspiralling binaries, and both provide complementary information

that can be used to determine the evolved mass distribution of PBHs as a function of redshift, as well as their spatial distribution.

Hyperbolic encounters are single scattering events where the majority of the energy is released near the point of closest approach, and have a characteristic peak frequency which is a function of only three variables (see Fig 22): the impact parameter b, the eccentricity e and the total mass of the system $M_{\rm tot} = m_1 + m_2$. Furthermore, the duration of such events is of the order of a few milliseconds to several hours, depending on those parameters. The case of inspiralling and merging PBH has been studied extensively, see e.g. Clesse and García-Bellido (2017a, 2017b), and estimated the production of a few tens of events/year/Gpc^3 in the range of $m_{\rm PBH} \sim \mathcal{O}(10-100)\, M_\odot$. In García-Bellido and Nesseris (2017, 2018) it was shown that, within the parameter space of the clustered PBH scenario (Clesse and García-Bellido 2015, 2017b), we can expect a similar but somewhat lower rate of GW burst events in the millisecond range (Fig. 22).

The waveforms of the GW emission in hyperbolic encounters are very different from those of the inspiralling binaries, since the majority of the energy is released near the point of closest approach, generating a burst of GWs with a characteristic "tear-drop" shape of the emission in the time-frequency domain (García-Bellido and Nesseris 2017, 2018). The burst has a characteristic peak frequency

$$f_{\rm peak} = 0.32\,{\rm mHZ} \times \frac{\beta(e+1)}{(e-1)}\frac{\rm AU}{b}, \tag{112}$$

which corresponds to the maximum GW emission and depends only on the impact parameter b, the total mass of the system $M_{\rm tot}$ and the eccentricity of the hyperbolic orbit $e = \sqrt{1 + b^2 v_0^4 / G^2 M_{\rm tot}^2}$, where v_0 is the asymptotic relative velocity of the encounter and $\beta \equiv v_0/c$. The maximum strain amplitude and power of the GW burst is given by

$$h_{\rm c}^{\rm max} = 3.24 \times 10^{-23} \frac{R_{\rm s}({\rm km})}{d_{\rm L}({\rm Gpc})} \frac{q\beta^2 g_{\rm max}}{(1+q)^2}, \tag{113}$$

$$P_{\rm max}(e) = 5.96 \times 10^{26} L_\odot \frac{q^2\beta^{10}}{(1+q)^4}\frac{(e+1)}{(e-1)^5}, \tag{114}$$

where $L_\odot$ is the solar luminosity, $R_{\rm s}$ is the Schwarzschild radius associated to the

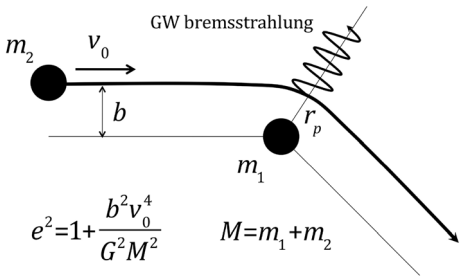

Fig. 22 The scattering of one BH of mass m_2 on another of mass m_1 induces the emission of gravitational waves which is maximal at the point of closest approach, $r_{\rm p}$ Image reproduced with permission

total mass, $q \equiv m_1/m_2$ is the binary mass ratio, $m_1 = qm_2 \geq m_2$ and $g_{\max} = 2\sqrt{18(e+1) + 5e^2/(e-1)}$.

GW signals in the LISA range could be generated by close hyperbolic encounters (CHE) of an IMBH and a SMBH as expected in the centers of galaxies, as well as from encounters of two SMBHs that could occur during galaxy collisions at low redshift. In the first case, an IMBH of mass $m_2 = 10^3 M_\odot$ and a SMBH of mass $m_1 = 10^6 M_\odot$, with an impact parameter $b = 1$AU and velocity $v_0 = 0.05\,c$ gives an eccentricity parameter of $e = 1.031$ with a duration of the event of 440 s. The maximum stress amplitude would be $h_c^{\max} = 1.02 \times 10^{-19}$ at a distance $d_L = 1$, with the peak at frequency $f_{\rm peak} = 1.05$ mHz, well within the sensitivity band of LISA. In a hyperbolic encounter between two SMBHs of equal masses $m_1 = m_2 = 10^6 M_\odot$ with impact parameter $b = 10$ AU and relative velocity $v_0 = 0.015c$, the eccentricity is low, $e = 1.01$, and the stress amplitude is huge, $h_c^{\max} = 2.22 \times 10^{-17}$ at $f_{\rm peak} = 1.51 \times 10^{-4}$HZ, which falls again in the LISA sensitivity range.

The event rate can be estimated by the cross-section of a CHE event, which is given by $\sigma = \pi b^2 = \pi (GM_{\rm tot}/v_0^2)^2 (e^2 - 1)$. In the picture of the local density contrast $\delta_{\rm loc}$, the total event rate for a generic PBH mass function is given by (García-Bellido et al. 2022)

$$\frac{{\rm d}\tau^{\rm CHE}}{{\rm d}m_1\,{\rm d}m_2} \approx 6.1 \times 10^{-8}\,{\rm yr}^{-1}{\rm Gpc}^{-3}\,h^4 \left(\frac{\Omega_{\rm DM}}{0.25}\right)^2 \left(\frac{\delta_{\rm loc}}{10^8}\right) \frac{f(m_1)}{m_1} \frac{f(m_2)}{m_2} \frac{M^2}{m_1\,m_2} \frac{e^2-1}{(v_0/c)^3}\,. \tag{115}$$

These CHE events are very common in dense clusters formed soon after recombination, while the PBH scatter off each other and puff-up the cluster. Some of these events loose so much energy in their GW emission that they end up in bounded systems. Many also are responsible for the disruption of previously formed binaries. All in all, there is a significant production of gravitational waves from CHE that can contribute to a SGWB early on. In the next Sections we will explore such a stochastic background from CHE events across the history of the universe, and will see that it can be significant for a wide PBH mass function, even in the LISA range of frequencies.

4.4 How to distinguish PBH from astrophysical binaries

In this Section we elaborate on which observable may be used to assess or rule out the primordial origin of an individual merger event. We follow the comprehensive description given in Franciolini et al. (2022b). A systematic strategy to use these discriminators is summarized in the flowchart of Fig. 23, based on the predictions of the standard PBH scenario where binaries are assembled in the early Universe. Notice that most of predictions would still apply to a much larger class of models, see Franciolini et al. (2022b) for more details.

One can identify two "smoking-gun" signatures of the primordial scenario, which are high redshift mergers and sub-solar masses. A general prediction of the PBH model is a merger rate density which grows monotonically with redshift (Ali-

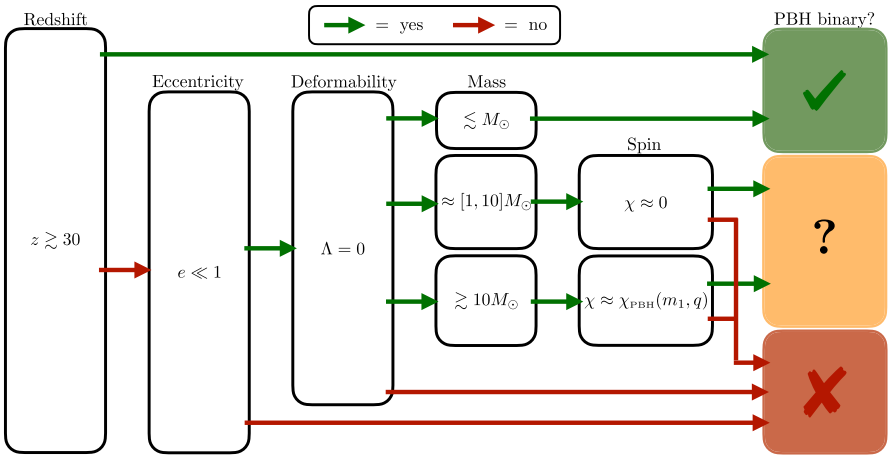

Fig. 23 Schematic flowchart representing how to systematically rule out or potentially assess the primordial origin of a binary merger. These criteria are based on measurements of the redshift z, eccentricity e, tidal deformability Λ, component masses m, and dimensionless spin χ. Each arrow indicates if the condition in the box is met (green) or violated (red), while the marks indicate: ✓) likely to be a PBH binary; ✗) cannot to be a PBH binary; **?**) may be a PBH binary. Image reproduced with permission from Franciolini et al. (2022b), copyright by APS Image reproduced with permission

Haïmoud et al. 2017; Raidal et al. 2019; De Luca et al. 2020d). Focusing on early binaries, one expects $R^{\rm EB}(z) \propto (t(z)/t(z=0))^{-34/37}$, extending up to redshifts $z \gtrsim \mathcal{O}(10^3)$. On the contrary, astrophysical-origin mergers are generically not expected to occur at $z \gtrsim 30$, even though the redshift corresponding to the epoch of first star formation is still poorly known. To give a conservative estimate, theoretical calculations and cosmological simulations suggest star formation does not precede $z \sim 40$ (Schneider et al. 2000, 2002, 2003; Bromm 2006; Tornatore et al. 2007; Trenti and Stiavelli 2009; de Souza et al. 2011; Koushiappas and Loeb 2017b; Mocz et al. 2020; Liu and Bromm 2020a). Additionally, the time delay between Pop III star formation and BBH mergers was estimated to be around $\mathcal{O}(10)$ M*yr* (Kinugawa et al. 2014, 2016; Hartwig et al. 2016; Belczynski et al. 2017; Inayoshi et al. 2017; Liu and Bromm 2020b, a; Kinugawa et al. 2020; Tanikawa et al. 2021; Singh et al. 2022a), implying merger redshifts $z \gtrsim 30$ to represent smoking guns for primordial binaries (Koushiappas and Loeb 2017b; De Luca et al. 2021c; Ng et al. 2022a). Observations of such distant events may be characterised by large measurement uncertainties on the inferred luminosity distance due to the low SNR at 3 G detectors (Ng et al. 2022a; Franciolini et al. 2022b; Martinelli et al. 2022; Ng et al. 2023), including LISA. However, it was recently shown that focusing on constraining the merger rate evolution at redshift larger than $\mathcal{O}(10)$ may allow to constrain PBH populations up to abundances as low as $f_{\rm PBH} \approx 10^{-5}$ (Ng et al. 2022b) in the solar mass range, even accounting for the contamination of Pop III binaries.

Sub-solar BHs are not expected in standard stellar evolution.[8] Other compact objects like white dwarfs, brown dwarfs, or exotic compact objects (Cardoso and Pani 2019) (e.g. boson stars; Guo et al. 2019b) may be misinterpreted as sub-solar PBHs. Distinguishing PBHs from other compact objects requires taking into account tidal disruption and tidal deformability measurements. Less compact objects like brown and white dwarfs are expected to be tidally disrupted well before the contact frequency. This leads to a different GW signature, see Franciolini et al. (2022b) and refererences therein for more details on the observability of these effects.

Another key prediction of the primordial model involves the eccentricity e of PBH binaries. While formed with large eccentricity at high redshift, PBH binaries then have enough time to circularize before the GW signal can enter the observation band of current and future detectors. Therefore, observing a non-zero eccentricity would rule out the interpretation as a primordial binary formed in the early Universe, while it may still be compatible with a PBH binary formed in the late-time universe (Cholis et al. 2016; Wang and Nitz 2021). Finally, the spin distribution of PBHs inherits characteristic mass-spin correlations induced by accretion effects, as discussed in Sect. 3.10. Using this criterion for determining the possible primordial nature of individual GW events would require reducing uncertainties on the accretion model. However, searching for signatures of this correlation can also be performed on a population level. This was recently done in Franciolini and Pani (2022) focusing on the GWTC-3 catalog, finding a similar correlation (indistinguishable at this stage from the one present in dynamically formed astrophysical binaries) may be present in the data.

In Sect. 6, dedicated to correlating GWs with LSS, we will mention further possibilities of distinguishing astrophysical and primordial merger populations through measurements of the event bias.

4.5 Summary

The calculation of PBH merger rates or encounter rates has been a very active line of research during the last few years, with some important twists. Two main binary formation channels have been envisaged: early binaries that formed quickly in the radiation era when two PBHs formed sufficiently close to each other, and late binaries that can form inside PBH clusters, when two PBHs pass sufficiently close to each other to form a bound system. Today, it is still unclear which binary formation channel provides the most important merger rates on the mass scales probed by LVK, especially since these rates depend on the exact shape of the PBH mass function, on the dark matter fraction made of PBHs, on the clustering properties, on accretion, possible hierarchical mergers, on binary disruptions, etc. It is also debated if the limits on those rates coming from the latest GW observations favor or disfavor PBHs as the dark matter.

We tried to list all these limitations and we now attempt to summarize the current status: at first, the merger rates of early binaries were found to importantly surpass the

[8] See, however, Shandera et al. (2018), Kouvaris et al. (2018) for models in which subsolar BHs are born out of dark sector interactions or capture of asteroidal mass PBHs (Oncins et al. 2022).

ones of late binaries in clusters, at least in the standard scenario of cosmological structure formation. However, on the one hand, N-body simulations have revealed several mechanisms that importantly suppress those rates if PBHs constitute a significant fraction of the dark matter, due to binary disruption by other PBHs, by matter fluctuations, and above all by the PBH clusters seeded by the inevitable Poisson fluctuations in the initial PBH distribution. On the other hand, the same effects should be responsible for a boost of the merger rates of late binaries in these PBH clusters, at a level comparable to that of early binaries on solar-mass scales, if PBHs significantly contribute to the dark matter. An important difference between early and late binary merger rates is the mass dependence, roughly going like $1/m_{\rm PBH}^{32/37}$ for early binaries and $1/m_{\rm PBH}^{11/21}$, by taking into account the halo mass distribution, for late binaries (Bird et al. 2016). Another difference is the redshift evolution of those rates. In both cases, however, it seems very disfavored that all the dark matter is made of $30M_\odot$ black holes. The scenario where the PBH mass function peaks at the solar mass scale, where the QCD transition should have favored PBH formation, may represent an alternative possibility, provided the overall abundance is below the current observational constraints in that mass range, see in particular Petač et al. (2022), Gorton and Green (2022), Juan et al. (2022), De Luca et al. (2022b), Franciolini et al. (2022e).

5 Stochastic backgrounds

5.1 From second-order curvature fluctuations

If PBHs are generated by the collapse of large density perturbations, they are unavoidably associated to the emission of induced GWs at second order by the same scalar perturbations, due to the intrinsic nonlinear nature of gravity (Tomita 1975; Matarrese et al. 1994; Acquaviva et al. 2003; Mollerach et al. 2004; Ananda et al. 2007; Baumann et al. 2007a).[9] The origin of these multimessenger signals is therefore not coming from PBHs themselves but from the underlying cosmological curvature perturbations (including ones that do not lead to PBHs. As a consequence, the conclusions will be robust to changes in the astrophysical evolution of PBHs (accretion and merger history) and clustering effects (Ünal et al. 2021). The phenomenological implications have been investigated in various contexts also associated to PBHs (Saito and Yokoyama 2009; Bugaev and Klimai 2010; Saito and Yokoyama 2010; García-Bellido et al. 2017; Ando et al. 2018; Bartolo et al. 2018, 2019c, b; Clesse et al. 2018; Ünal 2019; Wang et al. 2019; Domènech 2020; Domènech et al. 2020, 2022; Pi and Sasaki 2020; Ragavendra et al. 2021; Fumagalli

[9] We stress that we do not refer here to the GWs produced only in the overdense regions that contract at horizon crossing due to the gravitational force (De Luca et al. 2019b), but from everywhere in the Universe, due to the general increase of the power of the density perturbations at small scales. See also here Lin et al. (2020), Chen et al. (2021a), Kawai and Kim (2021), Lin et al. (2023), Papanikolaou et al. (2022), Ivanov et al. (2022), Zhang (2022), Yi (2023), Cheong et al. (2022), Feng et al. (2023), Zhang et al. (2022), Arya et al. (2024), Tzerefos et al. (2023), Papanikolaou et al. (2024c) for studies within modified gravity setups.

et al. 2021a, 2022a; Yuan et al. 2019) (see recent reviews by Yuan and Huang 2021a; Domènech 2021). This will be also a conclusive test for the intriguing proposal that the seeds of the SMBHs are formed by PBHs (Duechting 2004; Belotsky et al. 2014; Clesse and García-Bellido 2015; Nakama et al. 2016; García-Bellido et al. 2016).

Such a source of GWs is present at all scales, but due to the necessary enhancement of the scalar power spectrum responsible for the generation of PBHs around the characteristic scale $k_\star$, it will peak in the frequency range around $f_\star = k_\star/2\pi$, and can thus reach the detection sensitivities of many GW experiments like LISA. Since the emission mostly occurs when the corresponding scales cross the horizon, one can relate the GW frequency to the PBHs mass $m_{\rm PBH}$ as (see for example Saito and Yokoyama 2010; García-Bellido et al. 2017)

$$f \simeq 6\,{\rm mHz}\sqrt{\gamma}\left(\frac{m_{\rm PBH}}{10^{-12}M_\odot}\right)^{-1/2}, \tag{116}$$

where the parameter γ describes the efficiency of the gravitational collapse into PBHs.

There are several current and future experiments searching for a SGWB in various frequency ranges. In the ultra-low frequency range (around nHz), the observations at Pulsar Timing Array (PTA) experiments like NANOGrav (Agazie et al. 2023b, c), EPTA (in combination with InPTA) (Antoniadis et al. 2024, 2023a, b), PPTA (Reardon et al. 2023a; Zic et al. 2023; Reardon et al. 2023b) and CPTA (Xu et al. 2023), give rise to the most stringent constraints on the GWs abundance. Future experiments like SKA (Dewdney et al. 2009) (see also Moore et al. 2015) will greatly improve the sensitivity.

In the LVK frequency range, an additional constraint has been set by the non-observation of a stochastic background after O1-O2 runs (Abbott et al. 2019a). These searches can be translated into a constraint on the amplitude of the comoving curvature perturbation at the corresponding scales (Inomata and Nakama 2019; Ünal et al. 2021). Those bounds are also affecting the maximum allowed PBH fraction of DM with the hypothesis that they originate from the collapse of density perturbations. Detailed studies with the LVK data affecting the mass range $[10^{-20}, 10^{-18}]M_\odot$ are reported in Kapadia et al. (2020). Also, in Cai et al. (2019b), the dependence of the result on non-Gaussianities is also investigated, finding that local non-Gaussianity can for example alleviate the bounds (see Sect. 5.3 for details). This is possible for two main reasons: (i) Non-Gaussianity can allow PBHs to be produced more efficiently for the same power spectra, as the tail of the non-Gaussian probability distribution function of the perturbations has more area/probability for the perturbations greater than the threshold. (ii) Due to several contractions of the curvature field within non-Gaussian correlators, there is a higher symmetry factor compared to the Gaussian case. Hence, non-Gaussian perturbations can produce a large fraction of PBHs with a smaller amplitude power spectrum, and therefore with a smaller amount of sourced GWs.

SKA (Moore et al. 2015; Zhao et al. 2013) is the next-generation PTA experiment that will probe primordial perturbations very sensitively (Byrnes et al. 2019; Inomata and Nakama 2019; Kalaja et al. 2019; Gow et al. 2020). It has been recently shown

in Ünal et al. (2021) that PTA-SKA combined with CMB distortions will robustly test the PBHs from inflationary fluctuations, namely they will detect the stochastic GW background or distortion signatures and possibly make a extraordinary discovery or constrain the PBHs heavier than a solar mass for 13 orders of magnitude $(1-10^{13}M_\odot)$ to a completely negligible amount $\frac{\rho_{\rm PBH}}{\rho_{\rm DM}}<10^{-10}$.

Finally, the LISA experiment will be able to provide insights for the intermediate frequencies around the mHz, such that the peak of the signal falls within the LISA sensitivity band for PBH masses around $m_{\rm PBH}\sim\mathcal{O}(10^{-15}-10^{-8})M_\odot$ (Saito and Yokoyama 2009; García-Bellido et al. 2017; Bartolo et al. 2019c; Cai et al. 2019a; Ünal 2019; Bhaumik and Jain 2021).

In the following, we review the procedure to compute the induced SGWB spectrum from primordial scalar perturbations. First of all, let us define the scalar and tensor perturbations in the Newtonian gauge as

$$\mathrm{d}s^2=a^2\left\{-(1+2\Psi)\mathrm{d}\eta^2+\left[(1-2\Psi)\delta_{ij}+\frac{1}{2}h_{ij}\right]\mathrm{d}x^i\mathrm{d}x^j\right\},\tag{117}$$

where we neglected the anisotropic stress. The GWs emission is captured by the equation of motion for the GWs[10] as

$$h_{ij}''+2\mathcal{H}h_{ij}'-\nabla^2h_{ij}=-16\mathcal{T}_{ij}^{\ell m}\left[\Psi\partial_\ell\partial_m\Psi+2\partial_\ell\Psi\partial_m\Psi-\partial_\ell\left(\frac{\Psi'}{\mathcal{H}}+\Psi\right)\partial_m\left(\frac{\Psi'}{\mathcal{H}}+\Psi\right)\right],\tag{118}$$

where derivatives are taken with respect to conformal time η, $\mathcal{H}\equiv a'/a$ is the conformal Hubble parameter, and the source is evaluated assuming a radiation-dominated (RD) epoch,[11] The solution of the first order equation of motion in a radiation-dominated Universe relates the Bardeen's potential Ψ to the gauge invariant comoving curvature perturbation through (Lyth and Riotto 1999)

$$\Psi(\eta,\vec{k})=\frac{2}{3}T(k\eta)\zeta(\vec{k}),\qquad\text{where}\qquad T(z)=\frac{9}{z^2}\left[\frac{\sin(z/\sqrt{3})}{z/\sqrt{3}}-\cos(z/\sqrt{3})\right].\tag{119}$$

One can decompose the tensor field in Fourier space as

$$h_{ij}(\eta,\vec{x})=\int\frac{\mathrm{d}^3k}{(2\pi)^3}\sum_{\lambda=R,L}h_\lambda(\eta,\vec{k})\,e_{ij,\lambda}(\hat{k})\,\mathrm{E}^{i\vec{k}\cdot\vec{x}},\tag{120}$$

where h_λ are the two helicity modes. Introducing the dimensionless variables $x=p/k$ and $y=|\vec{k}-\vec{p}|/k$, the GWs emitted take the form, see for example (Espinosa et al. 2018),

[10] We do not consider the free-streaming effect of neutrinos on the GW amplitude (Weinberg 2004).

[11] The projector $\mathcal{T}_{ij}^{\ell m}$ to the transverse and traceless component is defined in Fourier space in terms of the polarisation tensors $e_{ij}^{\lambda}(\vec{k})$ the chiral basis (Lr) as $\tilde{\mathcal{T}}_{ij}^{\ell m}(\vec{k})=e_{ij}^{L}(\vec{k})\otimes e^{L\ell m}(\vec{k})+e_{ij}^{R}(\vec{k})\otimes e^{R\ell m}(\vec{k})$. The normalisation adopted is $e_{ij,\lambda}(\vec{k})e^{*}_{ij,\lambda'}(\vec{k})=\delta_{\lambda\lambda'}$.

$$h_\lambda(\eta,\vec{k}) = \frac{4}{9k^3\eta}\int \frac{\mathrm{d}^3p}{(2\pi)^3}\,\mathrm{E}^*_\lambda(\vec{k},\vec{p})\zeta(\vec{p})\zeta(\vec{k}-\vec{p})[\mathcal{I}_\mathrm{c}(x,y)\cos(k\eta)+\mathcal{I}_\mathrm{s}(x,y)\sin(k\eta)], \tag{121}$$

where $\mathrm{E}_\lambda(\vec{k},\vec{p}) \equiv \mathrm{E}_{ij,\lambda}(\hat{k})\vec{p}_i\vec{p}_j$, and two functions $\mathcal{I}_{\mathrm{c,s}}$ are (Espinosa et al. 2018; Kohri and Terada 2018)

$$\mathcal{I}_\mathrm{c}(x,y) = -36\pi\frac{(s^2+d^2-2)^2}{(s^2-d^2)^3}\theta(s-1) \tag{122}$$

$$\mathcal{I}_\mathrm{s}(x,y) = -36\frac{(s^2+d^2-2)}{(s^2-d^2)^2}\left[\frac{(s^2+d^2-2)}{(s^2-d^2)}\log\frac{(1-d^2)}{|s^2-1|}+2\right], \tag{123}$$

with

$$d \equiv \frac{1}{\sqrt{3}}|x-y|, \qquad s \equiv \frac{1}{\sqrt{3}}(x+y), \qquad (d,s)\in[0,1/\sqrt{3}]\times[1/\sqrt{3},+\infty). \tag{124}$$

The definition of the energy density associated to GWs is (Misner et al. 1973; Maggiore 2000; Flanagan and Hughes 2005)

$$\rho_\mathrm{GW} = \frac{M_\mathrm{PI}^2}{4}\left\langle \dot{h}_{ab}(t,\vec{x})\dot{h}_{ab}(t,\vec{x})\right\rangle_T, \tag{125}$$

where the angular brackets denote a time average performed on a timescale T much greater than the GW phase oscillations ($Tk_i \gg 1$) but much smaller than the cosmological time ($TH \ll 1$).

Assuming that the scalar perturbations ζ are Gaussian (see the next sections for a possible relaxation of this assumption), one finds

$$\begin{aligned}\left\langle \rho_\mathrm{GW}(\eta,\vec{x})\right\rangle &\equiv \rho_\mathrm{c}(\eta)\int \mathrm{d}\ln k\;\Omega_\mathrm{GW}(\eta,k)\\ &= \frac{2\pi^4M_\mathrm{p}^2}{81\eta^2a^2}\int\frac{\mathrm{d}^3k_1\mathrm{d}^3p_1}{(2\pi)^6}\frac{1}{k_1^4}\frac{\left[p_1^2-(\vec{k}_1\cdot\vec{p}_1)^2/k_1^2\right]^2}{p_1^3\left|\vec{k}_1-\vec{p}_1\right|^3}\mathcal{P}_\zeta(p_1)\mathcal{P}_\zeta(|\vec{k}_1-\vec{p}_1|)\\ &\quad\left[\mathcal{I}_\mathrm{c}^2(\vec{k}_1,\vec{p}_1)+\mathcal{I}_\mathrm{s}^2(\vec{k}_1,\vec{p}_1)\right],\end{aligned} \tag{126}$$

as a function of the curvature perturbation power spectrum $\mathcal{P}_\zeta$. In the first line, we have defined the fractional GW energy density for log interval Ω_GW, in terms of the critical energy density of a spatially flat Universe, $\rho_\mathrm{c} = 3H_0^2M_\mathrm{p}^2$.

The current GW abundance can then be obtained as

$$\Omega_{\rm GW}(\eta_0,k)=\frac{a_{\rm f}^4\rho_{\rm GW}(\eta_{\rm f},k)}{\rho_{\rm r}(\eta_0)}\Omega_{\rm r,0}=\frac{g_*(\eta_{\rm f})}{g_*(\eta_0)}\left(\frac{g_{*\rm s}(\eta_0)}{g_{*\rm s}(\eta_f)}\right)^{4/3}\Omega_{\rm r,0}\Omega_{\rm GW}(\eta_{\rm f},k), \quad (127)$$

in terms of the present radiation energy density fraction $\Omega_{\rm r,0}$ if the neutrinos were massless and the effective degrees of freedom for entropy density $g_{*\rm s}$. For the frequencies of interest, using the relation with the temperature of the universe at the time of horizon crossing $f\simeq 8\,{\rm mHZ}(g_*/10)^{1/4}(T/10^6\,{\rm GeV})$, one can show that the emission of GWs takes place at $\eta_{\rm f}$ (with corresponding scale factor $a_{\rm f}$) well before the time at which top quarks start annihilating, above which we can assume a radiation-dominated Universe with constant effective degrees of freedom.

As one can see, the GW's abundance depends on the curvature perturbation power spectrum. One possibility is represented by a monochromatic power spectrum with support at the momentum scale $k_\star$

$$\mathcal{P}_\zeta(k)=A_{\rm s}\,k_\star\delta(k-k_\star), \quad (128)$$

enhanced with respect to the power spectrum on large CMB scales, for which the current GWs abundance can be computed analytically as (see also Saito and Yokoyama 2010; Bugaev and Klimai 2010)

$$\begin{aligned}\Omega_{\rm GW}(\eta_0,k)=&\frac{\Omega_{\rm r,0}A_{\rm s}^2}{15552}\frac{g_*(\eta_{\rm f})}{g_*(\eta_0)}\left(\frac{g_{*S}(\eta_0)}{g_{*S}(\eta_{\rm f})}\right)^{4/3}\left(\frac{4k_\star}{k}-\frac{k}{k_\star}\right)^2\\&\theta(2k_\star-k)\left[\mathcal{I}_{\rm c}^2\left(\frac{k_\star}{k},\frac{k_\star}{k}\right)+\mathcal{I}_{\rm s}^2\left(\frac{k_\star}{k},\frac{k_\star}{k}\right)\right],\end{aligned} \quad (129)$$

where θ is the Heaviside step function.

A more realistic spectrum is provided by a log-normal shape with width σ

$$\mathcal{P}_\zeta(k)=A_\zeta\exp\left(-\frac{\ln^2(k/k_\star)}{2\sigma^2}\right), \quad (130)$$

whose abundance is shown by the black line of Fig. 24, compared to the monochromatic shape in red. For illustrative purposes, the power spectra peak scale has been chosen to be the one at which LISA has its maximum sensitivity, i.e. $f_\star=f_{\rm LISA}\sim 3.4\,{\rm mHZ}$ where $f_\star\equiv k_\star/2\pi$, corresponding to PBH with masses around $10^{-12}M_\odot$, while the parameters were chosen in order to have PBHs which account for the totality of the DM. One can see that the curves fall well within the sensitivity curves of LISA. It is thus clear that if PBHs of such masses, produced from the collapse of sizeable primordial fluctuations, represent the totality (or a fraction) of the dark matter, LISA will be able to measure the GWs sourced during the PBH formation time for a wide variety of PBH masses.

The spectral shapes present differences at high frequencies, because of the absence of the sharp cut-off at $2f_\star$ characteristic of the Dirac delta case, and at lower frequencies, since physical spectra would typically give a white-noise ($\propto f^3$) behaviour (Espinosa et al. 2018; Cai et al. 2020), while the slow fall-off of the monochromatic case is an unphysical effect of assuming such a power spectrum.

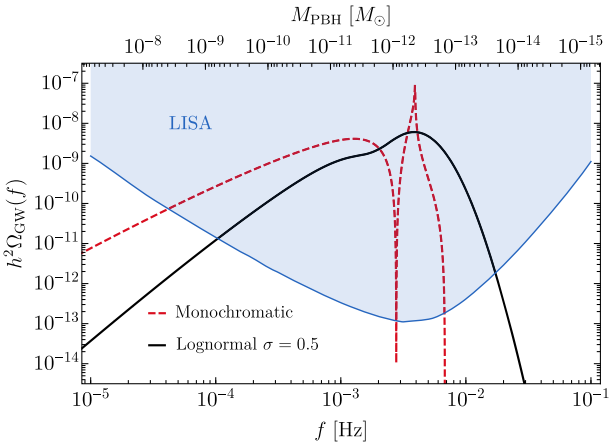

Fig. 24 Induced GWs spectra for both examples considered in Eqs. (128) and (130), for the parameters choice $A_{\rm s} = 0.033$, $A_\zeta = 0.044$ and $\sigma = 0.5$. For comparison, we also show the estimated sensitivity for LISA (Amaro-Seoane et al. 2017), following the proposed design (4y, 2.5 Gm of length, 6 links). The PBH mass corresponding to the characteristic frequency is depicted on the top horizontal axis, according to Eq. (116) Image reproduced with permission

Furthermore, in the latter a resonant effect at $f \sim 2f_\star/\sqrt{3}$ produces the spike, see for example Ananda et al. (2007).

As one can appreciate from Eq. (121), the non-linear coupling to the curvature perturbation naturally leads to an intrinsically non-Gaussian GW signal imprinted in phase correlations. However, it has been shown in Bartolo et al. (2019b, 2019c) (see also Bartolo et al. 2018; Margalit et al. 2020), that the coherence is washed out by the propagation of the waves in the perturbed Universe mainly due to time delay effects originated from the presence of large scale variations of gravitational potential. This is simply a consequence of the central limit theorem applied to a number $N \sim (k_\star \eta_0)^2 \ggg 1$ of independent lines of sight (Bartolo et al. 2019b). Possible small deformations smearing the GW spectrum can also arise from similar effects (Domcke et al. 2020).

5.2 Gauge invariance of the SGWB spectrum

The fact that tensor modes are generated at second-order in perturbation theory raises the issue of the possible gauge dependence of the result commonly computed in the Newtonian gauge. Indeed, second order tensor modes, contrary to the first order ones, are not gauge invariant. This issue has been recently highlighted in the literature (Hwang et al. 2017; Domènech and Sasaki 2018; Gong 2022; Tomikawa and Kobayashi 2020; Lu et al. 2020).

A physical observable is however not dependent on gauge choices by definition and it can be identified by understanding how the measurement in GW experiments is performed. The description of the detector's response to the GW signal can be best performed in the so-called transverse-traceless (TT) frame (Maggiore 2008; De Luca et al. 2020b), particularly in space based experiments like LISA. The TT frame is

defined as the one where the coordinates are fixed with the position of the mirrors and the effect of the passing GWs is captured by the delay of the arrival times between the arms of the experiment. The peculiarity of the LISA experiment is due to the relation between the characteristic frequency observable and the arm length L, which is $f_{\rm LISA}L \sim \mathcal{O}(1)$. The TT choice is optimal because it avoids keeping track of the otherwise large corrections $\mathcal{O}(fL)$ appearing if expanding around a locally inertial reference frame. Indeed, the projected sensitivity curves for the interferometer LISA are provided in such a frame.

One should remark that, during the period in which the source of the tensor mode is active and therefore the tensor field is coupled to the scalar perturbations at second-order in perturbation theory, it retains a gauge dependence and cannot be identified with the freely-propagating GW, which can be treated linearly and is therefore gauge invariant.

In the case of the production of tensor degrees of freedom from scalar perturbation during a radiation-dominated phase of the Universe, the source is active only when the scalar perturbations re-enter the horizon. Once produced, the GWs effectively decouple from the second order source and behave like linear perturbations of the metric in the late-time limit well within the cosmological horizon. Therefore, the initial gauge dependence of the result is lost (De Luca et al. 2020b; Inomata and Terada 2020; Yuan et al. 2020) and does not affect the spectrum shown in Fig. 24.

5.3 Impact of primordial non-Gaussianity on scalar induced SGWB

As discussed above, the existence of amplified primordial fluctuations at small scales can lead to PBHs and also accompanying scalar induced (secondary) SGWB. Depending on the amplification/enhancement scale, this background can be detected at different frequencies with various GW experiments including LISA, PTA-SKA, DECIGO and BBO. Since the physical scales for PBHs of mass less than million solar mass correspond to very small sub-galactic distances (perturbation wavelength $<$ kpc), the nonlinearity of scalar fluctuations in the current Universe prevents us from extracting primordial information about such small scales. However, the freely propagating SGWB sourced by primordial curvature fluctuations could be an excellent probe for these scales. The spectral shape of the scalar induced (or secondary) SGWB can be influenced by the statistical properties of the scalar density perturbations. Therefore, the detection and spectral analysis of the induced/secondary GW background can also shed light on the properties of the inflationary era.

Since the SGWB is sourced directly by the primordial curvature fluctuations in the horizon re-entry, it is natural to expect to observe some statistical properties of these scalar fluctuations in the SGWB spectrum. The SGWB includes a 4-pt function of the primordial curvature perturbations ($P_h \propto \langle h^2 \rangle \propto \langle \zeta^4 \rangle$ see also Eqs. (121) and (126)), hence for a Gaussian case, it can be reduced to only powers of a 2-pt function (see left panel of Fig. 25). In the presence of non-Gaussianity, a 4-pt correlator can not be written in terms of power spectra exactly.

Curvature perturbations with non-Gaussianity that can be expressed in terms of quadratic order Gaussian curvature perturbations contribute to GWs with 5 more diagrams given in Figs. 25 and 26. Note that the interaction could be of local form, or might include time and position derivatives. Hence, the topologies of these five diagrams are independent of the interaction type and universal for curvature perturbations with the form

$$\zeta = \zeta_g + O \cdot \zeta_g^2. \tag{131}$$

Here O is an operator acting on a quadratic order Gaussian field. It can be constant or depend on space and time. For two powers of interaction, we have 2 diagrams in Fig. 25

- Hybrid, since the power spectrum of one leg is tree level and the other one is the interaction;
- Walnut, due to the walnut shape. Note that the walnut topology diagram can be obtained by two different contractions.

For 4 powers of interaction, there are 3 diagrams given in Fig. 26

- Reducible, since this diagram can be reduced to a 1 loop diagram;
- Planar and Non-planar, respectively, as their topology can or cannot be drawn on a plane.

The properties of the spectrum have been studied in a number of references. For instance, Nakama et al. (2017) estimated the order of magnitude of the SGWB in the presence of non-Gaussianity. In García-Bellido et al. (2017), the SGWB spectrum was computed in the presence of large non-Gaussianities, and in such a case the main contribution to the SGWB comes from the 3 diagrams given in Fig. 26. The SGWB spectrum in the presence of small non-Gaussianity has been computed in Ünal (2019) with the diagrams in Figs. 25 and 26. Small non-Gaussianities have also been studied in Atal and Domènech (2021), Cai et al. (2019a).

It is important to note that Walnut diagram topology has two distinct contributions from two distinct contractions. This missing point in previous studies has been identified and computed carefully in Adshead et al. (2021). With these results, the whole diagrams have been completed up to quartic order in interaction ($f_{\rm NL}^4$) and quadratic order in scalar density perturbations. The scalar induced SGWB with scalar non-Gaussianities has been worked out in Yuan and Huang (2021b) up to third order

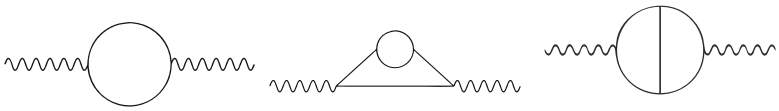

Fig. 25 Nonvanishing diagrams for $\mathcal{O}(f_{\rm NL}^0)$ (left) and $\mathcal{O}(f_{\rm NL}^2)$: center and right, called Hybrid and Walnut diagrams due to their topology and shape. Images reproduced with permission from Ünal (2019), copyright by APS Image reproduced with permission

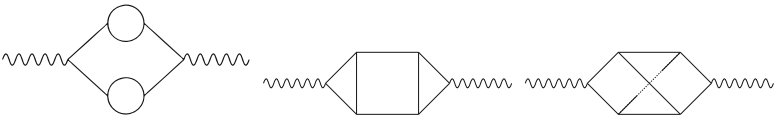

Fig. 26 Diagrams of $\mathcal{O}(f_{\rm NL}^4)$, called (from left to right) Reducible, Planar and non-Planar due to their topological properties. Images reproduced with permission from Ünal (2019), copyright by APS; see also García-Bellido et al. (2017) Image reproduced with permission

in density perturbations. The contribution of higher order in perturbation theory do not change the peak amplitude, but since higher order correlation includes convolution of higher number of propagators, the maximum frequency of external legs grow linearly with this number. Therefore, instead of sharp decrease in the high frequency regime, there are corrections at high frequencies from higher-order terms which slows down the decrease of the spectrum.[12]

The following results about the imprints of non-Gaussianity on the secondary/induced GW spectrum have been found:

- Non-Gaussianity can enhance the production efficiency of the SGWB. Namely, for the same amplitude of Gaussian or non-Gaussian scalar fluctuations, the resulting SGWB has a larger amplitude for non-Gaussian than for Gaussian fluctuations.
- Because non-Gaussianity is a result of interactions, this leads to a convolution in the momentum space and to a broader distribution of scalar fluctuations, with a peak at frequencies about $\mathcal{O}(1)$ higher, especially if the curvature fluctuations have a narrow spectrum.
- In the limit of large non-Gaussianities, the diagrams in Fig. 26 are important and dominate the signal. For small and mild non-Gaussianities, the signal is dominated by the diagrams in Fig. 25.

Some of the results above can be visualized in Fig. 27, where $\Omega_{\rm GW}$ indicates the total GW spectrum, $\Omega_{\rm GW}^{\rm g}$ indicates GWs from Gaussian scalar perturbations, and $\Omega_{\rm GW}^{\rm NG}$ GWs from non-Gaussian scalar perturbations.[13] Due to the interactions of the scalar perturbations, the high frequency regime of the SGWB is dominated by the NG scalar perturbations. This fact can lead to a second peak whose amplitude is set by the strength of the interactions, ie. the non-Gaussianity parameter $f_{\rm NL}$. If the NG contribution is considerable, the SGWB leads to two peaks, as shown in the right panel of Fig. 27. The second peak, which results from interactions/non-Gaussian perturbations, is at a frequency about $\mathcal{O}(1)$ times higher with respect to the first peak from Gaussian perturbations. It can be seen on the left panel of the same Figure that

[12] Explicitly, $\zeta + \zeta \to h$ interaction allows GW to have highest frequency at $2k_{UV}$ due to momentum conservation, k_{UV} is the highest momentum in scalar perturbations, on the other hand for $\zeta + \zeta + \zeta \to h$ interaction, GW has the highest frequency at $3k_{UV}$.

[13] Recall that induced GWs are sourced by scalar sources at quadratic order hence they are inherently non-Gaussian. By G and NG symbols we indicate the statistical properties of scalar perturbations sourcing GWs.

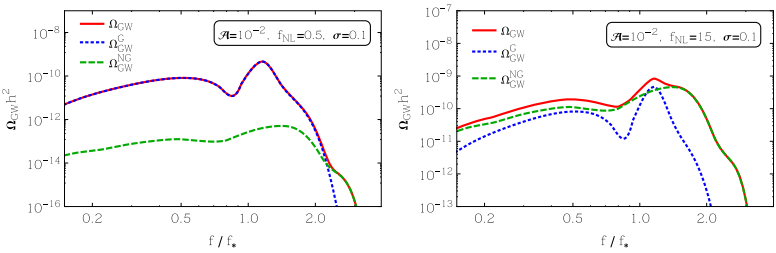

Fig. 27 Second peak produced by primordial non-Gaussian component of curvature perturbations. Image reproduced with permission from Ünal (2019), copyright by APS Image reproduced with permission

even if the NG contribution is tiny, it still dominates the large frequency regime of the GW spectrum and produces an abrupt second bump at smaller amplitudes which can be detected with sensitive next generation GW experiments, such as LISA, Cosmic Explorer, DECIGO and PTA-SKA, and allow probing non-Gaussianity as sensitive as $f_{\rm NL} \sim 0.5$ (Ünal 2019). This level of non-Gaussianity could be probed even better than using next generation CMB and LSS experiments.

In Garcia-Saenz et al. (2023), the impact of primordial non-Gaussianity on the scalar induced SGWB has been studied beyond the generalized local ansatz (131), paying attention to whether it can self-consistently be important in concrete early-universe scenarios. As pointed out above, the gravitational waves spectrum can be split into two contributions: the one set by the power spectrum, and the one determined by the connected four point function of the curvature perturbation, namely the primordial trispectrum. First, it is shown that this trispectrum-induced gravitational wave spectrum can always be written as a sum of three "channels" contributions, independently of the precise shape of the trispectrum. Second, the question addressed in Garcia-Saenz et al. (2023) is: can the trispectrum be observationally relevant for the scalar induced SGWB in conventional set-ups where non-Gaussianity provides subleading corrections to the Gaussian scalar signal?, i.e. in inflationary scenarios where interactions generating non-Gaussianity maintain perturbative control. Formulating a precise quantitative criterion ensuring perturbative control in strongly scale-dependent theories is difficult and model-dependent. Hence, the focus of Garcia-Saenz et al. (2023) is on scale-invariant theories. In this context, it is shown that neither regular trispectrum shapes peaking in the so-called equilateral configurations, nor local trispectrum shapes diverging in soft momentum limits, can contribute significantly. Indeed, those contributions are always bound to be smaller than an order-one (or smaller) number multiplying the relative one-loop correction to the scalar power spectrum, necessarily much smaller than unity in order for the theory to be under perturbative control. This result is shown to be also valid in a toy-model for the phenomenologically more relevant situation of a scale-dependent scalar spectrum, calling for more in-depth investigations of this question.

5.4 Induced SGWB anisotropies

It is interesting to note that the induced SGWB associated with PBH production[14] will present some angular anisotropies, which can be quantified by computing the two-point correlation function of the density field in different directions. The LISA experiment will be able to detect anisotropies with an angular resolution of $\ell \lesssim 15$ (Contaldi et al. 2020) (see also Baker et al. 2021a), which will require the spatial points to be separated by a non-negligible fraction of the present horizon. Since the characteristic scales of the perturbations generating the SGWB are much smaller than those distances, $k_* \, |\vec{x} - \vec{y}| \gg 1$, and that the emission takes place near horizon crossing with the assumption of Gaussian scalar perturbations, the Equivalence Principle dictates that the anisotropies decay as $(k_* |\vec{x} - \vec{y}|)^{-2}$. Therefore, the anisotropy coarse grained with the resolution of the experiment will be undetectable (Bartolo et al. 2020a). Another possibility, as far as anisotropies imprinted at formation are concerned, is given by the presence of non-Gaussianity which, by providing a correlation between small and large scales, may allow large scale modulation of power and lead to a large-scale anisotropy (Bartolo et al. 2020a). Finally, the propagation of GWs across disconnected regions of the Universe leads to large-scale anisotropies at detection (Alba and Maldacena 2016; Contaldi 2017; Cusin et al. 2017, 2019a; Jenkins and Sakellariadou 2018; Bartolo et al. 2019a, 2020b; Renzini and Contaldi 2019; Bertacca et al. 2020).

Assuming a local, scale-invariant, shape of non-Gaussianity $\zeta = \zeta_{\rm g} + \frac{3}{5} f_{\rm NL} \, \zeta_{\rm g}^2$ and taking into account propagation effects, one can compute the two-point correlation function of the direction dependent GW energy density contrast $\delta_{\rm GW}(\eta, \vec{x}, k) = \Omega_{\rm GW}(\eta, \vec{x}, k)/\Omega_{\rm GW}(\eta, k) - 1$, defined as the relative difference between the direction dependent GW energy density and its monopole contribution, in a spherical harmonics decomposition as (following the notation used in Bartolo et al. 2020a)

$$\left\langle \delta_{{\rm GW},\ell m} \delta^*_{{\rm GW},\ell' m'} \right\rangle = \delta_{\ell \ell'} \delta_{m m'} \, \hat{C}_\ell(k), \tag{132}$$

where (Bartolo et al. 2020a)

$$\sqrt{\frac{\ell(\ell+1)}{2\pi} \, \hat{C}_\ell(k)} \simeq \frac{3}{5} \left| 1 + \tilde{f}_{\rm NL}(k) \right| \left| 4 - \frac{\partial \ln \Omega_{\rm GW}(\eta, \, k)}{\partial \ln k} \right| \mathcal{P}^{1/2}_{\zeta_{\rm L}}, \tag{133}$$

and k denotes the momentum on small-scales. Here $\mathcal{P}_{\zeta_{\rm L}}$ denotes the power spectrum at large scales, while the momentum dependent non-Gaussian parameter is defined as

[14] The generation of a SGWB in the early Universe may also happen due to other mechanisms, possibly with characteristic anisotropic signatures, see for example García-Bellido et al. (2016), Cook and Sorbo (2012), Guzzetti et al. (2016), Bartolo et al. (2016), Ricciardone and Tasinato (2018), Caprini and Figueroa (2018), Geller et al. (2018), Dimastrogiovanni et al. (2020).

$$\tilde{f}_{\rm NL}(k) \equiv \frac{8 f_{\rm NL}}{4 - \frac{\partial \ln \Omega_{\rm GW}(\eta, k)}{\partial \ln k}}. \tag{134}$$

The presence of non-Gaussianity in the curvature perturbation, constrained by the Planck collaboration to be $-11.1 \lesssim f_{\rm NL} \lesssim 9.3$ at 95% C.L. (Akrami et al. 2020a), would also induce a significant variation on large scales of the PBH abundance through the modulation of the power on small scales induced by the long modes. If PBHs compose a non-negligible fraction of the DM, the presence of isocurvature modes in the DM density fluid associated to the non-Gaussianity (Young and Byrnes 2015) is strongly constrained by the CMB observations (Akrami et al. 2020b).

In Fig. 28, we show the expected GW anisotropy for the choice of a monochromatic and log-normal small-scale power spectrum of the curvature perturbation peaked at the LISA maximum sensitivity frequency. The dot-dashed lines identify the corresponding GW abundance at the present epoch evaluated at the peak frequency, while the colored region identifies the range of parameters allowed by the Planck constraints, and we choose the non-linear parameter $f_{\rm NL} \gtrsim -1/3$ to avoid the failure of the perturbative approach in the computation of the PBH abundance happening at larger negative values, see for example (Young and Byrnes 2013; Yoo et al. 2019). One finds that if a large fraction of the dark matter is composed of PBH, one expects a highly isotropic and Gaussian SGWB, up to propagation effects. On the contrary, the detection of a large amount of anisotropy in the signal associated to the PBH formation scenario would imply that only a small fraction of the DM can be accounted by PBHs (Bartolo et al. 2020a).

5.5 From PBH poisson fluctuations

At small scales, the gravitational interaction between individual PBHs (scattering, merging, etc.) results in the production of GWs. In this section, we are interested in the large-scale counterpart of this signal, i.e. at distances much larger than the mean separation length between PBHs, for which PBHs can be described by a pressureless fluid. This fluid is endowed with density perturbations, which can be treated within

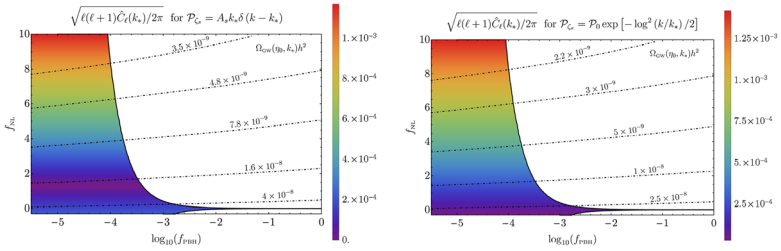

Fig. 28 Contour plot showing the amount of GWs anisotropy in the parameter space of $f_{\rm PBH}$ and $f_{\rm NL}$ allowed by the Planck constraints for the choice of a monochromatic and log-normal small-scale power spectrum, respectively, with peak frequency around the maximum sensitivity of LISA. The dot-dashed lines identify the corresponding present GWs abundance. Image reproduced with permission from Bartolo et al. (2020a), copyright by IOP and SISSA Image reproduced with permission

the framework of cosmological perturbation theory. In particular, these PBH density perturbations induce the production of GWs through second-order effects studied both in the context of general relativity (Papanikolaou et al. 2021; Domènech et al. 2021) as well in the context of modified gravity (Papanikolaou et al. 2022, 2023b).

To be explicit, we assume that PBHs form in a radiation-dominated, homogeneous Universe (at large scales, primordial curvature perturbations provide a contribution to inhomogeneities but they are negligible compared to the ones generated by PBHs, at least in the range of scales we are interested in). One can therefore view PBHs as a dust fluid, formed from the transition of a fraction of the radiation energy density into PBH dust matter. Assuming that PBHs are randomly distributed at formation time (i.e. they have Poisson statistics), the energy density associated to them is inhomogeneous while the total energy density of the background is homogeneous. Consequently, the energy density perturbation of the PBH matter field can be described by an isocurvature Poisson fluctuation. If the initial abundance of PBHs is large enough, PBHs can potentially dominate the Universe energy density content and in that case the isocurvature PBH energy density perturbation in the radiation era is converted into an adiabatic curvature perturbation deep in the PBH dominated era. These early PBH dominated eras can be naturally driven by ultralight PBHs, which evaporate before BBN (García-Bellido et al. 1996; Hidalgo et al. 2012; Martin et al. 2020b; Zagorac et al. 2019) and addressing a plethora of cosmological problems, most importantly that of Hubble tension (Hooper et al. 2019; Papanikolaou 2023b).

At second-order in cosmological perturbation theory, the gravitational potential of these Poisson distributed PBHs induce a SGWB which may be detected by LISA (Papanikolaou et al. 2021; Domènech et al. 2021). More precisely, as found in Papanikolaou et al. (2021), this gravitational potential gives rise to the following power spectrum for Φ:

$$\mathcal{P}_\Phi(k) = \frac{2}{3\pi}\left(\frac{k}{k_{\rm UV}}\right)^3 \left(5 + \frac{4}{9}\frac{k^2}{k_{\rm d}^2}\right)^{-2}, \tag{135}$$

where Φ is the Bardeen gravitational potential, $k_{\rm d}$ is the comoving scale exiting the Hubble radius at PBH domination time and $k_{\rm UV} \equiv a/\bar{r}$, where $\bar{r}$ corresponds to the mean PBH separation distance. Note that $k > k_{\rm UV}$ corresponds to distances within the mean separation distance, where the granularity of the PBH matter field and the associated non-linear effects become important, and where the gas of PBHs cannot be described by a fluid anymore. This is why the above expression should be restricted to $k < k_{\rm UV}$ with $k_{\rm UV}$ acting as a UV cutoff (hence the notation). Since $\bar{r} \propto a$, $k_{\rm UV}$ is a fixed comoving scale. From Eq. (135), one can see that $\mathcal{P}_\Phi$ is made of two branches: when $k \ll k_{\rm d}$, $\mathcal{P}_\Phi \propto k^3$, while $\mathcal{P}_\Phi \propto 1/k$ when $k \gg k_{\rm d}$. It reaches a maximum when $k \sim k_{\rm d}$, where $\mathcal{P}_\Phi$ is of order $(k_{\rm d}/k_{\rm UV})^3$.

The energy density of the associated induced GWs can be computed according to the prescription described in Sect. 5.1, where one should use the linear transfer function during a matter (PBH) dominated era. One can show that it peaks at the comoving scale that exits the Hubble radius at the onset of the PBH domination era (Papanikolaou et al. 2021). This scale corresponds to the frequency displayed in Fig. 29 as a function of the fraction of the Universe made of PBHs at the time they

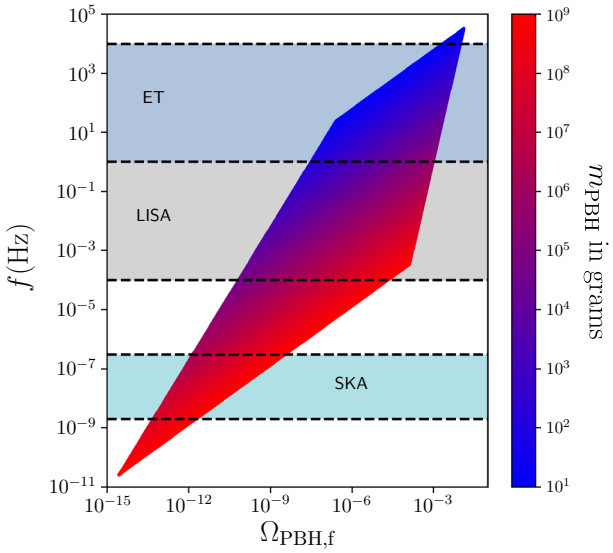

Fig. 29 Frequency at which the GWs induced by a dominating gas of PBHs peak, as a function of their energy density fraction at the time they form, $\Omega_{\mathrm{PBH,f}}$ (horizontal axis), and their mass m_{PBH} (colour coding). The region of parameter space that is displayed corresponds to values of m_{PBH} and $\Omega_{\mathrm{PBH,f}}$, such that black holes form after inflation, dominate the Universe content for a transient period and Hawking evaporate before BBN. We also impose that the induced GWs do not lead to a backreaction problem before they evaporate, see Papanikolaou et al. (2021) for more details. For comparison, the frequency detection bands of ET, LISA and SKA are shown. Image reproduced with permission from Papanikolaou et al. (2021), copyright by IOP and SISSA Image reproduced with permission

form, and their mass (assuming an initial monochromatic distribution of PBHs). One can see that a substantial fraction of parameter space lies within the LISA detection band. This would provide a unique access to ultralight PBHs, which otherwise cannot be detected through the PBH merging channel or the second-order induced GW channel presented in Sect. 5.1.

Let us point out that the calculation of the precise amplitude of the signal is more complex as it implies to follow its transition from the PBH-dominated era to the subsequent radiation-dominated (RD) era. This is why Papanikolaou et al. (2021) was followed up by Inomata et al. (2020), Domènech et al. (2021) where, by considering a monochromatic PBH mass function and a sudden transition from the PBH-dominated era to the radiation era after evaporation, it was found that the GW signal discussed here is not suppressed due to the PBH → RD transition and it can be detectable from LISA and other GW experiments. In fact, the fate of the signal through the transition depends on whether the transition is sharp or slow. In particular, on the one hand, when the transition is gradual, the gravitational potential oscillates with a decreasing amplitude (Inomata et al. 2019b), suppressing in this way the signal. On the other hand, if the transition is sudden, the gravitational potential oscillates very fast with large amplitudes up to the end of the transition and therefore the GW signal is expected to be enhanced in this case (Inomata et al. 2019a).

It is also important to mention that another calculation was performed in Kozaczuk et al. (2022), where the contribution from scales for which the density contrast becomes non linear during the PBH-dominated era was removed (note that the gravitational potential always remains linear). Assuming again a monochromatic PBH mass function, a reduction was found in the GW signal which removed it from the reach of LISA, while remaining accessible by other GW experiments like BBO. However, to fully access the signal, one should take into account more realistic extended mass functions which will make PBHs evaporate at different times, leading in this way to a longer period of PBH-domination, a fact which can potentially enhance the detectability of the signal discussed here. However, if the transition is gradual due to different PBH evaporation times, this will give an extra suppression as found in Inomata et al. (2019b). One therefore is met with two competitive effects which should be considered together in the case of a calculation with realistic extended mass distributions. Interestingly, as it was shown recently in Papanikolaou (2022a) if one accounts for a cosmologically motivated power-law primordial curvature power spectrum for the generation of an extended PBH mass function, they can find that despite the gradualness of the transition the GW signal can be detectable by LISA and can serve as a novel probe to constrain cosmological parameters of the early Universe. It is worth to mention as well that as pointed out recently in Papanikolaou et al. (2024b), the portal of GWs induced by PBH energy density fluctuations can serve also a novel probe of primordial non-Gaussianities.

5.6 From PBH mergers

5.6.1 Formulation

Overlapped GWs from PBH mergers form a SGWB. The spectral shape of the SGWB, its constraints by GW observations, and its implication to PBH physics have been discussed in the literature (Mandic et al. 2016; Clesse and García-Bellido 2017a; Wang et al. 2018; Raidal et al. 2017; Chen et al. 2019; Wang et al. 2019; De Luca et al. 2020d; Bavera et al. 2022; Bagui and Clesse 2022). For a binary system with a circular orbit, the single source energy spectrum $\frac{dE_{GW}}{d\ln f_r}$ for the inspiral phase is given by

$$\frac{dE_{GW}}{d\ln f_r} = \frac{\pi^{2/3}}{3}\mathcal{M}_c^{5/3}(Gf_r)^{2/3}, \tag{136}$$

where $f_r = (1+z)f$ is the GW frequency in the source frame with f being the frequency at the observer. One may use a more accurate fitting formula, which includes the contributions of the inspiral, merger, and ringdown parts of the BBH waveform (see (Ajith et al. 2011) for the details). The amplitude of the SGWB is given by summing up the energy spectrum of each binary system and by taking into account the merger rate distribution. At the end, the GW spectral abundance is written as

$$\Omega_{\rm GW}(f) = \frac{1}{\rho_{\rm c}} \int_0^{z_{\rm max}} {\rm d}z \, \frac{N(z)}{(1+z)} \frac{{\rm d}E_{\rm GW}}{{\rm d}\ln f_{\rm r}}, \tag{137}$$

where $\rho_{\rm c}$ is the critical density of the Universe, $\rho_{\rm c} = \frac{3H_0^2}{8\pi G}$. Here $N(z)$ is the number density of GW events at redshift z and can be related to the merger rate in a comoving volume from the previous section $R_{\rm EB/LB}$

$$N(z) = \frac{R_{\rm EB/LB}}{(1+z)H(z)}. \tag{138}$$

In the case of a broad mass distribution, we have to integrate Eq. (137) over the BH masses, m_1 and m_2, and we get (Clesse and García-Bellido 2017a)

$$\begin{aligned} \Omega_{\rm GW}(f) = & \frac{8\pi^{5/3} G^{5/3}}{9H_0^2} f^{2/3} \int_0^{z_{\rm max}} {\rm d}z \, \frac{1}{H(z)(1+z)^{4/3}} \\ & \times \int {\rm d}\ln m_1 \int {\rm d}\ln m_2 \, R_{\rm EB/LB} \mathcal{M}_{\rm c}^{5/3}(m_1, m_2). \end{aligned} \tag{139}$$

The maximum frequency at the observer is determined by the innermost stable circular orbit which is given by

$$f_{\rm ISCO} \approx 4.4\,{\rm kHZ} \, \frac{M_\odot}{m_1 + m_2} \frac{1}{1+z}. \tag{140}$$

This can be translated to the maximum redshift as

$$z_{\rm max} = \frac{f}{f_{\rm ISCO}} - 1. \tag{141}$$

As described in Sect. 4, there are two binary formation channels, dubbed early and late binaries. Below, we discuss the SGWB for each case.

5.6.2 Early binaries

The SGWB from early binaries is obtained by inserting the corresponding merging rate distribution of Eq. (101) into the above expression, Eq. (139). Since the merging rate depends on the redshift z, $R_{\rm EB}(z, m_1, m_2) = R_{\rm EB}(m_1, m_2) \times (t(z)/t_0)^{-34/37-0.29}$ for $f_{\rm PBH} = 1$, with $t(z)$ being the elapsed time between the Big Bang and a certain redshift z, this redshift-dependent factor can be included in the integral over z (Bagui and Clesse 2022),

$$\int_0^{z_{\rm max}} \frac{(t(z)/t_0)^{-34/37-0.29}}{(1+z)^{4/3} H(z)} {\rm d}z = 5.92 H_0^{-1}, \tag{142}$$

where $z_{\rm max} \simeq 100$, as discussed in Sect. 4.1.3. The integral on the masses can be performed by direct numerical integration or by using a Monte-Carlo method as in Clesse and García-Bellido (2017a), e.g. for a synthetic population of 10^6 BHs.

Expressing the merging rate in $\mathrm{yr}^{-1}\mathrm{Gpc}^{-3}$, the chirp mass in solar masses $M_\odot$ and the frequency in Hz, one obtains

$$\Omega_{\rm GW}(f)h^2 \simeq 6.46\times10^{-14}\int \mathrm{d}\ln m_1 \int \mathrm{d}\ln m_2 \left(\frac{R_{\rm EB}(m_1,m_2)}{\mathrm{yr}^{-1}\mathrm{Gpc}^{-3}}\right)\left(\frac{f}{\mathrm{HZ}}\right)^{2/3}\left(\frac{\mathcal{M}_{\rm c}}{M_\odot}\right)^{5/3}, \tag{143}$$

where the constant h takes the value $h = 0.67$. The resulting SGWB coming from early PBH binaries following a log-normal mass function (with mean mass $\mu = 2.5M_\odot$ and width $\sigma = 1$) as well as a mass distribution with thermal features are displayed in Fig. 30, as a function of the frequency. In the log-normal case, one notices that the spectrum reaches its highest point at 100 Hz and is suppressed at lower frequencies, whereas in the broad mass distribution case including QCD-induced features, it peaks at $10^{-6}, 10^{-3}$ and around 100 Hz. In the latter case, for ground-based detectors, one observes that the SGWB is above the projections for the LVK and ET detector designs, but just below the current limits imposed by the third observing run of LVK. The next observing runs of LVK may therefore be decisive for the detection of this SGWB. In addition, the detected signal by NANOGrav located within the interval $10^{-8} - 10^{-7}$ Hz with $\Omega_{\rm GW}h^2 \sim 10^{-9}$ (gray window, see Sect. 7.6.4 for more details) could be interpreted as a background of GWs in the model for late binaries in clusters (see next Subsection). However, in the early binaries model, the amplitude of the SGWB is always lower than the signal detected by NANOGrav, and therefore this model can not explain the observed signal. The detectability with LISA will be discussed in Sect. 8. The dependence of the SGWB on the PBH masses for

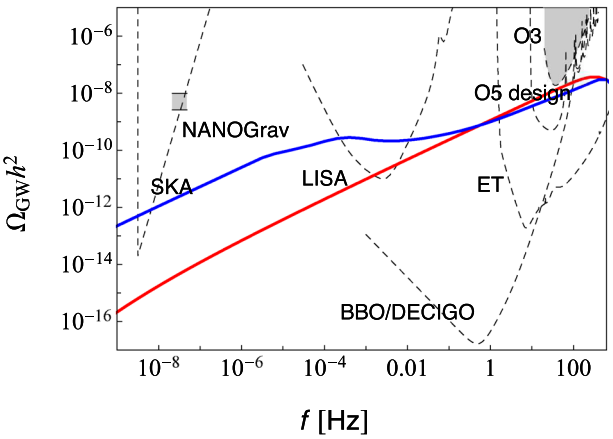

Fig. 30 The SGWB spectrum $\Omega_{\rm GW}h^2$ for early PBH binaries with a log-normal mass function (in red, with central mass $\mu = 2.5M_\odot$ and width $\sigma = 1$) and a broad mass distribution with scalar spectral index $n_{\rm s} = 0.970$ (in blue), and $f_{\rm PBH} = 1$. The numerical spectrum also shows the sensitivities of the ground-based interferometers: the LVK O3 Run, the final LVK and the Einstein Telescope (ET). The sensitivity of future space-based interferometers is also shown (LISA, BBO/DECIGO). The Pulsar Timing Array (PTA) considered here is the Square Kilometer Array (SKA) (Schmitz 2021). The NANOGrav 12.5 signal is represented by the gray square (see Sect. 7.6.4 for more details) Image reproduced with permission

the case of a broad mass function from the thermal history of the Universe is shown in Fig. 31.

5.6.3 Late binaries in clusters

In the case of late binary formation channel discussed in Sect. 4.2, the merger rate is given by Eq. (109). Substituting it into Eq. (139), the energy spectrum for the low-frequency inspiral regime can be estimated as

$$\Omega_{\rm GW}(f)h^2 \approx 2.41 \times 10^{-14} R_{\rm clust} \left(\frac{f}{\rm HZ}\right)^{2/3} \times \int {\rm d}m_1\, {\rm d}m_2 \frac{f(m_1) f(m_2)\, (m_1+m_2)^{23/21}}{(m_1\, m_2)^{5/7}}\,, \tag{144}$$

with the masses in solar masses and we use $h = 0.67$. In Fig. 32, we show the SGWB spectrum generated by late PBH binaries in clusters (we have chosen the virial velocity in those clusters to be $v_{\rm vir} = 5$ km/s, compatible with velocity dispersions in faint dwarf galaxies) for the log-normal mass function (with the central mass $\mu = 2.5 M_\odot$ and the variance $\sigma = 1$) and the thermal history mass distribution (with $n_{\rm s} = 0.97$ and no running). Here, the normalization is taken by requiring that the integral of the merger rate at $z = 0$ over the mass range $[5, 100] M_\odot$ gives a total rate of $38\,{\rm yr}^{-1}{\rm Gpc}^{-3}$. Note that the SGWB spectrum at lower frequency is highly uncertain, as it can be suppressed by many factors such as the tilt and running of the primordial curvature perturbation spectrum, and by the eventual presence of a cutoff in the merger rate due to the fact that massive PBHs become isolated (Braglia et al.

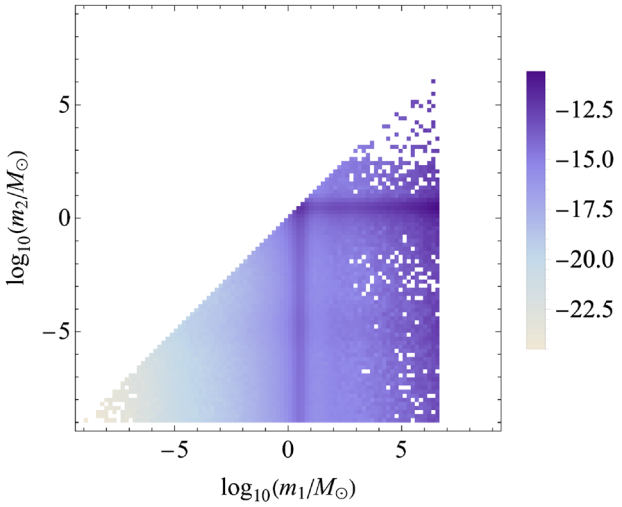

Fig. 31 Contribution to different PBH masses to the SGWB from early PBHs binaries (with $f_{\rm PBH} = 1$). The color bar indicates the values of the quantity $\log_{10}(\Omega_{\rm GW}h^2)$, which is represented as a function of the logarithm of the masses m_1 and m_2 of the PBHs following a mass distribution from the thermal history of the Universe (with $n_{\rm s} = 0.97$) for LISA frequencies (10^{-3} Hz). Image reproduced with permission from Bagui and Clesse (2022), copyright by Elsevier Image reproduced with permission

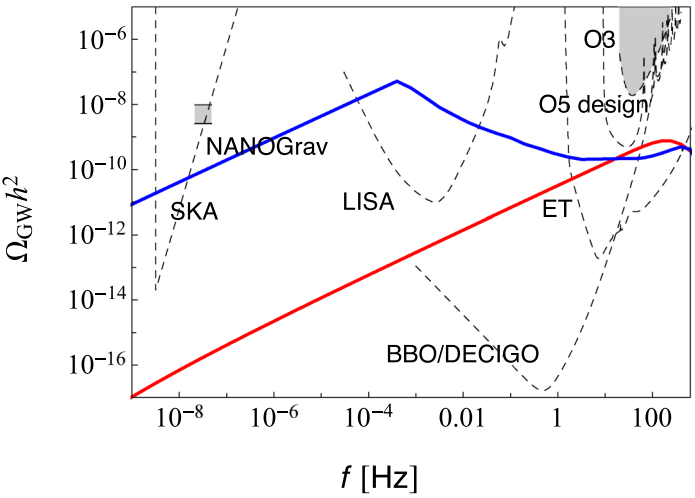

Fig. 32 The SGWB spectrum $\Omega_{GW}h^2$ for late PBH binaries in clusters with $f_{PBH} = 1$ for a log-normal mass function (in red, with the central mass $\mu = 2.5M_\odot$ and the width $\sigma = 1$) and a broad mass distribution (in blue, with $n_s = 0.97$ and no running). Note that here we use Ajith et al. (2011) for the single source GW energy spectrum instead of Eq. (139) Image reproduced with permission

2021b). We can see that, in the case of the log-normal mass function, the spectrum peaks around the ISCO frequency of PBH binaries (for $m_{PBH} = 2.5M_\odot$, we get $f_{ISCO} \sim 900$ Hz), while in the case of the thermal history mass function, we see that

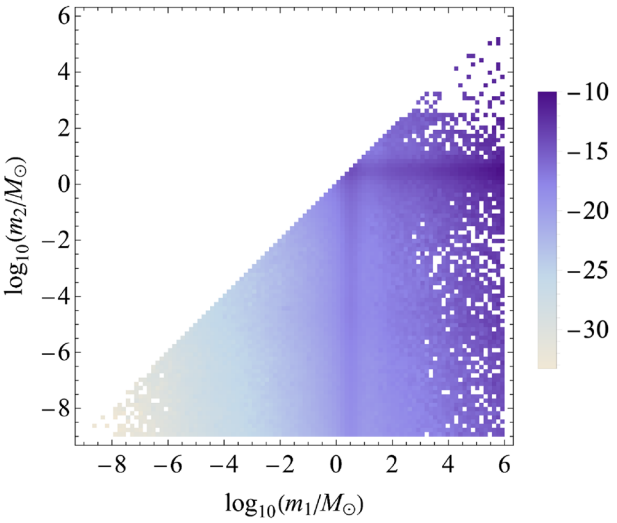

Fig. 33 The mass contribution to the SGWB from late PBHs binaries in clusters (with $f_{PBH} = 1$). The color bar indicates the values of the quantity $\log_{10}(\Omega_{GW}h^2)$, which is represented as a function of the logarithm of the masses m_1 and m_2 of the PBHs following a mass distribution from the thermal history of the

the SGWB is produced over a wide range of frequencies because of the wide mass distribution. In Fig. 33, we show which PBH masses contribute to the GW amplitude $\Omega_{\rm GW}$ at the LISA frequency 10^{-3}Hz. We can see that $2M_\odot$ mass PBHs paring with more massive ones are giving large contribution to the SGWB.

5.7 SGWB duty cycle

The SGWB of binary origin may have a characteristic property which could be used to infer the origin of BHs. If the interval between BBH events is larger than the typical duration of the signal, the waveforms do not overlap, and the SGWB becomes strongly non-Gaussian (sometimes referred to as intermittent or popcorn signal).

One of the quantities to characterize such a non-Gaussian characteristics of the SGWB is the so-called astrophysical duty cycle. The duty cycle gives the average number of events present in the frequency bin and can be defined using the event rate $\mathrm{d}R/\mathrm{d}z$ and the duration of the signal staying in the frequency bin $\mathrm{d}\bar{\tau}/\mathrm{d}f$ as

$$\frac{\mathrm{d}D}{\mathrm{d}f} = \int \mathrm{d}z \frac{\mathrm{d}R}{\mathrm{d}z}\frac{\mathrm{d}\bar{\tau}}{\mathrm{d}f}. \tag{145}$$

Here, $\mathrm{d}\bar{\tau}/\mathrm{d}f$ is determined by the chirp mass $\mathcal{M}_c^z = (1+z)\mathcal{M}_c$ as

$$\frac{\mathrm{d}\bar{\tau}}{\mathrm{d}f} = \frac{5}{96\pi^{8/3}}(G\mathcal{M}_c^z)^{-5/3} f^{-11/3}, \tag{146}$$

where $\mathcal{M}_c^z = (1+z)\mathcal{M}_c$. When the duty cycle is larger than unity, the GW events overlap, and the background is in the so-called *continuous* regime. On the other hand, if the interval between events is comparable or larger than the typical duration of the signal, the duty cycle becomes smaller than unity, and the statistical properties are strongly non-Gaussian. The value of the duty cycle can differ depending on the mass function and the redshift distribution. Thus, the non-Gaussian property could be used to distinguish primordial and astrophysical scenarios (Mukherjee and Silk 2020; Braglia et al. 2023a) together with the spectral shape (Mukherjee and Silk 2021).

5.8 From close encounters

Overlapped GWs from PBH close encounters can also form a SGWB (García-Bellido et al. 2022). The formulation is the same as the PBH mergers, Eq. (139). In the case of close hyperbolic encounters (CHE), the energy emitted per logarithmic frequency bin is given by (De Vittori et al. 2012; García-Bellido and Nesseris 2017)

$$\frac{\mathrm{d}E_{\rm GW}^{\rm CHE}}{\mathrm{d}\ln f_{\rm r}} = v\frac{\mathrm{d}E_{\rm GW}}{\mathrm{d}v} = \frac{4\pi}{45}\frac{G^3 m_1^2 m_2^2}{a^2 c^5 v_0} v^5 F_{\rm E}(v)\,, \tag{147}$$

where we have defined $v \equiv 2\pi v_0 f_{\rm r}$ and $v_0^2 \equiv a^3/GM$, and the semi-major axis a is related to the initial velocity as $a = GM/v_0^2$. The function $F_{\rm E}(v)$ describes the dependence on eccentricity e and it is given by (García-Bellido and Nesseris 2018)

$$
\begin{aligned}
v^5 F_{\rm E}(v) &\simeq \frac{12F(v)}{\pi y\,(1+y^2)^2}\, e^{-2v\,\xi(y)}\,,\\
F(v) &= v^2\big(1-y^2-3\,v\,y^3+4\,y^4+9\,v\,y^5+6\,v^2y^6\big)\,,\\
\xi(y) &= y-\tan^{-1}y\,,\\
y &= \sqrt{e^2-1}\,.
\end{aligned}
\tag{148}
$$

Substituting Eqs. (115) and (148) into Eq. (139), we can estimate the peak frequency

$$
f_{\rm peak} \simeq 4.3\,{\rm HZ}\left(\frac{y}{0.01}\right)^{-3}\left(\frac{M}{2000M_\odot}\right)^{1/2}\left(\frac{a}{1\,{\rm AU}}\right)^{-3/2}\,,
\tag{149}
$$

and the peak amplitude

$$
\begin{aligned}
\Omega_{\rm GW}(f_{\rm peak}) \approx & 0.9\times10^{-13}\,h\left(\frac{\Omega_{\rm m}}{0.3}\right)^{-1/2}\left(\frac{\Omega_{\rm DM}}{0.25}\right)^{2}\left(\frac{\delta_{\rm loc}}{10^8}\right)\left(\frac{a}{0.1{\rm AU}}\right)^{-2}\\
&\times\left(\frac{y}{0.01}\right)^{-5}\frac{m_1}{100M_\odot}\,\frac{m_2}{100M_\odot}\,\frac{m_1+m_2}{200M_\odot}\,.
\end{aligned}
\tag{150}
$$

In Fig. 34, we show the SGWB spectrum originating from close hyperbolic encounters, compared with the one from binary PBHs. We find that, for the modest

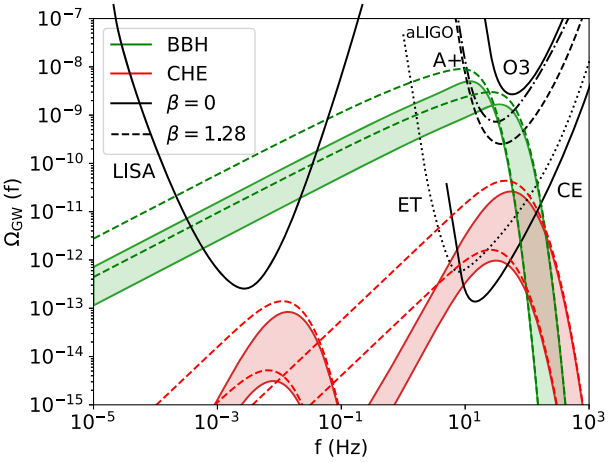

Fig. 34 Comparison of the SGWB spectrum originating from BBHs and CHEs, both for $\beta = 0$ (solid) and $\beta = 1.28$ (dashed), where β is a parameter characterizing the redshift dependence of the merger rate as $\tau^{\rm BBH} \propto (1+z)^{\beta}$. For the BBH curves, we take $m_1 = m_2 = 100 - 300\,M_\odot$ and $v_0 = 30$km/s. The CHE curves correspond to the same range of masses with $a_0 = 5$AU, $y_0 = 2\times10^{-3}$ for frequencies around 10 Hz, and $a_0 = 5\cdot10^7$AU, $y_0 = 10^{-5}$ in the mHz range. For all cases, we assume log-normal distributions for a_0, y_0 and the PBH mass, of respective widths $\sigma_a, \sigma_y = 0.1$, $\sigma_m = 0.5$, as well as $f_{\rm PBH} = 1$. The bands come from the possible range of parameters a_0 and y_0. For a smaller fraction of PBHs, the GW spectral amplitude simply scales as $\Omega_{\rm GW} \propto f_{\rm PBH}^2$. Image and estimated LISA sensitivity from García-Bellido et al. (2022), copyright by the author(s) Image reproduced with permission

choice of the parameter values, it is difficult to be reached by LISA. This difficulty can easily be understood if we rewrite Eq. (150) in terms of the peak frequency,

$$\begin{aligned}\Omega_{\rm GW}^{\rm CHE}(f_{\rm peak}) \approx 3.1\times 10^{-13}\, h \\ \times \left(\frac{\Omega_{\rm m}}{0.3}\right)^{-1/2}\left(\frac{\Omega_{\rm DM}}{0.25}\right)^{2}\left(\frac{\delta_{\rm loc}}{10^{8}}\right)\left(\frac{f_{\rm peak}}{50\,{\rm HZ}}\right)^{4/3} \\ \times \left(\frac{y}{0.01}\right)^{-1}\frac{m_1}{100M_\odot}\frac{m_2}{100M_\odot}\left(\frac{m_1+m_2}{200M_\odot}\right)^{1/3}.\end{aligned} \tag{151}$$

We can see that the maximum amplitude $\Omega_{\rm GW}^{\rm CHE}(f_{\rm peak})$ grows with $f_{\rm peak}^{4/3}$. Thus, the peak amplitude of the background decays significantly at low frequencies. However, we have observed that the peak amplitude tends to get enhanced when we make the log-normal distribution of the mass function wider. Thus, by considering a different PBH mass function, we may be able to find a case where the SGWB from CHEs gives an interesting contribution at the LISA frequency.

It is worth mentioning that it could be tested by third-generation ground-based GW detectors such as Einstein Telescope and Cosmic Explorer. Although the CHE curves are below the BBH curves, loud BBH events can be detected individually and subtracted from the data, which may allow us to probe the other SGWB component below the green curve.

5.9 Summary

In this section we have explored the different sources of SGWBs related to PBHs:

- The SGWB induced at second order by the large curvature fluctuations leading to PBH formation. Interestingly, it peaks at PTA frequencies for stellar-mass PBHs, which makes it a very complementary probe to test a possible primordial origin of GW events seen in ground-based detectors. This SGWB could be connected to the recent pulsar timing array observations, see Sect. 7.6.4 for more details. Future GW detectors like LISA, Cosmic Explorer and Einstein Telescope will probe small PBHs, in particular in the asteroid-mass range that remains so far unconstrained (see the section on the limits on the abundance of PBHs).
- The SGWB from the Poisson fluctuations in the initial PBH distribution, even if they were so small that they have totally evaporated. This mechanism could allow to probe the possible PBH formation at very high energy scales, up to the reheating phase and the GUT energy.
- The stochastic background from early binaries, in particular if PBHs have an extended mass function. In such a case the SGWB is boosted by the merging of binaries with extreme mass ratios.
- The stochastic background from late binaries in clusters, which for stellar-mass PBHs is smaller than the SGWB from early binaries at frequencies corresponding to ground-based GW detectors. Because the merger rates are not suppressed with

the PBH mass, it would however be the dominant background at low frequencies, i.e. in the LISA and PTA frequency range.

- The stochastic background from close hyperbolic PBH encounters in clusters, probably undetectable with LISA but in the range of future ground-based GW detectors.

The SGWB is therefore expected to be an interesting complementary signal that will help to distinguish between PBH formation models, mass functions, clustering histories and binary origins.

6 Gravitational-waves and large scale structure correlations

6.1 Introduction

Primordial black holes, both in the case where they comprise a large part of the dark matter or if they exist only in small numbers, are part of the Large-Scale Structure (LSS) of the Universe, and their observational relation with the other matter-energy components can be generally different with respect to black holes of stellar origin. By the time LISA will be online, there will be data from several large-scale structure experiments, both preceding and overlapping in time with LISA. These include observations from the ground and from space, such as DESI (Aghamousa et al. 2016a, b), the Vera Rubin Observatory (Blum et al. 2022), Euclid (Amendola et al. 2018), SPHEREx (Doré et al. 2014), Nancy Roman (Wenzl et al. 2022), ATLAS (Wang et al. 2019) and the SKAO (Weltman et al. 2020), all together providing galaxy catalogs over a very wide range of scales both in width and deepness, at unprecedented accuracy. It will therefore be paramount to take advantage of such data for PBH science. In this Section we discuss a few possible ways to use gravitational wave observations in combination with the LSS to constrain the existence and abundance of PBHs. LSS observations can be cross-correlated with different types of GW maps, both from the resolved mergers of compact objects and the stochastic backgrounds.

Cross-correlations between GWs from resolved compact object mergers and galaxies have been first investigated in Laguna et al. (2010). Later, it was suggested that the cross-correlation of mergers with EM counterparts could be used to constrain dark energy and modified gravity models (Camera and Nishizawa 2013). After the first detections of gravitational waves, Oguri (2016) investigated the possibility to constrain the distance-redshift relation using such correlations.

It was then shown that the cross-correlation of resolved mergers with LSS catalogs can be used to test primordial black hole scenarios (Raccanelli et al. 2016a; Raccanelli 2017; Scelfo et al. 2018, 2022) and different astrophysical models (Scelfo et al. 2020). More recently, an additional technique for constraining PBH abundances, formation channels and redshift distributions using only GW data has been proposed and studied (Libanore et al. 2022).

The GWxLSS probe became very popular and several different approaches have been suggested and investigated (see e.g., Raccanelli 2017; Scelfo et al. 2018; Cañas

Herrera et al. 2020; Calore et al. 2020), looking at both correlations with resolved sources and the SGWB (Cusin et al. 2018a; Jenkins et al. 2018, 2019a; Bertacca et al. 2020; Yang et al. 2020; Mukherjee and Silk 2020; Alonso et al. 2020). Here we present the main ideas and formalism developed so far; specific predictions for LISA and investigations involving similar analyses for extreme mass-ratio inspirals (EMRIs) and intermediate mass black holes (IMBHs) are currently being developed.

6.2 GW-galaxy cross-correlations for resolved events

The cross-correlation of LSS catalogs with maps of gravitational waves coming from the merger of compact objects will provide information on several astrophysical and cosmological parameters and models, and has been investigated in a variety of works from exploring ways to indirectly detect GWs to proper data correlations.

The idea of cross-correlations with the LSS in order to constrain the existence of PBHs and their abundances was first explored in Raccanelli et al. (2016a) and then further investigated in e.g., Raccanelli (2017), Scelfo et al. (2018, 2020). The possibility of using the GWxLSS correlation to test the existence of PBHs comes from the fact that primordial and astrophysical binary black holes trace the LSS in different ways. This reflects into the fact that the bias of the hosts of the binary system will be different when the BHs have different progenitors and formation channels. This bias quantifies the relation between underlying matter fluctuations and in the number of observed sources.

In Bird et al. (2016), it was shown that primordial black holes preferentially merge in lower biased objects and thus have a lower cross-correlation with luminous galaxies. This happens because binary PBHs would preferentially merge in halos with low velocity dispersion, which are low-mass halos and hence with very little or absent star formation; these objects have a bias $b < 1$. On the other hand, mergers of compact objects that are the endpoint of stellar evolution naturally happen for the vast majority within star forming-rich halos, which have larger galaxy bias values, $b > 1$. In the linear biasing scheme, b quantifies the relation between the underlying matter distribution and observed sources, $\delta_{\mathrm{O}} = b\delta_{\mathrm{m}}$. This reasoning is valid for PBH binary systems that form by capture (*late binary* formation scenario), as these systems form in the local Universe.

However, there is also another way to have mergers of PBH binaries, which we have referred to as *early binary* mergers. In this case, within the standard formation scenario (i.e., the collapse of primordial curvature perturbations at horizon re-entry), PBHs should form in the peaks of the initial matter distribution, and therefore they will trace the dark matter field. As a consequence, such mergers should be unbiased tracers of the underlying density field.

The overall catalog of PBH mergers will consequently be composed of a mixture of early and late binaries, with the total bias being the weighted average of the two.

Therefore, by measuring the amplitude of the angular cross-correlation of galaxy maps with catalogues of compact-object mergers, which directly depends on the bias of the mergers' hosts, one can statistically probe the abundance of PBH mergers. This information can also be used to discriminate between different astrophysical models (see e.g., Scelfo et al. 2020).

In order to measure the mergers' hosts bias, one can use the 3D angular power spectrum:

$$C_\ell^{\mathrm{GW}\times\mathrm{LSS}}(z_1,z_2)=\frac{2}{\pi}\int \mathrm{d}k\, k^2 P(k)\,\Psi_\ell^{\mathrm{GW}}(k,z_1)\Psi_\ell^{\mathrm{LSS}}(k,z_2)\,, \tag{152}$$

where $P(k)$ is the matter power spectrum and the kernels $\Psi_\ell^X(z)$ include the observational window functions and the relevant physical effects:

$$\Psi_\ell^X(k,z_i)=\int_{z_i-\Delta z}^{z_i+\Delta z} N^X(z)b^X(z)D(z)W(z)\Delta_\ell^X(k,z)\,\mathrm{d}z\,; \tag{153}$$

here X will be either GW or LSS, and W are observational window functions related to the experiment specifications (i.e., they include information on the redshift distribution and survey geometry and sensitivity). The Δ_ℓ terms are the (gauge-independent) observed overdensities and include effects from intrinsic clustering, peculiar velocity and Doppler contributions, lensing and gravitational potentials containing in this way information information on the underlying cosmological and astrophysical models. They are usually expressed as:

$$\Delta_\ell(k)=\Delta_\ell^{\mathrm{den}}(k,z)+\Delta_\ell^{\mathrm{rsd}}(k,z)+\Delta_\ell^{\mathrm{dop}}(k,z)+\Delta_\ell^{\mathrm{len}}(k,z)+\Delta_\ell^{\mathrm{gr}}(k,z)\,. \tag{154}$$

For details on these terms, their derivation and physical meaning, see e.g., Bonvin and Durrer (2011), Challinor and Lewis (2011), Raccanelli et al. (2016b), Scelfo et al. (2018).

6.3 GW-galaxy cross-correlations for the stochastic background

In addition to the signal from mergers detected by interferometers, there is another signal coming from the superposition of many unresolved sources. These will form a stochastic background of gravitational waves, as discussed in Sect. 5. Obviously, primordial black holes, if they exist, would contribute to this signal, and their associated GW backgrounds have been discussed in Sect. 5. This will be particularly relevant for LISA, as the SGWB is expected to be a product of LISA's observations.

In the same fashion as for the catalogs of resolved events described above, we can cross-correlate the stochastic background with the LSS; such correlation will contain information on the redshift distribution, mass function and clustering behavior of the sources. Moreover, the observed signal will be the combination of the stochastic GW background from astrophysical objects, denoted AGWB, the one from primordial black holes, and the one generated from inflation; disentangling the signal and distinguishing between the different sources will be of paramount importance to obtain information about black hole and early Universe physics, and one of the most promising ways to do so is thanks to the SGWB–LSS correlation.

Given that the GW energy density depends not only on astrophysical properties but also on cosmological perturbations, it will correlate with other cosmological probes; moreover, GWs will experience projection effects that will need to be accounted for in order to observe the signal in the appropriate frame (Bertacca et al.

2020; Bellomo et al. 2022). Some preliminary works on this have been done in the last few years, including forecasts for the cross-correlation signals between GW observatories and future galaxy surveys, as e.g., Euclid and SKA (see, e.g., Contaldi 2017; Cusin et al. 2017, 2018b, a; Jenkins et al. 2019a, 2018; Cusin et al. 2019b, 2020; Jenkins and Sakellariadou 2019; Jenkins et al. 2019b; Bertacca et al. 2020; Pitrou et al. 2020; Mukherjee and Silk 2020; Alonso et al. 2020).

In a similar way to the case of resolved mergers, the most natural observable is the angular cross power spectrum that correlates the energy density of the AGWB with galaxy number counts:

$$C_\ell^{\mathrm{AGWB}\times\mathrm{LSS}} = \frac{2}{\pi}\int \mathrm{d}k\, k^2 P(k)\Psi_\ell^{\mathrm{AGWB}}(k)\Psi_\ell^{\mathrm{LSS}}(k), \tag{155}$$

where most quantities are the same of Eq. (152), and the dependence on astrophysical models and parameters can be included in the expression for the AGWB energy density. This is usually written as the total GW energy density (denoted by the superscript TOT) per logarithmic frequency f_o and solid angle Ω_o along the line-of-sight $\hat{\mathbf{n}}$ of a SGWB, defined in e.g., Cusin et al. (2017), Bertacca et al. (2020) as

$$\Omega_{\mathrm{GW}}^{\mathrm{TOT}}(f_\mathrm{o},\hat{\mathbf{n}}) = \frac{f_\mathrm{o}}{\rho_\mathrm{c}}\frac{\mathrm{d}\rho_{\mathrm{GW}}^{\mathrm{TOT}}}{\mathrm{d}f_\mathrm{o}\mathrm{d}\Omega_\mathrm{o}}\ ; \tag{156}$$

this contains both a background, which is homogeneous and isotropic, and a direction-dependent contribution; the total relative fluctuation can thus be defined as (similarly to Eq. (132)):

$$\Delta_{\mathrm{AGWB}}^{\mathrm{TOT}}(f_\mathrm{o},\hat{\mathbf{n}}) = \frac{\Omega_{\mathrm{AGWB}}^{\mathrm{TOT}} - \bar{\Omega}_{\mathrm{AGWB}}^{\mathrm{TOT}}}{\bar{\Omega}_{\mathrm{AGWB}}^{\mathrm{TOT}}}\ . \tag{157}$$

Studies of the cross-correlation between the AGWB with galaxy number counts are presented in Cusin et al. (2018a), Mukherjee and Silk (2020), Cañas Herrera et al. (2020), Alonso et al. (2020), Cusin et al. (2019b); Yang et al. (2020), Bellomo et al. (2022). This allows a tomographic reconstruction of the redshift distribution of sources, and can be also useful for the shot noise characterization (in the case of ground-based detectors) (Alonso et al. 2020). The cross-correlation shows that the combination of galaxy surveys with the AGWB can be a powerful probe for GW physics and can be a robust observational probe for multi-messenger cosmology.

6.4 GW × LSS forecasts

Constraints on the presence of PBHs from measurements of the GWxLSS have been forecasted for the case of resolved GW signals, correlated with both galaxy surveys (Raccanelli et al. 2016a; Raccanelli 2017; Scelfo et al. 2018; Bosi et al. 2023) and intensity mapping experiments (Scelfo et al. 2022). Constraints coming from measurements of the stochastic background signal are currently being worked out. In this Section we introduce the formalism for obtaining such forecasts and report some of the results present in literature.

The correlation of two tracers (X, Y) can be estimated from tomographic maps of their number counts and evaluating their N-point statistics; in the case we consider here, this is the angular power spectrum $C_\ell^{XY}(z_i, z_j)$ of the tracer X in redshift bin z_i and the tracer Y in z_j. Assuming that the noise comes only from the standard shot noise contribution, the total signal extracted from the maps is:

$$\left\langle a_{\ell m}^{X}(z_i) a_{\ell' m'}^{Y^*}(z_j) \right\rangle = \delta_{\ell\ell'}\delta_{mm'}\tilde{C}_\ell^{XY}(z_i, z_j) = \delta_{\ell\ell'}\delta_{mm'}\left[C_\ell^{XY}(z_i, z_j) + \delta_{XY}\delta_{ij}\mathcal{N}_\ell^{X}(z_i)\right],$$

where $\mathcal{N}_\ell$ is the noise angular power spectrum.

The observed signal will receive contributions from several physical effects, coming from the cosmological perturbations described above, from density, velocity, lensing and gravity effects. It is important to include all of them to avoid mis-estimating parameters, best fit values and errors when doing parameter inference, as shown in Bellomo et al. (2022), Bernal et al. (2020).

Forecasts obtained so far have been based on the `Multi_CLASS` (Bellomo et al. 2020) and `GW_CLASS` codes (Bellomo et al. 2022). `Multi_CLASS` is the first public Boltzmann code that allows to compute the angular power spectrum for multiple galaxy (and other tracers) populations. The code lets the user specify specific properties of different tracers, such as its number density redshift distribution and bias, magnification bias and evolution bias parameters, while `GW_CLASS` calculates the stochastic signal from astrophysical mergers and accounts for all the astrophysical and projection effects contributions.

The first suggestion that this observable can be used to constrain PBHs was presented in Raccanelli et al. (2016a), where after introducing the concept, it is shown that the cross-correlation between galaxies mapped by future radio surveys and GW interferometers could distinguish between primordial and stellar origin of merging black holes. Such possibility depends on the merger rate of primordial black holes and the angular resolution of the GW interferometer. In that work, to obtain the results, a minimum-variance estimator was introduced for the *effective correlation amplitude*, $A_c \equiv r \times b_{GW}$, where r is the cross-correlation coefficient of Eq. (152). This cross-correlation coefficient parametrises the extent to which two biased tracers of the matter field are correlated (Tegmark and Peebles 1998).

The minimum-variance estimator for the effective correlation amplitude is given by (see e.g. Jeong and Kamionkowski 2012):

$$\widehat{A_c} = \frac{\Sigma_\ell \tilde{C}_\ell F_\ell / \mathrm{Var}[\tilde{C}_\ell]}{\Sigma_\ell F_\ell^2 / \mathrm{Var}[\tilde{C}_\ell]}, \tag{158}$$

where $\tilde{C}_\ell$ is the measured power spectrum and $F_\ell \equiv d\tilde{C}_\ell / d\widehat{A_c} \propto b_g$. The variance of this estimator is then:

$$\sigma^2_{\widehat{A_c}} = \left[\sum_\ell \frac{F_\ell^2}{\mathrm{Var}[\tilde{C}_\ell]}\right]^{-1}, \tag{159}$$

which can be used to forecast the measurement error when neglecting that of other parameters.

More generally, the measurement error for specific parameters in a given experiment can be estimated using Fisher analysis. For this case, we write the Fisher matrix as:

$$F_{\alpha\beta} = \sum_{\ell} \frac{\partial C_\ell}{\partial \vartheta_\alpha} \frac{\partial C_\ell}{\partial \vartheta_\beta} \sigma_{C_\ell}^{-2} \,, \tag{160}$$

where $\vartheta_\alpha = \{A_{\rm c}, b_{\rm g}\}$; the derivatives of the power spectra C_ℓ are evaluated at fiducial values $\bar{\vartheta}_\alpha$ corresponding to the scenario at hand, and σ_{C_ℓ} are errors in the power spectra.

The results in Raccanelli et al. (2016a) were obtained by computing the 2×2 Fisher matrix for the parameters $\{A_{\rm c}, b_{\rm g}\}$, using a prior on the galaxy bias corresponding to the precision reached by fitting the amplitude of the galaxy auto-correlation function $C_\ell^{\rm gg}$, using a value of $\ell_{\rm max} = 200$, which yields a $\sim 10\%$ precision in the measurement of the bias $b_{\rm g}$. For more details on this analysis, see Raccanelli et al. (2016a).

Subsequently, in Raccanelli (2017), such analysis was updated to include improved merger rate estimates from the LVK collaboration, for the correlation with different possible surveys with the SKA. In Fig. 35 we show forecasts for different experiments, considering different versions of LVK and ET correlated with HI and continuum SKA surveys. The bars show the constraints on $A_{\rm c}$ for different values of a parameter R that encapsulates uncertainties on the merger rate, which is degenerate with observation times from the gravitational wave interferometers.

Following this, in Scelfo et al. (2018), Libanore et al. (2023) these forecasts are updated by including all projection effects, and inserted in an analysis of a null hypothesis test by comparing two models, one in which the BHs origin is stellar, the other in which it is primordial. One model is assumed as a fiducial model. Then, by computing the signal-to-noise ratio (SNR), it is checked whether the alternative

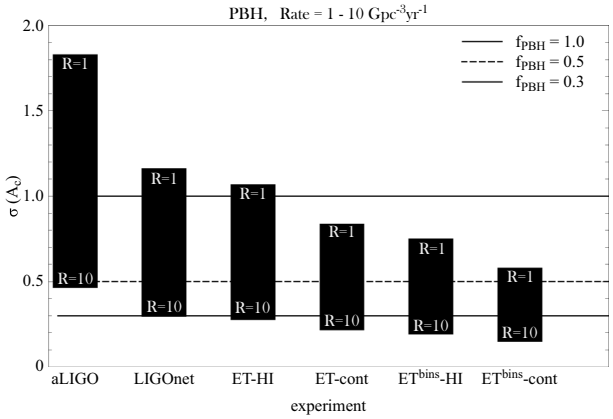

Fig. 35 Forecast errors on the cross-correlation amplitude, $A_{\rm c}$, for different experiment combinations, varying merger rates and years of observations. Each column corresponds to a GW detector experiment, for merger rates from 1 to 10 Gpc^{-3}yr^{-1}. Horizontal lines show the expected difference in the cross-correlation between (late binary) PBH and stellar binaries, for different values of $f_{\rm PBH}$ Image reproduced with permission

model can be differentiated from the fiducial one. The null hypothesis is that the model is indistinguishable from the fiducial, which happens for low values of the signal-to-noise ratio.

For instance, the distance of an alternative model from the fiducial can be quantified using a $\Delta\chi^2$ statistics. The $\Delta\chi^2$ is given by the logarithm of a likelihood, and the SNR can be written as:

$$\left(\frac{S}{N}\right) = f_{\rm sky}\sum_{2}^{\ell_{\rm max}}(2\ell+1)\left(\mathbf{C}_\ell^{\rm Alternative}-\mathbf{C}_\ell^{\rm Fiducial}\right)^T {\rm Cov}_\ell^{-1}\left(\mathbf{C}_\ell^{\rm Alternative}-\mathbf{C}_\ell^{\rm Fiducial}\right),$$

where $\mathbf{C}_\ell^T = \left(C_\ell^{\rm gg}(z_1,z_1),\cdots,C_\ell^{\rm gGW}(z_1,z_1),\cdots,C_\ell^{\rm GWGW}(z_1,z_1),\cdots\right)$, $f_{\rm sky}$ is the sky fraction covered by both GW and galaxy surveys and ${\rm Cov}_\ell$ is the covariance matrix, computed from the angular power spectra of the fiducial model.

In Fig. 36, we show the results where the fiducial model is taken to that of stellar BH mergers (see Scelfo et al. 2018). The bars span values between 0.1 and 10 for the factor r, (similarly to the case of Fig. 35, this parametrises the uncertainties on the BBH merger rates, which is degenerate with the observation time of the experiment).

After updates on the BBH merger rate and the specifications for the DESI survey (Aghamousa et al. 2016a), forecasts for the SNR for detecting a component of PBHs are shown in Bosi et al. (2023) and a summary plot can be found in Fig. 37. Here the color code is for the SNR, while on the x-axis is the fraction of PBH mergers from the total of observed BBH mergers observed by the Einstein Telescope, and on the y-axis the parameter r, as defined above.

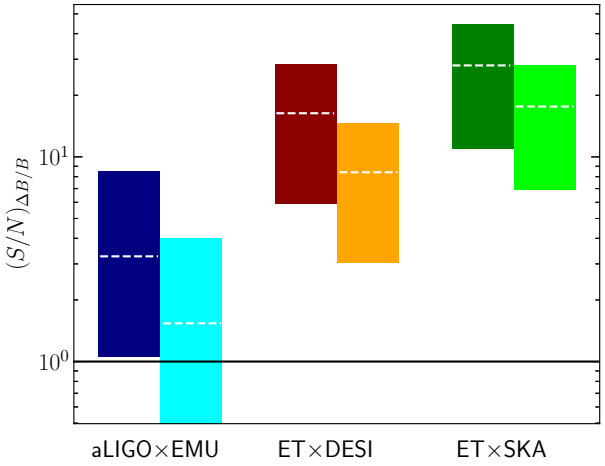

Fig. 36 Expected signal-to-noise ratio $(S/N)_{\Delta B/B}$ from the Fisher matrix analysis, for cross-correlations between GW observations (from either LVK or Einstein Telescope) and high-redshift LSS surveys (EMU, DESI and SKA), assuming stellar black holes for the fiducial scenario. In each case, the left bar corresponds to late PBH binaries and the right bar to early PBH binaries. Image reproduced with permission from Scelfo et al. (2018), copyright by IOP and SISSA Image reproduced with permission

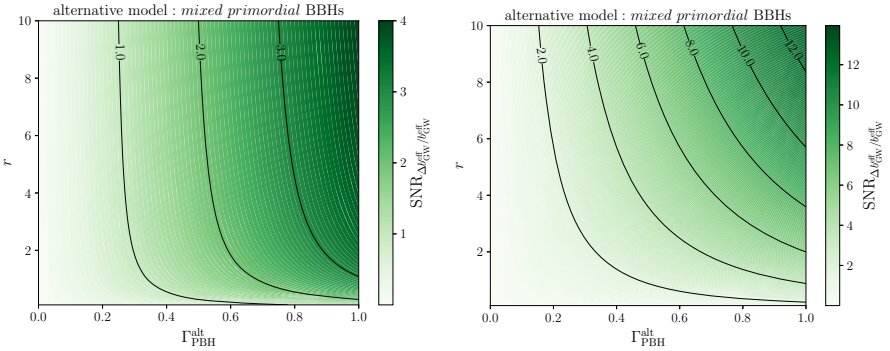

Fig. 37 SNR for detecting a fraction Γ of PBH mergers out of the total BBH mergers observed by the ET, as a function of the parameter r, cross-correlated with DESI. The left panel shows the result using just DESI x ET, while the right panel includes Planck priors. Results from Bosi et al. (2023) Image reproduced with permission

These results show that the presence of primordial black holes can be detected by using the cross-correlation with LSS and the fact that these objects cluster differently than astrophysical black hole mergers. Future GW detectors and LSS surveys will therefore allow a detection of a primordial component in the catalog of binary black hole mergers.

The cross-correlation forecasts shown so far are for the correlation of GWs with resolved galaxies; naturally, a similar analysis can be done for observations of intensity mapping. A first investigation for the 21 cm Intensity Mapping (IM) observed with the SKAO is presented in Scelfo et al. (2022), focusing on the IM of the neutral hydrogen (HI) from the proposed 21 cm IM survey with the SKAO and on resolved GW events from the merger of BBHs as detected by the Einstein Telescope (ET) (Sathyaprakash et al. 2012). A cross-correlation signal is expected, as both HI and GWs trace the cosmic density field, and once again they do so in different ways depending on astrophysical and cosmological models. In particular, for constraining the PBH abundance, results were obtained for the predicted IM from the SKAO correlated with GWs from ET.

6.5 Summary

Gravitational-wave observations of resolved black hole mergers and of the stochastic background can be cross-correlated with the LSS to constrain the existence and abundance of PBHs. This technique may provide additional information to test and constrain the different PBH scenarios, the PBH abundance within a broad range of masses, as well as binary formation channels. This will be of particular interest for the next generation of LSS surveys, such as DESI, Euclid and SKA, and gravitational-wave detectors like LISA, Einstein Telescope or Cosmic Explorer.

7 Current limits

The most stringent limits on $f_{\rm PBH}$ as a function of the PBH mass for a monochromatic mass function are represented in Fig. 38. Zooms on evaporation-based limits (between $10^{-19}M_\odot$ and $10^{-15}M_\odot$), on microlensing limits (between $10^{-11}M_\odot$ and $1M_\odot$) and on the multiple limits above $1\,M_\odot$ are shown in Fig. 39. These astrophysical and cosmological probes of PBHs can be divided in six categories, each related to the physical process at the origin of a PBH signature in observations:

1. Observations impacted by *black hole evaporation*
2. *Microlensing* observations
3. Observational signatures of the black hole *dynamics*
4. Observations impacted by the black hole *accretion*
5. Indirect constraints from *density fluctuations*

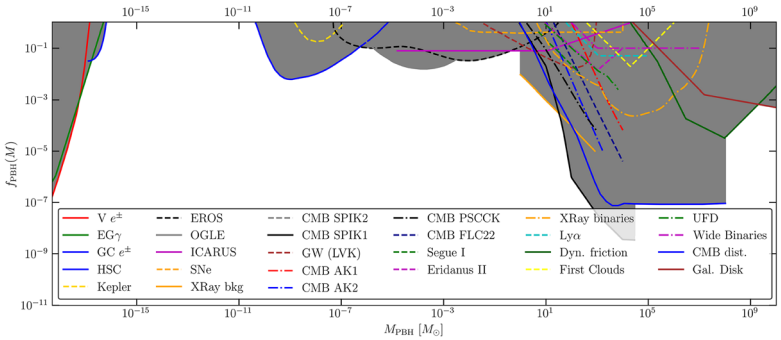

Fig. 38 We show the most stringent claimed constraints in the mass range of phenomenological interest. They come from the Hawking evaporation producing extra-galactic gamma-ray (EG γ) (Arbey et al. 2020), $e^\pm$ observations by Voyager 1 (V $e^\pm$) (Boudaud and Cirelli 2019), positron annihilations in the Galactic Center (GC e^+) (DeRocco and Graham 2019) and gamma-ray observations by INTEGRAL (INT) (Laha et al. 2020) (for other constraints in the ultra-light mass range see also Carr et al. 2010; Ballesteros et al. 2020a; Laha 2019; Poulter et al. 2019; Dasgupta et al. 2020; Laha et al. 2021). We plot microlensing searches by Subaru HSC (Niikura et al. 2019b; Smyth et al. 2020), MACHO/EROS (E) (Alcock et al. 2001; Allsman et al. 2001), Ogle (O) (Niikura et al. 2019a) and Icarus (I) (Oguri et al. 2018). Other constraints come from CMB distortions. In black dashed, we show the ones assuming disk accretion (Planck D in Serpico et al. (2020) and Poulin et al. (2017), from left to right) while in black solid the ones assuming spherical accretion (Planck S in Serpico et al. (2020) and both photo- and collisional ionization in Ali-Haïmoud and Kamionkowski (2017), from left to right). Only Serpico et al. (2020) includes the effect of the secondary dark matter halo in catalysing accretion. Additionally, constraints coming from X-rays (Xr) (Manshanden et al. 2019) and X-Ray binaries (XrB)(Inoue and Kusenko 2017) are shown. Dynamical limits coming from the disruption of wide binaries (WB) (Quinn et al. 2009), survival of star clusters in Eridanus II (EII) (Brandt 2016) and Segue I (SI) (Koushiappas and Loeb 2017a; Stegmann et al. 2020) are also shown. LVK stands for the constraint coming from LVK measurements (Ali-Haïmoud et al. 2017; Raidal et al. 2019; Vaskonen and Veermäe 2020; Wong et al. 2021). Constraints from Lyman-α forest observations (Lα) come from Murgia et al. (2019). We neglect the role of accretion which has been shown to affect constraints on masses larger than $\mathcal{O}(10)M_\odot$ (De Luca et al. 2020c, d) in a redshift dependent manner. See Carr et al. (2021c) for a comprehensive review on constraints on the PBH abundance. Notice that there are no stringent bounds in the asteroid mass range (Katz et al. 2018; Montero-Camacho et al. 2019) where LISA may constrain PBHs through the search of a second order SGWB Image reproduced with permission

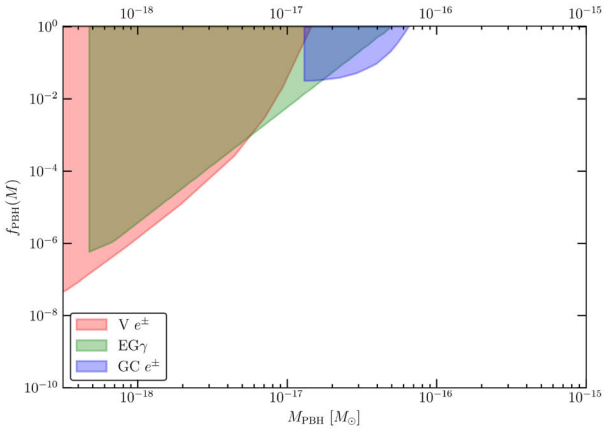
10^{-18}
10^{-17}
10^{-16}
10^{-15}
10^{0}
10^{-2}
10^{-4}
10^{-6}
10^{-8}
10^{-10}
$f_{\rm PBH}(M)$
V $e^{\pm}$
EGγ
GC $e^{\pm}$
$M_{\rm PBH}\ [M_\odot]$

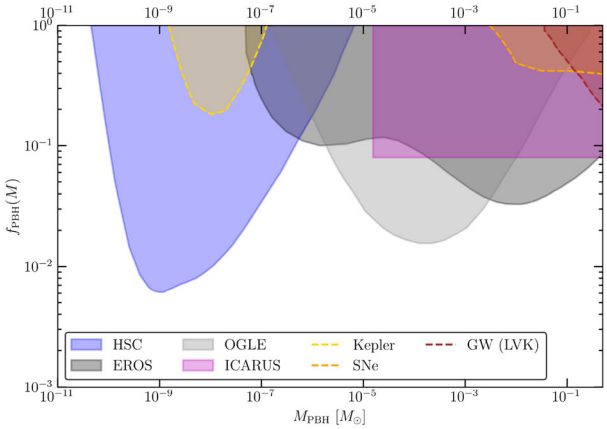
10^{-11}
10^{-9}
10^{-7}
10^{-5}
10^{-3}
10^{-1}
10^{0}
10^{-1}
10^{-2}
10^{-3}
$f_{\rm PBH}(M)$
HSC
EROS
OGLE
ICARUS
Kepler
SNe
GW (LVK)
$M_{\rm PBH}\ [M_\odot]$

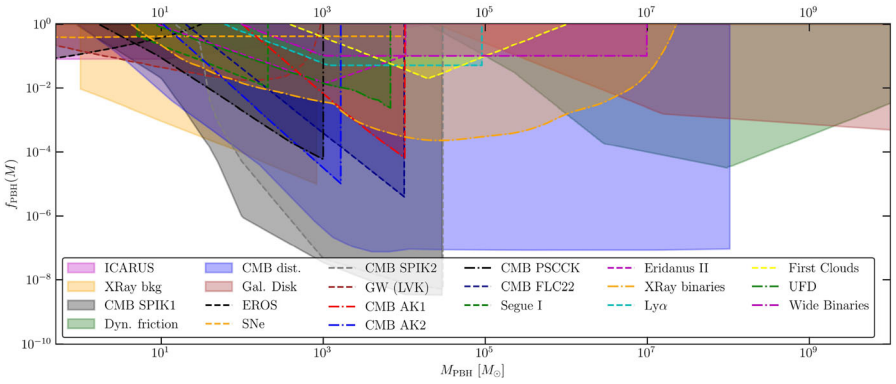
10^{1}
10^{3}
10^{5}
10^{7}
10^{9}
10^{0}
10^{-2}
10^{-4}
10^{-6}
10^{-8}
10^{-10}
$f_{\rm PBH}(M)$
ICARUS
XRay bkg
CMB SPIK1
Dyn. friction
CMB dist.
Gal. Disk
EROS
SNe
CMB SPIK2
GW (LVK)
CMB AK1
CMB AK2
CMB PSCCK
CMB FLC22
Segue I
Eridanus II
XRay binaries
Lyα
First Clouds
UFD
Wide Binaries
$M_{\rm PBH}\ [M_\odot]$

◀**Fig. 39** Zooms over some claimed limits on the PBH abundance $f_{\rm PBH}$ for a monochromatic distribution of mass $m_{\rm PBH}$, in the asteroid-mass range where constraints are dominated by various probes of PBH Hawking evaporation (top panel), in the planetary-mass and low stellar-mass range up to $m_{\rm PBH} \sim 10 M_\odot$ coming from microlensing surveys (middle panel), and in the range from stellar-mass up to the supermassive PBHs, from a combination of accretion, dynamical, GW and indirect constraints (bottom panel). The legend indicates the origin of each represented limit. It is worth noticing that all those limits are subject to important uncertainties and can be highly model dependent, moving up and down with different model and astrophysical assumptions. The possible limitations and sources of uncertainties are discussed in the text Image reproduced with permission

6. Signatures of PBHs in *gravitational-wave* observations

In this section, we review these current limits on the PBH abundance and comment on possible caveats and model dependences. We also discuss the possible observational evidences for the existence for PBHs, in relation with these limits.

7.1 PBH evaporation

We review here the PBH constraints relying on their evaporation. Let us note that the PBH mass is expressed in grams through this Section, and not in solar mass as for all the other probes, for a better consistency with the literature and because these constraints concern PBHs much lighter than a solar mass.

7.1.1 Big-bang nucleosythesis (BBN)

PBHs with masses $10^9 - 10^{13}$ g can affect the abundance of light elements produced during the Big-Bang Nucleosynthesis through Hawking radiation and the related emitted particles, allowing to set constraints on the abundance of low-mass PBHs (Carr et al. 2021c). In particular, for PBHs with masses $m_{\rm PBH} \approx 10^9 - 10^{10}$g, Hawking radiated mesons and antinucleons induce extra interconversion processes of protons to neutrons, increasing the neutron-to-proton ratio at the time of freeze-out of the weak interaction (Vainer and Naselskii 1978), and consequently leading to an increase in the final ^{4}He abundance (Miyama and Sato 1978). Regarding PBHs with masses $m_{\rm PBH} \approx 10^{10} - 10^{12}$g, long-lived high energy hadrons produced out of PBH evaporation, such as pions, kaons and nucleons, remain long enough in the ambient medium to trigger dissociation processes of light elements produced during BBN (Kohri and Yokoyama 2000), reducing the abundance of ^{4}He and increasing the one of d,^{3}He,^{6}Li and ^{7}Li. Finally, for PBHs with $m_{\rm PBH} \approx 10^{12} - 10^{13}$g, photons produced from the particle cascade process further dissociate ^{4}He, increasing the abundance of light synthesized elements (Keith et al. 2020; Acharya and Khatri 2020). However, it is important to stress that the BBN constraints carry out some uncertainties regarding the baryon-to-photon ratio, the reaction and the decay rates of the elements produced during the BBN processes (Kawasaki et al. 2005a, b).

7.1.2 Gamma-rays and neutrinos from Hawking radiation

The lifetime of a PBH due to its evaporation in standard model particles can be approximated as (Carr et al. 2010)

$$\tau \approx 400 \left(\frac{m_{\rm PBH}}{10^{10}\,{\rm g}} \right)^3 {\rm s}. \tag{161}$$

For a PBH with mass 5×10^{14} g, its lifetime is close to the age of Universe. Thus, such low-mass PBHs can be probed by looking for bursts of gamma rays. Such searches have been performed by the Water Cherenkov Observatories, Imaging Atmospheric Cherenkov Telescopes (IACTs) and gamma-ray space observatories. So far, no gamma-ray signal that could be due to PBH evaporation has been detected. The current limits are summarized in Table 3. These are expressed in terms of the PBH burst rate densities $\dot{B}_{\rm PBH}$, describing the number of bursts from PBH evaporation in the local Universe in a unit of volume per unit of time.

The observations of Galactic gamma-ray emission by INTEGRAL (Laha et al. 2020) also put a bound on the mass above which PBHs could constitute the entirety of DM, $m_{\rm PBH} > 1.2 \times 10^{17}$g, under some relatively conservative assumptions. New analysis of the diffuse soft gamma-ray emission towards the inner Galaxy measured by INTEGRAL/SPI over 16 years (Berteaud et al. 2022), implementing a spatial template fit of SPI data, an improved instrumental background model, and including the spatial distribution of MeV photons emitted by the evaporating PBHs into the fitting procedure, strengthens this lower bound to $m_{\rm PBH} \gtrsim 4 \times 10^{17}$g.

Table 3 Current limits on the local PBH burst rate density from different gamma-ray observatories

Experiment	$\dot{B}_{\rm PBH}$ Upper limit (pc^{-3}yr^{-1})	Burst duration (s)	$T_{\rm obs}$	References
Milagro	3.1×10^5 (99% CL)	0.001	1673 d	Abdo et al. (2015)
Milagro	1.2×10^4 (99% CL)	0.01	1673 d	Abdo et al. (2015)
Milagro	5.4×10^4 (99% CL)	0.1	1673 d	Abdo et al. (2015)
Milagro	3.6×10^4 (99% CL)	1	1673 d	Abdo et al. (2015)
Milagro	3.8×10^4 (99% CL)	10	1673 d	Abdo et al. (2015)
Milagro	6.9×10^4 (99% CL)	100	1673 d	Abdo et al. (2015)
VERITAS	2.22×10^4 (99% CL)	30	747 h	Archambault (2018)
H.E.S.S	4.9×10^4 (95% CL)	1	2600 h	Glicenstein et al. (2013)
H.E.S.S	1.4×10^4 (95% CL)	30	2600 h	Glicenstein et al. (2013)
H.E.S.S	5.6×10^4 (99% CL)	10	2860 h	Tavernier et al. (2020)
H.E.S.S	2.0×10^3 (95% CL)	120	4816 h	Aharonian et al. (2023)
Fermi-LAT	$7.2^{+8.1}_{-2.4} \times 10^3$ (99% CL)	1.26×10^8	1.26×10^8 s	Ackermann et al. (2018)
HAWC	$3.3^{+0.3}_{-0.1} \times 10^3$ (99% CL)	0.2	959 d	Albert et al. (2020)
HAWC	$3.5^{+0.4}_{-0.2} \times 10^3$ (99% CL)	1	959 d	Albert et al. (2020)
HAWC	$3.4^{+0.4}_{-0.1} \times 10^3$ (99% CL)	10	959 d	Albert et al. (2020)

The prospects for detection of gamma-ray signals from PBH evaporation for the future Southern Wide Field of View Gamma-ray Observatory (SWGO) have been estimated in López-Coto et al. (2021): it will be sensitive to local PBH burst rate densities $\dot{B}_{\rm PBH}$ of the order of $\sim 50\,{\rm pc}^{-3}{\rm yr}^{-1}$, improving by more than one order of magnitude the limits from current experiments.

7.1.3 Positron annihilation in the Galactic Center

PBH limits can be obtained with observations of the 511 keV line from the Galactic Center with INTEGRAL. Positrons produced by evaporating PBHs subsequently propagate throughout the Galaxy. As they annihilate, they contribute to the Galactic 511 keV line. Both monochromatic and log-normal mass distributions have been considered, e.g. giving the corresponding limit of $f_{\rm PBH} < 1$ for $m_{\rm PBH} \lesssim 2 \times 10^{17}$ g for a log-normal mass distribution with $\sigma = 0.5$ and $m_{\rm PBH} < 2 \times 10^{17}$ g with $\sigma = 0.1$ (DeRocco and Graham 2019). Estimates for different background assumptions (Ballesteros et al. 2020a) show that for the low ($\times 0.1$) power law background model, $f_{\rm PBH}$ can reach 1 up to $m_{\rm PBH} \sim 5 \times 10^{17}$g. Estimates for different mass distributions and spins (Dasgupta et al. 2020) give the mass limit $m_{\rm PBH} \sim 3 - 5 \times 10^{18}$ g for the log-normal mass distribution with $\sigma = 1$, $a^* = 0.5 - 1$ and $f_{\rm PBH} = 1$. It has been recently shown (Keith et al. 2022) that future MeV-scale gamma-ray observatories e-ASTROGAM or AMEGO would be able not only to detect the Hawking radiation from the Inner Galaxy, but also to precisely measure the abundance and mass distribution of PBHs responsible for the Galactic 511 keV line.

7.1.4 $e^{\pm}$ observations by Voyager 1

The measurements of interstellar low-energy (sub-GeV) $e^{\pm}$ flux are used to constrain the PBH fraction of DM in the Galaxy (Boudaud and Cirelli 2019). These electrons and positrons would be due to PBH evaporation. The obtained limits are based on local measurements, independent of the cosmological model. This flux must be shielded for Earth-bounded detectors by the magnetic field of the Sun. However, limits can be obtained from Voyager-1 measurements since it is now beyond the heliopause.

The Hawking radiation flux of $e^{\pm}$ is computed within the fully general diffusion-convection-reacceleration model of propagation with the parameters adjusted to the AMS-02 data. For the log-normal mass distribution of PBHs with a width σ larger than 1 and a central value $\mu \lesssim 10^{17}$ g, a PBH fraction larger than 1% of DM is excluded by the Voyager 1 data.

7.1.5 Ultra-faint dwarf galaxies

The ultra-faint dwarf galaxies (UFDGs), such as Leo T, also provide some limits on light, evaporating PBHs, through the heating of the interstellar medium gas (Kim 2021). The emitted energetic particles can heat and ionize the gas, in particular the fast electrons can deposit a substantial fraction of their energy and heat the interstellar

gas through the Coulomb interaction. The ultra-faint dwarf galaxy Leo T is of particular interest, not only because it is highly dark matter dominated but also because it has a large amount of neutral hydrogen and a relatively low metal abundance. In Kim (2021), limits are obtained for non-spinning PBHs, with masses between 2×10^{15} g and 10^{17} g as low as $f_{\rm PBH} \lesssim 10^{-3}$, i.e. more stringent than the limits from galactic and extragalactic emission. The possible spin of PBHs would affect the Hawking radiation, generally increasing the emission of particles, in particular ones with large spins. In comparison, stronger limits are obtained for spinning PBHs (Laha et al. 2021) than for non-spinning ones. In both cases, $f_{\rm PBH} = 1$ is claimed to be excluded for $m_{\rm PBH} \sim (2 - 2.5) \times 10^{16}$g.

7.1.6 CMB limits on Dark radiation

Evaporating PBHs in the mass range $[3 \times 10^{13}, 5 \times 10^{16}]$ g should have injected an exotic amount of electromagnetic energy in the Universe, which has an impact on the CMB anisotropies. This effect has been computed in Stöcker et al. (2018), using the `ExoCLASS` code that includes electromagnetic cascade calculations, initially developed in the context of WIMP annihilation. For a monochromatic mass function, the obtained bounds exclude PBHs as the main source of dark matter between 3×10^{13} and 2.5×10^{16}g, and are up to several orders of magnitude more stringent than the limits from the galactic gamma-ray background between 3×10^{13} and 3×10^{14} g. A similar analysis was conducted in Acharya and Khatri (2020), leading to limits at slightly lower masses, around 1.1×10^{13} g. See also Lucca et al. (2020) for the connection with CMB spectral distortions induced by the energy injection from evaporating PBHs. The non-standard energy injection problem has also been reformulated to account for an extended PBH mass distribution in Poulter et al. (2019). In comparison with a monochromatic mass function, the marginalised and log-normal ones have tighter exclusion bounds for heavier PBH masses, while at low PBH masses these two distributions exhibit weaker bounds than the delta distribution. In the future, experiments dedicated to the detection of the CMB spectral distortions or of the 21 cm signal from the dark ages could improve these limits. Finally, it has been pointed out in Nesseris et al. (2020) that the time-dependence of the matter density, as the PBH density decreases as they lose mass via Hawking radiation, can be formulated as an equivalent early dark energy model with varying equation of state $w(z)$. For instance, a population of ultra-light PBHs, decaying around neutrino decoupling, leads to a dark matter-radiation coupling altering the expansion history of the Universe, and alleviating the H_0 tension.

7.1.7 Neutrinos

For PBH masses between 10^{15} and 10^{17} g, black hole evaporation via Hawking radiation leads to sizeable fluxes of MeV neutrinos that could be detected with the next generation of detectors like Hyper-Kamiokande (Abe et al. 2018), JUNO (An et al. 2016), DUNE (Acciarri et al. 2016) and THEIA (Askins et al. 2020). Current experiments like SuperKamiokande already provide some limits on the PBH

abundance (Dasgupta et al. 2020; Bernal et al. 2022), but they are not yet competitive with gamma-ray limits. Those future experiments will have the ability to set complementary limits in the asteroid-mass range. The expected sensitivity of these experiments (Hyper-Kamiokande, JUNO, DUNE and THEIA) with various designs has been calculated in Wang et al. (2021), De Romeri et al. (2021), Bernal et al. (2022) for both monochromatic and log-normal PBH mass functions. Abundances as low as 10^{-6} could be probed for PBH with zero spin and even lower if PBHs have significant spin. DUNE and THEIA would also complement each other, because they are respectively sensitive to neutrino and antineutrino fluxes.

Neutrinos resulting from PBHs could also be observed in direct detection experiments, through coherent elastic neutrino-nucleus scattering (see Calabrese et al. 2022c).

High energy extra-galactic neutrinos can be used to put constraints on the local PBH burst rate density $\dot{B}_{\rm PBH}$ for both non-rotating ($a^\star = 0$) and rotating ($a^\star = 0.99$) black holes. The 90% C.L. limits from 10-years ν_μ IceCube data (Capanema et al. 2021) are presented in Table 4.

7.1.8 21 cm signal

The 21 cm line is an electromagnetic radiation spectral line created by an atomic transition between the two hyperfine levels of the 1s ground state of neutral hydrogen. This spectral line is of great interest and importance in cosmology as it seems to be the only known way to probe the dark ages of the Universe from the epoch of recombination to reionization. Observations of 21 cm are known to be very difficult to make, primarily because it is a faint signal and is usually plagued by interferences from various sources. However, a global 21 cm signal was claimed to be detected by the Experiment to Detect the Global Epoch of Reionization Signature (EDGES), which shows an absorption feature with an amplitude of $T_{21} \sim 500\,\mathrm{mK}$ centered at redshift $z \sim 17$, much stronger (by about a factor of 2) than expected in the ΛCDM model (Bowman et al. 2018). Various explanations, such as interactions between the dark matter particles and baryons, have been put forward to explain this anomalous signal. It must be noticed, however, that EDGES results were later contradicted the SARAS3 radiometer measurements (Singh et al. 2022b) that would

Table 4 Current limits on the local PBH burst rate density from IceCube (Capanema et al. 2021)

Experiment	$\dot{B}_{\rm PBH}$ Upper limit ($\mathrm{pc}^{-3}\mathrm{yr}^{-1}$])	Burst duration (s)	$T_{\rm obs}$
IceCube	1.7×10^7(90% CL, $a^\star = 0$)	10	10 years
IceCube	8.2×10^6 (90% CL, $a^\star = 0$)	10^2	10 years
IceCube	4.1×10^6 (90% CL, $a^\star = 0$)	10^3	10 years
IceCube	1.5×10^7 (90% CL, $a^\star = 0.99$)	10	10 years
IceCube	6.2×10^6 (90% CL, $a^\star = 0.99$)	10^2	10 years
IceCube	3.3×10^6 (90% CL, $a^\star = 0.99$)	10^3	10 years

exclude an astrophysical origin of the EDGES signal. Nevertheless, some limits can still be established on theoretical scenarios from the absence of a strong 21 cm signal.

In general, during that epoch, any additional sources, e.g. the dark matter annihilation or decay, will heat up the intergalactic medium (IGM) and increase the kinetic temperature that eventually determines the strength of the 21 cm signal. Therefore, observations of the EDGES experiment can, in principle, impose constraints on the properties of a dark matter scenario. It has been discussed that, in the context of 21 cm cosmology, PBHs can lead to multiple distinct observable effects: (i) The heating of the IGM due to their Hawking evaporation; (ii) The modification of the primordial power spectrum (and hence the halo mass function) induced by Poisson noise due to PBHs being point sources; (iii) A uniform heating and ionization of the IGM due to X-rays produced during accretion and (iv) A local modification of the temperature and density of the ambient medium surrounding isolated PBHs. Due to their Hawking evaporation, PBHs can affect the evolution of the IGM, and therefore their mass fraction can be constrained by the global 21 cm signal. Using this, the initial mass fraction of PBHs is constrained to be $\beta_{\rm PBH} \sim 2 \times 10^{-30}$ for very light PBHs in the mass range $6 \times 10^{13}\,{\rm g} \lesssim m_{\rm PBH} \lesssim 3 \times 10^{14}\,{\rm g}$ (Yang 2020). Considering PBH evaporation, in Mittal et al. (2022) the following limits have been found: $f_{\rm PBH} = 10^{-6.84}(m_{\rm PBH}/10^{15}\,{\rm g})^{3.75}$ in absence of X-ray heating and $f_{\rm PBH} \leq 10^{-9.73}(m_{\rm PBH}/10^{15}\,{\rm g})^{3.96}$ in presence of X-ray heating. The mass and spin are fundamental properties of a black hole, and they can substantially affect the BH evaporation rate. in Natwariya et al. (2021), the lower limits on masses of PBHs allowed to entirely constitute the DM have been found to be $1.5 \times 10^{17}\,{\rm g}$, $1.9 \times 10^{17}\,{\rm g}$, $3.9 \times 10^{17}\,{\rm g}$ and $6.7 \times 10^{17}\,{\rm g}$ for PBH spins 0, 0.5, 0.9 and 0.9999, respectively.

7.1.9 Limits from DM particle production

If evaporating PBHs are at present times a source of the boosted light DM particles, then the constraints on PBH mass and abundance can be obtained from the XENON1T data (Calabrese et al. 2022a). Considering DM masses smaller than 1 MeV, for low DM-nucleon cross-sections, the constraints on $f_{\rm PBH}$ are almost inversely proportional to the cross-section. However, for larger cross-sections the results might depend on the model of the DM propagation through Earth and atmosphere. The constraints are valid for the mass range $0.5 \lesssim m_{\rm PBH}/(10^{15} g) \lesssim 8.0$: the kinetic energy of particles emitted by more massive PBHs is too low, the less massive PBHs have evaporated nearly completely. For the DM particles interacting with electrons similar analyses are presented in Li and Liao (2022), Calabrese et al. (2022b).

7.1.10 Discussion and limitations

It is important to notice that all the limits on the PBH abundance in the asteroid mass range rely on the common assumption that PBHs evaporate through Hawking radiation. If the process of black hole evaporation is well established theoretically, its

existence is not proven observationally. Furthermore, it is still unclear whether quantum gravity effects would affect or not this process, see for example (Anchordoqui et al. 2022, 2023; Thoss et al. 2024), where for instance it is shown that the existence of one mesoscopic extra-dimension leads to a longer life-time of the PBHs and one can have an all-dark-matter interpretation in terms of PBHs in the mass range $10^{14} \lesssim m_{\rm PBH}/g \lesssim 10^{21}$. The efficiency of the evaporation through the different channels can also depend on the underlying particle physics theory. It is therefore important to keep in mind these possible limitations. Nevertheless, it is also worth noticing that such very light PBHs, if they exist, are the ideal target to probe and test the Hawking radiation hypothesis for the first time. It was also recently claimed that the memory burden effect limits by a factor two the PBH evaporation time, which may reopen some part of the allowed mass range, down to 10^6 kg (Alexandre et al. 2024).

The existence and importance of the Hawking radiation are not the only source of uncertainty on the abundance limits from PBH evaporation. The different source of uncertainties have been recently reviewed and critically analyzed in Auffinger (2022), especially coming from the instrument characteristics, the prediction of the (extra)galactic photon flux, the statistical method of signal-to-data comparison and the computation of the Hawking radiation rate. The constraints on PBHs are found to vary by several orders of magnitude, depending on the hypothesis. Even with an "ideal" experiment, PBHs can only be probed through Hawking radiation at masses below 10^{20} g, which is an intrinsic limitation of the phenomena.

In order to obtain those results, study the model dependence of the limits related to Hawking radiation and include all these uncertainties in the data analysis, the `BlackHawk` (Arbey and Auffinger 2019) and `Isatis` (Auffinger 2022) codes have been developed, allowing to compute the evaporation primary and secondary spectra of stable or long-lived particles, for any black hole distribution. We envisage to interface the PBH numerical tool developed in the context of the present review paper with these key tools.

7.2 Microlensing searches

One of the most stringent constraints on PBH as constituents of the dark matter in the Universe comes from the microlensing amplification of light from a distant star as a Massive Compact Halo Object (MACHO) moves across its line of sight. Microlensing events from lenses of less than one solar mass towards the Large Magellanic Cloud (LMC) where reported in the 1990s by several groups, but in the subsequent decades only upper bounds were published, until SUBARU and later OGLE reported events towards the galactic bulge and nearby Andromeda. The constraints on the halo abundance of those objects depend very much on the mass, velocity and spatial distribution in the halo. Most of these constraints are reported for a standard Navarro–Frenk–White (NFW) halo with virial velocities and a spatially uniform distribution of monochromatic (same mass) MACHOs, which put stringent constraints in the range of masses from 10^{-9} to $30\,M_\odot$. Above $10\,M_\odot$, it is essentially impossible to derive bounds on MACHOs due to the fact that the amplification light

curve lasts more than a decade, while no microlensing survey has monitored continuously the light from stars for so long. Below $10^{-9}\,M_\odot$, the wavelength of visible light is comparable to the Schwarzschild radius of the compact object, and we enter the regime of wave optics, where diffraction makes the constraints essentially disappear. One could search for PBHs with $m_{\rm PBH} < 10^{-9}\,M_\odot$ with light of shorter wavelength, like X-rays or gamma-rays, but sources that emit in those bands are typically not as abundant and stable as stars.

In the following subsections, we give a brief summary of the different microlensing constraints coming from different surveys.

7.2.1 Microlensing from stars in the Magellanic clouds

Microlensing observations of stars in the Large and Small Magellanic Clouds probe the fraction of the Galactic halo in MACHOs in a certain mass range (Paczynski 1986). The optical depth of the halo towards LMC and SMC is related to $f_{\rm PBH}$ by $\tau_{\rm L}^{\rm SMC} = 1.4\tau_{\rm L}^{\rm LMC} = 6.6 \times 10^{-7} f_{\rm PBH}$ for the standard halo model (Alcock et al. 2001). The MACHO project detected lenses with mass around $0.5\,M_\odot$ but concluded that their halo contribution could be at most 10% (Hamadache et al. 2006), while the EROS project excluded $6 \times 10^{-8}\,M_\odot < m_{\rm PBH} < 15\,M_\odot$ from dominating the halo (Allsman et al. 2001; Tisserand et al. 2007). Since then further limits in the range $0.1\,M_\odot < m_{\rm PBH} < 20\,M_\odot$ have come from the OGLE experiment (Wyrzykowski et al. 2011a, b). Very recently, even more stringent limits were claimed by OGLE that are also extended to heavier masses (Mróz et al. 2024a, b).

7.2.2 Microlensing from stars in the galactic bulge

Niikura et al. (2019a) have used data from a 5-year OGLE survey of the Galactic bulge to place much stronger limits in the range $10^{-6}\,M_\odot < m_{\rm PBH} < 10^{-4}\,M_\odot$, although they also claim some positive detections. The galactic bulge is a dense region of stars towards the galactic center where microlensing events are likely to occur. In fact, the OGLE collaboration has detected numerous microlensing events towards the bulge (Wyrzykowski et al. 2016), searching specifically for dark objects that amplify the light of stars behind them. Moreover, these stars are sufficiently close to Earth that one can use paralax measurements by GAIA to break degeneracies between mass and distance which plague magnification microlensing events. This use of the so-called astrometric microlensing has allowed Wyrzykowski and Mandel (2020) to conclusively detect black holes in the mass gap, in the range $2 - 5\,M_\odot$. Niikura et al. (2019a) also report microlensing events towards the galactic bulge in a lower mass range of Earth-mass primordial black holes. These are tantalizing hints of a multimodal population of primordial black holes in the halo of our galaxy, where non of the mass ranges are sufficient to comply 100% of all the dark matter halo.

7.2.3 Microlensing from stars in Andromeda

The Andromeda galaxy (M31) is too far away to resolve individual stars with a typical dedicated (small, 2 m) telescope, as most microlensing surveys do. Therefore they use a different technique called pixel lensing, which corresponds to single pixels brightening up over the length of the survey with a characteristic Paczinsky amplification curve due to a passing compact object. This technique was used by the POINT-AGAPE collaboration (Calchi Novati et al. 2005), who reported six microlensing events, which they argued could be interpreted as self-lensing of stars and this allowed them to conclude that 20% of the Milky Way halo in the direction of M31 could be in the form of $0.5 - 1.0\,M_\odot$ primordial black holes.

More recently, it was reported by Niikura et al. (2019b) the observation, with the Hyper Supreme Cam (HSC) on Subaru Telescope, of a microlensing event towards Andromeda by a compact body with mass in the range $10^{-10} - 10^{-5}\,M_\odot$. Give the detailed statistics of the observation, they claimed this could provide evidence for a non-zero component, at the level of few percent, for the dark matter halo to be in the form of primordial black holes.

7.2.4 Microlensing from quasars

Hawkins has claimed for many years that quasar microlensing data suggest the existence of PBH dark matter (Hawkins 1993). He originally argued for Jupiter-mass PBHs but later increased the mass estimate to $0.4M_\odot$ (Hawkins 2007). More recently, the detection of 24 microlensed quasars (Niikura et al. 2019a) suggests that up to 25% of galactic halos could be in PBHs with mass between 0.05 and $0.45M_\odot$. These events could also be explained by intervening stars, but in several cases the stellar region of the lensing galaxy is not aligned with the quasar, which suggests a population of subsolar halo objects with $f_{\rm PBH} \gtrsim 0.01$. Indeed, Hawkins has argued that the most plausible microlensers are PBHs, either in galactic halos or distributed along the lines of sight to the quasars (Hawkins 2020b).

7.2.5 Caustic crossing in giant arcs

Caustic crossing events in giant arcs are recently discovered phenomena that can be used to probe the existence of dark compact objects such as PBHs (Oguri et al. 2018). These observations correspond to highly magnified images of individual stars, inside giant arcs produced by the strong gravitational lensing of galaxy clusters. This technique is complementary to microlensing of stars and quasars. Compared to microlensing searches, the main difference comes from the existence of high magnification regions, convergence and shear fields, due to the cluster potential. Such environments are also required for quasar microlensing but here the source is different and is a simple star, not a quasar.

Kelly et al. (2018) reported the observation of such an event, the MACS J1149 Lensed Star 1 (LS1), also known as *Icarus*. It corresponds to a faint transient near the critical curve of the massive cluster MACS J1149.6+2223. It is interpreted as a

luminous star in a host galaxy at a redshift $z = 1.49$ which is highly magnified, by a factor of several thousands at the peak brightness, by a compact object that is very close to the critical curve of the foreground lens. The lens properties of this event seem to be consistent with a microlensing event induced by a star that contributes to the intra-cluster light but it can also be used to set constraints on the abundance of compact objects in this galaxy cluster. This leads to claimed limits, with different assumptions on the object transverse velocity, going down to $f_{\rm PBH} < 0.1$ (Oguri et al. 2018). These limits are independent on the object mass in the range between $10^{-5}\,M_\odot$ and $10\,M_\odot$ and become progressively less stringent at larger masses, up to $100 - 1000\,M_\odot$ depending on the assumptions.

Caustic crossing in giant arcs therefore appears to be a promising technique to probe the existence of PBHs that is complementary to other microlensing searches.

7.2.6 Microlensing of supernovae

One can also constrain the abundance of PBHs with stellar masses using supernovae surveys. A certain number of supernova light curves are expected to be lensed by PBHs, exhibiting a magnification of order $\mu \sim 0.1$ if PBHs constitute all the dark matter (Zumalacarregui and Seljak 2018). Nevertheless, it has been debated whether the current JLA and Union data already exclude $f_{\rm PBH} = 1$, especially in the case of broad PBH mass distributions (García-Bellido et al. 2018). The main discrepancy has to do with the assumed statistics and the treatment of outliers and other systematics, like the probability of amplification due to discrete sources along the line of sight (Boscá et al. 2022). Interestingly, the SNe limits are of the same order from $10M_\odot$ up to $10^4 M_\odot$.

7.2.7 Femtolensing

Additional limits on the PBH abundance have been established based on the femtolensing of gamma-ray bursts. Compared to microlensing, the terminology of femtolensing is used to refer to the very small angular distance between lensed images and applies to objects of very small masses. The effect is probed by searching for interferometry patterns in the energy spectrum of lensed objects (Gould 1992). One must nevertheless take into account that the wavelength of the electromagnetic radiation can become comparable to the Schwarzschild radius of the PBH, which implies a lower bound on the mass range probed with this technique. In Barnacka et al. (2012), a search for femtolensing events has been performed on the FERMI observations of gamma-ray bursts for which the redshifts were known. The absence of femtolensing events has been used to set constraints on the dark matter fraction in PBHs of mass between 5×10^{17} g and 10^{20} g, with a limit down to $f_{\rm PBH} \lesssim 0.04$.

7.2.8 Discussion and limitations

The robustness of microlensing limits is of very high importance and still controversial because this is the only observational technique to probe the abundance

of PBHs smaller than a solar mass, down to $10^{-10}M_{\odot}$. Another debated question is whether microlensing surveys of quasars or towards the galactic center only provide a limit on PBHs due to the lack of observations or also hint at their existence due to a series of observations.

The contribution of PBHs to the dark matter is also an interesting question. Deriving limits from microlensing surveys of stars in the Magellanic clouds depends on numerous astrophysical assumptions (velocity dispersion, galactic dark matter profile, etc...) and varying limits can be obtained with different hypothesis (Green 2016, 2017; Hawkins 2015, 2020b; Calcino et al. 2018; García-Bellido and Hawkins 2024). Wide mass distributions can also significantly alter the limits on their abundance, but without totally removing them. The clustering of PBHs was the main argument invoked to totally suppress the microlensing limits (García-Bellido and Clesse 2018; Carr et al. 2021b), even though it has been shown that this is not the case assuming initial Poisson distributed PBHs (Petač et al. 2022; Gorton and Green 2022). Furthermore, in the case of a large initial spatial clustering distribution beyond Poisson, it has been also recently shown that the combination of constraints from microlensing and Lyman-α forest completely rules out the parameter space for stellar-mass PBHs to be a dominant constituent of the dark matter (De Luca et al. 2022b).

7.3 Dynamical limits

7.3.1 PBH capture by neutron stars or white dwarfs

The asteroid-mass range, between $10^{-16}\,M_{\odot}$ and $10^{-10}\,M_{\odot}$ (10^{17} – 10^{23} g), is the only one for which there is a general consensus that PBHs can contribute up to the entirety of the dark matter. Nevertheless, if this mass window remains open nowadays, this has not been always the case. Some constraints had been proposed, coming from observations of neutron stars and white dwarfs (WD) in globular clusters (Capela et al. 2013b, a; Pani and Loeb 2014; Defillon et al. 2014) that can capture asteroid-mass PBHs falling at the center of the star and rapidly swallowing its material until it becomes a black hole. Such constraints therefore arise from the combination of a dynamical and an accretion process. But those limits have been relieved due to large uncertainties. It was initially claimed that $f_{\rm PBH}$ cannot exceed between 10^{-2} and 0.2, depending on the DM density in globular clusters. However, this approach is limited by our knowledge of the DM constitution of globular clusters. Using updated prescriptions, the limits from Capela et al. (2013a), Pani and Loeb (2014) have been then relieved in Montero-Camacho et al. (2019), re-opening the asteroid-mass range to full PBH-DM scenarios.

In Graham et al. (2015), it was proposed that the transit of PBHs through a white dwarf causes localized heating around the BH trajectory due to dynamical friction, eventually triggering a runaway thermonuclear fusion and causing the WD to explode as a supernova, even if the WD mass is below the Chandrasekhar limit. The constraints on PBHs were derived by using two classes of observations. One class comes from direct observations of WDs with known masses, whose existence places bounds on PBHs that are abundant enough that they would have transited the WD

with high probability. The second class arises from the measured rate of type Ia supernovae, that constrain PBHs with a low abundance and thus have a low probability of transit through a WD. The shape of the observed distribution of WD masses (with masses up to $1.25M_\odot$) excludes PBHs with masses $\sim 10^{19} - 10^{20}$g from being a dominant constituent of the local DM density, whereas the type Ia supernova rate disfavors BHs with masses between $10^{20} - 10^{22}$g. However, the latter is not a robust exclusion due to uncertainties in the methods used to determine the WD population with masses larger than $\sim 0.85M_\odot$ (necessary condition for a WD to explode due to a BH), and this mass could possibly change if the current simulation data used to derive it is refined. Measurements of WD binaries in GW observatories could be used in the future to further strengthen the BH bounds.

More recently, limits on PBH in the interesting asteroid-mass range between 10^{18} g and 10^{21} g based on the capture of PBHs by Sun-like stars in ultra-faint dwarf galaxies leading to its destruction, have been calculated in Esser and Tinyakov (2023). If one requires that no more than a fraction of stars $\xi = 0.5$ is destroyed, one obtains a limit on the PBH abundance of about $f_{\rm PBH} \lesssim 0.3$ in the above-mentioned mass range. But the constraints strongly depend on the possible value of ξ that is still fairly unknown. In Smirnov et al. (2024), it was suggested that the recent discovery of a population of faint supernovae (Ca-rich gap transients) may come from the explosion of white dwarfs, possibly due to PBH captures. Their unusual spatial distribution, predominantly at large distances from their presumed host galaxies, supports this hypothesis and the authors have shown that their spatial distribution matches well the distribution of dwarf spheroidal galaxies.

7.3.2 Ultra-faint dwarf galaxies

If PBHs above $10\,M_\odot$ constitute an important fraction of the dark matter, their regular encounters in highly dark matter dominated ultra-faint dwarf galaxies (UFDGs), such as in Segues I or in Eridanus II, should have induced their dynamical heating, allowing them to reach a half-light radii larger than 10 parsecs. This argument also applies to star clusters in UFDGs, like for Eridanus II. Relatively stringent limits from UFDGs have been first established in Brandt (2016), for monochromatic mass functions. These have been extended to log-normal PBH mass functions, including the effect of a central intermediate-mass BH, in Green (2016), or in Li et al. (2017). All these works basically exclude $f_{\rm PBH} = 1$ for $m_{\rm PBH} > 10\,M_\odot$. These limits are relatively solid because they rely on well-known Newtonian gravitational dynamics. Nevertheless, one should point out that these limits can be shifted if UFDGs host a central intermediate-mass black hole.

Another way to constrain PBHs from UFDGs is to consider the radial luminosity profile, given that stars must also be heated up by PBHs. In this case, Segue 1 provides the most stringent limit, excluding $f_{\rm PBH} = 1$ for $m_{\rm PBH} \sim 2\,M_\odot$ (Koushiappas and Loeb 2017a; Stegmann et al. 2020). However, these limits rely on astrophysical assumptions about the stellar mass distribution and they could change for wide-mass PBH models, depending on the existence and mass of a central intermediate-mass black hole, etc. Finally, UFDGs also provide an argument in favor of solar-mass

PBHs constituting an important fraction of the dark matter, given that there is no observation of such objects with a radius less than about 20 parsecs, whereas they would still be above the magnitude limit of the current instruments.

7.3.3 Dark Matter profile of dwarf galaxies (core-cusp problem)

The regular PBH-PBH interactions in a dense environment should prevent the formation of cusps in the central region of dwarf galaxies, possibly explaining the core-cusp problem. As first pointed out in Clesse and García-Bellido (2018), the gravitational scattering cross-section for PBHs in the stellar-mass range are of order $(0.1-1)\mathrm{cm}^2/\mathrm{g}$ and so PBHs are in essence a well motivated self-interacting dark matter model. But contrary to particle dark matter, this does not need exotic physics but relies on the only well-known interaction that is not included in the standard model of particle physics, gravitation. The core-cusp problem in the context of PBHs was then further explored in Boldrini et al. (2020). They found that the mechanism works well for PBHs of mass between 20 and $100\,M_\odot$, if they have $f_{\rm PBH}\sim 0.01$, but it would be less efficient and would allow larger abundances for PBHs of the order of the solar mass. Therefore, observations of low-mass dwarf galaxies provide at the same time a new limit on the PBH abundance and a possible hint for their existence. These limits imposed on the PBH abundance have been represented in Fig. 38.

7.3.4 Wide halo binaries

Wide stellar binaries can be destructed by the encounters with PBHs, therefore the existence of the undisrupted ones in the galactic halo also provides constraints on the PBH abundance (Carr and Sakellariadou 1999).

Using the analysis of Quinn et al. (2009), the following constraint at 2σ confidence level has been found (Carr et al. 2021c): $f_{\rm PBH}<500\,M_\odot/m_{\rm PBH}$ flattens above $M\sim 1000\,M_\odot$ with $f_{\rm PBH}\lesssim 0.5$. Using the results of (Monroy-Rodríguez and Allen 2014), where the low-mass limit was reduced from $500\,M_\odot$ to $21-78\,M_\odot$, $f_{\rm PBH}$ flattens at $m_{\rm PBH}\sim 100\,M_\odot$ with $f_{\rm PBH}\lesssim 0.1$ (Carr et al. 2021c). In Tian et al. (2020), by using a sample of 4351 halo wide binaries from the Gaia catalog, a break at $\sim$ 0.1 pc in the separation distribution has been detected. Any break in the power law for the separation distribution of wide halo binaries can be attributed to a disruption of the binary as a result of encountering MACHOs (e.g. PBHs). Therefore, this break implies $m_{\rm PBH}>10\,M_\odot$. These limits come from the expected disruption of such wide binaries when they encounter PBHs. They therefore strongly depend on the number density of PBHs, and they could vary if, for instance, a majority of PBHs live in clusters.

7.3.5 Disruption of stellar streams

Stellar streams have been observed in the Milky Way halo and are likely formed by the tidal stripping of progenitors. These would be perturbed by encounters with dark matter subhalos, such as PBH clusters. Some methods have been proposed to

distinguish the origin of perturbers, in particular the PBH-DM hypothesis form standard particle CDM (Montanari and García-Bellido 2022). Stellar streams like GD-1 could probe the abundance of haloes down to $10^3 M_\odot$, providing a test of the existence of PBHs.

7.3.6 PBHs in the solar system

The dynamics of objects in the Oort cloud suggests the possible existence of a not yet observed planet, referred as Planet Nine. It could also be a dark compact object several times the mass of the Earth, in orbit around the Sun in the Oort cloud. It has been suggested that Planet Nine is a PBH captured by the Sun (Scholtz and Unwin 2020) a long time ago. It was later proposed to search for the existence of such a PBH in the Oort cloud by probing the flares from accretion of small Oort cloud objects with LSST (Siraj and Loeb 2020), which could result in improved limits on PBH abundances, or by probing the associated Hawking radiation (Arbey and Auffinger 2020).

Alternatively, it has been proposed to probe asteroid-mass PBHs in orbit around the Earth by searching for their gravitational signatures in gravimeter networks (Namigata et al. 2022). But the obtained limits on the PBH abundance with the current gravimeter sensitivity are not yet relevant. Near-Earth PBHs could also leave imprints in gravimeters or in GNSS orbit products. One way to detect a PBH passing through the Earth would be to observe the induced seismic signatures (Luo et al. 2012).

All this nevertheless remains highly speculative and it is not clear, for instance, if a PBH captured by the Sun (or by the Earth) would remain on a stable orbit, or if its orbit would likely pass near the Earth. However, it must also be pointed out that discovering a PBH inside the Solar System would have tremendous implications and could even, in principle, allow in-situ investigations of a black hole (Witten 2020).

7.3.7 Discussion and limitations

Again, there are a series of limitations and uncertainties that restrict the range of applicability of the dynamical limits. In particular, let us mention that if most PBHs are regrouped in clusters, the limits from wide halo binaries would be strongly affected and possibly suppressed. These clusters could even be the ultra-faint-dwarf galaxies, for which observations show a minimum radius around a few tens of parsecs. Dynamical heating of UFDGs by PBHs can therefore be seen both as a limit and as a clue for the existence of such PBHs. For UFDGs, other sources of uncertainties come from the stellar population model, the exact DM profile and the existence of a central intermediate-mass black hole that typically makes limits less stringent. This illustrates that the border between observational limits and evidence is blurred and connected, and above all strongly model dependent. A similar conclusion applies to the asteroid-mass region, for which uncertainties on the DM content of globular clusters and the details of the tidal capture of small PBHs by neutrons stars or white dwarfs still make this range viable for a full PBH-DM scenario.

7.4 Accretion limits

7.4.1 Cosmic microwave background (CMB) anisotropies

Primordial black holes which experience a phase of accretion at the present epoch are subject to several constraints depending on their characteristic environment.

CMB anisotropies are impacted by accreting PBHs around the time of the recombination and until the completion of the reionization, leading to stringent limits on the abundance of PBHs heavier than around $10 - 100\,M_\odot$. The main idea behind these constraints is the following: in the early Universe, PBHs accrete primordial gas and then convert a fraction of the accreted mass to radiation. This results in the injection of energy into the primordial plasma, which affects its thermal and ionization histories, leading to CMB distortions in its frequency spectrum, as well as signatures in the CMB temperature and polarization angular power spectra.

When accretion comes into play, the first aspect to consider is its geometry, i.e. spherical accretion or accretion disk formation. The former is obtained when the characteristic angular momentum of the accreted gas at the Bondi radius (distance from the center at which the escape velocity equals the sound speed) is smaller than the angular momentum at the ISCO (Innermost Stable Circular Orbit) radius. The second aspect that must be taken into account is the local feedback. Indeed, radiation emanating from the accreting PBH may heat and ionize the accreting gas, influencing the radiative output. Moreover, as discussed in Ali-Haïmoud and Kamionkowski (2017), one can assume that (1) In the outermost region of the accretion flow, the ionization fraction is approximately equal to the background value. Radiative feedback is neglected, and Compton drag and cooling are included in the calculation. When the temperature of the gas reaches $\sim 10^4$ K, the gas gets collisionally ionized. This first limiting case is refered to as collisional ionization; (2) In the innermost region, the radiation from the PBH photoionizes the gas, which becomes fully ionized and adiabatically compressed. This second limiting case is referred to as photoionization. Furthermore, the accreting PBHs are moving with respect to the ambient gas with some relative velocity, which does not allow for a perfectly spherically-symmetric accretion. This relative velocity is comprised of (1) A Gaussian linear contribution on large scales $v_{\rm L}$ (derived in Ali-Haïmoud and Kamionkowski 2017); (2) A small-scale contribution $v_{\rm NL}$ due to non-linear clustering of PBHs (not examined in Ali-Haïmoud and Kamionkowski 2017).

Another key quantity is the radiative efficiency factor ϵ, which is strongly related to the geometry of the accretion flow and the accretion rate. It usually takes the value $\epsilon \sim 0.1$ for moderate or low disk accretion rate, that corresponds to the value inferred from BH observations. In the case of spherical accretion, one gets smaller values of the order of 10^{-5}. Finally, to compute the CMB bound, it is crucial to evaluate the total energy injection rate, by taking into consideration that not all radiation is equally effective. To compute the impact on the CMB, one has to quantify what amount of injected energy is actually deposited into the medium by using the *energy deposition functions*, and the last step is to include the spectrum of the radiation emitted through BH accretion. Let's note that each accretion scenario has a

distinctive energy injection history, that could in principle be distinguished in the CMB angular power spectrum (Poulin et al. 2017).

For PBHs more massive than $\sim 1\,M_\odot$, strong constraints were derived by Ricotti et al. (2008), while in Ali-Haïmoud and Kamionkowski (2017), CMB limits on the PBH abundance were re-examined in detail, based on previous works. In particular, in order to set the most conservative constraints on the PBH abundance, it is useful to compute the minimum PBH luminosity that is physically plausible and the accretion rate, taking into account the Compton drag and Compton cooling by CMB photons. Assuming a quasi-spherical accretion flow, a steady-state flow and a Newtonian approximation, the bounds derived show that in the collisional ionization limit, CMB anisotropy measurements by *Planck* exclude PBHs with masses $M \gtrsim 10^2 M_\odot$ from being the dominant DM component. In the photoionization limit, this threshold is lowered to $\sim 10 M_\odot$. These constraints are weaker than those derived in Ricotti et al. (2008).

As a side note, it is shown in Ali-Haïmoud and Kamionkowski (2017) that local Compton heating by the radiation produced by the accreting PBH can be safely neglected, i.e. one can neglect local thermal feedback. It is also demonstrated that it is not self-consistent to assume that ionizations proceed exclusively through photoionizations or collisional ionization, i.e. the level of ionization feedback is expected to lie between the two limiting cases. Finally, it was also derived that global heating of the plasma due to accreting PBHs does not leave any (observable) imprint on CMB spectral distortions.

In Poulin et al. (2017), it is argued that the spherical accretion approximation is likely not valid and that an *accretion disk* should form during the dark ages, between recombination and reionization. More precisely, all plausible estimates suggest that a disk forms soon after recombination, mainly due to the fact that, already before recombination, stellar-mass PBHs are in a non-linear regime (i.e. they are clustered in halos of bound objects, e.g. PBH binaries or big clumps containing thousands of PBHs). The main criterion necessary for disk formation considered in Poulin et al. (2017) is that the angular momentum of the material at accretion distance is sufficient to keep the matter in Keplerian rotation at a distance $\gg 3r_s$, where r_s is the Schwarzschild radius. To accumulate angular momentum, the accreted material must have significant velocity or density differences. Based on the angular momentum of the accreted gas, one can derive the condition required for a disk to form (Poulin et al. 2017). For instance, the disk formation criterion is likely satisfied if we consider an ideal, free-streaming homogeneous gas moving at a bulk motion with velocity of order v_L without dispersion, or when PBHs constitute an important fraction of the DM with $M \gtrsim M_\odot$.

The conservative constraints obtained in Poulin et al. (2017) (at 95% C.L. using data from *Planck* high-l TT TE EE+lensing) are represented in Fig. 38. One notices that the presence of disks improves the CMB constraints on PBH by at least two orders of magnitude, so that PBHs with masses $M \gtrsim 2M_\odot$ (with monochromatic mass distribution) are excluded from accounting for the totality of the DM. The constraints derived for the monochromatic case were also extended to a log-normal mass

distribution, and become more restrictive for a broader distribution (Poulin et al. 2017).

In Serpico et al. (2020), they extended previous calculation (Poulin et al. 2017) to account for the accretion of dominant, non-PBH DM particles onto PBH. The increased gravitational potential felt by the baryons enhances baryonic accretion and the PBH luminosity constrained by the CMB. The accreting DM halos around each PBH are treated via a toy model and numerical simulations, assuming that the ionization of gas in the dark ages due to accretion onto PBHs is homogeneous.

The toy model considered in Serpico et al. (2020) is used to determine the upper limit to the mass growth of the PBH via DM accretion. The most optimistic scenario for PBH growth is for a cold DM with no dispersion. The time evolution of the radius of a mass-shell around a PBH is found to be $M_{\rm halo} \simeq (3000/1+z)M_{\rm PBH}$, which is expected to break down at very late times. This conjecture is then verified via cosmological N-body simulations, where in order to model the halo growth, it is required that the DM halo is composed of many DM particles when it becomes comparable to the PBH mass. An important result is that when the halo is compact, the accreting baryons see a BH whose effective mass is the sum of the PBH and the DM halo masses. If the halo is large, only a fraction of its mass contributes to the accretion. This is the model used in Serpico et al. (2020) to compute the impact of PBH accretion onto the CMB.

The CMB constraints of Serpico et al. (2020) are obtained by taking into account the effect of accretion within DM halos. Supposing that PBHs are accreting at Eddington luminosity (luminosity at which accretion is balanced by radiation pressure in a spherical system), one gets the limit $f_{\rm PBH} < 2.9 \times 10^{-9}$. In absence of DM halos the constraints at 95% C.L. are stronger (by a factor ~ 4) than bounds derived in Poulin et al. (2017). Accounting for the DM halo leads to improved bounds for $f_{\rm PBH} \lesssim 10^{-2}$ and $f_{\rm PBH} \lesssim 0.2$ for the disk and spherical accretion cases, respectively. Eventually, the bounds flatten when $M \gtrsim 10^4 M_\odot$ as a consequence of the accretion that reaches the Eddington limit. CMB constraints exceed the ones coming from the non-observation of mergers by LVK, BBN, the non-observation of the SGWB, etc., for masses $M \gtrsim (20-50)M_\odot$. The CMB bounds remain dominant until $10^{3.5} M_\odot$, when they come close to the BBN ones. Specifically, it is excluded that PBH constitute the totality of the DM over the stellar mass range, and around $10 M_\odot$ no more than $f_{\rm PBH} \sim 0.1$ is allowed (Serpico et al. 2020).

Finally, a possible relaxation of the limits from CMB anisotropies has recently been suggested in Facchinetti et al. (2023), Piga et al. (2022), Agius et al. (2024). The work of Facchinetti et al. (2023) relies on a more realistic accretion model based on hydrodynamical simulations and conservative assumptions for the emission efficiency. This leads to limits that are up to 2 orders of magnitude less stringent than previously estimated, between 10 and $10^4\, M_\odot$, which reopens the possibility that PBHs might explain at the same time (at least a fraction of) the dark matter, some of the LVK binary BH mergers, and the existence of supermassive BHs. The work of Piga et al. (2022) takes a step towards the development of a more realistic PBH accretion by accounting the contribution of outflows, for various accretion geometries, ionization models and mass distributions in absence and in presence

of mechanical feedback and non-thermal emissions due to the outflows. More conservative limits were more recently obtained from a critical re-investigation of all the possible effects (Agius et al. 2024). In general, it seems that PBH accretion is rather complex physical process that is hard to assess, which induces large uncertainties in all the accretion-based limits.

7.4.2 21 cm signal

There are several limits based on the EDGES detection of the absorption signal of the global redshifted 21 cm line in the range $15 < z < 22$, see however the previous discussion about the exclusion of an astrophysical origin of the EDGES signal by SARAS3. The Poisson distribution of PBHs can lead to isocurvature perturbations and consequently to early structure formation. The DM annihilation is enhanced in early formed dense halos and modifies the ionization and temperature evolution of baryons. Using the redshift dependence of the EDGES signal (Tashiro and Kadota 2021a), the following constraint on PBH abundance has been found: $f_{\rm PBH} < 10^{-3.4}$ for $f_{\rm ann}\langle\sigma v\rangle/m_\chi = 3 \times 10^{-28}\,{\rm cm}^3/{\rm s/GeV}$, where m_χ denotes the DM mass.

PBHs can accrete the surrounding baryonic matter as well as DM particles from the surrounding halo. This results in the emission of high energy photons that are injected into the IGM, leading to changes in its thermal and ionization history via ionization, excitation and heating. For the PBHs accreting only baryons (Hektor et al. 2018), the following approximation for the constraint on the PBHs fraction has been found: $f_{\rm PBH} \leq C(\beta)(0.15/f_{\rm E})(\lambda/0.01)^{-(1+\beta)}(M_{\rm PBH}/10M_\odot)^{-(1+\beta)}$, where $C(\beta) = 0.00015 + 0.00051\beta + 0.0091\beta^2$ if $\beta \leq 0.37$ and $C(\beta) = 0.019\beta^{2.5}$ if $\beta > 0.37$ (here λ is the mass accretion parameter, $T_k = 8\,K$ the maximal gas temperatures allowed, and $f_{\rm E} < 1$ the effective energy absorption factor, assuming a monochromatic mass function). Including also DM particles accretion, in Yang (2021) for a differential 21 cm brightness temperature $\delta T_{21} \lesssim -100\,{\rm mK}$ the limit $f_{\rm PBH} \lesssim 2.6 \times 10^{-5}$ has been obtained for $m_{\rm PBH} = 10M_\odot$ and $f_{\rm PBH} \lesssim 2.6 \times 10^{-6}$ for $m_{\rm PBH} = 10^4 M_\odot$. These limits are weakened by a factor of order 3 for $\delta T_{21} \lesssim -50\,{\rm mK}$.

In Mena et al. (2019), it has been shown that future experiments like SKA and HERA could potentially improve the existing CMB bounds by more than an order of magnitude. The prospects for constraining PBHs with the future 21 cm forest observations have been discussed in Villanueva-Domingo and Ichiki (2022).

In Hasinger (2020) the contribution of accretion on PBHs to the observed low-frequency cosmic radio background (CRB), and thus to the EDGES signal, has been estimated. It has been found that for radio-quiet PBHs the contribution to the CRB constitutes at 1.4 GHz a fraction of 0.1% of the observed synchrotron radio background, mostly accumulated at $z \gtrsim 20$. This increases the depth of the 21 cm absorption line by only about 30%. However, some fraction of the radio-loud PBHs (e.g. 5% with 1000 times higher fluxes), as observed in the AGN population, will easily provide the 5% excess high-redshift radio background flux necessary to explain the EDGES observation.

7.4.3 Cosmic X-ray, infrared and radio backgrounds

Right after the first detection of gravitational-waves from a binary black hole merger, it has been proposed that a PBH origin would be supported by the spatial correlations between the source-subtracted infrared and X-ray backgrounds (Kashlinsky 2016), which have been measured at a 5σ level (Kashlinsky et al. 2018, 2005) and are unexplained by known sources. These correlations can be induced by DM halos seeded at higher redshift than in the standard CDM scenario by the Poisson fluctuations in the PBH distribution, if one has $f_{\rm PBH} m_{\rm PBH}/M_\odot \sim \mathcal{O}(1)$. In turn, matter accretion onto PBHs leads to X-ray emission while star formation in these halos leads to a spatially correlated infrared radiation. The possibility of this scenario was confirmed and explored in more details in Hasinger (2020), Cappelluti et al. (2022).

Recently, it has also been investigated if the observed excess of the cosmic X-ray and radio cosmic background by Chandra and ARCADE 2, suggesting an undiscovered population of emitters, could be explained by a high-redshift population of PBHs (Ziparo et al. 2022) distributed in DM halos and in the intergalactic medium. It was shown that the emission should dominantly come from small DM halos, with masses of order or smaller than $10^6\,M_\odot$ at high redshifts $z \gtrsim 6$. Interestingly, it was also found that even if PBHs account for the excess in the radio background, it cannot at the same time explain the X-ray cosmic background. This leads to limits on the PBH abundance, in particular in the $1 - 100\,M_\odot$ mass range, which are stronger than the microlensing limits or the bounds from ultra-faint dwarf galaxies, with $f_{\rm PBH} \lesssim 9 \times 10^{-3}\,M_\odot/m_{\rm PBH}$.

7.4.4 Limits from accretion at present epoch

A population of PBHs with masses around $\mathcal{O}(10 - -100) M_\odot$ in the Milky Way would be responsible for radio and X-ray emission if they experience a phase of accretion from the interstellar gas. By comparing the predicted emission with observation data in the VLA radio and Chandra X-ray catalogs, one can set a constraint on the fraction of dark matter in the form of PBHs to be of the order of $f_{\rm PBH} \lesssim (10^{-2} - 10^{-3})$ in the relevant mass range, depending on the assumed PBH mass function (Gaggero et al. 2017; Manshanden et al. 2019). This constraint is shown in Fig. 38 and denoted "Xr".

Second, the abundance of PBHs in the stellar or intermediate mass ranges, which interact with the interstellar medium emitting significant fluxes of X-ray photons, may be constrained by using the observed number density of X-ray binaries. In particular, by comparing the emitted radiation signals with the electromagnetic data, one can constrain the PBH abundance to be smaller than $f_{\rm PBH} \lesssim (10^{-2} - 10^{-3})$ in the considered mass range (Inoue and Kusenko 2017). This constraint is labelled "XrB" in Fig. 38.

Finally, a cosmology-independent constraint can be set on the PBH abundance based on the absence of gas heating in the interstellar medium due to PBH interactions. In particular, photon emission from accreting PBHs, dynamical friction, winds and jets emission from accretion disks may be constrained using data from the

Leo T dwarf galaxy, setting a bound on PBHs with masses in the range $(10^{-2} - 10^{6})M_{\odot}$ up to the percent level (Lu et al. 2021; Takhistov et al. 2022).

7.4.5 Discussion and limitations

Accretion limits, in particular limits from CMB temperature anisotropies, are claimed to set the most stringent limits on the abundance of PBHs between about $10M_{\odot}$ and $10^{4}M_{\odot}$, i.e. in the range that is particularly relevant for GW observations with ground-based and space-based detectors. Their strengths nevertheless depend on the details of the accretion (e.g. disk or spherical accretion). Given the possible complexity of the accretion process, it is possible that those limits significantly change if different assumptions are chosen, for instance for the velocity-dependence of the accretion process. One should also notice that the Poisson-induced clustering of PBHs were not taken into account in the calculation of these limits. Other sources of uncertainties come in the computation of the injected energy and the resulting changes in the evolution of the ionized fraction at high redshfit. Limits from the X-ray and radio emission in the galactic center have their own uncertainties, e.g. related to the dark matter distribution. The limits that were presented were nevertheless considered as relatively conservative.

An important implication that was recently discovered for the limits from CMB temperature anisotropies is that the existence of a particle dark matter component in addition to PBHs reinforce those limits on the abundance of PBHs, in such a way that they may become incompatible with an explanation of GW observations.

7.5 Indirect constraints from density fluctuations

7.5.1 CMB distortions

Enhanced primordial density perturbations producing PBHs will also generate CMB distortions by dumping energy into the primordial plasma in the wave-number range $1 \lesssim k/\mathrm{Mpc}^{-1} \lesssim 10^{4.5}$. The amount of distortion can be roughly estimated as $<\mu> \sim O(1)\, P_{\zeta}\, \Delta N$, where ΔN is the e-fold number duration of the enhanced perturbations, which is equivalent to $\ln\left[\frac{k_{\max}}{k_{\min}}\right]$. Assuming $\Delta N \sim O(1)$, one can probe the distortion level from the power spectrum, and current bounds are $<\mu> \lesssim 10^{-4}$ (Kohri et al. 2014; Nakama et al. 2018; Inomata and Nakama 2019; Byrnes et al. 2019; Kalaja et al. 2019; Gow et al. 2021; García-Bellido et al. 2017).

The PBH production is extremely sensitive to the tail of the statistical properties, i.e. probability distribution, of the primordial perturbations as discussed in Sect. 3. Hence, for highly efficient PBHs producing non-Gaussian perturbations, the distortion signal can be smaller and evade the current bounds. However, future experiments will reach remarkable sensitivities to probe both Gaussian and non-Gaussian primordial signals (Nakama et al. 2018; García-Bellido et al. 2017).

If scalar induced stochastic GW background is combined with CMB distortions, the probed PBH seed range will be $(0.1 - 10^{13})M_{\odot}$ (Ünal et al. 2021) (equivalently

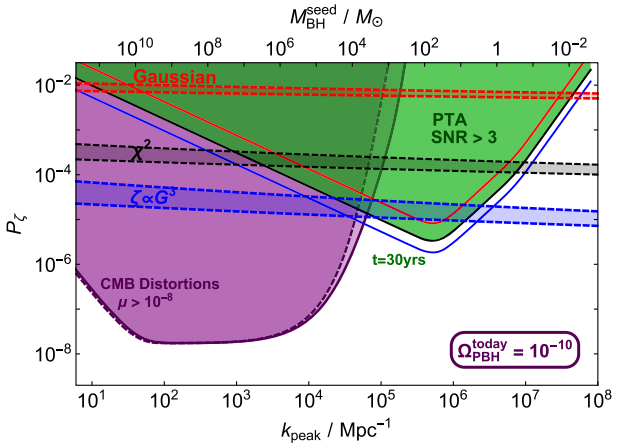

Fig. 40 Probing power of future PTA (SKA) and CMB distortion (PIXIE-like) experiments on primordial fluctuations for about 7 decades in wavenumbers and 13 decades in masses. Results are shown for inflationary perturbations that obey distinct probability distributions: Gaussian (red horizontal dashed line), chi-sqr (χ^2, black horizontal dashed line), cubic-Gaussian (G^3, blue horizontal dashed line), detectable if

the probed wavenumber range will be $1 \lesssim k/\mathrm{Mpc}^{-1} \lesssim 10^7$). These probes will also reach conclusive results about the intriguing possibility that PBHs could be the seeds of SMBHs, and with the detection of billion-solar-mass SMBHs at redshift higher than 6 (Schneider et al. 2023), this has become an even more pressing question. Since CMB distortions and scalar induced GWs are global cosmic signals associated with the formation/production of PBHs, the conclusions will be robust to modifications in: (i) Astrophysical evolution, such as merger and accretion history; (ii) The amplitude and statistical properties of the primordial perturbations (Gaussian versus non-Gaussian); (iii) The clustering effects. The combined probes are shown in Fig. 40, where non-detection of both signals will robustly constrain the PBH abundance to the negligible amount of $f_{\mathrm{PBH}} < 10^{-10}$ (Ünal et al. 2021).

Bosonic degrees of freedom scattering with spinning BHs can get energy from the rotational energy of BHs, and this phenomenon is called as superradiance. All BHs with enough spin can experience this process, but especially light PBHs, in the mass range, 10^{-33}–$1\,M_\odot$, can experience superradiance even for tiny spin values, 10^{-5}–10^{-2} (Ünal 2023). The instability rate of black hole is different for distinct types of perturbation, that is, scalar, vector, and tensor. Light PBHs can probe over 33 decades of bosons (scalar, vector and spin-2) in the mass range mentioned above, 10^{-12}–10^{21} eV.[15] This superradiance process boson mass range matches with the

[15] Bosons could be beyond Standard model particles such as axions and dark photons, also it could be Standard Model photon with effective mass due to plasma interactions. If spinning light PBHs are observed, this implies non-existence of superradiance for the given BHs and boson mass range, therefore this observation can imply either there are no such particles or their self/external interactions prevent them from superradiance. This results in bounds on the axion decay constant (inversely related to the strength of self-interaction) and its energy density (Ünal 2023).

plasma mass of photons, namely this allows light PBHs to amplify the photon production via superradiance and dump energy to CMB plasma, and if CMB cannot thermalize to have black-body spectrum this leads to CMB distortions, giving rise to bounds on PBHs depending on their masses (Pani and Loeb 2013).

7.5.2 Lyman-α forest

The constraints on PBHs can be obtained from the high-resolution high-redshift Lyman-α forest data since the Poisson fluctuations in the PBH number density induce a small-scale power enhancement departing from the standard CDM prediction. This enhancement can be interpreted as an isocurvature perturbation with the scale-invariant spectrum and isocurvature-to-adiabatic amplitude ratio for the monochromatic distribution: $f_{\rm iso} = \sqrt{\frac{k_\star^3 m_{\rm PBH} f_{\rm PBH}}{2\pi^2 \Omega_{\rm CDM} \rho_{\rm cr}} \frac{1}{A_{\rm s}}}$ (here $k_\star = 0.05/\text{Mpc}$ is the pivot scale) (Murgia et al. 2019). Using MIKE and HIRES/KECK samples of quasar spectra and a grid of hydrodynamic simulations exploring different values of astrophysical parameters, in Murgia et al. (2019) the marginalized upper limit $f_{\rm PBH} m_{\rm PBH} \sim 60\, M_\odot$ at 2σ on the PBH mass have been found for a monochromatic distribution. This has been obtained with a Gaussian prior on the reionization redshift, preventing the posterior distribution to peak on high redshift values that are disfavoured from the CMB and IGM observations.

7.5.3 El Gordo cluster and enhanced Halo Mass Functions

One of the most fascinating connections between PBHs and large scale structure (LSS) arises when one considers the effect of quantum diffusion in single field inflation with quasi-inflection points (Ezquiaga et al. 2020) as a natural way to generate large exponential tails in the density contrast PDF a fact that enhances the probability of collapse of small-scale fluctuations upon re-entry leading in this way to PBH formation. These highly non-Gaussian tails in the PDF can also be responsible at larger (galactic and cluster) scales for the enhancement of the halo mass function at high redshift (Ezquiaga et al. 2022), possibly explaining the increased abundance of massive galaxies seen by the James Webb Space Telescope at redshifs $z \sim 9 - 20$ (Finkelstein et al. 2022b), as well as significantly more massive clusters, like El Gordo (Asencio et al. 2020) at $z \sim 1$, than expected by the standard model ΛCDM. It remains to be shown whether such large deviation from the ΛCDM predictions for the halo mass function are compatible with LSS constraints. In the near future we may have deep imaging up to redshift $z \sim 20$ with both infrared and radio surveys like SKA, to test the enhanced exponential tails that could have given rise to PBHs in the early universe.

7.5.4 High-z galaxies from JWST

The James Webb Space Telescope (JWST) imaging program via the Cosmic Evolution Early Release Science (CEERS) survey recently reported a population of massive galaxy candidates at redshift $z \gtrsim 8$ with stellar masses of the order of

$10^9 M_\odot$ (Atek et al. 2022; Finkelstein et al. 2022a; Harikane et al. 2023; Naidu et al. 2022; Yan et al. 2023). A note of caution here is in order, as spectroscopic follow-up will be necessary to confirm current observation only based on photometry. However, if confirmed, such early formation of massive galaxies reported by the JWST is hardly reconcilable with the standard ΛCDM expectations. Recently, Labbé et al. (2023) derived the cumulative stellar mass density at $z = 8$ and 10 for $M_\star \gtrsim 10^{10}\ M_\odot$ based on 14 galaxy candidates with masses in the range $\sim 10^9 \div 10^{11}\ M_\odot$ at $7 < z < 11$ observed by the CEERS program. They found

$$\rho_*(>10^{10} M_\odot) \simeq 1.3^{+1.1}_{-0.6} \cdot 10^6 M_\odot\,\mathrm{Mpc}^{-3}, \tag{162}$$

at $z \simeq 10$. These values are larger than the ΛCDM predictions, even allowing maximum Star Formation Efficiency (SFE) $\epsilon = 1$, or invoking extreme value statistics (Lovell et al. 2022).

Recently, Liu and Bromm (2022), Hütsi et al. (2023) investigated the hypothesis that early structure formation was induced by the seeding effect of PBH induced Poisson isocurvature perturbations.[16] Their result shows that such early formation of massive galaxies is possible if the PBH abundance is such that $m_{\rm PBH} f_{\rm PBH} \gtrsim 6 \times 10^6\ (2 \times 10^5) M_\odot$ for SFE $\epsilon < 0.1\ (1)$. Such abundance for massive PBHs are ruled out by observations of the CMB μ-distortion, although this conclusion relies on the assumptions that primordial density fluctuations are sufficiently Gaussian and that PBHs formed in the standard scenario of primordial density fluctuations not growing during the radiation-dominated era. However, strong isocurvature perturbations of PBHs with $m_{\rm PBH} f_{\rm PBH} \gtrsim 170\, M_\odot$ are ruled out by high-z Lyman-α forest data (Murgia et al. 2019).

7.5.5 Ultra-compact mini haloes

It has been claimed in Adamek et al. (2019), Bertone et al. (2019) that a small fraction of dark matter made of PBHs is not compatible with the rest of the dark matter being made of weakly interacting massive particles (WIMPs) because PBHs should seed the formation of ultra-compact mini-halos with steep density profiles (DM overdensities formed around PBHs are also referred as DM spikes or mini-spikes; Boudaud et al. 2021). Then, the WIMPs in the dense innermost part of these halos would annihilate, which produces a detectable gamma-ray signal. The absence of detection allows to set limits on the PBH fraction in presence of WIMPs, of at most one billionth of the dark matter for PBH masses larger than $10^{-6} M_\odot$. An interesting corollary is that any firm detection of PBHs implies that the remaining dark matter cannot be constituted by WIMPs. Similar analysis, e.g. including the effect of primordial non-Gaussianity or the mass dependence of this limit in the case of light PBHs, have been performed in Nakama et al. (2019), Carr et al. (2021d), Kadota and Silk (2021). The s-wave and p-wave annihilation scenarios have been compared in Kadota and Tashiro (2022) where a stringent limit has been obtained for

[16] See also Biagetti et al. (2023), Menci et al. (2022), Gong et al. (2023) for different potential explanations.

the thermal relic p-wave with a WIMP mass of 100 GeV (see also Chanda et al. 2024). It has been also shown in Tashiro and Kadota (2021b) that WIMPs around PBHs enhance the heating and ionization in the intergalactic medium, due to WIMP annihilations, leading to comparable or even tighter bounds of the possible DM fraction made of PBHs, for instance $f_{\rm PBH} \lesssim \mathcal{O}(10^{-10} - 10^{-8})$ for a WIMP mass of order $10 - 10^3$ GeV with a conventional annihilation cross section $\langle \sigma v \rangle = 3 \times 10^{-26} {\rm cm}^3/{\rm s}$. Some of those limits were recently reanalyzed in Ginés et al. (2022). WIMP annihilation in ultra-compact mini-halos around PBHs can also lead to a potentially detectable neutrino signal (Freese et al. 2022) and the limits can be competitive with respect to gamma-ray searches (Boucenna et al. 2018) if PBHs are heavy. Another proposed way to probe DM dresses around PBHs is by observing the gravitational strong lensing of sources like fast radio bursts in the PBH mass range from $10\,M_\odot$ to $10^3\,M_\odot$ (Oguri et al. 2023).

The specific case of SU(2)L triplet fermion "winos," has been studied in Hertzberg et al. (2021). In this case as well, after the wino kinetic decoupling, DM particles are captured by PBHs leading to dark mini-halos, constrained by the production of narrow line gamma rays from wino annihilation in the Galactic Center. Another very specific scenario of parsec-size ultra-compact mini-halos around PBHs, in the context of the QCD axion dark matter, encountering neutron stars and leading to transient radio emissions due to resonant axion-photon conversion in the neutron star magnetosphere, has been explored in Nurmi et al. (2021).

Finally, it has recently been argued in Sten Delos and Silk (2023) that the large density fluctuations required for PBH formation should also lead to ultradense DM halos (see also Ricotti and Gould 2009; Kohri et al. 2014; Gosenca et al. 2017; Delos et al. 2018a, b; Nakama et al. 2019; Hertzberg et al. 2020; Ando et al. 2022) that would actually host a large fraction of the DM (in much greater abundance than PBHs), enabling a variety of new observational tests. This conclusion is viable as long as clustering of the dark matter is possible on the relevant scales (e.g. Bringmann 2009). The formation of such halos can already take place before matter-radiation equality (Kolb and Tkachev 1994; Berezinsky et al. 2010, 2013; Delos 2019; Sten Delos and Silk 2023), which occurred at redshift $z \simeq 3400$ (Aghanim et al. 2020) Due to their early formation, ultradense DM halos could be compact enough to produce detectable microlensing signatures. If a dark matter spike forms around a PBH binary, it would induce a dephasing that could be measured with future detectors (Cole et al. 2023a).

In Delos and Franciolini (2023) it is investigated whether the EROS, OGLE, and HSC surveys can probe these halos by fully accounting for finite source size and extended lens effects. Interestingly, current data by the EROS-2 (Tisserand et al. 2007), OGLE-IV (Niikura et al. 2019a) and Subaru-HSC (Niikura et al. 2019b) surveys may already constrain the amplitudes of primordial curvature perturbations in a new region of parameter space, even though this conclusion is sensitive to details about the internal structures of these ultradense halos. Adopting optimistic assumptions, HSC data would constrain a power spectrum that features an enhancement at scales $k \sim 10^7/{\rm Mpc}$, and an amplitude as low as $\mathcal{P}_\zeta \simeq 10^{-4}$ may be accessible. This range of scale is particularly interesting as it connects to

primordial black hole formation in a portion of the LVK mass range and the production of scalar induced gravitational waves in the nanohertz frequency range reachable by pulsar timing arrays. Further dedicated numerical simulations are required to investigate in details the central density reached by such DM halos, to which lensing constraints are particularly sensitive.

In summary, the study of dark matter halos, seeded or induced by the existence of PBHs, brings support for the incompatibility of the coexistence of PBHs and WIMPs and all-or-nothing scenarios.

7.5.6 Discussion and limitations

The primordial fluctuations at the origin of the formation of PBHs with masses above $60\,M_\odot$ can have left detectable signatures in the form of spectral distortions of the CMB black-body spectrum, which have been constrained by FIRAS, in high-redshift Lyman-α forest observations, which can typically probe smaller length scales than large scale structure surveys or CMB anisotropies, and in a GW background sourced at second order in perturbation theory that was discussed in a dedicated section. Those indirect probes are therefore independent of the details of the PBH formation and their subsequent complex evolution. They also depend on the statistical properties of primordial fluctuations, e.g. they can be suppressed in the presence of large non-Gaussianities. These indirect probes are therefore very interesting to discriminate between the possible PBH formation models in a way that is independent of the complex physical processes that could have impacted the PBH properties. This is of particular interest to constrain models with broad PBH distributions aiming at explaining LVK observations and SMBH seeds in a unified way. The absence of any detection of CMB distortions would bring support to non-Gaussian models or to scenarios where PBHs are not formed by primordial density fluctuations.

7.6 Gravitational waves

7.6.1 LVK GW mergers

The LVK collaboration has been searching for compact binary coalescences. By the end of the O3 run, 90 binary black hole (BBH) candidates have been found (Abbott et al. 2023a), providing rich information on the BH population (Abbott et al. 2023b). The latest catalog GWTC-3 indicates that the BBH merger rate is between 17.3 $\mathrm{Gpc}^{-3}\mathrm{yr}^{-1}$ and 45 $\mathrm{Gpc}^{-3}\mathrm{yr}^{-1}$ at a fiducial redshift $(z = 0.2)$.

Soon after the first discovery of the BBH event GW150914, it has been pointed out that the observed BBH could be of primordial origin (Bird et al. 2016; Sasaki et al. 2016; Clesse and García-Bellido 2017b). More detection of BBH events provided information on the merger rate and the chirp mass distribution, and Clesse and García-Bellido (2018) made the first MCMC analysis to infer the PBH mass function. Statistical tests have been performed with the GWTC-1 catalog to test the hypothesis that all or part of observed BBHs is primordial (Hall et al. 2020). The use of the effective spin parameter has also been discussed (Fernandez and Profumo

2019; García-Bellido et al. 2021c). With more events from GWTC-2, the combination of an astrophysical and a primordial BH population have been tested, both using phenomenological models to describe the ABH population (De Luca et al. 2021c; Hütsi et al. 2021c) as well as state-of-the-art astrophysical population synthesis results (Franciolini et al. 2022a). These analyses confirm it is difficult to explain all the features observed in the GWTC-3 catalog of events by means of a single binary population, while showing shortcomings of both astrophysical and primordial scenarios, but still allows for PBH to contribute to a fraction of the observed BBHs.

Indication of particular events has been also discussed. GW190521 has attracted attention because at least the primary component mass lies in the so-called pair-instability mass gap, where there should not be direct formation of stellar black holes, and the possibility of a primordial origin has been discussed in De Luca et al. (2021a). The events GW190425 and GW190814 have both companions with masses $[1.6-2.5]M_\odot$ and $[2.5-2.7]M_\odot$, which is unexpected if they originated from a neutron star or a stellar black hole. Vattis et al. (2020) discussed the possibility of PBH pairing with an astrophysical BH, and concluded that it is unlikely that such binaries form and merge within a Hubble time (see also Kritos et al. 2021; Sasaki et al. 2022). Jedamzik (2021, 2020), Carr et al. (2021b), Clesse and García-Bellido (2022) investigated the possibility that both the primary and secondary BHs are primordial considering the thermal history mass function, which indeed has a bump at a few $M_\odot$ and around $30-50M_\odot$ and explains the events very well, together with GW190521.

Recently, Franciolini et al. (2022e) performed the most comprehensive Bayesian population analysis of LVK data, that includes both BH and NS merger events, while testing the hypothesis that a fraction of events may come from the primordial scenario, where the latter is derived from first principles with the inclusion of QCD effects on the mass distribution. The results of such an analysis can currently only set an upper bound on the PBH fraction, showing the still limited constraining power of available data, but interestingly peaked up some aforementioned special events with high probability of being primordial (i.e. GW190924_021846, GW190814, GW190412, and GW190521). One peculiar property of the PBH channel, is that if it produced mergers in the NS mass range, due to the QCD enhancement and the critical collapse, it would necessarily produce a mass distribution which is wider the the one expected for astrophysical NS mergers (Franciolini et al. 2022e). This would inevitably predicts subsolar, as well as lower mass gap event mergers.

Due to the much improved sensitivity of future observation runs, we notice that O4 and O5 may have more chances to detect many PBH events. However, unless some of these events have smoking-gun features (Franciolini et al. 2022b), it would be hard to distinguish them from ordinary astrophysical channels. Therefore, an interesting prediction, reported in Table 5, is the number of subsolar and mass-gap events detectable in O4 and O5, assuming GW190814 is primordial. Such numbers can be considered conservative upper bounds, as well as complementary tests of the primordial origin of the aforementioned events. In particular, in O5 there could be as many as ≈ 8 subsolar events per year (but the 90% confidence interval is also compatible with zero events). Then O5 should detect one to a few dozen events per

Table 5 Assuming GW190814 had primordial origin, this table reports the 90% C.I. for the number of detected PBH events within GWTC-3, and predicted events (per year) with LVK O4 and O5 sensitivity

LVK observing run	$N^{det}_{\rm PBH}$	$N^{det}_{\rm PBH}$(SS)	$N^{det}_{\rm PBH}$(LMG)	$N^{det}_{\rm PBH}$(UMG)
O1-O3	[0.8, 22.4]	[0.0, 0.6]	[0.1, 2.3]	[0.0, 6.1]
O4	[1.9, 43.7]	[0.0, 1.3]	[0.3, 13.0]	[0.0, 13.1]
O5	[10.3, 216.7]	[0.0, 8.6]	[0.8, 25.2]	[0.0, 47.3]

We also indicate forecasted detections (within the 90% C.I.) that would fall in the subsolar ($m_1 < M_\odot$, SS), lower mass gap ($m_1 \in [2.5, 5]\, M_\odot$ and/or $m_2 \in [2.5, 5]\, M_\odot$, LMG) and upper mass gap ($m_1 > 50 M_\odot$, UMG) ranges. Table adapted from Franciolini et al. (2022e)

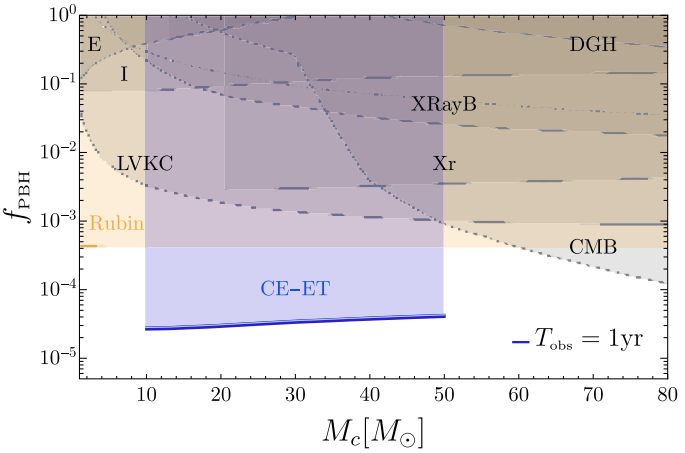

Fig. 41 Projected upper limit on $f_{\rm PBH}$ as a function of central PBH mass scale M_c (assuming a narrow log-normal mass distribution) obtained from null high redshift merger detections with one year of observations at a CE-ET network. See the main text for a discussion of the other (non-GW constraints). In yellow, we show forecasts for the limits that will be set by microlensing searches with the Rubin observatory (Drlica-Wagner et al. 2019; Bird et al. 2023). Image reproduced with permission from Ng et al. (2022b), copyright by the author(s) Image reproduced with permission

year in the lower mass-gap (and up to ≈ 50 upper mass-gap events), which might be more difficult to interpret in astrophysical scenarios.

Future observations at third generation experiments will be able to further constrain the abundance of PBHs in the LVK mass range by searching for high redshift PBH mergers, where the possible astrophysical contamination from Pop III mergers fades out (Ng et al. 2022b) (see also Nakamura et al. 2016; Koushiappas and Loeb 2017b; De Luca et al. 2021d; Pujolas et al. 2021; Ng et al. 2022a; Franciolini

et al. 2022b; Martinelli et al. 2022). This technique would allow to constrain the PBH abundance down to values as small as $f_{\rm PBH}\lesssim\mathcal{O}(10^{-5})$ in the standard scenario, see Fig. 41 (Ng et al. 2022b).[17]

7.6.2 LVK sub-solar searches

In addition to the standard compact binary coalescence search, the LVK has been updating the constraint on sub-solar mass binaries, where at least one binary component has a mass between $[0.2-1]M_\odot$ (Abbott et al. 2018, 2019c, 2022) (see also Nitz and Wang 2021a, b; Phukon et al. 2021; Nitz and Wang 2022). So far, no firm detection of such GWs has been reported, but four subsolar black hole candidates with false alarm rate smaller than $2\,{\rm yr}^{-1}$ and signal-to-noise ratio SNR >8 were reported in Phukon et al. (2021) after re-analysing the data from the second observing run within an extended mass range. If such a binary system were to be found with a clear statistical significance, it could be strong support for the existence of PBHs, since neither black holes nor neutron stars are expected to form below $\sim 1M_\odot$ through conventional stellar evolution. The recent analysis with the data from the first half of the LVK O3 run has provided a bound on the merger rate of subsolar binaries in the range $[220-24200]{\rm Gpc}^{-3}{\rm yr}^{-1}$. Assuming an isotropic distribution of equal-mass primordial black holes, the bound on the merger rate translates to the bound on the fraction of PBHs as $f_{\rm PBH}\equiv\Omega_{\rm PBH}/\Omega_{\rm DM}\lesssim 6\%$. Although the LVK collaboration papers have placed stringent constraints on the PBH abundance, they can be relaxed by two orders of magnitude if we take into account merger rate suppression due to binary disruption by early forming clusters, matter inhomogeneities and nearby PBHs (Phukon et al. 2021).

7.6.3 LVK SGWB

As mentioned in Sect. 5.6, overlapped GWs from binary PBHs form a SGWB. The most updated bound on the SGWB by the LVK O3 run is $\Omega_{\rm GW}<5.8\times10^{-9}$ at the 95% credible level for a flat (frequency-independent) SGWB (Abbott et al. 2021b). The first constraints on PBH abundance were argued in Wang et al. (2018) using the O1 data. The updated constraints by O2 and O3 data can be found in Raidal et al. (2017), Hütsi et al. (2021c). In addition, parameter estimation has been attempted by Mukherjee and Silk (2021) using the O3 data by considering both astrophysical and primordial components. The analysis provided weak constraints on the PBH merger rate and time delay parameter, while it indicated the difficulty of separating astrophysical and primordial BBH contributions with the current sensitivity of the detectors (see also Bavera et al. 2022). We may be able to obtain meaningful constraints on the PBH merger rate with the increased sensitivity of upcoming runs and future detectors.

[17] Such constraint becomes much more stringent if one assumes clustered PBH initial conditions, boosting the PBH merger rate (De Luca et al. 2021d). However, further work on understanding the merger rate of initially clustered scenarios is needed.

It is worth mentioning that the upper bound on the SGWB can provide constraints also on the ultralight PBHs in the mass range of $[10^{-20} - 10^{-19}]M_{\odot}$ through the scalar induced GWs. Those PBHs are strongly constrained by the Hawking radiation, but with the upgraded sensitivity, the ground-based interferometers could provide constraints that are several orders of magnitude stronger than existing constraints (Kapadia et al. 2020). The first constraint was demonstrated by (Kapadia et al. 2021) with the O2 data. See (Romero-Rodriguez et al. 2022) for the updated constraint by the O3 data.

7.6.4 PTAs and NANOGrav

As discussed in Sect. 5.1, enhanced density perturbations inevitably source stochastic GWs, dubbed as scalar induced GWs, or SIGW. The SIGW can be used to probe the small scale power spectrum (Nakama et al. 2017; Inomata and Nakama 2019; Byrnes et al. 2019; Cai et al. 2019b; Kalaja et al. 2019; Ünal et al. 2021; Papanikolaou 2022a). The amplitude of this signal can be estimated as $\Omega_{\rm GW} \sim (\text{symmetry factors}) \cdot \Omega_{\rm rad} \cdot P_{\zeta}^2$, where symmetry factors include possible contractions and different diagrams. Hence, it is seen that current PTA experiments can probe $P_{\zeta} > 10^{-2.5}$ at the nano-Hertz (nHz) scale.

In 2020, the NANOGrav collaboration first reported evidence in their 12.5-year dataset (Arzoumanian et al. 2020) for a common spectrum of a stochastic nature, representing the first hint of the existence of a nHz SGWB (also later on confirmed in Goncharov et al. 2021; Chen et al. 2021b; Antoniadis et al. 2022). However, at the time, no evidence was found for a quadrupolar spatial correlation (i.e. Hellings–Down (HD) curve; Hellings and Downs 1983), necessary to interpret the signal as a GW background consistent with General Relativity. Interestingly, the more recent PTA data released in 2023 by the NANOGrav (Agazie et al. 2023b, c), EPTA (in combination with InPTA) (Antoniadis et al. 2023b, a, 2024), PPTA (Reardon et al. 2023a; Zic et al. 2023; Reardon et al. 2023b) and CPTA (Xu et al. 2023) collaborations, gathered significant evidence for a HD angular correlation.

Focusing on the most stringent dataset, the latest NANOGrav 15-yr, the reported observations can be fitted by a smooth power law with a scaling $\Omega_{\rm GW} \propto f^{(1.6,2.3)}$ at 1σ. It is known that supermassive black hole binaries produce a SGWB with a scaling $\Omega_{\rm GW} \propto f^{2/3}$ (Phinney 2001) if binary evolution is GW driven, which is currently disfavoured at 2σ by the NANOGrav 15-year data (Agazie et al. 2023a; Afzal et al. 2023). Nevertheless, environmental and statistical effects may play a relevant role, and lead to a steeper scaling (Sesana et al. 2008; Kocsis and Sesana 2011; Kelley et al. 2017; Perrodin and Sesana 2018; Ellis et al. 2023; Agazie et al. 2023a; Afzal et al. 2023; Ghoshal and Strumia 2024). At the present stage, current data does not allow to rule-out (or rule-in) a cosmological origin for the observed signal, which may also be due to first-order phase transitions (Arzoumanian et al. 2021; Xue et al. 2021; Nakai et al. 2021; Di Bari et al. 2021; Sakharov et al. 2021; Li et al. 2021; Ashoorioon et al. 2022; Benetti et al. 2022; Barir et al. 2023; Hindmarsh and Kume 2023; Gouttenoire and Volansky 2024; Baldes et al. 2023; Ghosh et al. 2024; Gouttenoire 2023), cosmic strings and domain walls (Ellis and Lewicki 2021;

Datta et al. 2021; Samanta and Datta 2021; Buchmüller et al. 2020, 2021; Blasi et al. 2021; Ramazanov et al. 2022; Babichev et al. 2022; Gorghetto et al. 2021; Blanco-Pillado et al. 2021b; Ferreira et al. 2023; An and Yang 2024; Qiu and Yu 2023; Zeng et al. 2023; King et al. 2024; Babichev et al. 2023; Kitajima et al. 2024; Barman et al. 2023; Blasi et al. 2023; Lazarides et al. 2023; Cai et al. 2023; Gouttenoire and Vitagliano 2024), and inflationary first order tensor perturbations (Vagnozzi 2023; García-Bellido et al. 2017; Ünal et al. 2024) (see also for other explanations Franciolini et al. 2024b; Madge et al. 2023; Figueroa et al. 2024; García-Bellido et al. 2024; Murai and Yin 2023).

Standard PBH formation scenarios generating a population of subsolar PBHs are related to the emission of an induced SGWB, which may explain current PTA detections (Vaskonen and Veermäe 2021; De Luca et al. 2021g; Bhaumik and Jain 2021; Inomata et al. 2021a; Kohri and Terada 2021; Domènech and Pi 2022; Vagnozzi 2021; Namba and Suzuki 2020; Sugiyama et al. 2021; Zhou et al. 2020; Lin et al. 2023; Rezazadeh et al. 2022; Kawasaki and Nakatsuka 2021; Ahmed et al. 2022; Yi and Fei 2023; Yi 2023; Zhao and Wang 2023; Dandoy et al. 2023; Zhao et al. 2023; Ferrante et al. 2023a; Cai et al. 2024; Franciolini et al. 2023; Balaji et al. 2023; Liu et al. 2024; You et al. 2023; Jin et al. 2023; Zhao et al. 2024; Wang et al. 2024a, b; Firouzjahi and Talebian 2023; Liu et al. 2024; Basilakos et al. 2024a, b; Abe and Tada 2023; Inomata et al. 2024). In Fig. 42 we show the parameter space that would be compatible with PTA signal and how this relates to PBH overproduction constraints (see also Sect. 3 for a discussion on the uncertainties affecting the computation of the PBH abundance).

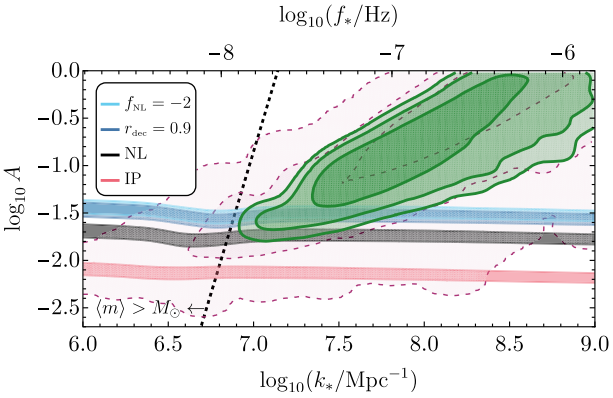

Fig. 42 The green and purple posterior indicate the 1, 2, 3σ contours obtained fitting to NANOGrav15 and EPTA dataset, respectively. This plot assumed a broken power law curvature spectrum with a fixed growth index $n = 4$ and varying decay power law index after the peak located at k_*. A indicates the power spectral peak amplitude and we indicate on top the corresponding peak SGWB frequency. We also show the corresponding PBH abundance for different models: Gaussian curvature perturbations including non-linear effects (black), quasi-inflection-point models with $\beta = 3$ (red), curvaton models with $r_{\rm dec} = 0.9$ (blue) and negative f_{NL} (cyan) (see Table 1 and references therein for more details). The colored bands cover values of PBH abundance in the range $f_{\rm PBH} \in (1, 10^{-3})$ from top to bottom. The dashed line indicates an average PBH mass $\langle m \rangle = M_\odot$. We point the reader to Sect. 3 for a discussion on the uncertainties affecting the computation of the PBH abundance. Image reproduced with permission from Franciolini et al. (2023), copyright by APS Image reproduced with permission

Due to the extreme sensitivity of PBHs to the statistics of the primordial perturbations, it is also possible to reduce or enhance the abundance of PBHs efficiently via non-Gaussian perturbations. This could result in a larger/smaller amplitude of curvature perturbations and of the associated SIGWs. On the one hand, assuming a fixed abundance of PBHs, negative non-Gaussianities would be able to enhance the associated amplitude of the GW signal, bringing it closer to the range preferred by PTA observations. On the other hand, positive non-Gaussianities could reduce Ω_{GW} allowing this scenarios to escape the sensitivity level of current PTA experiments.

Future nHz frequency gravitational wave detectors will reach remarkable sensitivities, provided a potential astrophysical background can be tamed. Therefore, with future PTA-SKA experiments we will either detect or rule out conclusively the cosmological signals accompanying the formation of PBHs. PTA-SKA will robustly probe PBH mass formation in the range $[0.1 - 10^4]M_\odot$. This regime is extremely important for both astrophysical sources such as stellar mass BH binaries, intermediate BHs and SMBH seeds. In Fig. 43, from Ünal et al. (2021), we show the PTA-SKA detection capabilities of the stochastic GW background sourced by primordial scalar perturbations which obey different statistical distributions: Gaussian, chi-sqr (χ^2) and cubic-Gaussian (G^3) for the cases i) $f_{\rm PBH} \sim 1$ (i.e PBHs constituting all the DM) and ii) $f_{\rm PBH} = 10^{-10}$.

One should point out here as well the possibility of future nHz PTA-SKA GW detectors to observe ultralight PBHs in the mass range $10^7 - 10^9$ g given that the peak frequency associated to the scalar induced GWs sourced by Poisson PBH energy density fluctuations, related to the PBH spatial distribution, is well within the PTA-SKA frequency range (Papanikolaou et al. 2021). This potential detectability of such small mass PBHs is very important given the fact that these ultralight PBHs

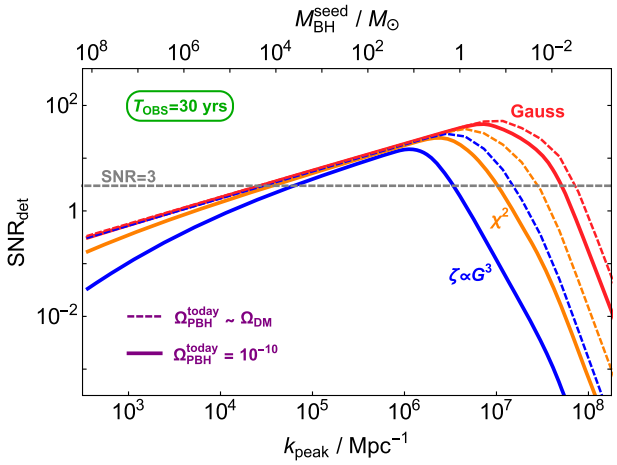

Fig. 43 PTA-SKA detection capabilities of the stochastic GW background sourced by scalar perturbations with distinct primordial statistical distributions: Gaussian (red), chi-sqr (χ^2, orange) and cubic-Gaussian (G^3, blue) for i) $f_{\rm PBH} \sim 1$ (i.e. PBHs constituting all the DM) and ii) $f_{\rm PBH} = 10^{-10}$. Image reproduced with permission from Ünal et al. (2021), copyright by APS Image reproduced with permission

evaporate before BBN so they do not leave another direct observational imprint of their existence.

7.6.5 Continuous and high-frequency GWs from planetary-mass PBHs

PBH binary systems with a planetary chirp mass should emit very weak continuous GWs in the frequency range of ground-based interferometers, many years before they actually merge. It has been proposed to search for continuous waves from PBH binaries in our galaxy (Miller et al. 2021), either towards the galactic center or in the solar system vicinity. However, the current limits on continuous waves do not yet provide significant limits on the PBH abundance (Miller et al. 2022), even for the models with the highest merger rates. However, future instruments like Einstein Telescope should be able to probe $f_{\rm PBH}$ between 10^{-2} and 1.

When they merge, these low-mass PBH binaries emit gravitational waves in the MHz or GHz range. These could be probed with high-frequency GW detectors like resonant microwave cavities, which could probe $f_{\rm PBH}$ down to about 10^{-3} (Herman et al. 2021; Aggarwal et al. 2021). Additionally, one recent proposal involving resonant LC circuits may represent the best option in terms of individual merger detection prospects in the range $(1-100)$ MHz. It was also shown in Franciolini et al. (2022d) that a detection of the stochastic gravitational wave background produced by unresolved light PBH binaries is possible only if the theoretical sensitivity of the proposed Gaussian beam detector is achieved. Such a detector, whose feasibility is subject to various caveats, may be able to rule-out some scenarios for asteroidal mass primordial black hole dark matter (see Franciolini et al. 2022d and references therein for more details).

7.6.6 Discussion and limitations

Gravitational wave observations already provide both limits on the PBH abundance and possible hints in favor of the PBH hypothesis. There is a rather general agreement that the observations of black hole mergers around $30\,M_\odot$ do not allow for more than about a percent of the dark matter to be made of PBHs of this mass.

Exceptional GW events, e.g. including at least one black hole in the pair-instability mass gap (like GW190521), with one object in the low-mass gap or at least heavier than most of neutron stars (like GW190814 and GW190421) without electromagnetic counterparts, mergers with low mass ratios and small individual spins (like GW190814), with statistical evidence for a black hole spin not aligned or anti-aligned with orbital momentum, as well as the measured low effective spins, provide a series of indications that challenge most standard stellar-origin scenarios and suggest alternative formation mechanisms. Among these alternatives, the PBH hypothesis is a front-runner together with scenarios of stellar black hole binary formation in dense environments like globular clusters or nearby AGNs. All these observations are also pushing the odds in favor of PBHs when one performs model comparisons based on Bayesian statistics. But the statistical significance of these

observations, as well as the large theoretical uncertainties on both PBHs and stellar black hole models, do not yet allow to draw a definitive conclusion.

If at least some of the detected black holes are primordial, this suggests a somehow extended mass function, which is also more realistic theoretically. This means that thermal effects induced by the QCD transition needs to be taken into account, as recently done in Franciolini et al. (2022e), Escrivà et al. (2023), which have important effects in the stellar mass range and can modify the merger rate distribution previously derived with phenomenological lognormal models.

Limits on GW backgrounds is another way to already probe the possible DM fraction made of PBHs, but these limits highly depend on the model parameters and are impacted by the merger rate uncertainties or by the possible non-Gaussian statistics of scalar perturbations in the case of a SGWB from second order perturbations. Nevertheless, it has been claimed that the possible signal from PTAs at nHz frequencies could come from the scalar perturbations leading to stellar-mass or planetary-mass PBHs.

Altogether, GWs appear to be a very novel and promising way to probe and set a limit on the abundance of PBHs. Once again, one must be cautious because of the large model uncertainties, but the intriguing LVK observations provide a very strong motivation to investigate further the PBH hypothesis with improved models and Bayesian statistical methods. Among the GW signatures of PBHs, signals from the coalescence of subsolar black holes provide the most compelling way to distinguish between stellar and primordial origin. A few candidates have been recently found but whose statistical significance is too limited to claim a detection. Upcoming data will have the ability to detect subsolar PBHs if they significantly contribute to the dark matter.

7.7 Summary

There are dozens of ways to probe and constrain the abundance of PBHs, which have been reviewed in this section. If one strictly follows the claimed limits and assume a monochromatic distribution, it seems excluded that PBHs account for the entirety of the dark matter below $10^{-16}M_\odot$ due to limits based on PBH evaporation through Hawking radiation and above $10^{-10}M_\odot$ due to microlensing limits up to the solar mass scale, and multiple other astrophysical and cosmological observations at masses above a solar mass. This has fed the interest for the asteroid-mass region that until know remains open, even if some limits have been claimed from the capture of PBHs by stars, but still using quite specific assumptions.

It is however worth noticing that the situation is in reality much less simplistic, and that all the limits rely on assumptions that can be debated and that very often are also model dependent. The simplest example of the mitigation of these limits is probably the fact that all the evaporation-based limits rely on a still unproven physical phenomena mixing quantum theory and gravity. If for any reason our current description of the Hawking radiation is incorrect or if it is less efficient than expected, all the limits on the PBH abundance below $10^{-16}M_\odot$ disappear. Lots of work have tried to examine the validity of the assumptions in different contexts and

these were also discussed in this section. It is also worth noticing that the strength of the microlensing limits can vary depending on the PBH clustering, on the galactic halo profiles, etc. Another example of how limits can change depending on assumptions is provided by CMB limits, varying by many orders of magnitude depending on the details of the accretion process onto PBHs or on the dark matter content.

Besides asteroid-mass PBHs, one can also notice that in the solar-mass region, the number of probes is limited to microlensing and X-ray limits and are not extremely stringent, varying between 10^{-2} and 10^{-1}. For quite extended PBH mass functions, it could remain a viable possibility that the main peak of PBHs arises within this range as one could expect from the QCD-transition. Scenarios combining a peak in the asteroid-mass range and a peak in the solar-mass range, possibly explaining GW observations, are also an interesting possibility.

Finally, one should note that limits on PBH abundances cohabit with possible positive evidence (Carr et al. 2024), e.g. from detected microlensing events, cosmic background properties supporting the high redshift existence of PBH clusters, and obviously GW observations and the intriguing properties of black hole binary mergers. Most of these evidences point to the stellar-mass region.

Taken all these considerations into account, it seems indeed difficultly plausible that all the dark matter is made of planetary-mass or intermediate mass (above $10M_\odot$) PBHs. But both the asteroid-mass region and the stellar-mass region remain of very high interest, especially in the context of extended mass distributions. But strong claims are probably premature given the remaining large level of uncertainties for all the probes.

8 Detectability with LISA

In this section, we aim at summarizing the different ways with which the LISA mission can probe PBHs, and the possible impact that LISA will have on our understanding of the viable PBH models, in particular their mass function, merging rates, and the underlying formation scenarios. Remarkably, we emphasize that not only LISA will be able to probe intermediate-mass PBHs but also solar-mass and subsolar mass PBHs, and even tiny PBHs formed at very high energies in the early Universe that would have entirely evaporated, due to the Poisson fluctuations and the resulting SGWB they would have left.

8.1 SGWB from second order curvature fluctuations

The generation of PBHs from the collapse of sizeable density perturbations is unavoidably associated with the emission of a SGWB at second order in perturbation theory, whose characteristic frequency can be related to the PBH mass (Yuan and Huang 2021a; Domènech 2021). It has been found that the formation of PBHs with masses around $\mathcal{O}(10^{-15} - 10^{-8})M_\odot$, where they can comprise the dark matter in the Universe, corresponds to the emission of a SGWB with frequency and abundance well within the LISA sensitivity curve (Bartolo et al. 2019b).

The properties of such a SGWB can be summarised as follows:

- The shape of the signal depends on the power spectrum of the curvature perturbations and is model dependent. However, the behaviour at low frequencies is predicted to be scaling like $\sim k^3$ due to causality arguments (Cai et al. 2020).[18]
- Even though GW signals have an intrinsic non-Gaussian nature at emission epoch, their coherence in phase correlations is washed out by their propagation in the perturbed Universe due to time delay effects generated by large scale variations of the gravitational potential, leading to a completely low-redshift Gaussian signal at the LISA detector (Bartolo et al. 2019c).
- The presence of local scale-invariant primordial non-Gaussianities in the scalar curvature perturbation would be responsible in modifying the shape and abundance of the GW spectrum (Ünal 2019), as well as inducing a large amount of anisotropies in the SGWB, potentially detectable by LISA (Bartolo et al. 2022), if PBHs comprise only a small fraction of the dark matter in the Universe (Bartolo et al. 2020a).

These predictions can be used to disentangle this signal from other SGWBs of different nature.

8.2 SGWB from ultralight evaporated PBHs

LISA will also probe the formation of PBHs of mass between 10 g and 10^9 g that are too light to have survived until today, due to Hawking evaporation. In particular, a SGWB comes from the Poisson fluctuations in the spatial distribution of these PBHs at formation (Papanikolaou et al. 2021). These Poisson fluctuations correspond actually to scalar inhomogeneities, sourcing a SGWB at second order. This will be particularly interesting in the context of modified-gravity setups (Papanikolaou et al. 2022, 2023b) that could be constrained or even ruled out using the SGWB from ultralight PBHs.

Through this PBH-induced SGWB, LISA will indirectly probe the early Universe at energies up to the scale of grand-unified theory, including inflationary models, even if these PBHs have quickly evaporated.

8.3 SGWB from early binaries

As seen in Fig. 30, the SGWB amplitude for a log-normal mass function with central mass $\mu = 2.5M_\odot$ and width $\sigma = 1$ reaches its peak at around 100 Hz, and starts to be greatly suppressed below the LISA frequencies. For the thermal broad-mass function, one notices in Fig. 31 the important contribution to the SGWB from binaries composed of intermediate and solar-mass PBH (coming from the electron peak and the QCD peak in the PBH mass function respectively, see Fig. 13). These low-mass-ratio binaries start to boost the SGWB below 0.1 Hz by up to 3 orders of magnitude

[18] See Domènech et al. (2020), Hook et al. (2021), Witkowski et al. (2022) where the impact of thermal history on the SGWB spectral shape was investigated.

at most, compared to the log-normal case (Fig. 30). In particular, one can notice a bump in the SGWB around 10^{-3} Hz, originating from the bump around $10^6 M_\odot$ in the broad PBH mass function. The shape of the background could therefore give us important details about the PBH mass function and allow for precise reconstruction. The SGWB spectral index ($\mathrm{d}\log\Omega_{\rm GW}/\mathrm{d}\log f$) is overall positive for the early binaries contrary to the late-time PBH binaries (see next Subsection), thus probing the SGWB spectral index at the LISA frequencies could be a way to differentiate PBH binaries in clusters from early PBH binaries.

8.4 SGWB from late binaries

Similarly to the early binaries case, the SGWB amplitude for a log-normal mass function is much lower at the LISA frequencies, but we can still expect a detection if the GW amplitude is high enough to be detected by LVK. In the case of a thermal history mass function, the SGWB amplitude is enhanced at LISA frequencies because we have more massive PBHs paring with the $2M_\odot$ PBHs (see Figs. 32 and 33). The overall amplitude is determined by the merger rate, which still has a large uncertainty. As discussed in Sect. 4.2, it can be enhanced by increasing the PBH density in clusters and/or lowering the PBH velocity. Further observations by LVK would provide useful implications on the merger rate to refine the prediction on the SGWB amplitude at LISA frequency.

8.5 Intermediate-mass binary mergers

As shown in Fig. 21 for two typical models, intermediate-mass PBHs between 10^3 and $10^5 M_\odot$ that are contributing to the dark matter at the sub-percent level at most, due to other limits in this range, could merge with rates above $10^{-3}\mathrm{yr}^{-1}\mathrm{Gpc}^{-3}$. Interestingly, this mass range corresponds to GW frequencies where LISA has the highest range, effectively probing any merger in the observable Universe up to redshifts of 100 to 1000. This means that even if the merger rate is lower than in the stellar-range, LISA could detect more than a few of these mergers every year. Determining the merger rate and redshift distribution of intermediate-mass BH mergers is therefore a promising way to constrain the PBH mass functions and clustering properties, possibly linking them to the seeds of supermassive black holes.

8.6 Extreme mass ratio inspirals

The capability of LISA of targeting low frequency regimes makes it an ideal experiment for the search of GW signals generated from the inspiral of a subsolar mass compact object that could have a primordial origin around a supermassive black hole (SMBH). GW constraints can be set on the PBH abundance from the expected PBH-SMBH merger rate (Guo et al. 2019a; Kuhnel et al. 2020). In particular, a null-detection during a 5-year operation of the experiment would constrain the PBH abundance to values smaller than $f_{\rm PBH} \lesssim 3 \times 10^{-4}$ for PBHs masses in the range $(10^{-2} - 1)\, M_\odot$ (Guo et al. 2019a). Furthermore, the detection of these extreme mass-

ratio inspirals at LISA will be crucial in the search for subsolar-mass black holes, given the unparalleled precision in measuring the mass of the secondary object at subpercent level for PBHs as light as $\mathcal{O}(0.01)M_\odot$ up to luminosity distances around hundred megaparsecs (Barsanti et al. 2022). This would allow the claim of detection of a subsolar-mass black hole with very high statistical confidence.

8.7 High-redshift binary mergers

It is challenging to explain how supermassive black holes can exist in only partially reionized environments at redshifts as high as $z \gtrsim 7$ (Banados et al. 2018). If the seeds of these black holes come from the first population of stars, this typically needs super-Eddington accretion rate and large mass seeds. Another possible mechanism is the direct collapse of gas into BHs. Both models have their caveats. Even if one invokes super-Eddington accretion, it is very challenging for these seeds to reach sufficiently large masses to explain observations. PBHs are an alternative explanation to the existence of SMBHs since they can provide seeds of intermediate-mass BHs at higher redshift than for the other astrophysical mechanisms (Duechting 2004; Kawasaki et al. 2012; Clesse and García-Bellido 2015; Bernal et al. 2018; De Luca et al. 2023a). Therefore, the easiest way to distinguish PBH seeds from other candidates is to observe intermediate-mass or even supermassive black holes at $z \gtrsim 20$, prior to star formation.

The astrophysical range of LISA will allow for the observation of IMBBH mergers at redshifts $z > 20$ with a SNR larger than five, for equal-mass mergers and progenitor masses between $10^3\,M_\odot$ and $10^6\,M_\odot$ (Colpi et al. 2024). The possible merger rates of PBHs for a broad mass function with the imprints of the thermal history, shown in Fig. 21, can be larger than $\mathcal{O}(1)\mathrm{yr}^{-1}$ for primordial IMBBHs that would be formed in PBH clusters at high redshift. The existence of these clusters is relevant since they would also form in the standard Press–Schechter theory. LISA observations will be complementary to those of Earth-based GW detectors, like CE and ET, which will probe mergers with lower masses, and to future PTA limits from SKA, which will probe eventual mergers of SMBHs.

8.8 Combination with LVK observations

Numerous compact binary coalescences with total mass between $10\,M_\odot$ and $100\,M_\odot$ and a merger frequency in the range probed by Earth-based interferometers will also be detected by LISA due to the GW emission in the inspiral phase, as illustrated in Fig. 44. This provides a unique way to determine months or even years in advance when and in which sky location these mergers are going to occur. It will be then easier to search for electromagnetic counterparts of mergers. Parameter reconstruction will also be improved, which could also help to better determine the source location, distance and redshift. According to Sesana (2016), up to hundreds of binary black hole mergers could be pre-determined with an accuracy of about 10 s and $1\,\mathrm{deg}^2$, as well as a chirp mass reconstruction at the 10^{-6} level. The latest analysis (Klein et al. 2022) uses the state-of-art waveforms and Bayesian parameter

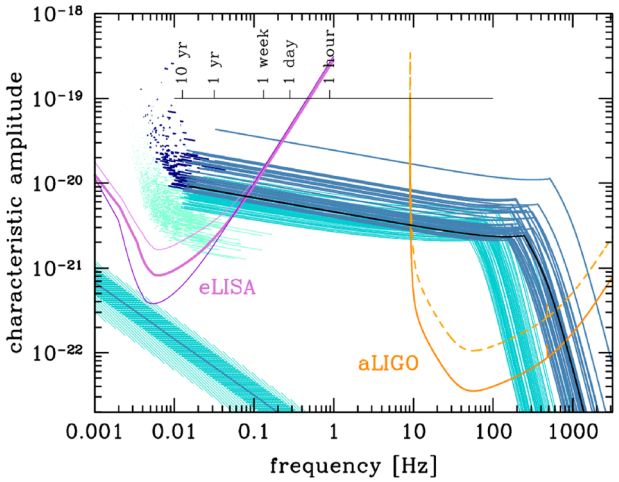

Fig. 44 Illustration of the concept of multi-band GW astronomy, combining (e)LISA and aLIGO (LVK). Each blue line corresponds to a trajectory in the strain-frequency plane for black hole mergers. The horizontal time scale corresponds to the probed time before the merger. Image reproduced with permission from Sesana (2016), copyright by APS Image reproduced with permission

estimation for both frequency bands to assess the potential of multi-band GW observations of the stellar-mass BBHs starting from 3 years before the merger (LISA) up to the coalescence (ground-based detectors: upgraded LVK or 3 G – either ET or CE). Such observations will allow to determine all 17 parameters describing the binary with at least percent-level accuracy, possibly to identify a likely host galaxy and to alert about the expected merger days in advance significantly improving the chances of detection of any electromagnetic signature associated with it.

In Franciolini et al. (2022b) the measurement accuracy by LISA, ET and LVK has been quantified for such PBH binary discriminators as eccentricity, spin and mass-spin correlation, as well as the horizon redshift for subsolar-mass mergers with negligible spins and eccentricity has been determined.

A better reconstruction of the black hole mass, rate and redshift distribution will help to distinguish between primordial and stellar scenarios, as well as the black hole environment and binary formation channel (merger from a cluster, stellar binary origin, AGNs...). This could be particularly the case for mergers with black hole masses in the pair-instability mass gaps that would be seen as short bursts in LVK detectors, not allowing for a precise mass reconstruction. LISA will significantly help to determine their still enigmatic (possibly primordial) origin.

8.9 Quasi-monochromatic continuous waves from subsolar PBHs

It has been pointed out in Pujolas et al. (2021), Barsanti et al. (2022), Guo and Miller (2022) that LISA will probe the existence of galactic subsolar PBHs in binaries with very long coalescence times up to distances of tens of kiloparsecs, allowing to probe the galactic center or PBH clusters in the galactic dark matter halo. This range is

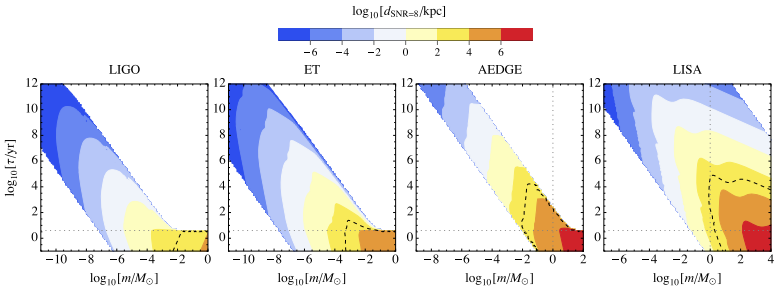

Fig. 45 Distance for which a circular binary of total mass m and coalescence time τ leads to quasi-continuous gravitational waves detectable with a SNR = 8 in different detectors. The expectations for LISA are shown in the right panel. Image reproduced with permission from Pujolas et al. (2021), copyright by APS Image reproduced with permission

shown in the right panel of Fig. 45 coming from Pujolas et al. (2021) as a function of the binary mass and time before collapse. The most interesting region is probably for $10^{-2}M_\odot < m < 1M_\odot$ and collapse time τ up to 10^8 years, for which the range is of order of tens of parsecs.

Therefore, with the use of continuous-wave methods, LISA will be able to probe different mass and collapse time scales than ground-based instruments like Einstein telescope (De Luca et al. 2021d). It will therefore be complementary to probe the existence of subsolar black holes or primordial origin in our galaxy, which if they are found, would lead to groundbreaking implications in cosmology.

8.10 Observing near-Earth asteroid-mass primordial black holes

The LISA instrument will have the sensitivity to detect the gravitational influence of dark matter clumps or dark asteroid-mass compact objects like tiny primordial black holes passing nearby the detector. This possibility was recently studied in Baum et al. (2022) (see also the old work by Seto and Cooray 2004).

With typical galactic velocities of hundreds kilometers per second, the signal duration is of order of hours or days, and would correspond to a burst at a frequency of order 10^{-6}–10^{-4} Hz, within the LISA sensitivity band. Since the signal would come from a transient change in the acceleration on the three mirrors resulting from the gravitational force exerted by the compact object, the shape of the signal is expected to be different than for a gravitational-wave tensor fluctuation. Therefore specific analysis tools are probably needed to search for them, but those could be used to detect near-Earth asteroids as well, which would be an interesting bi-product of such an analysis. For instance, one expects one observable transit every 20 years (Baum et al. 2022) for PBHs with mass of order 10^{14} kg, if they constitute all the DM density. The expected LISA range to asteroid-mass PBHs and the corresponding rate of expected events is shown in Fig. 46.

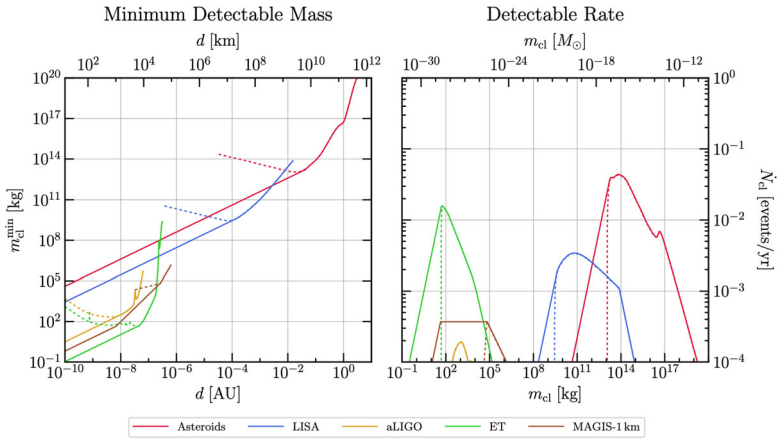

Fig. 46 Left: Expected mass of dark matter clumps or compact objects like PBHs $m_{\rm cl}$ in the inner solar system that could be detected at a distance d by LISA and other types of gravitational-wave detectors, due to the transient acceleration of test masses (which for LISA corresponds to the mirrors in the three space probes). Right: Corresponding rate of expected observable events as a function of the object mass, if they comprise all the dark matter and assuming galactic velocities. Image reproduced with permission from Baum et al. (2022), copyright by APS Image reproduced with permission

Observing tiny primordial black holes in the solar system would be clearly revolutionary and LISA will probably be the first instrument to reach the required sensitivity to make such a great achievement.

8.11 Summary

LISA will have the ability to probe primordial black holes of a very broad range of masses, based on different signals and GW production mechanisms:

- 10^3 – $10^9\,M_\odot$: GWs from the merging of intermediate-mass and supermassive black holes, including at redshift $z \gtrsim 20$, and their SGWB.
- 10 – $100\,M_\odot$: GWs from the merging of binaries with extreme-mass ratios and their SGWB.
- 0.01 – $1\,M_\odot$: Quasi-continuous GWs from sub-solar PBH in our galaxy.
- 10^{-15} – $10^{-8}\,M_\odot$: SGWB from second order perturbations.
- 10^{-19} – $10^{-16}\,M_\odot$: Newtonian gravitational force from PBHs in the inner solar system.
- $< 10^{-20}\,M_\odot$: SGWB induced by Poisson PBH energy density fluctuations.

This includes the two best ways to almost unambiguously prove the existence of PBHs, i.e. detecting subsolar black holes (in binaries with extreme mass ratios) and black holes at higher redshift than the stellar formation scenario can account for.

As a consequence, LISA will be an instrument of premiere importance in order to probe the existence of PBHs, which will be complementary to other astrophysical and cosmological signals, as well as other types of GW detectors.

9 Conclusions

Since the first detection of gravitational waves in 2015, primordial black holes (PBHs) have been the subject of an exponential growth of interest. Not only could PBHs explain some of the LVK black hole mergers but they could also have important cosmological consequences in cosmology: their existence would unveil new high-energy physics needed for their formation in the early Universe, they could significantly contribute to or even entirely constitute the dark matter, they may be related to baryogenesis, may have seeded supermassive black holes at the center of galaxies, and may as well have significantly modified the formation and growth of structures through the Universe's history.

With this work, we provide a review including the most recent scenarios of primordial black hole formation. The most up-to-date formalisms to be used for end-to-end calculations of their gravitational-wave signatures are also reviewed. A particular emphasis is placed on the observational perspectives in the context of the LISA mission. The present astrophysical and cosmological limits are also briefly reviewed and discussed, as well as the possible clues for their existence.

Among the plethora of formation mechanisms, we have discussed in particular the recent classes of models in which PBHs are formed from Gaussian or non-Gaussian inhomogeneities that could be produced from quantum fluctuations or quantum diffusion of one or more scalar fields during inflation. Wherever possible, we provided the concrete formula to be used to calculate the primordial power spectrum of curvature fluctuations in these models and their possible non-Gaussian statistics. We went beyond the standard formalism of PBH formation by reviewing recent progress on the relation between the curvature perturbation and the density contrast, the model-dependent computation of the overdensity threshold leading to PBH formation, including thermal effects at the QCD transition that provide a good theoretical motivation for a peak in the PBHs distribution at the stellar-mass scale (possibly associated with LVK observations). We also went beyond the standard computation of the present PBH mass function and spin distribution by including non-trivial effects related to accretion, which have been studied recently.

PBHs can lead to different types of signatures in gravitational-wave observations and we have reviewed their calculation in a model-dependent way. We provided the most recent prescriptions for the calculation of the PBH merging rates, for different binary formation mechanisms (early binaries, binaries formed in clusters, disrupted binaries). These mergers would leave distinct GW signatures that are searched for with GW template-based methods. The PBH mass function and the underlying formation model could be reconstructed from the rate, mass, spin and redshift

distribution of black hole mergers with present and future gravitational-wave interferometers. Recent analysis of LVK observations have revealed that there could be some statistical significance in favor of the PBHs hypothesis, depending on which astrophysical channels one compares them to. Another source of GWs comes from the transient bursts produced during close hyperbolic encounters, for which we also provide the expected rate and typical shape. Besides transient events, PBH binaries and hyperbolic encounters should also have produced a stochastic GW background covering the full frequency range accessible with observations of pulsar timing arrays, LISA and ground-based interferometers. The general formalism to compute this background has been reviewed and particular examples based on broad PBH mass functions including thermal effects have been given and discussed. At second order in perturbation theory, one gets another source of gravitational-waves associated with PBHs, coming from the large density fluctuations that are at the origin of their formation or, for lighter PBHs which have already evaporated today, that are produced by their Poisson distribution. We have reviewed the most recent prescriptions to calculate these SGWBs for any PBH model, and discussed their observability.

The future LISA space-based interferometer will probe PBHs in several ways. First, by searching for intermediate-mass PBH mergers. Based on the expected noise power spectral density, we estimated the number and distribution of PBH merger events in some models. LISA will also be able to detect mergers with very low mass ratios, for instance between an intermediate-mass PBH and a solar-mass PBH produced at the QCD transition. Also, it will probe the SGWB from PBH binaries, which could be strongly boosted for wide PBH mass functions, compared to a peaked PBH mass function. Therefore, LISA will be very useful to disentangle the different possible PBH mass functions and formation scenarios. Searching for high-redshift mergers is another way to distinguish astrophysical and primordial origins of black holes and test the hypothesis that supermassive black hole seeds are primordial. Finally, the broad gravitational-wave frequency range covered by LISA will allow to probe the stochastic GW background induced by scalar perturbations, corresponding to PBH scales ranging from $10^{-15}M_\odot$ to $10^{-8}M_\odot$, therefore covering the interesting asteroid-mass range where there is no significant limit on the PBH abundance. By probing a scalar-induced background from Poisson fluctuations in even lighter, evaporating PBHs, that would have totally disappeared from the Universe today due to Hawking evaporation. This would be another unique way to probe physics at much higher scales than can be done with particle accelerators.

Our work will soon be accompanied by a numerical code to compute all these gravitational-wave observations, for a wide variety of models. This code is currently under development and testing, but some of our key figures were already produced using it. This is a first promising perspective of this work. Then, our review also sheds light on the physical processes that are still subject of large uncertainties, like the role of PBH accretion and clustering, or the PBH binary disruption. We also discuss the fact that all signatures are highly model dependent.

One important conclusion of our analysis of the recent literature on PBHs is that strong claims, in one or another direction, are certainly premature and generally rely

on hypotheses that are very hard to test. Thus, there is still a huge amount of work to be done before making precise predictions. We therefore encourage others to pursue this direction and hope that our work will provide motivation and tools for researchers from other fields to join the growing PBH community.

Acknowledgements E.B. and S.C. acknowledge support from the Belgian Francqui Foundation through a start-up grant and to the Belgian Fund for Research FNRS-F.R.S. through the *Mandat d'impulsion scientifique* MIS/VA - F.4509.22 and an IISN grant. V.DL. is supported by funds provided by the Center for Particle Cosmology at the University of Pennsylvania. JME is supported by the European Union's Horizon 2020 research and innovation program under the Marie Sklodowska-Curie grant agreement No. 847523 INTERACTIONS, and by VILLUM FONDEN (grant no. 53101 and 37766). The work of G.F. partly received financial support provided under the European Union's H2020 ERC, Starting Grant agreement no. DarkGRA–757480 and under the MIUR PRIN programme, and support from the Amaldi Research Center funded by the MIUR program "Dipartimento di Eccellenza" (CUP: B81I18001170001). J.G.B., E. R.M., and S.K.DEar acknowledge support from the Spanish Research Project PID2021-123012NB-C43 [MICINN-FEDER], and the Centro de Excelencia Severo Ochoa Program CEX2020-001007-S at IFT, funded by MCIN/AEI/10.13039/501100011033. C.J. is supported in part by the National Key Research and Development Program of China Grant No. 2021YFC2203004, and by the FNRS-FRIA Grant No. 1. E.070.19F and the FNRS *Fonds de la Recherche Scientifique* Grant No. T.0198.19. R.K.J. acknowledges financial support from the new faculty seed start-up grant of IISc, the Core Research Grant CRG/2018/002200 from the Science and Engineering Research Board, Department of Science and Technology, Government of India and the Infosys Foundation, Bangalore through the Infosys Young Investigator award. S.K. is supported by the Spanish Atracción de Talento contract no. 2019-T1/TIC-13177 granted by Comunidad de Madrid, the I+D grant PID2020-118159GA-C42 funded by MCIN/AEI/10.13039/501100011033, the Consolidación Investigadora 2022 grant CNS2022-135211 and the i-LINK 2021 grant LINKA20416 of CSIC, and Japan Society for the Promotion of Science (JSPS) KAKENHI Grant no. 20H01899, 20H05853, and 23H00110. I.M. has received funding from the European Union's Horizon2020 research and innovation programme under the Marie Skłodowska-Curie grant agreement No 754496. TP acknowledges financial support from the *Foundation for Education and European Culture in Greece* as well as from the *Fondation CFM pour la Recherche in France* and from the *Alexander S. Onassis Public Benefit Foundation* through the scholarship FZO 059-1/2018–2019. A.Ra. acknowledges funding from the Italian Ministry of University and Research (MUR) through the "Dipartimenti di eccellenza" project "Science of the Universe". A.R. is supported by the Boninchi Foundation. S.RP. is supported by the European Research Council under the European Union's Horizon 2020 research and innovation programme (Starting Grant agreement No 758792, project GEODESI). C.U. is supported by Ben Gurion University Kreitman Fellowship and the Israel Academy of Sciences and Humanities (IASH) & Council for Higher Education (CHE) Excellence Fellowship Program for International Postdoctoral Researchers, also European Structural and Investment Funds and the Czech Ministry of Education, Youth and Sports (Project CoGraDS - CZ.02.1.01/0.0/0.0/15 003/0000437). D.W. is supported by UK STFC grants ST/S000550/1 and ST/W001225/1. E.B. is supported by the FNRS-IISN (under grant number 4.4501.19).

References

Aad G et al (2019) Measurement of the top-quark mass in $t\bar{t}+1$-jet events collected with the ATLAS detector in pp collisions at $\sqrt{s}=8$ TeV. JHEP 11:150. https://doi.org/10.1007/JHEP11(2019)150. arXiv:1905.02302 [hep-ex]

Abbott B et al (2016) Observation of gravitational waves from a binary black hole merger. Phys Rev Lett 116(6):061102. https://doi.org/10.1103/PhysRevLett.116.061102. arXiv:1602.03837 [gr-qc]

Abbott BP et al (2018b) Search for subsolar-mass ultracompact binaries in advanced LIGO's first observing run. Phys Rev Lett 121(23):231103. https://doi.org/10.1103/PhysRevLett.121.231103. arXiv:1808.04771 [astro-ph.CO]

Abbott B et al (2019a) Search for the isotropic stochastic background using data from Advanced LIGO's second observing run. Phys Rev D 100(6):061101. https://doi.org/10.1103/PhysRevD.100.061101. arXiv:1903.02886 [gr-qc]

Abbott BP et al (2019) GWTC-1: a gravitational-wave transient catalog of compact binary mergers observed by LIGO and Virgo during the first and second observing runs. Phys Rev X 9(3):031040. https://doi.org/10.1103/PhysRevX.9.031040. arXiv:1811.12907 [astro-ph.HE]

Abbott BP et al (2019c) Search for subsolar mass ultracompact binaries in advanced LIGO's second observing run. Phys Rev Lett 123(16):161102. https://doi.org/10.1103/PhysRevLett.123.161102. arXiv:1904.08976 [astro-ph.CO]

Abbott R et al (2021a) GWTC-2: compact binary coalescences observed by LIGO and Virgo during the first half of the third observing run. Phys Rev X 11:021053. https://doi.org/10.1103/PhysRevX.11.021053. arXiv:2010.14527 [gr-qc]

Abbott R et al (2021b) Upper limits on the isotropic gravitational-wave background from Advanced LIGO and Advanced Virgo's third observing run. Phys Rev D 104(2):022004. https://doi.org/10.1103/PhysRevD.104.022004. arXiv:2101.12130 [gr-qc]

Abbott R et al (2022) Search for subsolar-mass binaries in the first half of advanced LIGO's and advanced Virgo's third observing run. Phys Rev Lett 129(6):061104. https://doi.org/10.1103/PhysRevLett.129.061104. arXiv:2109.12197 [astro-ph.CO]

Abbott R et al (2023a) GWTC-3: compact binary coalescences observed by LIGO and Virgo during the second part of the third observing run. Phys Rev X 13(4):041039. https://doi.org/10.1103/PhysRevX.13.041039. arXiv:2111.03606 [gr-qc]

Abbott R et al (2023b) Population of merging compact binaries inferred using gravitational waves through GWTC-3. Phys Rev X 13(1):011048. https://doi.org/10.1103/PhysRevX.13.011048. arXiv:2111.03634 [astro-ph.HE]

Abbott R et al (2023c) Search for subsolar-mass black hole binaries in the second part of Advanced LIGO's and Advanced Virgo's third observing run. Mon Not R Astron Soc 524(4):5984–5992. https://doi.org/10.1093/mnras/stad588. [Erratum: Mon. Not. R. Astron. Soc. 526, 6234 (2023)] arXiv:2212.01477 [astro-ph.HE]

Abdo A et al (2015) Milagro limits and HAWC sensitivity for the rate-density of evaporating primordial black holes. Astropart Phys 64:4–12. https://doi.org/10.1016/j.astropartphys.2014.10.007. arXiv:1407.1686 [astro-ph.HE]

Abe KT, Tada Y (2023) Translating nano-Hertz gravitational wave background into primordial perturbations taking account of the cosmological QCD phase transition. Phys Rev D 108(10):L101304. https://doi.org/10.1103/PhysRevD.108.L101304. arXiv:2307.01653 [astro-ph.CO]

Abe K, et al (2018) HyperKamiokande design report. arXiv e-prints arXiv:1805.04163 [physics.ins-det]

Acciarri R, et al (2016) Long-baseline neutrino facility (LBNF) and deep underground neutrino experiment (DUNE): conceptual design report, Volume 1: The LBNF and DUNE Projects. arXiv e-prints arXiv:1601.05471 [physics.ins-det]

Acharya SK, Khatri R (2020) CMB and BBN constraints on evaporating primordial black holes revisited. JCAP 06:018. https://doi.org/10.1088/1475-7516/2020/06/018. arXiv:2002.00898 [astro-ph.CO]

Ackermann M et al (2018) Search for gamma-ray emission from local primordial black holes with the Fermi Large Area Telescope. Astrophys J 857(1):49. https://doi.org/10.3847/1538-4357/aaac7b. arXiv:1802.00100 [astro-ph.HE]

Acquaviva V, Bartolo N, Matarrese S et al (2003) Second order cosmological perturbations from inflation. Nucl Phys B 667:119–148. https://doi.org/10.1016/S0550-3213(03)00550-9. arXiv:astro-ph/0209156

Adamek J, Byrnes CT, Gosenca M et al (2019) WIMPs and stellar-mass primordial black holes are incompatible. Phys Rev D 100(2):023506. https://doi.org/10.1103/PhysRevD.100.023506. arXiv:1901.08528 [astro-ph.CO]

Adams FC, Bond J, Freese K et al (1993) Natural inflation: particle physics models, power law spectra for large scale structure, and constraints from COBE. Phys Rev D 47:426–455. https://doi.org/10.1103/PhysRevD.47.426. arXiv:hep-ph/9207245

Adshead P, Lozanov KD, Weiner ZJ (2021) Non-Gaussianity and the induced gravitational wave background. JCAP 10:080. https://doi.org/10.1088/1475-7516/2021/10/080. arXiv:2105.01659 [astro-ph.CO]

Afzal A et al (2023) The NANOGrav 15 yr data set: search for signals from new physics. Astrophys J Lett 951(1):L11. https://doi.org/10.3847/2041-8213/acdc91. arXiv:2306.16219 [astro-ph.HE]

Agazie G et al (2023a) The NANOGrav 15 yr data set: constraints on supermassive black hole binaries from the gravitational-wave background. Astrophys J Lett 952(2):L37. https://doi.org/10.3847/2041-8213/ace18b. arXiv:2306.16220 [astro-ph.HE]

Agazie G et al (2023b) The NANOGrav 15 yr data set: evidence for a gravitational-wave background. Astrophys J Lett 951(1):L8. https://doi.org/10.3847/2041-8213/acdac6. arXiv:2306.16213 [astro-ph.HE]

Agazie G et al (2023c) The NANOGrav 15 yr data set: observations and timing of 68 millisecond pulsars. Astrophys J Lett 951(1):L9. https://doi.org/10.3847/2041-8213/acda9a. arXiv:2306.16217 [astro-ph.HE]

Aggarwal N et al (2021) Challenges and opportunities of gravitational-wave searches at MHz to GHz frequencies. Living Rev Relativ 24:4. https://doi.org/10.1007/s41114-021-00032-5. arXiv:2011.12414 [gr-qc]

Aghamousa A, et al (2016a) The DESI experiment part i: science, targeting, and survey design. arXiv e-prints arXiv:1611.00036 [astro-ph.IM]

Aghamousa A, et al (2016b) The DESI experiment part II: instrument design. arXiv e-prints arXiv:1611.00037 [astro-ph.IM]

Aghanim N et al (2020) Planck 2018 results. VI. Cosmological parameters. Astron Astrophys 641:A6. https://doi.org/10.1051/0004-6361/201833910. [Erratum: Astron. Astrophys. 652, C4 (2021)] arXiv:1807.06209 [astro-ph.CO]

Agius D, Essig R, Gaggero D et al (2024) Feedback in the dark: a critical examination of CMB bounds on primordial black holes. JCAP 07:003. https://doi.org/10.1088/1475-7516/2024/07/003. arXiv:2403.18895 [hep-ph]

Aharonian F et al (2023) Search for the evaporation of primordial black holes with H.E.S.S. JCAP 04:040. https://doi.org/10.1088/1475-7516/2023/04/040. arXiv:2303.12855 [astro-ph.HE]

Ahmed W, Junaid M, Zubair U (2022) Primordial black holes and gravitational waves in hybrid inflation with chaotic potentials. Nucl Phys B 984:115968. https://doi.org/10.1016/j.nuclphysb.2022.115968. arXiv:2109.14838 [astro-ph.CO]

Ajith P et al (2011) Inspiral-merger-ringdown waveforms for black-hole binaries with non-precessing spins. Phys Rev Lett 106:241101. https://doi.org/10.1103/PhysRevLett.106.241101. arXiv:0909.2867 [gr-qc]

Akrami Y et al (2020a) Planck 2018 results. IX. Constraints on primordial non-Gaussianity. Astron Astrophys 641:A9. https://doi.org/10.1051/0004-6361/201935891. arXiv:1905.05697 [astro-ph.CO]

Akrami Y et al (2020b) Planck 2018 results. X. Constraints on inflation. Astron Astrophys 641:A10. https://doi.org/10.1051/0004-6361/201833887. arXiv:1807.06211 [astro-ph.CO]

Alba V, Maldacena J (2016) Primordial gravity wave background anisotropies. JHEP 03:115. https://doi.org/10.1007/JHEP03(2016)115. arXiv:1512.01531 [hep-th]

Albert A et al (2020) Constraining the local burst rate density of primordial black holes with HAWC. JCAP 04:026. https://doi.org/10.1088/1475-7516/2020/04/026. arXiv:1911.04356 [astro-ph.HE]

Alcock C et al (1997) The MACHO project LMC microlensing results from the first two years and the nature of the galactic dark halo. Astrophys J 486:697–726. https://doi.org/10.1086/304535. arXiv:astro-ph/9606165

Alcock C et al (2001) The MACHO project: microlensing detection efficiency. Astrophys J Suppl 136:439–462. https://doi.org/10.1086/322529. arXiv:astro-ph/0003392

Alexandre A, Dvali G, Koutsangelas E (2024) New mass window for primordial black holes as dark matter from the memory burden effect. Phys Rev D 110(3):036004. https://doi.org/10.1103/PhysRevD.110.036004. arXiv:2402.14069 [hep-ph]

Ali-Haïmoud Y (2018) Correlation function of high-threshold regions and application to the initial small-scale clustering of primordial black holes. Phys Rev Lett 121(8):081304. https://doi.org/10.1103/PhysRevLett.121.081304. arXiv:1805.05912 [astro-ph.CO]

Ali-Haïmoud Y, Kamionkowski M (2017) Cosmic microwave background limits on accreting primordial black holes. Phys Rev D 95(4):043534. https://doi.org/10.1103/PhysRevD.95.043534. arXiv:1612.05644 [astro-ph.CO]

Ali-Haïmoud Y, Kovetz ED, Kamionkowski M (2017) Merger rate of primordial black-hole binaries. Phys Rev D 96(12):123523. https://doi.org/10.1103/PhysRevD.96.123523. arXiv:1709.06576 [astro-ph.CO]

Allahverdi R, Enqvist K, García-Bellido J et al (2006) Gauge invariant MSSM inflaton. Phys Rev Lett 97:191304. https://doi.org/10.1103/PhysRevLett.97.191304. arXiv:hep-ph/0605035

Allahverdi R, Enqvist K, García-Bellido J et al (2007) MSSM flat direction inflation: slow roll, stability, fine tunning and reheating. JCAP 06:019. https://doi.org/10.1088/1475-7516/2007/06/019. arXiv:hep-ph/0610134

Allsman R et al (2001) MACHO project limits on black hole dark matter in the 1–30 solar mass range. Astrophys J Lett 550:L169. https://doi.org/10.1086/319636. arXiv:astro-ph/0011506

Alonso D, Cusin G, Ferreira PG et al (2020) Detecting the anisotropic astrophysical gravitational wave background in the presence of shot noise through cross-correlations. Phys Rev D 102(2):023002. https://doi.org/10.1103/PhysRevD.102.023002. arXiv:2002.02888 [astro-ph.CO]

Amaro-Seoane P et al (2023) Astrophysics with the Laser Interferometer Space Antenna. Living Rev Relativ 26:2. https://doi.org/10.1007/s41114-022-00041-y. arXiv:2203.06016 [gr-qc]

Amaro-Seoane P, et al (2017) Laser Interferometer Space Antenna. arXiv e-prints arXiv:1702.00786 [astro-ph.IM]

Ambartsumian VA (1937) On the statistics of double stars. AZh 14:207–219

Amendola L et al (2018) Cosmology and fundamental physics with the Euclid satellite. Living Rev Relativ 21:2. https://doi.org/10.1007/s41114-017-0010-3. arXiv:1606.00180 [astro-ph.CO]

An F et al (2016) Neutrino physics with JUNO. J Phys G 43(3):030401. https://doi.org/10.1088/0954-3899/43/3/030401. arXiv:1507.05613 [physics.ins-det]

An H, Yang C (2024) Gravitational waves produced by domain walls during inflation. Phys Rev D 109 (12):123508. https://doi.org/10.1103/PhysRevD.109.123508. arXiv:2304.02361 [hep-ph]

Ananda KN, Clarkson C, Wands D (2007) The Cosmological gravitational wave background from primordial density perturbations. Phys Rev D 75:123518. https://doi.org/10.1103/PhysRevD.75.123518. arXiv:gr-qc/0612013

Anber MM, Sorbo L (2010) Naturally inflating on steep potentials through electromagnetic dissipation. Phys Rev D 81:043534. https://doi.org/10.1103/PhysRevD.81.043534. arXiv:0908.4089 [hep-th]

Anchordoqui LA, Antoniadis I, Lust D (2022) Dark dimension, the swampland, and the dark matter fraction composed of primordial black holes. Phys Rev D 106(8):086001. https://doi.org/10.1103/PhysRevD.106.086001. arXiv:2206.07071 [hep-th]

Anchordoqui LA, Antoniadis I, Lust D (2023) The dark universe: primordial black hole $\rightleftharpoons$ dark graviton gas connection. Phys Lett B 840:137844. https://doi.org/10.1016/j.physletb.2023.137844. arXiv:2210.02475 [hep-th]

Ando S, Hiroshima N, Ishiwata K (2022) Constraining the primordial curvature perturbation using dark matter substructure. Phys Rev D 106(10):103014. https://doi.org/10.1103/PhysRevD.106.103014. arXiv:2207.05747 [astro-ph.CO]

Ando K, Inomata K, Kawasaki M et al (2018) Primordial black holes for the LIGO events in the axionlike curvaton model. Phys Rev D 97(12):123512. https://doi.org/10.1103/PhysRevD.97.123512. arXiv:1711.08956 [astro-ph.CO]

Ando K, Vennin V (2021) Power spectrum in stochastic inflation. JCAP 04:057. https://doi.org/10.1088/1475-7516/2021/04/057. arXiv:2012.02031 [astro-ph.CO]

Antoniadis J et al (2022) The international pulsar timing array second data release: search for an isotropic gravitational wave background. Mon Not R Astron Soc 510(4):4873–4887. https://doi.org/10.1093/mnras/stab3418. arXiv:2201.03980 [astro-ph.HE]

Antoniadis J et al (2023a) The second data release from the European Pulsar Timing Array - I. The dataset and timing analysis. Astron Astrophys 678:A48. https://doi.org/10.1051/0004-6361/202346841. arXiv:2306.16224 [astro-ph.HE]

Antoniadis J et al (2023b) The second data release from the European Pulsar Timing Array - III. Search for gravitational wave signals. Astron Astrophys 678:A50. https://doi.org/10.1051/0004-6361/202346844. arXiv:2306.16214 [astro-ph.HE]

Antoniadis J et al (2024) The second data release from the European Pulsar Timing Array - IV. Implications for massive black holes, dark matter, and the early Universe. Astron Astrophys 685:A94. https://doi.org/10.1051/0004-6361/202347433. arXiv:2306.16227 [astro-ph.CO]

Araya IJ, Rubio ME, San Martin M et al (2021) Magnetic field generation from PBH distributions. Mon Not R Astron Soc 503(3):4387–4399. https://doi.org/10.1093/mnras/stab729. arXiv:2012.09585 [astro-ph.CO]

Arbey A, Auffinger J (2019) BlackHawk: a public code for calculating the Hawking evaporation spectra of any black hole distribution. Eur Phys J C 79(8):693. https://doi.org/10.1140/epjc/s10052-019-7161-1. arXiv:1905.04268 [gr-qc]

Arbey A, Auffinger J, Silk J (2020) Constraining primordial black hole masses with the isotropic gamma ray background. Phys Rev D 101(2):023010. https://doi.org/10.1103/PhysRevD.101.023010. arXiv:1906.04750 [astro-ph.CO]

Arbey A, Auffinger J (2020) Detecting Planet 9 via Hawking radiation. arXiv e-prints arXiv:2006.02944 [gr-qc]

Archambault S (2018) Search for Primordial Black Hole Evaporation with VERITAS. PoS ICRC2017:691. https://doi.org/10.22323/1.301.0691, arXiv:1709.00307 [astro-ph.HE]

Arun KG et al (2022) New horizons for fundamental physics with LISA. Living Rev Relativ 25:4. https://doi.org/10.1007/s41114-022-00036-9. arXiv:2205.01597 [gr-qc]

Arya R, Jain RK, Mishra AK (2024) Primordial black holes dark matter and secondary gravitational waves from warm Higgs-G inflation. JCAP 02:034. https://doi.org/10.1088/1475-7516/2024/02/034. arXiv:2302.08940 [astro-ph.CO]

Arzoumanian Z et al (2020) The NANOGrav 12.5 yr data set: search for an isotropic stochastic gravitational-wave background. Astrophys J Lett 905(2):L34. https://doi.org/10.3847/2041-8213/abd401. arXiv:2009.04496 [astro-ph.HE]

Arzoumanian Z et al (2021) Searching for gravitational waves from cosmological phase transitions with the NANOGrav 12.5-year dataset. Phys Rev Lett 127(25):251302. https://doi.org/10.1103/PhysRevLett.127.251302. arXiv:2104.13930 [astro-ph.CO]

Asencio E, Banik I, Kroupa P (2020) A massive blow for ΛCDM – the high redshift, mass, and collision velocity of the interacting galaxy cluster El Gordo contradicts concordance cosmology. Mon Not R Astron Soc 500(4):5249–5267. https://doi.org/10.1093/mnras/staa3441. arXiv:2012.03950 [astro-ph.CO]

Ashoorioon A, Rezazadeh K, Rostami A (2022) NANOGrav signal from the end of inflation and the LIGO mass and heavier primordial black holes. Phys Lett B 835:137542. https://doi.org/10.1016/j.physletb.2022.137542. arXiv:2202.01131 [astro-ph.CO]

Askins M et al (2020) THEIA: an advanced optical neutrino detector. Eur Phys J C 80(5):416. https://doi.org/10.1140/epjc/s10052-020-7977-8. arXiv:1911.03501 [physics.ins-det]

Atal V, Domènech G (2021) Probing non-Gaussianities with the high frequency tail of induced gravitational waves. JCAP 06:001. https://doi.org/10.1088/1475-7516/2021/06/001. arXiv:2103.01056 [astro-ph.CO]

Atal V, Garriga J, Marcos-Caballero A (2019) Primordial black hole formation with non-Gaussian curvature perturbations. JCAP 09:073. https://doi.org/10.1088/1475-7516/2019/09/073. arXiv:1905.13202 [astro-ph.CO]

Atal V, Sanglas A, Triantafyllou N (2020) LIGO/Virgo black holes and dark matter: the effect of spatial clustering. JCAP 11:036. https://doi.org/10.1088/1475-7516/2020/11/036. arXiv:2007.07212 [astro-ph.CO]

Atek H, Shuntov M, Furtak LJ et al (2022) Revealing galaxy candidates out to z $\sim$ 16 with jwst observations of the lensing cluster smacs0723. Mon Not R Astron Soc 519(1):1201–1220. https://doi.org/10.1093/mnras/stac3144. arXiv:2207.12338 [astro-ph.GA]

Aubourg E et al (1993) Evidence for gravitational microlensing by dark objects in the galactic halo. Nature 365:623–625. https://doi.org/10.1038/365623a0

Auclair P et al (2023) Cosmology with the Laser Interferometer Space Antenna. Living Rev Relativ 26:5. https://doi.org/10.1007/s41114-023-00045-2. arXiv:2204.05434 [astro-ph.CO]

Auclair P, Vennin V (2021) Primordial black holes from metric preheating: mass fraction in the excursion-set approach. JCAP 02:038. https://doi.org/10.1088/1475-7516/2021/02/038. arXiv:2011.05633 [astro-ph.CO]

Auffinger J (2022) Limits on primordial black holes detectability with Isatis: a BlackHawk tool. Eur Phys J C 82(4):384. https://doi.org/10.1140/epjc/s10052-022-10199-y. arXiv:2201.01265 [astro-ph.HE]

Babichev E, Gorbunov D, Ramazanov S et al (2022) Gravitational shine of dark domain walls. JCAP 04 (04):028. https://doi.org/10.1088/1475-7516/2022/04/028. arXiv:2112.12608 [hep-ph]
Babichev E, Gorbunov D, Ramazanov S et al (2023) NANOGrav spectral index γ=3 from melting domain walls. Phys Rev D 108(12):123529. https://doi.org/10.1103/PhysRevD.108.123529. arXiv:2307.04582 [hep-ph]
Bagui E, Clesse S (2022) A boosted gravitational wave background for primordial black holes with broad mass distributions and thermal features. Phys Dark Univ 38:101115. https://doi.org/10.1016/j.dark.2022.101115. arXiv:2110.07487 [astro-ph.CO]
Baibhav V et al (2021) Probing the nature of black holes: deep in the mHz gravitational-wave sky. Exper Astron 51(3):1385–1416. https://doi.org/10.1007/s10686-021-09741-9. arXiv:1908.11390 [astro-ph.HE]
Baker J et al (2021a) High angular resolution gravitational wave astronomy. Exper Astron 51(3):1441–1470. https://doi.org/10.1007/s10686-021-09712-0. arXiv:1908.11410 [astro-ph.HE]
Baker MJ, Breitbach M, Kopp J, et al (2021b) Detailed calculation of primordial black hole formation during first-order cosmological phase transitions. arXiv e-prints arXiv:2110.00005 [astro-ph.CO]
Baker MJ, Breitbach M, Kopp J, et al (2021c) Primordial black holes from first-order cosmological phase transitions. arXiv e-prints arXiv:2105.07481 [astro-ph.CO]
Balaji S, Domènech G, Franciolini G (2023) Scalar-induced gravitational wave interpretation of PTA data: the role of scalar fluctuation propagation speed. JCAP 10:041. https://doi.org/10.1088/1475-7516/2023/10/041. arXiv:2307.08552 [gr-qc]
Baldes I, Dichtl M, Gouttenoire Y, et al (2023) Bubbletrons. arXiv e-prints arXiv:2306.15555 [hep-ph]
Ballesteros G, Coronado-Blázquez J, Gaggero D (2020a) X-ray and gamma-ray limits on the primordial black hole abundance from Hawking radiation. Phys Lett B 808:135624. https://doi.org/10.1016/j.physletb.2020.135624. arXiv:1906.10113 [astro-ph.CO]
Ballesteros G, Rey J, Rompineve F (2020b) Detuning primordial black hole dark matter with early matter domination and axion monodromy. JCAP 06:014. https://doi.org/10.1088/1475-7516/2020/06/014. arXiv:1912.01638 [astro-ph.CO]
Ballesteros G, Rey J, Taoso M et al (2020c) Primordial black holes as dark matter and gravitational waves from single-field polynomial inflation. JCAP 07:025. https://doi.org/10.1088/1475-7516/2020/07/025. arXiv:2001.08220 [astro-ph.CO]
Ballesteros G, Serpico PD, Taoso M (2018) On the merger rate of primordial black holes: effects of nearest neighbours distribution and clustering. JCAP 10:043. https://doi.org/10.1088/1475-7516/2018/10/043. arXiv:1807.02084 [astro-ph.CO]
Ballesteros G, Taoso M (2018) Primordial black hole dark matter from single field inflation. Phys Rev D 97 (2):023501. https://doi.org/10.1103/PhysRevD.97.023501. arXiv:1709.05565 [hep-ph]
Banados E et al (2018) An 800-million-solar-mass black hole in a significantly neutral Universe at redshift 7.5. Nature 553(7689):473–476. https://doi.org/10.1038/nature25180. arXiv:1712.01860 [astro-ph.GA]
Banerjee S, Papanikolaou T, Saridakis EN (2022) Constraining F(R) bouncing cosmologies through primordial black holes. Phys Rev D 106(12):124012. https://doi.org/10.1103/PhysRevD.106.124012. arXiv:2206.01150 [gr-qc]
Bardeen JM, Bond J, Kaiser N et al (1986) The statistics of peaks of gaussian random fields. Astrophys J 304:15–61. https://doi.org/10.1086/164143
Bardeen JM, Press WH, Teukolsky SA (1972) Rotating black holes: locally nonrotating frames, energy extraction, and scalar synchrotron radiation. Astrophys J 178:347. https://doi.org/10.1086/151796
Barir J, Geller M, Sun C et al (2023) Gravitational waves from incomplete inflationary phase transitions. Phys Rev D 108(11):115016. https://doi.org/10.1103/PhysRevD.108.115016. arXiv:2203.00693 [hep-ph]
Barman B, Borah D, Jyoti Das S et al (2023) Scale of Dirac leptogenesis and left-right symmetry in the light of recent PTA results. JCAP 10:053. https://doi.org/10.1088/1475-7516/2023/10/053. arXiv:2307.00656 [hep-ph]
Barnaby N, Namba R, Peloso M (2011) Phenomenology of a Pseudo-scalar inflaton: naturally large nongaussianity. JCAP 04:009. https://doi.org/10.1088/1475-7516/2011/04/009. arXiv:1102.4333 [astro-ph.CO]
Barnacka A, Glicenstein JF, Moderski R (2012) New constraints on primordial black holes abundance from femtolensing of gamma-ray bursts. Phys Rev D 86:043001. https://doi.org/10.1103/PhysRevD.86.043001. arXiv:1204.2056 [astro-ph.CO]

Barrow JD, Carr BJ (1996) Formation and evaporation of primordial black holes in scalar - tensor gravity theories. Phys Rev D 54:3920–3931. https://doi.org/10.1103/PhysRevD.54.3920

Barsanti S, De Luca V, Maselli A et al (2022) Detecting subsolar-mass primordial black holes in extreme mass-ratio inspirals with LISA and einstein telescope. Phys Rev Lett 128(11):111104. https://doi.org/10.1103/PhysRevLett.128.111104. arXiv:2109.02170 [gr-qc]

Bartolo N et al (2016) Science with the space-based interferometer LISA. IV: probing inflation with gravitational waves. JCAP 12:026. https://doi.org/10.1088/1475-7516/2016/12/026. arXiv:1610.06481 [astro-ph.CO]

Bartolo N et al (2022) Probing anisotropies of the stochastic gravitational wave background with LISA. JCAP 11:009. https://doi.org/10.1088/1475-7516/2022/11/009. arXiv:2201.08782 [astro-ph.CO]

Bartolo N, Bertacca D, De Luca V et al (2020a) Gravitational wave anisotropies from primordial black holes. JCAP 02:028. https://doi.org/10.1088/1475-7516/2020/02/028. arXiv:1909.12619 [astro-ph.CO]

Bartolo N, Bertacca D, Matarrese S et al (2019a) Anisotropies and non-gaussianity of the cosmological gravitational wave background. Phys Rev D 100(12):121501. https://doi.org/10.1103/PhysRevD.100.121501. arXiv:1908.00527 [astro-ph.CO]

Bartolo N, Bertacca D, Matarrese S et al (2020b) Characterizing the cosmological gravitational wave background: anisotropies and non-gaussianity. Phys Rev D 102(2):023527. https://doi.org/10.1103/PhysRevD.102.023527. arXiv:1912.09433 [astro-ph.CO]

Bartolo N, Domcke V, Figueroa DG et al (2018) Probing non-gaussian stochastic gravitational wave backgrounds with LISA. JCAP 11:034. https://doi.org/10.1088/1475-7516/2018/11/034. arXiv:1806.02819 [astro-ph.CO]

Bartolo N, De Luca V, Franciolini G et al (2019b) Primordial black hole dark matter: LISA serendipity. Phys Rev Lett 122(21):211301. https://doi.org/10.1103/PhysRevLett.122.211301. arXiv:1810.12218 [astro-ph.CO]

Bartolo N, De Luca V, Franciolini G et al (2019c) Testing primordial black holes as dark matter with LISA. Phys Rev D 99(10):103521. https://doi.org/10.1103/PhysRevD.99.103521. arXiv:1810.12224 [astro-ph.CO]

Basilakos S, Nanopoulos DV, Papanikolaou T et al (2024a) Gravitational wave signatures of no-scale supergravity in NANOGrav and beyond. Phys Lett B 850:138507. https://doi.org/10.1016/j.physletb.2024.138507. arXiv:2307.08601 [hep-th]

Basilakos S, Nanopoulos DV, Papanikolaou T et al (2024b) Induced gravitational waves from flipped SU(5) superstring theory at nHz. Phys Lett B 849:138446. https://doi.org/10.1016/j.physletb.2024.138446. arXiv:2309.15820 [astro-ph.CO]

Bassett BA, Kaiser DI, Maartens R (1999a) General relativistic preheating after inflation. Phys Lett B 455:84–89. https://doi.org/10.1016/S0370-2693(99)00478-5. arXiv:hep-ph/9808404

Bassett BA, Tamburini F, Kaiser DI et al (1999b) Metric preheating and limitations of linearized gravity. 2. Nucl Phys B 561:188–240. https://doi.org/10.1016/S0550-3213(99)00495-2. arXiv:hep-ph/9901319

Bassett BA, Tsujikawa S (2001) Inflationary preheating and primordial black holes. Phys Rev D 63:123503. https://doi.org/10.1103/PhysRevD.63.123503. arXiv:hep-ph/0008328 [hep-ph]

Bassett BA, Viniegra F (2000) Massless metric preheating. Phys Rev D 62:043507. https://doi.org/10.1103/PhysRevD.62.043507. arXiv:hep-ph/9909353

Baum S, Fedderke MA, Graham PW (2022) Searching for dark clumps with gravitational-wave detectors. Phys Rev D 106(6):063015. https://doi.org/10.1103/PhysRevD.106.063015. arXiv:2206.14832 [astro-ph.CO]

Baumann D, Steinhardt PJ, Takahashi K et al (2007a) Gravitational wave spectrum induced by primordial scalar perturbations. Phys Rev D 76:084019. https://doi.org/10.1103/PhysRevD.76.084019. arXiv:hep-th/0703290

Baumann D, Steinhardt PJ, Turok N (2007b) Primordial Black Hole Baryogenesis. arXiv e-prints arXiv:hep-th/0703250

Bavera SS, Franciolini G, Cusin G et al (2022) Stochastic gravitational-wave background as a tool for investigating multi-channel astrophysical and primordial black-hole mergers. Astron Astrophys 660:A26. https://doi.org/10.1051/0004-6361/202142208. arXiv:2109.05836 [astro-ph.CO]

Belczynski K, Ryu T, Perna R et al (2017) On the likelihood of detecting gravitational waves from Population III compact object binaries. Mon Not R Astron Soc 471(4):4702–4721. https://doi.org/10.1093/mnras/stx1759. arXiv:1612.01524 [astro-ph.HE]

Bellomo N, Bernal JL, Scelfo G et al (2020) Beware of commonly used approximations. Part I. Errors in forecasts. JCAP 10:016. https://doi.org/10.1088/1475-7516/2020/10/016. arXiv:2005.10384 [astro-ph.CO]

Bellomo N, Bertacca D, Jenkins AC et al (2022) CLASS_GWB: robust modeling of the astrophysical gravitational wave background anisotropies. JCAP 06(06):030. https://doi.org/10.1088/1475-7516/2022/06/030. arXiv:2110.15059 [gr-qc]

Bellomo N, Bertacca D, Jenkins AC et al (2022) CLASS_GWB: robust modeling of the astrophysical gravitational wave background anisotropies. JCAP 6:030. https://doi.org/10.1088/1475-7516/2022/06/030. arXiv:2110.15059 [gr-qc]

Belotsky KM, Dmitriev AE, Esipova EA et al (2014) Signatures of primordial black hole dark matter. Modern Phys Lett A 29(37):1440005. https://doi.org/10.1142/S0217732314400057. arXiv:1410.0203 [astro-ph.CO]

Benetti M, Graef LL, Vagnozzi S (2022) Primordial gravitational waves from NANOGrav: a broken power-law approach. Phys Rev D 105(4):043520. https://doi.org/10.1103/PhysRevD.105.043520. arXiv:2111.04758 [astro-ph.CO]

Berezinsky V, Dokuchaev V, Eroshenko Y et al (2010) Superdense cosmological dark matter clumps. Physical Review D 81(10):103529. https://doi.org/10.1103/PhysRevD.81.103529. arXiv:1002.3444 [astro-ph.CO]

Berezinsky VS, Dokuchaev VI, Eroshenko YN (2013) Formation and internal structure of superdense dark matter clumps and ultracompact minihaloes. JCAP 11:059. https://doi.org/10.1088/1475-7516/2013/11/059. arXiv:1308.6742 [astro-ph.CO]

Berlin A, Blas D, Tito D'Agnolo R et al (2022a) Detecting high-frequency gravitational waves with microwave cavities. Phys Rev D 105(11):116011. https://doi.org/10.1103/PhysRevD.105.116011. arXiv:2112.11465 [hep-ph]

Berlin A, et al (2022b) Searches for new particles, dark matter, and gravitational waves with SRF cavities. arXiv e-prints arXiv:2203.12714 [hep-ph]

Bernal JL, Bellomo N, Raccanelli A et al (2020) Beware of commonly used approximations. Part II. Estimating systematic biases in the best-fit parameters. JCAP 10:017. https://doi.org/10.1088/1475-7516/2020/10/017. arXiv:2005.09666 [astro-ph.CO]

Bernal N, Muñoz Albornoz V, Palomares-Ruiz S et al (2022) Current and future neutrino limits on the abundance of primordial black holes. JCAP 10:068. https://doi.org/10.1088/1475-7516/2022/10/068. arXiv:2203.14979 [hep-ph]

Bernal JL, Raccanelli A, Verde L et al (2018) Signatures of primordial black holes as seeds of supermassive black holes. JCAP 05:017. https://doi.org/10.1088/1475-7516/2018/05/017. [Erratum: JCAP 01, E01 (2020)] arXiv:1712.01311 [astro-ph.CO]

Bertacca D, Ricciardone A, Bellomo N et al (2020) Projection effects on the observed angular spectrum of the astrophysical stochastic gravitational wave background. Phys Rev D 101(10):103513. https://doi.org/10.1103/PhysRevD.101.103513. arXiv:1909.11627 [astro-ph.CO]

Berteaud J, Calore F, Iguaz J et al (2022) Strong constraints on primordial black hole dark matter from 16 years of INTEGRAL/SPI observations. Phys Rev D 106(2):023030. https://doi.org/10.1103/PhysRevD.106.023030. arXiv:2202.07483 [astro-ph.HE]

Bertone G, Coogan AM, Gaggero D et al (2019) Primordial black holes as silver bullets for new physics at the weak scale. Phys Rev D 100(12):123013. https://doi.org/10.1103/PhysRevD.100.123013. arXiv:1905.01238 [hep-ph]

Bezrukov FL, Shaposhnikov M (2008) The standard model higgs boson as the inflaton. Phys Lett B 659:703–706. https://doi.org/10.1016/j.physletb.2007.11.072. arXiv:0710.3755 [hep-th]

Bhagwat S, De Luca V, Franciolini G et al (2021) The importance of priors on LIGO-Virgo parameter estimation: the case of primordial black holes. JCAP 01:037. https://doi.org/10.1088/1475-7516/2021/01/037. arXiv:2008.12320 [astro-ph.CO]

Bhattacharya T et al (2014) QCD phase transition with chiral quarks and physical quark masses. Phys Rev Lett 113(8):082001. https://doi.org/10.1103/PhysRevLett.113.082001. arXiv:1402.5175 [hep-lat]

Bhaumik N, Jain RK (2020) Primordial black holes dark matter from inflection point models of inflation and the effects of reheating. JCAP 01:037. https://doi.org/10.1088/1475-7516/2020/01/037. arXiv:1907.04125 [astro-ph.CO]

Bhaumik N, Jain RK (2021) Small scale induced gravitational waves from primordial black holes, a stringent lower mass bound, and the imprints of an early matter to radiation transition. Phys Rev D 104(2):023531. https://doi.org/10.1103/PhysRevD.104.023531. arXiv:2009.10424 [astro-ph.CO]

Biagetti M, Franciolini G, Kehagias A et al (2018) Primordial black holes from inflation and quantum diffusion. JCAP 07:032. https://doi.org/10.1088/1475-7516/2018/07/032. arXiv:1804.07124 [astro-ph.CO]

Biagetti M, Franciolini G, Riotto A (2023) High-redshift JWST observations and primordial non-gaussianity. Astrophys J 944(2):113. https://doi.org/10.3847/1538-4357/acb5ea. arXiv:2210.04812 [astro-ph.CO]

Biagetti M, De Luca V, Franciolini G et al (2021) The formation probability of primordial black holes. Phys Lett B 820:136602. https://doi.org/10.1016/j.physletb.2021.136602. arXiv:2105.07810 [astro-ph.CO]

Bicknell G, Henriksen RN (1979) Formation of primordial black holes. Astrophys J 232:670–682

Bird S et al (2023) Snowmass 2021 cosmic frontier white paper: primordial black hole dark matter. Phys Dark Univ 41:101231. https://doi.org/10.1016/j.dark.2023.101231. arXiv:2203.08967 [hep-ph]

Bird S, Cholis I, Muñoz JB et al (2016) Did LIGO detect dark matter? Phys Rev Lett 116(20):201301. https://doi.org/10.1103/PhysRevLett.116.201301. arXiv:1603.00464 [astro-ph.CO]

Bjorkmo T, Ferreira RZ, Marsh MCD (2019) Mild non-gaussianities under perturbative control from rapid-turn inflation models. JCAP 12:036. https://doi.org/10.1088/1475-7516/2019/12/036. arXiv:1908.11316 [hep-th]

Blanco-Pillado JJ, Olum KD, Wachter JM (2021b) Comparison of cosmic string and superstring models to NANOGrav 12.5-year results. Phys Rev D 103(10):103512. https://doi.org/10.1103/PhysRevD.103.103512. arXiv:2102.08194 [astro-ph.CO]

Blanco-Pillado JJ, Olum KD, Vilenkin A (2021a) No black holes from cosmic string cusps. arXiv e-prints arXiv:2101.05040 [astro-ph.CO]

Blasi S, Brdar V, Schmitz K (2021) Has NANOGrav found first evidence for cosmic strings? Phys Rev Lett 126(4):041305. https://doi.org/10.1103/PhysRevLett.126.041305. arXiv:2009.06607 [astro-ph.CO]

Blasi S, Mariotti A, Rase A et al (2023) Axionic domain walls at pulsar timing arrays: QCD bias and particle friction. JHEP 11:169. https://doi.org/10.1007/JHEP11(2023)169. arXiv:2306.17830 [hep-ph]

Blum B, et al (2022) Snowmass2021 cosmic frontier white paper: rubin observatory after LSST. In: 2022 Snowmass summer study, arXiv:2203.07220

Boehm C, Kobakhidze A, O'hare CAJ et al (2021) Eliminating the LIGO bounds on primordial black hole dark matter. JCAP 03:078. https://doi.org/10.1088/1475-7516/2021/03/078. arXiv:2008.10743 [astro-ph.CO]

Boldrini P, Miki Y, Wagner AY et al (2020) Cusp-to-core transition in low-mass dwarf galaxies induced by dynamical heating of cold dark matter by primordial black holes. Mon Not R Astron Soc 492(4):5218–5225. https://doi.org/10.1093/mnras/staa150. arXiv:1909.07395 [astro-ph.CO]

Bondi H (1952) On spherically symmetrical accretion. Mon Not R Astron Soc 112:195. https://doi.org/10.1093/mnras/112.2.195

Bonvin C, Durrer R (2011) What galaxy surveys really measure. Phys Rev D 84:063505. https://doi.org/10.1103/PhysRevD.84.063505. arXiv:1105.5280 [astro-ph.CO]

Bosch-Ramon V, Bellomo N (2020) Mechanical feedback effects on primordial black hole accretion. Astron Astrophys 638:A132. https://doi.org/10.1051/0004-6361/202037537. arXiv:2004.11224 [astro-ph.CO]

Boscá V, Fleury P, García-Bellido J (2022) Accurate modelling of extragalactic microlensing by compact objects. JCAP 10:098. https://doi.org/10.1088/1475-7516/2022/10/098. arXiv:2205.00991 [astro-ph.CO]

Bosi M, Bellomo N, Raccanelli A (2023) Constraining extended cosmologies with GWxLSS cross-correlations. JCAP 11:086. https://doi.org/10.1088/1475-7516/2023/11/086. arXiv:2306.03031 [astro-ph.CO]

Boucenna SM, Kuhnel F, Ohlsson T et al (2018) Novel constraints on mixed dark-matter scenarios of primordial black holes and WIMPs. JCAP 07:003. https://doi.org/10.1088/1475-7516/2018/07/003. arXiv:1712.06383 [hep-ph]

Boudaud M, Cirelli M (2019) Voyager 1 $e^{\pm}$ further constrain primordial black holes as dark matter. Phys Rev Lett 122(4):041104. https://doi.org/10.1103/PhysRevLett.122.041104. arXiv:1807.03075 [astro-ph.HE]

Boudaud M, Lacroix T, Stref M et al (2021) In-depth analysis of the clustering of dark matter particles around primordial black holes. Part I. Density profiles. JCAP 08:053. https://doi.org/10.1088/1475-7516/2021/08/053. arXiv:2106.07480 [astro-ph.CO]

Bowman JD, Rogers AEE, Monsalve RA et al (2018) An absorption profile centred at 78 megahertz in the sky-averaged spectrum. Nature 555(7694):67–70. https://doi.org/10.1038/nature25792. arXiv:1810.05912 [astro-ph.CO]

Braglia M, Chen X, Hazra DK (2021a) Probing primordial features with the stochastic gravitational wave background. JCAP 03:005. https://doi.org/10.1088/1475-7516/2021/03/005. arXiv:2012.05821 [astro-ph.CO]

Braglia M, García-Bellido J, Kuroyanagi S (2021b) Testing primordial black holes with multi-band observations of the stochastic gravitational wave background. JCAP 12(12):012. https://doi.org/10.1088/1475-7516/2021/12/012. arXiv:2110.07488 [astro-ph.CO]

Braglia M, García-Bellido J, Kuroyanagi S (2023a) Tracking the origin of black holes with the stochastic gravitational wave background popcorn signal. Mon Not R Astron Soc 519(4):6008–6019. https://doi.org/10.1093/mnras/stad082. arXiv:2201.13414 [astro-ph.CO]

Braglia M, Hazra DK, Finelli F et al (2020) Generating PBHs and small-scale GWs in two-field models of inflation. JCAP 08:001. https://doi.org/10.1088/1475-7516/2020/08/001. arXiv:2005.02895 [astro-ph.CO]

Braglia M, Linde A, Kallosh R et al (2023b) Hybrid α-attractors, primordial black holes and gravitational wave backgrounds. JCAP 04:033. https://doi.org/10.1088/1475-7516/2023/04/033. arXiv:2211.14262 [astro-ph.CO]

Brandt TD (2016) Constraints on MACHO dark matter from compact stellar systems in ultra-faint dwarf galaxies. Astrophys J Lett 824(2):L31. https://doi.org/10.3847/2041-8205/824/2/L31. arXiv:1605.03665 [astro-ph.GA]

Bringmann T (2009) Particle models and the small-scale structure of dark matter. New J Phys 11:105027. https://doi.org/10.1088/1367-2630/11/10/105027. arXiv:0903.0189 [astro-ph.CO]

Brito R, Cardoso V, Pani P (2015) Black holes as particle detectors: evolution of superradiant instabilities. Class Quant Grav 32(13):134001. https://doi.org/10.1088/0264-9381/32/13/134001. arXiv:1411.0686 [gr-qc]

Bromm V (2006) High-redshift gamma-ray bursts from population III progenitors. Astrophys J 642:382. https://doi.org/10.1086/500799. arXiv:astro-ph/0509303

Brown AR (2018) Hyperbolic inflation. Phys Rev Lett 121(25):251601. https://doi.org/10.1103/PhysRevLett.121.251601. arXiv:1705.03023 [hep-th]

Buchmüller W, Domcke V, Schmitz K (2020) From NANOGrav to LIGO with metastable cosmic strings. Phys Lett B 811:135914. https://doi.org/10.1016/j.physletb.2020.135914. arXiv:2009.10649 [astro-ph.CO]

Buchmüller W, Domcke V, Schmitz K (2021) Stochastic gravitational-wave background from metastable cosmic strings. JCAP 12(12):006. https://doi.org/10.1088/1475-7516/2021/12/006. arXiv:2107.04578 [hep-ph]

Bugaev E, Klimai P (2010) Induced gravitational wave background and primordial black holes. Phys Rev D 81:023517. https://doi.org/10.1103/PhysRevD.81.023517. arXiv:0908.0664 [astro-ph.CO]

Bugaev EV, Klimai PA (2013) Primordial black hole constraints for curvaton models with predicted large non-Gaussianity. Int J Mod Phys D 22:1350034. https://doi.org/10.1142/S021827181350034X. arXiv:1303.3146 [astro-ph.CO]

Bugaev E, Klimai P (2014) Axion inflation with gauge field production and primordial black holes. Phys Rev D 90(10):103501. https://doi.org/10.1103/PhysRevD.90.103501. arXiv:1312.7435 [astro-ph.CO]

Byrnes CT, Cole PS, Patil SP (2019) Steepest growth of the power spectrum and primordial black holes. JCAP 06:028. https://doi.org/10.1088/1475-7516/2019/06/028. arXiv:1811.11158 [astro-ph.CO]

Byrnes CT, Copeland EJ, Green AM (2012) Primordial black holes as a tool for constraining non-Gaussianity. Phys Rev D 86:043512. https://doi.org/10.1103/PhysRevD.86.043512. arXiv:1206.4188 [astro-ph.CO]

Byrnes CT, Hindmarsh M, Young S et al (2018) Primordial black holes with an accurate QCD equation of state. JCAP 08:041. https://doi.org/10.1088/1475-7516/2018/08/041. arXiv:1801.06138 [astro-ph.CO]

Bödeker D, Kühnel F, Oldengott IM et al (2021) Lepton flavor asymmetries and the mass spectrum of primordial black holes. Phys Rev D 103(6):063506. https://doi.org/10.1103/PhysRevD.103.063506. arXiv:2011.07283 [astro-ph.CO]

Cai YF, He XC, Ma XH et al (2023) Limits on scalar-induced gravitational waves from the stochastic background by pulsar timing array observations. Sci Bull 68:2929–2935. https://doi.org/10.1016/j.scib.2023.10.027. arXiv:2306.17822 [gr-qc]

Cai RG, Liu TB, Wang SJ (2018) Sensitivity of primordial black hole abundance on the reheating phase. Phys Rev D 98(4):043538. https://doi.org/10.1103/PhysRevD.98.043538. arXiv:1806.05390 [astro-ph.CO]
Cai YF, Ma XH, Sasaki M et al (2022a) Highly non-gaussian tails and primordial black holes from single-field inflation. JCAP 12:034. https://doi.org/10.1088/1475-7516/2022/12/034. arXiv:2207.11910 [astro-ph.CO]
Cai YF, Ma XH, Sasaki M et al (2022b) One small step for an inflaton, one giant leap for inflation: a novel non-gaussian tail and primordial black holes. Phys Lett B 834:137461. https://doi.org/10.1016/j.physletb.2022.137461. arXiv:2112.13836 [astro-ph.CO]
Cai Rg, Pi S, Sasaki M (2019a) Gravitational waves induced by non-gaussian scalar perturbations. Phys Rev Lett 122(20):201101. https://doi.org/10.1103/PhysRevLett.122.201101. arXiv:1810.11000 [astro-ph.CO]
Cai RG, Pi S, Sasaki M (2020) Universal infrared scaling of gravitational wave background spectra. Phys Rev D 102(8):083528. https://doi.org/10.1103/PhysRevD.102.083528. arXiv:1909.13728 [astro-ph.CO]
Cai RG, Pi S, Wang SJ et al (2019b) Pulsar timing array constraints on the induced gravitational waves. JCAP 10:059. https://doi.org/10.1088/1475-7516/2019/10/059. arXiv:1907.06372 [astro-ph.CO]
Cai Y, Zhu M, Piao YS (2024) Primordial black holes from null energy condition violation during inflation. Phys Rev Lett 133(2):021001. https://doi.org/10.1103/PhysRevLett.133.021001. arXiv:2305.10933 [gr-qc]
Calabrese R, Chianese M, Fiorillo DFG et al (2022a) Direct detection of light dark matter from evaporating primordial black holes. Phys Rev D 105(2):L021302. https://doi.org/10.1103/PhysRevD.105.L021302. arXiv:2107.13001 [hep-ph]
Calabrese R, Chianese M, Fiorillo DFG et al (2022b) Electron scattering of light new particles from evaporating primordial black holes. Phys Rev D 105(10):103024. https://doi.org/10.1103/PhysRevD.105.103024. arXiv:2203.17093 [hep-ph]
Calabrese R, Fiorillo DFG, Miele G et al (2022c) Primordial black hole dark matter evaporating on the neutrino floor. Phys Lett B 829:137050. https://doi.org/10.1016/j.physletb.2022.137050. arXiv:2106.02492 [hep-ph]
Calchi Novati S et al (2005) POINT-AGAPE pixel lensing survey of M31: evidence for a MACHO contribution to galactic halos. Astron Astrophys 443:911. https://doi.org/10.1051/0004-6361:20053135. arXiv:astro-ph/0504188
Calchi Novati S, Mirzoyan S, Jetzer P et al (2013) Microlensing towards the SMC: a new analysis of OGLE and EROS results. Mon Not R Astron Soc 435:1582. https://doi.org/10.1093/mnras/stt1402. arXiv:1308.4281 [astro-ph.GA]
Calcino J, García-Bellido J, Davis TM (2018) Updating the MACHO fraction of the Milky Way dark halowith improved mass models. Mon Not R Astron Soc 479(3):2889–2905. https://doi.org/10.1093/mnras/sty1368. arXiv:1803.09205 [astro-ph.CO]
Caldwell RR, Casper P (1996) Formation of black holes from collapsed cosmic string loops. Phys Rev D 53:3002–3010. https://doi.org/10.1103/PhysRevD.53.3002. arXiv:gr-qc/9509012
Caldwell RR, Gates E (1993) Constraints on cosmic strings due to black holes formed from collapsed cosmic string loops. Phys Rev D 48:2581–2586. https://doi.org/10.1103/PhysRevD.48.2581. arXiv:hep-ph/9306221
Calore F, Cuoco A, Regimbau T et al (2020) Cross-correlating galaxy catalogs and gravitational waves: a tomographic approach. Phys Rev Res 2:023314. https://doi.org/10.1103/PhysRevResearch.2.023314. arXiv:2002.02466 [astro-ph.CO]
Camera S, Nishizawa A (2013) Beyond concordance cosmology with magnification of gravitational-wave standard sirens. Phys Rev Lett 110(15):151103. https://doi.org/10.1103/PhysRevLett.110.151103. arXiv:1303.5446 [astro-ph.CO]
Capanema A, Esmaeili A, Esmaili A (2021) Evaporating primordial black holes in gamma ray and neutrino telescopes. JCAP 12:051. https://doi.org/10.1088/1475-7516/2021/12/051. arXiv:2110.05637 [hep-ph]
Capela F, Pshirkov M, Tinyakov P (2013a) Constraints on primordial black holes as dark matter candidates from capture by neutron stars. Phys Rev D 87(12):123524. https://doi.org/10.1103/PhysRevD.87.123524. arXiv:1301.4984 [astro-ph.CO]
Capela F, Pshirkov M, Tinyakov P (2013b) Constraints on primordial black holes as dark matter candidates from star formation. Phys Rev D 87(2):023507. https://doi.org/10.1103/PhysRevD.87.023507. arXiv:1209.6021 [astro-ph.CO]

Capozziello S, De Laurentis M, De Paolis F et al (2008) Gravitational waves from hyperbolic encounters. Mod Phys Lett A 23:99–107. https://doi.org/10.1142/S0217732308026236. arXiv:0801.0122 [gr-qc]
Cappelluti N, Hasinger G, Natarajan P (2022) Exploring the high-redshift PBH-ΛCDM universe: early black hole seeding, the first stars and cosmic radiation backgrounds. Astrophys J 926(2):205. https://doi.org/10.3847/1538-4357/ac332d. arXiv:2109.08701 [astro-ph.CO]
Caprini C, Figueroa DG (2018) Cosmological backgrounds of gravitational waves. Class Quant Grav 35 (16):163001. https://doi.org/10.1088/1361-6382/aac608. arXiv:1801.04268 [astro-ph.CO]
Cardoso V, Pani P (2019) Testing the nature of dark compact objects: a status report. Living Rev Relativ 22:4. https://doi.org/10.1007/s41114-019-0020-4. arXiv:1904.05363 [gr-qc]
Carr BJ (1975) The Primordial black hole mass spectrum. Astrophys J 201:1–19. https://doi.org/10.1086/153853
Carr B, Clesse S, García-Bellido J (2021a) Primordial black holes from the QCD epoch: linking dark matter, baryogenesis and anthropic selection. Mon Not R Astron Soc 501(1):1426–1439. https://doi.org/10.1093/mnras/staa3726. arXiv:1904.02129 [astro-ph.CO]
Carr B, Clesse S, García-Bellido J et al (2021b) Cosmic conundra explained by thermal history and primordial black holes. Phys Dark Univ 31:100755. https://doi.org/10.1016/j.dark.2020.100755. arXiv:1906.08217 [astro-ph.CO]
Carr B, Clesse S, García-Bellido J et al (2024) Observational evidence for primordial black holes: a positivist perspective. Phys Rept 1054:1–68. https://doi.org/10.1016/j.physrep.2023.11.005. arXiv:2306.03903 [astro-ph.CO]
Carr BJ, Coley AA (2011) Persistence of black holes through a cosmological bounce. Int J Mod Phys D 20:2733–2738. https://doi.org/10.1142/S0218271811020640. arXiv:1104.3796 [astro-ph.CO]
Carr B, Dimopoulos K, Owen C et al (2018) Primordial black hole formation during slow reheating after inflation. Phys Rev D 97(12):123535. https://doi.org/10.1103/PhysRevD.97.123535. arXiv:1804.08639 [astro-ph.CO]
Carr BJ, Gilbert JH, Lidsey JE (1994) Black hole relics and inflation: limits on blue perturbation spectra. Phys Rev D 50:4853–4867. https://doi.org/10.1103/PhysRevD.50.4853. arXiv:astro-ph/9405027
Carr BJ, Hawking SW (1974) Black holes in the early Universe. Mon Not R Astron Soc 168:399–415
Carr BJ, Kohri K, Sendouda Y et al (2010) New cosmological constraints on primordial black holes. Phys Rev D 81:104019. https://doi.org/10.1103/PhysRevD.81.104019. arXiv:0912.5297 [astro-ph.CO]
Carr B, Kohri K, Sendouda Y et al (2021c) Constraints on primordial black holes. Rept Prog Phys 84 (11):116902. https://doi.org/10.1088/1361-6633/ac1e31. arXiv:2002.12778 [astro-ph.CO]
Carr B, Kuhnel F (2019) Primordial black holes with multimodal mass spectra. Phys Rev D 99 (10):103535. https://doi.org/10.1103/PhysRevD.99.103535. arXiv:1811.06532 [astro-ph.CO]
Carr B, Kuhnel F (2020) Primordial black holes as dark matter: recent developments. Ann Rev Nucl Part Sci 70:355–394. https://doi.org/10.1146/annurev-nucl-050520-125911. arXiv:2006.02838 [astro-ph.CO]
Carr B, Kuhnel F, Visinelli L (2021d) Black holes and WIMPs: all or nothing or something else. Mon Not R Astron Soc 506(3):3648–3661. https://doi.org/10.1093/mnras/stab1930. arXiv:2011.01930 [astro-ph.CO]
Carr BJ, Lidsey JE (1993) Primordial black holes and generalized constraints on chaotic inflation. Phys Rev D 48:543–553. https://doi.org/10.1103/PhysRevD.48.543
Carr BJ, Sakellariadou M (1999) Dynamical constraints on dark matter in compact objects. Astrophys J 516(1):195–220. https://doi.org/10.1086/307071
Carr B, Silk J (2018) Primordial black holes as generators of cosmic structures. Mon Not R Astron Soc 478 (3):3756–3775. https://doi.org/10.1093/mnras/sty1204. arXiv:1801.00672 [astro-ph.CO]
Carr B, Tenkanen T, Vaskonen V (2017) Primordial black holes from inflaton and spectator field perturbations in a matter-dominated era. Phys Rev D 96(6):063507. https://doi.org/10.1103/PhysRevD.96.063507. arXiv:1706.03746 [astro-ph.CO]
Carrilho P, Malik KA, Mulryne DJ (2019) Dissecting the growth of the power spectrum for primordial black holes. Phys Rev D 100(10):103529. https://doi.org/10.1103/PhysRevD.100.103529. arXiv:1907.05237 [astro-ph.CO]
Cañas Herrera G, Contigiani O, Vardanyan V (2020) Cross-correlation of the astrophysical gravitational-wave background with galaxy clustering. Phys Rev D 102(4):043513. https://doi.org/10.1103/PhysRevD.102.043513. arXiv:1910.08353 [astro-ph.CO]
Challinor A, Lewis A (2011) The linear power spectrum of observed source number counts. Phys Rev D 84:043516. https://doi.org/10.1103/PhysRevD.84.043516. arXiv:1105.5292 [astro-ph.CO]

Chanda P, Scholtz J, Unwin J (2024) Improved constraints on dark matter annihilations around primordial black holes. JHEP 07:273. https://doi.org/10.1007/JHEP07(2024)273. arXiv:2209.07541 [hep-ph]
Chapline GF (1975) Cosmological effects of primordial black holes. Nature 253(5489):251–252. https://doi.org/10.1038/253251a0
Chen S et al (2021b) Common-red-signal analysis with 24-yr high-precision timing of the European Pulsar Timing Array: inferences in the stochastic gravitational-wave background search. Mon Not R Astron Soc 508(4):4970–4993. https://doi.org/10.1093/mnras/stab2833. arXiv:2110.13184 [astro-ph.HE]
Chen ZC, Huang QG (2018) Merger rate distribution of primordial-black-hole binaries. Astrophys J 864 (1):61. https://doi.org/10.3847/1538-4357/aad6e2. arXiv:1801.10327 [astro-ph.CO]
Chen ZC, Huang F, Huang QG (2019) Stochastic gravitational-wave background from binary black holes and binary neutron stars and implications for LISA. Astrophys J 871(1):97. https://doi.org/10.3847/1538-4357/aaf581. arXiv:1809.10360 [gr-qc]
Chen JW, Liu J, Xu HL et al (2017) Tracing primordial black holes in nonsingular bouncing cosmology. Phys Lett B 769:561–568. https://doi.org/10.1016/j.physletb.2017.03.036. arXiv:1609.02571 [gr-qc]
Chen P, Koh S, Tumurtushaa G (2021a) Primordial black holes and induced gravitational waves from inflation in the Horndeski theory of gravity. arXiv e-prints arXiv:2107.08638 [gr-qc]
Cheng SL, Lee DS, Ng KW (2024) Primordial perturbations from ultra-slow-roll single-field inflation with quantum loop effects. JCAP 03:008. https://doi.org/10.1088/1475-7516/2024/03/008. arXiv:2305.16810 [astro-ph.CO]
Cheong DY, Kohri K, Park SC (2022) The inflaton that could: primordial black holes and second order gravitational waves from tachyonic instability induced in Higgs-R ^{2} inflation. JCAP 10:015. https://doi.org/10.1088/1475-7516/2022/10/015. arXiv:2205.14813 [hep-ph]
Cheong DY, Lee SM, Park SC (2021) Primordial black holes in Higgs-R^2 inflation as the whole of dark matter. JCAP 01:032. https://doi.org/10.1088/1475-7516/2021/01/032. arXiv:1912.12032 [hep-ph]
Chisholm JR (2006) Clustering of primordial black holes: basic results. Phys Rev D 73:083504. https://doi.org/10.1103/PhysRevD.73.083504. arXiv:astro-ph/0509141
Chisholm JR (2011) Clustering of Primordial Black Holes. II. Evolution of Bound Systems. Phys Rev D 84:124031. https://doi.org/10.1103/PhysRevD.84.124031. arXiv:1110.4402 [astro-ph.CO]
Cholis I, Kovetz ED, Ali-Haïmoud Y et al (2016) Orbital eccentricities in primordial black hole binaries. Phys Rev D 94(8):084013. https://doi.org/10.1103/PhysRevD.94.084013. arXiv:1606.07437 [astro-ph.HE]
Cicoli M, Diaz VA, Pedro FG (2018) Primordial black holes from string inflation. JCAP 06:034. https://doi.org/10.1088/1475-7516/2018/06/034. arXiv:1803.02837 [hep-th]
Clesse S (2011) Hybrid inflation along waterfall trajectories. Phys Rev D 83:063518. https://doi.org/10.1103/PhysRevD.83.063518. arXiv:1006.4522 [gr-qc]
Clesse S, Garbrecht B, Zhu Y (2014) Non-gaussianities and curvature perturbations from hybrid inflation. Phys Rev D 89(6):063519. https://doi.org/10.1103/PhysRevD.89.063519. arXiv:1304.7042 [astro-ph.CO]
Clesse S, García-Bellido J (2015) Massive primordial black holes from hybrid inflation as dark matter and the seeds of galaxies. Phys Rev D 92(2):023524. https://doi.org/10.1103/PhysRevD.92.023524. arXiv:1501.07565 [astro-ph.CO]
Clesse S, García-Bellido J (2015) Massive primordial black holes from hybrid inflation as dark matter and the seeds of galaxies. Phys Rev D 92(2):023524. https://doi.org/10.1103/PhysRevD.92.023524. arXiv:1501.07565 [astro-ph.CO]
Clesse S, García-Bellido J (2017a) Detecting the gravitational wave background from primordial black hole dark matter. Phys Dark Univ 18:105–114. https://doi.org/10.1016/j.dark.2017.10.001. arXiv:1610.08479 [astro-ph.CO]
Clesse S, García-Bellido J (2017b) The clustering of massive primordial black holes as dark matter: measuring their mass distribution with advanced LIGO. Phys Dark Univ 15:142–147. https://doi.org/10.1016/j.dark.2016.10.002. arXiv:1603.05234 [astro-ph.CO]
Clesse S, García-Bellido J (2018) Seven hints for primordial black hole dark matter. Phys Dark Univ 22:137–146. https://doi.org/10.1016/j.dark.2018.08.004. arXiv:1711.10458 [astro-ph.CO]
Clesse S, García-Bellido J (2022) GW190425, GW190521 and GW190814: three candidate mergers of primordial black holes from the QCD epoch. Phys Dark Univ 38:101111. https://doi.org/10.1016/j.dark.2022.101111. arXiv:2007.06481 [astro-ph.CO]
Clesse S, García-Bellido J, Orani S (2018) Detecting the stochastic gravitational wave background from primordial black hole formation. arXiv e-prints arXiv:1812.11011 [astro-ph.CO]

Cole PS, Coogan A, Kavanagh BJ et al (2023a) Measuring dark matter spikes around primordial black holes with einstein telescope and cosmic explorer. Phys Rev D 107(8):083006. https://doi.org/10.1103/PhysRevD.107.083006. arXiv:2207.07576 [astro-ph.CO]

Cole PS, Gow AD, Byrnes CT et al (2023b) Primordial black holes from single-field inflation: a fine-tuning audit. JCAP 08:031. https://doi.org/10.1088/1475-7516/2023/08/031. arXiv:2304.01997 [astro-ph.CO]

Cole PS, Gow AD, Byrnes CT et al (2024) Smooth vs instant inflationary transitions: steepest growth re-examined and primordial black holes. JCAP 05:022. https://doi.org/10.1088/1475-7516/2024/05/022. arXiv:2204.07573 [astro-ph.CO]

Colpi M, et al (2024) LISA Definition Study Report. arXiv e-prints arXiv:2402.07571 [astro-ph.CO]

Contaldi CR (2017) Anisotropies of gravitational wave backgrounds: a line of sight approach. Phys Lett B 771:9–12. https://doi.org/10.1016/j.physletb.2017.05.020. arXiv:1609.08168 [astro-ph.CO]

Contaldi CR, Pieroni M, Renzini AI et al (2020) Maximum likelihood map-making with the Laser Interferometer Space Antenna. Phys Rev D 102(4):043502. https://doi.org/10.1103/PhysRevD.102.043502. arXiv:2006.03313 [astro-ph.CO]

Cook JL, Sorbo L (2012) Particle production during inflation and gravitational waves detectable by ground-based interferometers. Phys Rev D 85:023534. https://doi.org/10.1103/PhysRevD.85.023534. [Erratum: Phys. Rev. D 86, 069901 (2012)] arXiv:1109.0022 [astro-ph.CO]

Copeland EJ, Liddle AR, Lidsey JE et al (1998) Black holes and gravitational waves in string cosmology. Phys Rev D 58:063508. https://doi.org/10.1103/PhysRevD.58.063508. arXiv:gr-qc/9803070

Copeland EJ, Liddle AR, Lyth DH et al (1994) False vacuum inflation with Einstein gravity. Phys Rev D 49:6410–6433. https://doi.org/10.1103/PhysRevD.49.6410. arXiv:astro-ph/9401011

Cotner E, Kusenko A (2017) Primordial black holes from scalar field evolution in the early universe. Phys Rev D 96(10):103002. https://doi.org/10.1103/PhysRevD.96.103002. arXiv:1706.09003 [astro-ph.CO]

Cremonini S, Lalak Z, Turzynski K (2011) Strongly coupled perturbations in two-field inflationary models. JCAP 03:016. https://doi.org/10.1088/1475-7516/2011/03/016. arXiv:1010.3021 [hep-th]

Cruz-Osorio A, Lora-Clavijo FD, Herdeiro C (2021) GW190521 formation scenarios via relativistic accretion. JCAP 07:032. https://doi.org/10.1088/1475-7516/2021/07/032. arXiv:2101.01705 [astro-ph.HE]

Cruz-Osorio A, Rezzolla L (2020) Common-envelope dynamics of a stellar-mass black hole: general relativistic simulations. Astrophys J 894(2):147. https://doi.org/10.3847/1538-4357/ab89aa. arXiv:2004.13782 [gr-qc]

Cusin G, Durrer R, Ferreira PG (2019a) Polarization of a stochastic gravitational wave background through diffusion by massive structures. Phys Rev D 99(2):023534. https://doi.org/10.1103/PhysRevD.99.023534. arXiv:1807.10620 [astro-ph.CO]

Cusin G, Dvorkin I, Pitrou C et al (2018a) First predictions of the angular power spectrum of the astrophysical gravitational wave background. Phys Rev Lett 120:231101. https://doi.org/10.1103/PhysRevLett.120.231101. arXiv:1803.03236 [astro-ph.CO]

Cusin G, Dvorkin I, Pitrou C et al (2019b) Properties of the stochastic astrophysical gravitational wave background: astrophysical sources dependencies. Phys Rev D 100(6):063004. https://doi.org/10.1103/PhysRevD.100.063004. arXiv:1904.07797 [astro-ph.CO]

Cusin G, Dvorkin I, Pitrou C et al (2020) Stochastic gravitational wave background anisotropies in the mHz band: astrophysical dependencies. Mon Not R Astron Soc 493(1):L1–L5. https://doi.org/10.1093/mnrasl/slz182. arXiv:1904.07757 [astro-ph.CO]

Cusin G, Pitrou C, Uzan JP (2017) Anisotropy of the astrophysical gravitational wave background: analytic expression of the angular power spectrum and correlation with cosmological observations. Phys Rev D 96(10):103019. https://doi.org/10.1103/PhysRevD.96.103019. arXiv:1704.06184 [astro-ph.CO]

Cusin G, Pitrou C, Uzan JP (2018b) The signal of the gravitational wave background and the angular correlation of its energy density. Phys Rev D 97(12):123527. https://doi.org/10.1103/PhysRevD.97.123527. arXiv:1711.11345 [astro-ph.CO]

Dalianis I, Kehagias A, Tringas G (2019) Primordial black holes from α-attractors. JCAP 01:037. https://doi.org/10.1088/1475-7516/2019/01/037. arXiv:1805.09483 [astro-ph.CO]

Dandoy V, Domcke V, Rompineve F (2023) Search for scalar induced gravitational waves in the International Pulsar Timing Array data release 2 and NANOgrav 12.5 years datasets. SciPost Phys Core 6:060. https://doi.org/10.21468/SciPostPhysCore.6.3.060. arXiv:2302.07901 [astro-ph.CO]

Dasgupta B, Laha R, Ray A (2020) Neutrino and positron constraints on spinning primordial black hole dark matter. Phys Rev Lett 125(10):101101. https://doi.org/10.1103/PhysRevLett.125.101101. arXiv:1912.01014 [hep-ph]

Datta S, Ghosal A, Samanta R (2021) Baryogenesis from ultralight primordial black holes and strong gravitational waves from cosmic strings. JCAP 08:021. https://doi.org/10.1088/1475-7516/2021/08/021. arXiv:2012.14981 [hep-ph]

Davoudiasl H (2019) LIGO/Virgo black holes from a first order quark confinement phase transition. Phys Rev Lett 123(10):101102. https://doi.org/10.1103/PhysRevLett.123.101102. arXiv:1902.07805 [hep-ph]

De Luca V, Bellomo N (2023) Accretion, emission, mass and spin evolution. arXiv e-prints arXiv:2312.14097 [astro-ph.CO]

De Luca V, Desjacques V, Franciolini G et al (2019a) The initial spin probability distribution of primordial black holes. JCAP 05:018. https://doi.org/10.1088/1475-7516/2019/05/018. arXiv:1903.01179 [astro-ph.CO]

De Luca V, Desjacques V, Franciolini G et al (2019b) Gravitational waves from peaks. JCAP 09:059. https://doi.org/10.1088/1475-7516/2019/09/059. arXiv:1905.13459 [astro-ph.CO]

De Luca V, Desjacques V, Franciolini G et al (2020a) The clustering evolution of primordial black holes. JCAP 11:028. https://doi.org/10.1088/1475-7516/2020/11/028. arXiv:2009.04731 [astro-ph.CO]

De Luca V, Desjacques V, Franciolini G et al (2021a) GW190521 mass gap event and the primordial black hole scenario. Phys Rev Lett 126(5):051101. https://doi.org/10.1103/PhysRevLett.126.051101. arXiv:2009.01728 [astro-ph.CO]

De Luca V, Franciolini G, Kehagias A et al (2019c) The ineludible non-gaussianity of the primordial black hole abundance. JCAP 07:048. https://doi.org/10.1088/1475-7516/2019/07/048. arXiv:1904.00970 [astro-ph.CO]

De Luca V, Franciolini G, Kehagias A et al (2020b) On the gauge invariance of cosmological gravitational waves. JCAP 03:014. https://doi.org/10.1088/1475-7516/2020/03/014. arXiv:1911.09689 [gr-qc]

De Luca V, Franciolini G, Kehagias A et al (2021b) Standard model baryon number violation seeded by black holes. Phys Lett B 819:136454. https://doi.org/10.1016/j.physletb.2021.136454. arXiv:2102.07408 [astro-ph.CO]

De Luca V, Franciolini G, Kehagias A et al (2022a) Primordial black holes in matter-dominated eras: the role of accretion. Phys Lett B 832:137265. https://doi.org/10.1016/j.physletb.2022.137265. arXiv:2112.02534 [astro-ph.CO]

De Luca V, Franciolini G, Pani P et al (2020c) Constraints on primordial black holes: the importance of accretion. Phys Rev D 102(4):043505. https://doi.org/10.1103/PhysRevD.102.043505. arXiv:2003.12589 [astro-ph.CO]

De Luca V, Franciolini G, Pani P et al (2020d) Primordial black holes confront LIGO/Virgo data: current situation. JCAP 06:044. https://doi.org/10.1088/1475-7516/2020/06/044. arXiv:2005.05641 [astro-ph.CO]

De Luca V, Franciolini G, Pani P et al (2020e) The evolution of primordial black holes and their final observable spins. JCAP 04:052. https://doi.org/10.1088/1475-7516/2020/04/052. arXiv:2003.02778 [astro-ph.CO]

De Luca V, Franciolini G, Pani P et al (2021c) Bayesian evidence for both astrophysical and primordial black holes: mapping the GWTC-2 catalog to third-generation detectors. JCAP 05:003. https://doi.org/10.1088/1475-7516/2021/05/003. arXiv:2102.03809 [astro-ph.CO]

De Luca V, Franciolini G, Pani P et al (2021d) The minimum testable abundance of primordial black holes at future gravitational-wave detectors. JCAP 11:039. https://doi.org/10.1088/1475-7516/2021/11/039. arXiv:2106.13769 [astro-ph.CO]

De Luca V, Franciolini G, Riotto A (2020f) On the primordial black hole mass function for broad spectra. Phys Lett B 807:135550. https://doi.org/10.1016/j.physletb.2020.135550. arXiv:2001.04371 [astro-ph.CO]

De Luca V, Franciolini G, Riotto A (2021e) Bubble correlation in first-order phase transitions. Phys Rev D 104(12):123539. https://doi.org/10.1103/PhysRevD.104.123539. arXiv:2110.04229 [hep-ph]

De Luca V, Franciolini G, Riotto A (2021f) Constraining the initial primordial black hole clustering with CMB distortion. Phys Rev D 104(6):063526. https://doi.org/10.1103/PhysRevD.104.063526. arXiv:2103.16369 [astro-ph.CO]

De Luca V, Franciolini G, Riotto A (2021g) NANOGrav data hints at primordial black holes as dark matter. Phys Rev Lett 126(4):041303. https://doi.org/10.1103/PhysRevLett.126.041303. arXiv:2009.08268 [astro-ph.CO]

De Luca V, Franciolini G, Riotto A et al (2022b) Ruling out initially clustered primordial black holes as dark matter. Phys Rev Lett 129(19):191302. https://doi.org/10.1103/PhysRevLett.129.191302. arXiv:2208.01683 [astro-ph.CO]

De Luca V, Franciolini G, Riotto A (2023a) Heavy primordial black holes from strongly clustered light black holes. Phys Rev Lett 130(17):171401. https://doi.org/10.1103/PhysRevLett.130.171401. arXiv:2210.14171 [astro-ph.CO]

De Luca V, Kehagias A, Riotto A (2023b) How well do we know the primordial black hole abundance: the crucial role of nonlinearities when approaching the horizon. Phys Rev D 108(6):063531. https://doi.org/10.1103/PhysRevD.108.063531. arXiv:2307.13633 [astro-ph.CO]

De Luca V, Riotto A (2022) A note on the abundance of primordial black holes: use and misuse of the metric curvature perturbation. Phys Lett B 828:137035. https://doi.org/10.1016/j.physletb.2022.137035. arXiv:2201.09008 [astro-ph.CO]

DeRocco W, Graham PW (2019) Constraining primordial black hole abundance with the galactic 511 keV line. Phys Rev Lett 123(25):251102. https://doi.org/10.1103/PhysRevLett.123.251102. arXiv:1906.07740 [astro-ph.CO]

Defillon G, Granet E, Tinyakov P et al (2014) Tidal capture of primordial black holes by neutron stars. Phys Rev D 90(10):103522. https://doi.org/10.1103/PhysRevD.90.103522. arXiv:1409.0469 [gr-qc]

Delos MS (2019) Evolution of dark matter microhalos through stellar encounters. Phys Rev D 100(8):083529. https://doi.org/10.1103/PhysRevD.100.083529. arXiv:1907.13133 [astro-ph.CO]

Delos MS, Erickcek AL, Bailey AP et al (2018a) Are ultracompact minihalos really ultracompact? Phys Rev D 97(4):041303. https://doi.org/10.1103/PhysRevD.97.041303. arXiv:1712.05421 [astro-ph.CO]

Delos MS, Erickcek AL, Bailey AP et al (2018b) Density profiles of ultracompact minihalos: implications for constraining the primordial power spectrum. Phys Rev D 98(6):063527. https://doi.org/10.1103/PhysRevD.98.063527. arXiv:1806.07389 [astro-ph.CO]

Delos MS, Franciolini G (2023) Lensing constraints on ultradense dark matter halos. Phys Rev D 107(8):083505. https://doi.org/10.1103/PhysRevD.107.083505. arXiv:2301.13171 [astro-ph.CO]

Deng H, Vilenkin A (2017) Primordial black hole formation by vacuum bubbles. JCAP 12:044. https://doi.org/10.1088/1475-7516/2017/12/044. arXiv:1710.02865 [gr-qc]

Desjacques V, Riotto A (2018) Spatial clustering of primordial black holes. Phys Rev D 98(12):123533. https://doi.org/10.1103/PhysRevD.98.123533. arXiv:1806.10414 [astro-ph.CO]

Dewdney PE, Hall PJ, Schilizzi RT et al (2009) The square kilometre Array. IEEE Proc 97(8):1482–1496. https://doi.org/10.1109/JPROC.2009.2021005

de Jong E, Aurrekoetxea JC, Lim EA (2022) Primordial black hole formation with full numerical relativity. JCAP 03(03):029. https://doi.org/10.1088/1475-7516/2022/03/029. arXiv:2109.04896 [astro-ph.CO]

De Romeri V, Martínez-Miravé P, Tórtola M (2021) Signatures of primordial black hole dark matter at DUNE and THEIA. JCAP 10:051. https://doi.org/10.1088/1475-7516/2021/10/051. arXiv:2106.05013 [hep-ph]

De Vittori L, Jetzer P, Klein A (2012) Gravitational wave energy spectrum of hyperbolic encounters. Phys Rev D 86:044017. https://doi.org/10.1103/PhysRevD.86.044017. arXiv:1207.5359 [gr-qc]

Di Bari P, Marfatia D, Zhou YL (2021) Gravitational waves from first-order phase transitions in Majoron models of neutrino mass. JHEP 10:193. https://doi.org/10.1007/JHEP10(2021)193. arXiv:2106.00025 [hep-ph]

Dimastrogiovanni E, Fasiello M, Tasinato G (2020) Searching for fossil fields in the gravity sector. Phys Rev Lett 124(6):061302. https://doi.org/10.1103/PhysRevLett.124.061302. arXiv:1906.07204 [astro-ph.CO]

Dolgov A, Silk J (1993) Baryon isocurvature fluctuations at small scales and baryonic dark matter. Phys Rev D 47:4244–4255. https://doi.org/10.1103/PhysRevD.47.4244

Dolgov AD, Naselsky PD, Novikov ID (2000) Gravitational waves, baryogenesis, and dark matter from primordial black holes. arXiv e-prints arXiv:astro-ph/0009407

Domcke V, Garcia-Cely C, Rodd NL (2022) Novel search for high-frequency gravitational waves with low-mass axion haloscopes. Phys Rev Lett 129(4):041101. https://doi.org/10.1103/PhysRevLett.129.041101. arXiv:2202.00695 [hep-ph]

Domcke V, Jinno R, Rubira H (2020) Deformation of the gravitational wave spectrum by density perturbations. JCAP 06:046. https://doi.org/10.1088/1475-7516/2020/06/046. arXiv:2002.11083 [astro-ph.CO]

Domcke V, Muia F, Pieroni M et al (2017) PBH dark matter from axion inflation. JCAP 07:048. https://doi.org/10.1088/1475-7516/2017/07/048. arXiv:1704.03464 [astro-ph.CO]

Domènech G (2020) Induced gravitational waves in a general cosmological background. Int J Mod Phys D 29(03):2050028. https://doi.org/10.1142/S0218271820500285. arXiv:1912.05583 [gr-qc]
Domènech G (2021) Scalar induced gravitational waves review. Universe 7(11):398. https://doi.org/10.3390/universe7110398. arXiv:2109.01398 [gr-qc]
Domènech G, Lin C, Sasaki M (2021) Gravitational wave constraints on the primordial black hole dominated early universe. JCAP 04:062. https://doi.org/10.1088/1475-7516/2021/04/062. arXiv:2012.08151 [gr-qc]
Domènech G, Passaglia S, Renaux-Petel S (2022) Gravitational waves from dark matter isocurvature. JCAP 03(03):023. https://doi.org/10.1088/1475-7516/2022/03/023. arXiv:2112.10163 [astro-ph.CO]
Domènech G, Pi S (2022) NANOGrav hints on planet-mass primordial black holes. Sci China Phys Mech Astron 65(3):230411. https://doi.org/10.1007/s11433-021-1839-6. arXiv:2010.03976 [astro-ph.CO]
Domènech G, Pi S, Sasaki M (2020) Induced gravitational waves as a probe of thermal history of the universe. JCAP 08:017. https://doi.org/10.1088/1475-7516/2020/08/017. arXiv:2005.12314 [gr-qc]
Domènech G, Sasaki M (2018) Hamiltonian approach to second order gauge invariant cosmological perturbations. Phys Rev D 97(2):023521. https://doi.org/10.1103/PhysRevD.97.023521. arXiv:1709.09804 [gr-qc]
Doré O, et al (2014) Cosmology with the SPHEREX All-Sky Spectral Survey. arXiv e-prints arXiv:1412.4872 [astro-ph.CO]
Drlica-Wagner A, et al (2019) Probing the fundamental nature of dark matter with the large synoptic survey telescope. arXiv:1902.01055
Duechting N (2004) Supermassive black holes from primordial black hole seeds. Phys Rev D 70:064015. https://doi.org/10.1103/PhysRevD.70.064015. arXiv:astro-ph/0406260
Easther R, Flauger R, Gilmore JB (2011) Delayed reheating and the breakdown of coherent oscillations. JCAP 04:027. https://doi.org/10.1088/1475-7516/2011/04/027. arXiv:1003.3011 [astro-ph.CO]
Ellis J, Fairbairn M, Hütsi G et al (2023) Prospects for future binary black hole gravitational wave studies in light of PTA measurements. Astron Astrophys 676:A38. https://doi.org/10.1051/0004-6361/202346268. arXiv:2301.13854 [astro-ph.CO]
Ellis J, Lewicki M (2021) Cosmic string interpretation of NANOGrav pulsar timing data. Phys Rev Lett 126(4):041304. https://doi.org/10.1103/PhysRevLett.126.041304. arXiv:2009.06555 [astro-ph.CO]
Enqvist K, Nurmi S, Podolsky D et al (2008) On the divergences of inflationary superhorizon perturbations. JCAP 04:025. https://doi.org/10.1088/1475-7516/2008/04/025. arXiv:0802.0395 [astro-ph]
Escrivà A, Bagui E, Clesse S (2023) Simulations of PBH formation at the QCD epoch and comparison with the GWTC-3 catalog. JCAP 05:004. https://doi.org/10.1088/1475-7516/2023/05/004. arXiv:2209.06196 [astro-ph.CO]
Escrivà A, Germani C, Sheth RK (2020) Universal threshold for primordial black hole formation. Phys Rev D 101(4):044022. https://doi.org/10.1103/PhysRevD.101.044022. arXiv:1907.13311 [gr-qc]
Escrivà A, Germani C, Sheth RK (2021) Analytical thresholds for black hole formation in general cosmological backgrounds. JCAP 01:030. https://doi.org/10.1088/1475-7516/2021/01/030. arXiv:2007.05564 [gr-qc]
Escrivà A, Tada Y, Yokoyama S et al (2022) Simulation of primordial black holes with large negative non-Gaussianity. JCAP 05(05):012. https://doi.org/10.1088/1475-7516/2022/05/012. arXiv:2202.01028 [astro-ph.CO]
Espinosa JR, Racco D, Riotto A (2018) A cosmological signature of the SM higgs instability: gravitational waves. JCAP 09:012. https://doi.org/10.1088/1475-7516/2018/09/012. arXiv:1804.07732 [hep-ph]
Esser N, Tinyakov P (2023) Constraints on primordial black holes from observation of stars in dwarf galaxies. Phys Rev D 107(10):103052. https://doi.org/10.1103/PhysRevD.107.103052. arXiv:2207.07412 [astro-ph.HE]
Ezquiaga JM, García-Bellido J (2018) Quantum diffusion beyond slow-roll: implications for primordial black-hole production. JCAP 08:018. https://doi.org/10.1088/1475-7516/2018/08/018. arXiv:1805.06731 [astro-ph.CO]
Ezquiaga JM, García-Bellido J, Ruiz Morales E (2018) Primordial black hole production in critical higgs inflation. Phys Lett B 776:345–349. https://doi.org/10.1016/j.physletb.2017.11.039. arXiv:1705.04861 [astro-ph.CO]
Ezquiaga JM, García-Bellido J, Vennin V (2020) The exponential tail of inflationary fluctuations: consequences for primordial black holes. JCAP 03:029. https://doi.org/10.1088/1475-7516/2020/03/029. arXiv:1912.05399 [astro-ph.CO]

Ezquiaga JM, García-Bellido J, Vennin V (2022 [arXiv:2207.06317]) Massive galaxy clusters like El Gordo hint at primordial quantum diffusion. Phys Rev Lett arXiv:2207.06317 [astro-ph.CO]
Facchinetti G, Lucca M, Clesse S (2023) Relaxing CMB bounds on primordial black holes: the role of ionization fronts. Phys Rev D 107(4):043537. https://doi.org/10.1103/PhysRevD.107.043537. arXiv:2212.07969 [astro-ph.CO]
Feng JX, Zhang F, Gao X (2023) Scalar induced gravitational waves from Chern-Simons gravity during inflation era. JCAP 07:047. https://doi.org/10.1088/1475-7516/2023/07/047. arXiv:2302.00950 [gr-qc]
Fernandez N, Profumo S (2019) Unraveling the origin of black holes from effective spin measurements with LIGO-Virgo. JCAP 08:022. https://doi.org/10.1088/1475-7516/2019/08/022. arXiv:1905.13019 [astro-ph.HE]
Ferrante G, Franciolini G, Iovino AJunior et al (2023a) Primordial black holes in the curvaton model: possible connections to pulsar timing arrays and dark matter. JCAP 06:057. https://doi.org/10.1088/1475-7516/2023/06/057. arXiv:2305.13382 [astro-ph.CO]
Ferrante G, Franciolini G, Iovino AJunior et al (2023b) Primordial non-Gaussianity up to all orders: theoretical aspects and implications for primordial black hole models. Phys Rev D 107(4):043520. https://doi.org/10.1103/PhysRevD.107.043520. arXiv:2211.01728 [astro-ph.CO]
Ferreira RZ (2020) Non-Gaussianities in models of inflation with large and negative entropic masses. JCAP 08:034. https://doi.org/10.1088/1475-7516/2020/08/034. arXiv:2003.13410 [astro-ph.CO]
Ferreira RZ, Notari A, Pujolas O et al (2023) Gravitational waves from domain walls in pulsar timing array datasets. JCAP 02:001. https://doi.org/10.1088/1475-7516/2023/02/001. arXiv:2204.04228 [astro-ph.CO]
Ferrer F, Masso E, Panico G et al (2019) Primordial black holes from the QCD axion. Phys Rev Lett 122 (10):101301. https://doi.org/10.1103/PhysRevLett.122.101301. arXiv:1807.01707 [hep-ph]
Figueroa DG, Pieroni M, Ricciardone A et al (2024) Cosmological background interpretation of pulsar timing array data. Phys Rev Lett 132(17):171002. https://doi.org/10.1103/PhysRevLett.132.171002. arXiv:2307.02399 [astro-ph.CO]
Finelli F, Brandenberger RH (1999) Parametric amplification of gravitational fluctuations during reheating. Phys Rev Lett 82:1362–1365. https://doi.org/10.1103/PhysRevLett.82.1362. arXiv:hep-ph/9809490
Finkelstein SL, Bagley MB, Haro PA et al (2022b) A long time ago in a galaxy far, far away: a candidate z 12 galaxy in early JWST CEERS imaging. Astrophys J Lett 940(2):L55. https://doi.org/10.3847/2041-8213/ac966e. arXiv:2207.12474 [astro-ph.GA]
Finkelstein SL, Bagley MB, Arrabal Haro P, et al (2022a) A long time ago in a galaxy far, far away: a candidate z 12 Galaxy in Early JWST CEERS Imaging. arXiv e-prints arXiv:2207.12474. arXiv:2207.12474 [astro-ph.GA]
Firouzjahi H (2023) One-loop corrections in power spectrum in single field inflation. JCAP 10:006. https://doi.org/10.1088/1475-7516/2023/10/006. arXiv:2303.12025 [astro-ph.CO]
Firouzjahi H, Nassiri-Rad A, Noorbala M (2019) Stochastic ultra slow roll inflation. JCAP 01:040. https://doi.org/10.1088/1475-7516/2019/01/040. arXiv:1811.02175 [hep-th]
Firouzjahi H, Riotto A (2023) Sign of non-Gaussianity and the primordial black holes abundance. Phys Rev D 108(12):123504. https://doi.org/10.1103/PhysRevD.108.123504. arXiv:2309.10536 [astro-ph.CO]
Firouzjahi H, Riotto A (2024) Primordial Black Holes and loops in single-field inflation. JCAP 02:021. https://doi.org/10.1088/1475-7516/2024/02/021. arXiv:2304.07801 [astro-ph.CO]
Firouzjahi H, Talebian A (2023) Induced gravitational waves from ultra slow-roll inflation and pulsar timing arrays observations. JCAP 10:032. https://doi.org/10.1088/1475-7516/2023/10/032. arXiv:2307.03164 [gr-qc]
Flanagan EE, Hughes SA (2005) The basics of gravitational wave theory. New J Phys 7:204. https://doi.org/10.1088/1367-2630/7/1/204. arXiv:gr-qc/0501041
Flores MM, Kusenko A, Sasaki M (2024) Revisiting formation of primordial black holes in a supercooled first-order phase transition. Phys Rev D 110(1):015005. https://doi.org/10.1103/PhysRevD.110.015005. arXiv:2402.13341 [hep-ph]
Franciolini G, Baibhav V, De Luca V et al (2022a) Searching for a subpopulation of primordial black holes in LIGO-Virgo gravitational-wave data. Phys Rev D 105(8):083526. https://doi.org/10.1103/PhysRevD.105.083526. arXiv:2105.03349 [gr-qc]
Franciolini G, Cotesta R, Loutrel N et al (2022b) How to assess the primordial origin of single gravitational-wave events with mass, spin, eccentricity, and deformability measurements. Phys Rev D 105(6):063510. https://doi.org/10.1103/PhysRevD.105.063510. arXiv:2112.10660 [astro-ph.CO]

Franciolini G, Iovino AJunior, Vaskonen V (2023) Recent gravitational wave observation by pulsar timing arrays and primordial black holes: the importance of non-gaussianities. Phys Rev Lett 131 (20):201401. https://doi.org/10.1103/PhysRevLett.131.201401. arXiv:2306.17149 [astro-ph.CO]

Franciolini G, Iovino AJ, Taoso M et al (2024a) Perturbativity in the presence of ultraslow-roll dynamics. Phys Rev D 109(12):123550. https://doi.org/10.1103/PhysRevD.109.123550. arXiv:2305.03491 [astro-ph.CO]

Franciolini G, Kehagias A, Matarrese S et al (2018) Primordial black holes from inflation and non-gaussianity. JCAP 03:016. https://doi.org/10.1088/1475-7516/2018/03/016. arXiv:1801.09415 [astro-ph.CO]

Franciolini G, Kritos K, Berti E et al (2022c) Primordial black hole mergers from three-body interactions. Phys Rev D 106(8):083529. https://doi.org/10.1103/PhysRevD.106.083529. arXiv:2205.15340 [astro-ph.CO]

Franciolini G, Maharana A, Muia F (2022d) Hunt for light primordial black hole dark matter with ultrahigh-frequency gravitational waves. Phys Rev D 106(10):103520. https://doi.org/10.1103/PhysRevD.106.103520. arXiv:2205.02153 [astro-ph.CO]

Franciolini G, Musco I, Pani P et al (2022e) From inflation to black hole mergers and back again: gravitational-wave data-driven constraints on inflationary scenarios with a first-principle model of primordial black holes across the QCD epoch. Phys Rev D 106(12):123526. https://doi.org/10.1103/PhysRevD.106.123526. arXiv:2209.05959 [astro-ph.CO]

Franciolini G, Pani P (2022) Searching for mass-spin correlations in the population of gravitational-wave events: The GWTC-3 case study. Phys Rev D 105(12):123024. https://doi.org/10.1103/PhysRevD.105.123024. arXiv:2201.13098 [astro-ph.HE]

Franciolini G, Racco D, Rompineve F (2024b) Footprints of the QCD crossover on cosmological gravitational waves at pulsar timing arrays. Phys Rev Lett 132(8):081001. https://doi.org/10.1103/PhysRevLett.132.081001. arXiv:2306.17136 [astro-ph.CO]

Franciolini G, Urbano A (2022) Primordial black hole dark matter from inflation: the reverse engineering approach. Phys Rev D 106(12):123519. https://doi.org/10.1103/PhysRevD.106.123519. arXiv:2207.10056 [astro-ph.CO]

Franciolini G (2021) Primordial black holes: from theory to gravitational wave observations. PhD thesis, Geneva U., Dept. Theor. Phys., https://doi.org/10.13097/archive-ouverte/unige:156136, arXiv:2110.06815

Freese K, Frieman JA, Olinto AV (1990) Natural inflation with pseudo - Nambu-Goldstone bosons. Phys Rev Lett 65:3233–3236. https://doi.org/10.1103/PhysRevLett.65.3233

Freese K, Galstyan I, Sandick P et al (2022) Neutrino point source searches for dark matter spikes. JCAP 08:065. https://doi.org/10.1088/1475-7516/2022/08/065. arXiv:2202.01126 [astro-ph.CO]

Freigang J, Lust D, Nian GE et al (2023) Cosmic acceleration and turns in the Swampland. JCAP 11:080. https://doi.org/10.1088/1475-7516/2023/11/080. arXiv:2306.17217 [hep-th]

Fujita T, Kawasaki M, Tada Y et al (2013) A new algorithm for calculating the curvature perturbations in stochastic inflation. JCAP 12:036. https://doi.org/10.1088/1475-7516/2013/12/036. arXiv:1308.4754 [astro-ph.CO]

Fumagalli J, Bhattacharya S, Peloso M et al (2024) One-loop infrared rescattering by enhanced scalar fluctuations during inflation. JCAP 04:029. https://doi.org/10.1088/1475-7516/2024/04/029. arXiv:2307.08358 [astro-ph.CO]

Fumagalli J, Garcia-Saenz S, Pinol L et al (2019) Hyper-non-gaussianities in inflation with strongly nongeodesic motion. Phys Rev Lett 123(20):201302. https://doi.org/10.1103/PhysRevLett.123.201302. arXiv:1902.03221 [hep-th]

Fumagalli J, Palma GA, Renaux-Petel S et al (2022a) Primordial gravitational waves from excited states. JHEP 03:196. https://doi.org/10.1007/JHEP03(2022)196. arXiv:2111.14664 [astro-ph.CO]

Fumagalli J, Pieroni M, Renaux-Petel S et al (2022b) Detecting primordial features with LISA. JCAP 07 (07):020. https://doi.org/10.1088/1475-7516/2022/07/020. arXiv:2112.06903 [astro-ph.CO]

Fumagalli J, Renaux-Petel S, Ronayne JW et al (2023) Turning in the landscape: a new mechanism for generating primordial black holes. Phys Lett B 841:137921. https://doi.org/10.1016/j.physletb.2023.137921. arXiv:2004.08369 [hep-th]

Fumagalli J, Renaux-Petel S, Witkowski LT (2021a) Oscillations in the stochastic gravitational wave background from sharp features and particle production during inflation. JCAP 08:030. https://doi.org/10.1088/1475-7516/2021/08/030. arXiv:2012.02761 [astro-ph.CO]

Fumagalli J, Renaux-Petel S, Witkowski LT (2021b) Resonant features in the stochastic gravitational wave background. JCAP 08:059. https://doi.org/10.1088/1475-7516/2021/08/059. arXiv:2105.06481 [astro-ph.CO]
Fumagalli J (2023) Absence of one-loop effects on large scales from small scales in non-slow-roll dynamics. arXiv e-prints arXiv:2305.19263 [astro-ph.CO]
Gaggero D, Bertone G, Calore F et al (2017) Searching for primordial black holes in the radio and X-ray sky. Phys Rev Lett 118(24):241101. https://doi.org/10.1103/PhysRevLett.118.241101. arXiv:1612.00457 [astro-ph.HE]
Garcia-Saenz S, Pinol L, Renaux-Petel S et al (2023) No-go theorem for scalar-trispectrum-induced gravitational waves. JCAP 03:057. https://doi.org/10.1088/1475-7516/2023/03/057. arXiv:2207.14267 [astro-ph.CO]
Garcia-Saenz S, Renaux-Petel S (2018) Flattened non-Gaussianities from the effective field theory of inflation with imaginary speed of sound. JCAP 11:005. https://doi.org/10.1088/1475-7516/2018/11/005. arXiv:1805.12563 [hep-th]
Garcia-Saenz S, Renaux-Petel S, Ronayne J (2018) Primordial fluctuations and non-Gaussianities in sidetracked inflation. JCAP 07:057. https://doi.org/10.1088/1475-7516/2018/07/057. arXiv:1804.11279 [astro-ph.CO]
García-Bellido J (2017) Massive primordial black holes as dark matter and their detection with gravitational waves. J Phys Conf Ser 840(1):012032. https://doi.org/10.1088/1742-6596/840/1/012032. arXiv:1702.08275 [astro-ph.CO]
García-Bellido J (2019) Primordial black holes and the origin of the matter-antimatter asymmetry. Phil Trans Roy Soc Lond A 377(2161):20190091. https://doi.org/10.1098/rsta.2019.0091
García-Bellido J, Carr B, Clesse S (2021a) Primordial black holes and a common origin of baryons and dark matter. Universe 8(1):12. https://doi.org/10.3390/universe8010012. arXiv:1904.11482 [astro-ph.CO]
García-Bellido J, Clesse S (2018) Constraints from microlensing experiments on clustered primordial black holes. Phys Dark Univ 19:144–148. https://doi.org/10.1016/j.dark.2018.01.001. arXiv:1710.04694 [astro-ph.CO]
García-Bellido J, Clesse S, Fleury P (2018) Primordial black holes survive SN lensing constraints. Phys Dark Univ 20:95–100. https://doi.org/10.1016/j.dark.2018.04.005. arXiv:1712.06574 [astro-ph.CO]
García-Bellido J, Jaraba S, Kuroyanagi S (2022) The stochastic gravitational wave background from close hyperbolic encounters of primordial black holes in dense clusters. Phys Dark Univ 36:101009. https://doi.org/10.1016/j.dark.2022.101009. arXiv:2109.11376 [gr-qc]
García-Bellido J, Linde AD, Wands D (1996) Density perturbations and black hole formation in hybrid inflation. Phys Rev D 54:6040–6058. https://doi.org/10.1103/PhysRevD.54.6040. arXiv:astro-ph/9605094
García-Bellido J, Murayama H, White G (2021b) Exploring the early Universe with Gaia and Theia. JCAP 12(12):023. https://doi.org/10.1088/1475-7516/2021/12/023. arXiv:2104.04778 [hep-ph]
García-Bellido J, Nesseris S (2017) Gravitational wave bursts from Primordial Black Hole hyperbolic encounters. Phys Dark Univ 18:123–126. https://doi.org/10.1016/j.dark.2017.10.002. arXiv:1706.02111 [astro-ph.CO]
García-Bellido J, Nesseris S (2018) Gravitational wave energy emission and detection rates of Primordial Black Hole hyperbolic encounters. Phys Dark Univ 21:61–69. https://doi.org/10.1016/j.dark.2018.06.001. arXiv:1711.09702 [astro-ph.HE]
García-Bellido J, Nuño Siles JF, Ruiz Morales E (2021c) Bayesian analysis of the spin distribution of LIGO/Virgo black holes. Phys Dark Univ 31:100791. https://doi.org/10.1016/j.dark.2021.100791. arXiv:2010.13811 [astro-ph.CO]
García-Bellido J, Papageorgiou A, Peloso M et al (2024) A flashing beacon in axion inflation: recurring bursts of gravitational waves in the strong backreaction regime. JCAP 01:034. https://doi.org/10.1088/1475-7516/2024/01/034. arXiv:2303.13425 [astro-ph.CO]
García-Bellido J, Peloso M, Ünal C (2016) Gravitational waves at interferometer scales and primordial black holes in axion inflation. JCAP 12:031. https://doi.org/10.1088/1475-7516/2016/12/031. arXiv:1610.03763 [astro-ph.CO]
García-Bellido J, Peloso M, Ünal C (2017) Gravitational wave signatures of inflationary models from primordial black hole dark matter. JCAP 09:013. https://doi.org/10.1088/1475-7516/2017/09/013. arXiv:1707.02441 [astro-ph.CO]
García-Bellido J, Ruiz Morales E (2017) Primordial black holes from single field models of inflation. Phys Dark Univ 18:47–54. https://doi.org/10.1016/j.dark.2017.09.007. arXiv:1702.03901 [astro-ph.CO]

García-Bellido J (2018) Primordial Black Holes. PoS EDSU2018:042. https://doi.org/10.22323/1.335.0042
García-Bellido J, Hawkins M (2024) Reanalysis of the MACHO constraints on PBH in the light of Gaia DR3 data. arXiv e-prints arXiv:2402.00212 [astro-ph.GA]
Garriga J, Sakellariadou M (1993) Effects of friction on cosmic strings. Phys Rev D 48:2502–2515. https://doi.org/10.1103/PhysRevD.48.2502. arXiv:hep-th/9303024
Garriga J, Vilenkin A (1993) Black holes from nucleating strings. Phys Rev D 47:3265–3274. https://doi.org/10.1103/PhysRevD.47.3265. arXiv:hep-ph/9208212
Garriga J, Vilenkin A, Zhang J (2016) Black holes and the multiverse. JCAP 02:064. https://doi.org/10.1088/1475-7516/2016/02/064. arXiv:1512.01819 [hep-th]
Ge S (2020) Sublunar-mass primordial black holes from closed axion domain walls. Phys Dark Univ 27:100440. https://doi.org/10.1016/j.dark.2019.100440. arXiv:1905.12182 [hep-ph]
Geller M, Hook A, Sundrum R et al (2018) Primordial anisotropies in the gravitational wave background from cosmological phase transitions. Phys Rev Lett 121(20):201303. https://doi.org/10.1103/PhysRevLett.121.201303. arXiv:1803.10780 [hep-ph]
Geller SR, Qin W, McDonough E et al (2022) Primordial black holes from multifield inflation with nonminimal couplings. Phys Rev D 106(6):063535. https://doi.org/10.1103/PhysRevD.106.063535. arXiv:2205.04471 [hep-th]
Germani C, Musco I (2019) Abundance of primordial black holes depends on the shape of the inflationary power spectrum. Phys Rev Lett 122(14):141302. https://doi.org/10.1103/PhysRevLett.122.141302. arXiv:1805.04087 [astro-ph.CO]
Ghosh T, Ghoshal A, Guo HK et al (2024) Did we hear the sound of the Universe boiling? Analysis using the full fluid velocity profiles and NANOGrav 15-year data. JCAP 05:100. https://doi.org/10.1088/1475-7516/2024/05/100. arXiv:2307.02259 [astro-ph.HE]
Ghoshal A, Strumia A (2024) Probing the Dark Matter density with gravitational waves from supermassive binary black holes. JCAP 02:054. https://doi.org/10.1088/1475-7516/2024/02/054. arXiv:2306.17158 [astro-ph.CO]
Ginés EU, Mena O, Witte SJ (2022) Revisiting constraints on WIMPs around primordial black holes. Phys Rev D 106(6):063538. https://doi.org/10.1103/PhysRevD.106.063538. arXiv:2207.09481 [astro-ph.CO]
Glicenstein JF, Barnacka A, Vivier M, et al (2013) Limits on Primordial Black Hole evaporation with the H.E.S.S. array of Cherenkov telescopes. In: 33rd International Cosmic Ray Conference, p 0930, arXiv:1307.4898
Goncharov B et al (2021) On the evidence for a common-spectrum process in the search for the nanohertz gravitational-wave background with the parkes pulsar timing array. Astrophys J Lett 917(2):L19. https://doi.org/10.3847/2041-8213/ac17f4. arXiv:2107.12112 [astro-ph.HE]
Gong JO (2022) Analytic integral solutions for induced gravitational waves. Astrophys J 925(1):102. https://doi.org/10.3847/1538-4357/ac3a6c. arXiv:1909.12708 [gr-qc]
Gong JO, Stewart ED (2001) The density perturbation power spectrum to second order corrections in the slow roll expansion. Phys Lett B 510:1–9. https://doi.org/10.1016/S0370-2693(01)00616-5. arXiv:astro-ph/0101225 [astro-ph]
Gong Y, Yue B, Cao Y et al (2023) Fuzzy dark matter as a solution to reconcile the stellar mass density of high-z massive galaxies and reionization history. Astrophys J 947(1):28. https://doi.org/10.3847/1538-4357/acc109. arXiv:2209.13757 [astro-ph.CO]
Gorghetto M, Hardy E, Nicolaescu H (2021) Observing invisible axions with gravitational waves. JCAP 06:034. https://doi.org/10.1088/1475-7516/2021/06/034. arXiv:2101.11007 [hep-ph]
Gorton M, Green AM (2022) Effect of clustering on primordial black hole microlensing constraints. JCAP 08(08):035. https://doi.org/10.1088/1475-7516/2022/08/035. arXiv:2203.04209 [astro-ph.CO]
Gosenca M, Adamek J, Byrnes CT et al (2017) 3D simulations with boosted primordial power spectra and ultracompact minihalos. Phys Rev D 96(12):123519. https://doi.org/10.1103/PhysRevD.96.123519. arXiv:1710.02055 [astro-ph.CO]
Gould A (1992) Femtolensing of gamma-ray bursters. Astrophys J Lett 386:L5. https://doi.org/10.1086/186279
Gouttenoire Y (2023) First-order phase transition interpretation of pulsar timing array signal is consistent with solar-mass black holes. Phys Rev Lett 131(17):171404. https://doi.org/10.1103/PhysRevLett.131.171404. arXiv:2307.04239 [hep-ph]
Gouttenoire Y, Vitagliano E (2024) Domain wall interpretation of the PTA signal confronting black hole overproduction. Phys Rev D 110(6):L061306. https://doi.org/10.1103/PhysRevD.110.L061306. arXiv:2306.17841 [gr-qc]

Gouttenoire Y, Volansky T (2024) Primordial black holes from supercooled phase transitions. Phys Rev D 110(4):043514. https://doi.org/10.1103/PhysRevD.110.043514. arXiv:2305.04942 [hep-ph]
Gow AD, Assadullahi H, Jackson JHP et al (2023) Non-perturbative non-Gaussianity and primordial black holes. EPL 142(4):49001. https://doi.org/10.1209/0295-5075/acd417. arXiv:2211.08348 [astro-ph.CO]
Gow AD, Byrnes CT, Cole PS et al (2021) The power spectrum on small scales: robust constraints and comparing PBH methodologies. JCAP 02:002. https://doi.org/10.1088/1475-7516/2021/02/002. arXiv:2008.03289 [astro-ph.CO]
Gow AD, Byrnes CT, Hall A et al (2020) Primordial black hole merger rates: distributions for multiple LIGO observables. JCAP 01:031. https://doi.org/10.1088/1475-7516/2020/01/031. arXiv:1911.12685 [astro-ph.CO]
Gow AD, Byrnes CT, Cole PS, et al (2020) The power spectrum on small scales: robust constraints and comparing PBH methodologies. arXiv e-prints arXiv:2008.03289. arXiv:2008.03289 [astro-ph.CO]
Graham PW, Rajendran S, Varela J (2015) Dark matter triggers of supernovae. Phys Rev D 92(6):063007. https://doi.org/10.1103/PhysRevD.92.063007. arXiv:1505.04444 [hep-ph]
Green AM (2016) Microlensing and dynamical constraints on primordial black hole dark matter with an extended mass function. Phys Rev D 94(6):063530. https://doi.org/10.1103/PhysRevD.94.063530. arXiv:1609.01143 [astro-ph.CO]
Green AM (2017) Astrophysical uncertainties on stellar microlensing constraints on multi-Solar mass primordial black hole dark matter. Phys Rev D 96(4):043020. https://doi.org/10.1103/PhysRevD.96.043020. arXiv:1705.10818 [astro-ph.CO]
Green AM, Liddle AR (1997) Constraints on the density perturbation spectrum from primordial black holes. Phys Rev D 56:6166–6174. https://doi.org/10.1103/PhysRevD.56.6166. arXiv:astro-ph/9704251
Green AM, Liddle AR, Riotto A (1997) Primordial black hole constraints in cosmologies with early matter domination. Phys Rev D 56:7559–7565. https://doi.org/10.1103/PhysRevD.56.7559. arXiv:astro-ph/9705166
Green AM, Malik KA (2001) Primordial black hole production due to preheating. Phys Rev D 64:021301. https://doi.org/10.1103/PhysRevD.64.021301. arXiv:hep-ph/0008113 [hep-ph]
Groot Nibbelink S, van Tent BJW (2002) Scalar perturbations during multiple field slow-roll inflation. Class Quant Grav 19:613–640. https://doi.org/10.1088/0264-9381/19/4/302. arXiv:hep-ph/0107272
Groot Nibbelink S, van Tent BJW (2000) Density perturbations arising from multiple field slow roll inflation. arXiv e-prints arXiv:hep-ph/0011325
Gröbner M, Jetzer P, Haney M et al (2020) A note on the gravitational wave energy spectrum of parabolic and hyperbolic encounters. Class Quant Grav 37(6):067002. https://doi.org/10.1088/1361-6382/ab6be2. arXiv:2001.05187 [gr-qc]
Guo HK, Shu J, Zhao Y (2019a) Using LISA-like Gravitational wave detectors to search for primordial black holes. Phys Rev D 99(2):023001. https://doi.org/10.1103/PhysRevD.99.023001. arXiv:1709.03500 [astro-ph.CO]
Guo HK, Sinha K, Sun C (2019b) Probing boson stars with extreme mass ratio inspirals. JCAP 09:032. https://doi.org/10.1088/1475-7516/2019/09/032. arXiv:1904.07871 [hep-ph]
Guo HK, Miller A (2022) Searching for mini extreme mass ratio inspirals with gravitational-wave detectors. arXiv e-prints arXiv:2205.10359 [astro-ph.IM]
Guzzetti M, Bartolo N, Liguori M et al (2016) Gravitational waves from inflation. Riv Nuovo Cim 39(9):399–495. https://doi.org/10.1393/ncr/i2016-10127-1. arXiv:1605.01615 [astro-ph.CO]
Hall A, Gow AD, Byrnes CT (2020) Bayesian analysis of LIGO-Virgo mergers: primordial vs. astrophysical black hole populations. Phys Rev D 102:123524. https://doi.org/10.1103/PhysRevD.102.123524. arXiv:2008.13704 [astro-ph.CO]
Hamadache C et al (2006) Galactic bulge microlensing optical depth from eros-2. Astron Astrophys 454:185–199. https://doi.org/10.1051/0004-6361:20064893. arXiv:astro-ph/0601510
Harada T, Yoo CM, Kohri K (2013) Threshold of primordial black hole formation. Phys Rev D 88(8):084051. https://doi.org/10.1103/PhysRevD.88.084051. [Erratum: Phys. Rev. D 89, 029903 (2014)] arXiv:1309.4201 [astro-ph.CO]
Harada T, Yoo CM, Kohri K et al (2016) Primordial black hole formation in the matter-dominated phase of the Universe. Astrophys J 833(1):61. https://doi.org/10.3847/1538-4357/833/1/61. arXiv:1609.01588 [astro-ph.CO]

Harada T, Yoo CM, Kohri K et al (2017) Spins of primordial black holes formed in the matter-dominated phase of the Universe. Phys Rev D 96(8):083517. https://doi.org/10.1103/PhysRevD.96.083517. [Erratum: Phys. Rev. D 99, 069904 (2019)] arXiv:1707.03595 [gr-qc]

Harada T, Yoo CM, Kohri K et al (2021) Spins of primordial black holes formed in the radiation-dominated phase of the universe: first-order effect. Astrophys J 908(2):140. https://doi.org/10.3847/1538-4357/abd9b9. arXiv:2011.00710 [astro-ph.CO]

Harikane Y, Ouchi M, Oguri M, et al (2023) A comprehensive study of galaxies at z $\sim$ 9–16 found in the early JWST data: ultraviolet luminosity functions and cosmic star formation history at the pre-reionization epoch. Astrophys J Suppl 265(1). https://doi.org/10.3847/1538-4365/acaaa9, arXiv:2208.01612 [astro-ph.GA]

Hartwig T, Volonteri M, Bromm V et al (2016) Gravitational waves from the remnants of the first stars. Mon Not R Astron Soc 460(1):L74–L78. https://doi.org/10.1093/mnrasl/slw074. arXiv:1603.05655 [astro-ph.GA]

Hasinger G (2020) Illuminating the dark ages: cosmic backgrounds from accretion onto primordial black hole dark matter. JCAP 07:022. https://doi.org/10.1088/1475-7516/2020/07/022. arXiv:2003.05150 [astro-ph.CO]

Hawking S (1971) Gravitationally collapsed objects of very low mass. Mon Not R Astron Soc 152:75

Hawking SW (1975) Particle creation by black holes. Commun Math Phys 43:199–220. https://doi.org/10.1007/BF02345020. ([Erratum: Commun. Math. Phys. 46, 206 (1976)])

Hawking SW (1989) Black holes from cosmic strings. Phys Lett B 231:237–239. https://doi.org/10.1016/0370-2693(89)90206-2

Hawking SW (1990) Gravitational radiation from collapsing cosmic string loops. Phys Lett B 246:36–38. https://doi.org/10.1016/0370-2693(90)91304-T

Hawking SW, Moss IG, Stewart JM (1982) Bubble collisions in the very early universe. Phys Rev D 26:2681. https://doi.org/10.1103/PhysRevD.26.2681

Hawkins MRS (1993) Gravitational microlensing, quasar variability and missing matter. Nature 366 (6452):242–245. https://doi.org/10.1038/366242a0

Hawkins MRS (2007) Timescale of variation and the size of the accretion disc in active galactic nuclei. Astron Astrophys 462:581. https://doi.org/10.1051/0004-6361:20066283. arXiv:astro-ph/0611491

Hawkins MRS (2015) A new look at microlensing limits on dark matter in the Galactic halo. Astron Astrophys 575:A107. https://doi.org/10.1051/0004-6361/201425400. arXiv:1503.01935 [astro-ph.GA]

Hawkins MRS (2020a) SDSS J1004+4112: the case for a galaxy cluster dominated by primordial black holes. Astron Astrophys 643:A10. https://doi.org/10.1051/0004-6361/202038670. arXiv:2010.15007 [astro-ph.CO]

Hawkins MRS (2020b) The signature of primordial black holes in the dark matter halos of galaxies. Astron Astrophys 633:A107. https://doi.org/10.1051/0004-6361/201936462. arXiv:2001.07633 [astro-ph.GA]

Hawkins MRS (2022) New evidence for a cosmological distribution of stellar mass primordial black holes. Mon Not R Astron Soc 512(4):5706–5714. https://doi.org/10.1093/mnras/stac863. arXiv:2204.09143 [astro-ph.CO]

Heggie DC (1975) Binary evolution in stellar dynamics. Mon Not R Astron Soc 173:729–787. https://doi.org/10.1093/mnras/173.3.729

Hektor A, Hütsi G, Marzola L et al (2018) Constraining primordial black holes with the EDGES 21 cm absorption signal. Phys Rev D 98(2):023503. https://doi.org/10.1103/PhysRevD.98.023503. arXiv:1803.09697 [astro-ph.CO]

Helfer T, Aurrekoetxea JC, Lim EA (2019) Cosmic string loop collapse in full general relativity. Phys Rev D 99(10):104028. https://doi.org/10.1103/PhysRevD.99.104028. arXiv:1808.06678 [gr-qc]

Hellings RW, Downs GS (1983) Upper limits on the isotropic gravitational radiation background from pulsar timing analysis. Astrophys J Lett 265:L39–L42. https://doi.org/10.1086/183954

Herman N, Füzfa A, Lehoucq L et al (2021) Detecting planetary-mass primordial black holes with resonant electromagnetic gravitational-wave detectors. Phys Rev D 104(2):023524. https://doi.org/10.1103/PhysRevD.104.023524. arXiv:2012.12189 [gr-qc]

Herman N, Lehoucq L, Fúzfa A (2023) Electromagnetic antennas for the resonant detection of the stochastic gravitational wave background. Phys Rev D 108(12):124009. https://doi.org/10.1103/PhysRevD.108.124009. arXiv:2203.15668 [gr-qc]

Hertzberg MP, Nurmi S, Schiappacasse ED et al (2021) Shining primordial black holes. Phys Rev D 103 (6):063025. https://doi.org/10.1103/PhysRevD.103.063025. arXiv:2011.05922 [hep-ph]

Hertzberg MP, Schiappacasse ED, Yanagida TT (2020) Implications for dark matter direct detection in the presence of LIGO-motivated primordial black holes. Phys Lett B 807:135566. https://doi.org/10.1016/j.physletb.2020.135566. arXiv:1910.10575 [astro-ph.CO]

Hertzberg MP, Yamada M (2018) Primordial black holes from polynomial potentials in single field inflation. Phys Rev D 97(8):083509. https://doi.org/10.1103/PhysRevD.97.083509. arXiv:1712.09750 [astro-ph.CO]

Hidalgo JC, Urena-Lopez LA, Liddle AR (2012) Unification models with reheating via Primordial Black Holes. Phys Rev D 85:044055. https://doi.org/10.1103/PhysRevD.85.044055. arXiv:1107.5669 [astro-ph.CO]

Hindmarsh M, Kume J (2023) Multi-messenger constraints on Abelian-Higgs cosmic string networks. JCAP 04:045. https://doi.org/10.1088/1475-7516/2023/04/045. arXiv:2210.06178 [astro-ph.CO]

Hook A, Marques-Tavares G, Racco D (2021) Causal gravitational waves as a probe of free streaming particles and the expansion of the Universe. JHEP 02:117. https://doi.org/10.1007/JHEP02(2021)117. arXiv:2010.03568 [hep-ph]

Hooper D, Ireland A, Krnjaic G (2023) Cosmological magnetic fields from primordial Kerr-Newman black holes. Phys Rev D 107(10):103524. https://doi.org/10.1103/PhysRevD.107.103524. arXiv:2206.04066 [astro-ph.CO]

Hooper D, Krnjaic G, McDermott SD (2019) Dark radiation and superheavy dark matter from black hole domination. JHEP 08:001. https://doi.org/10.1007/JHEP08(2019)001. arXiv:1905.01301 [hep-ph]

Hotchkiss S, Mazumdar A, Nadathur S (2011) Inflection point inflation: WMAP constraints and a solution to the fine-tuning problem. JCAP 06:002. https://doi.org/10.1088/1475-7516/2011/06/002. arXiv:1101.6046 [astro-ph.CO]

Hoyle F, Lyttleton RA (1939) The effect of interstellar matter on climatic variation. Proceedings of the Cambridge Philosophical Society 35(3):405. https://doi.org/10.1017/S0305004100021150

Hoyle F, Lyttleton RA (1940a) On the accretion of interstellar matter by stars. Proc Cambridge Philos Soc 36(3):325. https://doi.org/10.1017/S0305004100017369

Hoyle F, Lyttleton RA (1940b) On the physical aspects of accretion by stars. Proc Cambridge Philos Soc 36(4):424. https://doi.org/10.1017/S0305004100017461

Hwang JC, Jeong D, Noh H (2017) Gauge dependence of gravitational waves generated from scalar perturbations. Astrophys J 842(1):46. https://doi.org/10.3847/1538-4357/aa74be. arXiv:1704.03500 [astro-ph.CO]

Hütsi G, Koivisto T, Raidal M et al (2021a) Cosmological black holes are not described by the Thakurta metric: LIGO-Virgo bounds on PBHs remain unchanged. Eur Phys J C 81(11):999. https://doi.org/10.1140/epjc/s10052-021-09803-4. arXiv:2105.09328 [astro-ph.CO]

Hütsi G, Raidal M, Urrutia J et al (2023) Did JWST observe imprints of axion miniclusters or primordial black holes? Phys Rev D 107(4):043502. https://doi.org/10.1103/PhysRevD.107.043502. arXiv:2211.02651 [astro-ph.CO]

Hütsi G, Raidal M, Vaskonen V et al (2021c) Two populations of LIGO-Virgo black holes. JCAP 03:068. https://doi.org/10.1088/1475-7516/2021/03/068. arXiv:2012.02786 [astro-ph.CO]

Hütsi G, Raidal M, Veermäe H (2019) Small-scale structure of primordial black hole dark matter and its implications for accretion. Phys Rev D 100(8):083016. https://doi.org/10.1103/PhysRevD.100.083016. arXiv:1907.06533 [astro-ph.CO]

Hütsi G, Koivisto T, Raidal M, et al (2021b) Reply to "Comment on: Cosmological black holes are not described by the Thakurta metric". arXiv e-prints arXiv:2106.02007 [astro-ph.CO]

Iacconi L, Assadullahi H, Fasiello M et al (2022) Revisiting small-scale fluctuations in α-attractor models of inflation. JCAP 06(06):007. https://doi.org/10.1088/1475-7516/2022/06/007. arXiv:2112.05092 [astro-ph.CO]

Inayoshi K, Hirai R, Kinugawa T et al (2017) Formation pathway of Population III coalescing binary black holes through stable mass transfer. Mon Not R Astron Soc 468(4):5020–5032. https://doi.org/10.1093/mnras/stx757. arXiv:1701.04823 [astro-ph.HE]

Inman D, Ali-Haïmoud Y (2019) Early structure formation in primordial black hole cosmologies. Phys Rev D 100(8):083528. https://doi.org/10.1103/PhysRevD.100.083528. arXiv:1907.08129 [astro-ph.CO]

Inomata K, Braglia M, Chen X et al (2023) Questions on calculation of primordial power spectrum with large spikes: the resonance model case. JCAP 04:011. https://doi.org/10.1088/1475-7516/2023/04/011. arXiv:2211.02586 [astro-ph.CO]

Inomata K, Kawasaki M, Mukaida K et al (2017) Inflationary primordial black holes for the LIGO gravitational wave events and pulsar timing array experiments. Phys Rev D 95(12):123510. https://doi.org/10.1103/PhysRevD.95.123510. arXiv:1611.06130 [astro-ph.CO]

Inomata K, Kawasaki M, Mukaida K et al (2018) Double inflation as a single origin of primordial black holes for all dark matter and LIGO observations. Phys Rev D 97(4):043514. https://doi.org/10.1103/PhysRevD.97.043514. arXiv:1711.06129 [astro-ph.CO]

Inomata K, Kawasaki M, Mukaida K et al (2020) Gravitational wave production right after a primordial black hole evaporation. Phys Rev D 101(12):123533. https://doi.org/10.1103/PhysRevD.101.123533. arXiv:2003.10455 [astro-ph.CO]

Inomata K, Kawasaki M, Mukaida K et al (2021a) NANOGrav results and LIGO-Virgo primordial black holes in axionlike curvaton models. Phys Rev Lett 126(13):131301. https://doi.org/10.1103/PhysRevLett.126.131301. arXiv:2011.01270 [astro-ph.CO]

Inomata K, Kohri K, Nakama T et al (2019a) Enhancement of gravitational waves induced by scalar perturbations due to a sudden transition from an early matter era to the radiation era. Phys Rev D 100 (4):043532. https://doi.org/10.1103/PhysRevD.100.043532. arXiv:1904.12879 [astro-ph.CO]

Inomata K, Kohri K, Nakama T et al (2019b) Gravitational waves induced by scalar perturbations during a gradual transition from an early matter era to the radiation era. JCAP 10:071. https://doi.org/10.1088/1475-7516/2019/10/071. arXiv:1904.12878 [astro-ph.CO]

Inomata K, Kohri K, Terada T (2024) Detected stochastic gravitational waves and subsolar-mass primordial black holes. Phys Rev D 109(6):063506. https://doi.org/10.1103/PhysRevD.109.063506. arXiv:2306.17834 [astro-ph.CO]

Inomata K, McDonough E, Hu W (2021b) Primordial black holes arise when the inflaton falls. Phys Rev D 104(12):123553. https://doi.org/10.1103/PhysRevD.104.123553. arXiv:2104.03972 [astro-ph.CO]

Inomata K, McDonough E, Hu W (2022) Amplification of primordial perturbations from the rise or fall of the inflaton. JCAP 02(02):031. https://doi.org/10.1088/1475-7516/2022/02/031. arXiv:2110.14641 [astro-ph.CO]

Inomata K, Nakama T (2019) Gravitational waves induced by scalar perturbations as probes of the small-scale primordial spectrum. Phys Rev D 99(4):043511. https://doi.org/10.1103/PhysRevD.99.043511. arXiv:1812.00674 [astro-ph.CO]

Inomata K, Terada T (2020) Gauge independence of induced gravitational waves. Phys Rev D 101 (2):023523. https://doi.org/10.1103/PhysRevD.101.023523. arXiv:1912.00785 [gr-qc]

Inoue Y, Kusenko A (2017) New X-ray bound on density of primordial black holes. JCAP 10:034. https://doi.org/10.1088/1475-7516/2017/10/034. arXiv:1705.00791 [astro-ph.CO]

Ioka K, Chiba T, Tanaka T et al (1998) Black hole binary formation in the expanding universe: three body problem approximation. Phys Rev D 58:063003. https://doi.org/10.1103/PhysRevD.58.063003. arXiv:astro-ph/9807018

Ivanov P (1997) Nonlinear metric perturbations and production of primordial black holes. Phys Rev D 57:7145–7154. https://doi.org/10.1103/PhysRevD.57.7145. arXiv:astro-ph/9708224

Ivanov VR, Ketov SV, Pozdeeva EO et al (2022) Analytic extensions of Starobinsky model of inflation. JCAP 03(03):058. https://doi.org/10.1088/1475-7516/2022/03/058. arXiv:2111.09058 [gr-qc]

Ivanov P, Naselsky P, Novikov I (1994) Inflation and primordial black holes as dark matter. Phys Rev D 50:7173–7178. https://doi.org/10.1103/PhysRevD.50.7173

Jackson JHP, Assadullahi H, Koyama K et al (2022) Numerical simulations of stochastic inflation using importance sampling. JCAP 10:067. https://doi.org/10.1088/1475-7516/2022/10/067. arXiv:2206.11234 [astro-ph.CO]

Jain RK, Chingangbam P, Gong JO et al (2009) Punctuated inflation and the low CMB multipoles. JCAP 01:009. https://doi.org/10.1088/1475-7516/2009/01/009. arXiv:0809.3915 [astro-ph]

Jain RK, Chingangbam P, Sriramkumar L et al (2010) The tensor-to-scalar ratio in punctuated inflation. Phys Rev D 82:023509. https://doi.org/10.1103/PhysRevD.82.023509. arXiv:0904.2518 [astro-ph.CO]

James-Turner C, Weil DPB, Green AM et al (2020) Constraints on the cosmic string loop collapse fraction from primordial black holes. Phys Rev D 101(12):123526. https://doi.org/10.1103/PhysRevD.101.123526. arXiv:1911.12658 [astro-ph.CO]

Jangra P, Kavanagh BJ, Diego JM (2023) Impact of dark matter spikes on the merger rates of Primordial Black Holes. JCAP 11:069. https://doi.org/10.1088/1475-7516/2023/11/069. arXiv:2304.05892 [astro-ph.CO]

Jaraba S, García-Bellido J (2021) Black hole induced spins from hyperbolic encounters in dense clusters. Phys Dark Univ 34:100882. https://doi.org/10.1016/j.dark.2021.100882. arXiv:2106.01436 [gr-qc]

Jedamzik K (1997) Primordial black hole formation during the QCD epoch. Phys Rev D 55:5871–5875. https://doi.org/10.1103/PhysRevD.55.R5871. arXiv:astro-ph/9605152

Jedamzik K (2020) Primordial black hole dark matter and the LIGO/Virgo observations. JCAP 09:022. https://doi.org/10.1088/1475-7516/2020/09/022. arXiv:2006.11172 [astro-ph.CO]
Jedamzik K (2021) Consistency of primordial black hole dark matter with LIGO/Virgo merger rates. Phys Rev Lett 126(5):051302. https://doi.org/10.1103/PhysRevLett.126.051302. arXiv:2007.03565 [astro-ph.CO]
Jedamzik K, Lemoine M, Martin J (2010) Collapse of small-scale density perturbations during preheating in single field inflation. JCAP 09:034. https://doi.org/10.1088/1475-7516/2010/09/034. arXiv:1002.3039 [astro-ph.CO]
Jedamzik K, Niemeyer JC (1999) Primordial black hole formation during first order phase transitions. Phys Rev D 59:124014. https://doi.org/10.1103/PhysRevD.59.124014. arXiv:astro-ph/9901293
Jedamzik K, Sigl G (2000) On metric preheating. Phys Rev D 61:023519. https://doi.org/10.1103/PhysRevD.61.023519. arXiv:hep-ph/9906287
Jenkins AC, O'Shaughnessy R, Sakellariadou M et al (2019a) Anisotropies in the astrophysical gravitational-wave background: the impact of black hole distributions. Phys Rev Lett 122 (11):111101. https://doi.org/10.1103/PhysRevLett.122.111101. arXiv:1810.13435 [astro-ph.CO]
Jenkins AC, Romano JD, Sakellariadou M (2019b) Estimating the angular power spectrum of the gravitational-wave background in the presence of shot noise. Phys Rev D 100(8):083501. https://doi.org/10.1103/PhysRevD.100.083501. arXiv:1907.06642 [astro-ph.CO]
Jenkins AC, Sakellariadou M (2018) Anisotropies in the stochastic gravitational-wave background: formalism and the cosmic string case. Phys Rev D 98(6):063509. https://doi.org/10.1103/PhysRevD.98.063509. arXiv:1802.06046 [astro-ph.CO]
Jenkins AC, Sakellariadou M (2019) Shot noise in the astrophysical gravitational-wave background. Phys Rev D 100(6):063508. https://doi.org/10.1103/PhysRevD.100.063508. arXiv:1902.07719 [astro-ph.CO]
Jenkins AC, Sakellariadou M, Regimbau T et al (2018) Anisotropies in the astrophysical gravitational-wave background: predictions for the detection of compact binaries by LIGO and Virgo. Phys Rev D 98(6):063501. https://doi.org/10.1103/PhysRevD.98.063501. arXiv:1806.01718 [astro-ph.CO]
Jenkins AC, Sakellariadou M (2020) Primordial black holes from cusp collapse on cosmic strings. arXiv e-prints arXiv:2006.16249 [astro-ph.CO]
Jeong D, Kamionkowski M (2012) Clustering fossils from the early universe. Phys Rev Lett 108 (25):251301. https://doi.org/10.1103/PhysRevLett.108.251301. arXiv:1203.0302 [astro-ph.CO]
Jin JH, Chen ZC, Yi Z et al (2023) Confronting sound speed resonance with pulsar timing arrays. JCAP 09:016. https://doi.org/10.1088/1475-7516/2023/09/016. arXiv:2307.08687 [astro-ph.CO]
Joana C (2022) Gravitational dynamics in Higgs inflation: preinflation and preheating with an auxiliary field. Phys Rev D 106(2):023504. https://doi.org/10.1103/PhysRevD.106.023504. arXiv:2202.07604 [astro-ph.CO]
Juan JI, Serpico PD, Franco Abellán G (2022) The QCD phase transition behind a PBH origin of LIGO/Virgo events? JCAP 07(07):009. https://doi.org/10.1088/1475-7516/2022/07/009. arXiv:2204.07027 [astro-ph.CO]
Jung TH, Okui T (2021) Primordial black holes from bubble collisions during a first-order phase transition. arXiv e-prints arXiv:2110.04271 [hep-ph]
Kadota K, Silk J (2021) Boosting small-scale structure via primordial black holes and implications for sub-GeV dark matter annihilation. Phys Rev D 103(4):043530. https://doi.org/10.1103/PhysRevD.103.043530. arXiv:2012.03698 [astro-ph.CO]
Kadota K, Tashiro H (2022) Primordial black hole dark matter in the presence of p-wave WIMP annihilation. JCAP 03(03):045. https://doi.org/10.1088/1475-7516/2022/03/045. arXiv:2112.04179 [astro-ph.CO]
Kalaja A, Bellomo N, Bartolo N et al (2019) From primordial black holes abundance to primordial curvature power spectrum (and back). JCAP 10:031. https://doi.org/10.1088/1475-7516/2019/10/031. arXiv:1908.03596 [astro-ph.CO]
Kallosh R, Linde A (2022) Dilaton-axion inflation with PBHs and GWs. JCAP 08(08):037. https://doi.org/10.1088/1475-7516/2022/08/037. arXiv:2203.10437 [hep-th]
Kamenshchik AY, Tronconi A, Vardanyan T et al (2019) Non-canonical inflation and primordial black holes production. Phys Lett B 791:201–205. https://doi.org/10.1016/j.physletb.2019.02.036. arXiv:1812.02547 [gr-qc]
Kannike K, Marzola L, Raidal M et al (2017) Single field double inflation and primordial black holes. JCAP 09:020. https://doi.org/10.1088/1475-7516/2017/09/020. arXiv:1705.06225 [astro-ph.CO]

Kapadia SJ, Lal Pandey K, Suyama T et al (2021) Search for the stochastic gravitational-wave background induced by primordial curvature perturbations in LIGO's second observing run. Astrophys J Lett 910 (1):L4. https://doi.org/10.3847/2041-8213/abe86e. arXiv:2009.05514 [gr-qc]

Kapadia SJ, Pandey KL, Suyama T et al (2020) Prospects for probing ultralight primordial black holes using the stochastic gravitational-wave background induced by primordial curvature perturbations. Phys Rev D 101(12):123535. https://doi.org/10.1103/PhysRevD.101.123535. arXiv:2005.05693 [astro-ph.CO]

Karam A, Koivunen N, Tomberg E et al (2023) Anatomy of single-field inflationary models for primordial black holes. JCAP 03:013. https://doi.org/10.1088/1475-7516/2023/03/013. arXiv:2205.13540 [astro-ph.CO]

Karnesis N et al (2024) The Laser Interferometer Space Antenna mission in Greece White Paper. Int J Mod Phys D 33(07n08):2450027. https://doi.org/10.1142/S0218271824500275. arXiv:2209.04358 [gr-qc]

Kashlinsky A (2016) LIGO gravitational wave detection, primordial black holes and the near-IR cosmic infrared background anisotropies. Astrophys J Lett 823(2):L25. https://doi.org/10.3847/2041-8205/823/2/L25. arXiv:1605.04023 [astro-ph.CO]

Kashlinsky A, Arendt RG, Atrio-Barandela F et al (2018) Looking at cosmic near-infrared background radiation anisotropies. Rev Mod Phys 90(2):025006. https://doi.org/10.1103/RevModPhys.90.025006. arXiv:1802.07774 [astro-ph.CO]

Kashlinsky A, Arendt RG, Mather J et al (2005) Tracing the first stars with fluctuations of the cosmic infrared background. Nature 438(7064):45–50. https://doi.org/10.1038/nature04143. arXiv:astro-ph/0511105 [astro-ph]

Kashlinsky A, et al (2019) Electromagnetic probes of primordial black holes as dark matter. arXiv e-prints arXiv:1903.04424 [astro-ph.CO]

Katz A, Kopp J, Sibiryakov S et al (2018) Femtolensing by dark matter revisited. JCAP 12:005. https://doi.org/10.1088/1475-7516/2018/12/005. arXiv:1807.11495 [astro-ph.CO]

Kavanagh BJ, Gaggero D, Bertone G (2018) Merger rate of a subdominant population of primordial black holes. Phys Rev D 98(2):023536. https://doi.org/10.1103/PhysRevD.98.023536. arXiv:1805.09034 [astro-ph.CO]

Kawai S, Kim J (2021) Primordial black holes from Gauss-Bonnet-corrected single field inflation. Phys Rev D 104(8):083545. https://doi.org/10.1103/PhysRevD.104.083545. arXiv:2108.01340 [astro-ph.CO]

Kawana K, Xie KP (2022) Primordial black holes from a cosmic phase transition: the collapse of Fermi-balls. Phys Lett B 824:136791. https://doi.org/10.1016/j.physletb.2021.136791. arXiv:2106.00111 [astro-ph.CO]

Kawasaki M, Kitajima N, Yanagida TT (2013) Primordial black hole formation from an axionlike curvaton model. Phys Rev D 87(6):063519. https://doi.org/10.1103/PhysRevD.87.063519. arXiv:1207.2550 [hep-ph]

Kawasaki M, Kohri K, Moroi T (2005a) Big-Bang nucleosynthesis and hadronic decay of long-lived massive particles. Phys Rev D 71:083502. https://doi.org/10.1103/PhysRevD.71.083502. arXiv:astro-ph/0408426

Kawasaki M, Kohri K, Moroi T (2005b) Hadronic decay of late-decaying particles and Big-Bang Nucleosynthesis. Phys Lett B 625:7–12. https://doi.org/10.1016/j.physletb.2005.08.045. arXiv:astro-ph/0402490

Kawasaki M, Kusenko A, Tada Y et al (2016) Primordial black holes as dark matter in supergravity inflation models. Phys Rev D 94(8):083523. https://doi.org/10.1103/PhysRevD.94.083523. arXiv:1606.07631 [astro-ph.CO]

Kawasaki M, Kusenko A, Yanagida TT (2012) Primordial seeds of supermassive black holes. Phys Lett B 711:1–5. https://doi.org/10.1016/j.physletb.2012.03.056. arXiv:1202.3848 [astro-ph.CO]

Kawasaki M, Nakatsuka H (2019) Effect of nonlinearity between density and curvature perturbations on the primordial black hole formation. Phys Rev D 99(12):123501. https://doi.org/10.1103/PhysRevD.99.123501. arXiv:1903.02994 [astro-ph.CO]

Kawasaki M, Nakatsuka H (2021) Gravitational waves from type II axion-like curvaton model and its implication for NANOGrav result. JCAP 05:023. https://doi.org/10.1088/1475-7516/2021/05/023. arXiv:2101.11244 [astro-ph.CO]

Kawasaki M, Sugiyama N, Yanagida T (1998) Primordial black hole formation in a double inflation model in supergravity. Phys Rev D 57:6050–6056. https://doi.org/10.1103/PhysRevD.57.6050. arXiv:hep-ph/9710259

Kehagias A, Musco I, Riotto A (2019) Non-gaussian formation of primordial black holes: effects on the threshold. JCAP 12:029. https://doi.org/10.1088/1475-7516/2019/12/029. arXiv:1906.07135 [astro-ph.CO]

Keith C, Hooper D, Blinov N et al (2020) Constraints on primordial black holes from big bang nucleosynthesis revisited. Phys Rev D 102(10):103512. https://doi.org/10.1103/PhysRevD.102.103512. arXiv:2006.03608 [astro-ph.CO]

Keith C, Hooper D, Linden T et al (2022) Sensitivity of future gamma-ray telescopes to primordial black holes. Phys Rev D 106(4):043003. https://doi.org/10.1103/PhysRevD.106.043003. arXiv:2204.05337 [astro-ph.HE]

Kelley LZ, Blecha L, Hernquist L (2017) Massive black hole binary mergers in dynamical galactic environments. Mon Not R Astron Soc 464(3):3131–3157. https://doi.org/10.1093/mnras/stw2452. arXiv:1606.01900 [astro-ph.HE]

Kelly PL et al (2018) Extreme magnification of an individual star at redshift 1.5 by a galaxy-cluster lens. Nat Astron 2(4):334–342. https://doi.org/10.1038/s41550-018-0430-3. arXiv:1706.10279 [astro-ph.GA]

Khlopov MY (2010) Primordial black holes. Res Astron Astrophys 10:495–528. https://doi.org/10.1088/1674-4527/10/6/001. arXiv:0801.0116 [astro-ph]

Khlopov M, Malomed BA, Zeldovich IB (1985) Gravitational instability of scalar fields and formation of primordial black holes. Mon Not R Astron Soc 215:575–589

Khlopov MY, Polnarev AG (1980) Primordial black holes as a cosmological test of grand unification. Phys Lett B 97:383–387. https://doi.org/10.1016/0370-2693(80)90624-3

Kim H (2021) A constraint on light primordial black holes from the interstellar medium temperature. Mon Not R Astron Soc 504(4):5475–5484. https://doi.org/10.1093/mnras/stab1222. arXiv:2007.07739 [hep-ph]

Kim HI, Lee CH (1996) Constraints on the spectral index from primordial black holes. Phys Rev D 54:6001–6007. https://doi.org/10.1103/PhysRevD.54.6001

Kim JE, Nilles HP, Peloso M (2005) Completing natural inflation. JCAP 01:005. https://doi.org/10.1088/1475-7516/2005/01/005. arXiv:hep-ph/0409138

King SF, Marfatia D, Rahat MH (2024) Toward distinguishing Dirac from Majorana neutrino mass with gravitational waves. Phys Rev D 109(3):035014. https://doi.org/10.1103/PhysRevD.109.035014. arXiv:2306.05389 [hep-ph]

Kinugawa T, Inayoshi K, Hotokezaka K et al (2014) Possible indirect confirmation of the existence of Pop III massive stars by gravitational wave. Mon Not R Astron Soc 442(4):2963–2992. https://doi.org/10.1093/mnras/stu1022. arXiv:1402.6672 [astro-ph.HE]

Kinugawa T, Miyamoto A, Kanda N et al (2016) The detection rate of inspiral and quasi-normal modes of Population III binary black holes which can confirm or refute the general relativity in the strong gravity region. Mon Not R Astron Soc 456(1):1093–1114. https://doi.org/10.1093/mnras/stv2624. arXiv:1505.06962 [astro-ph.SR]

Kinugawa T, Nakamura T, Nakano H (2020) Chirp mass and spin of binary black holes from first star remnants. Mon Not R Astron Soc 498(3):3946–3963. https://doi.org/10.1093/mnras/staa2511. arXiv:2005.09795 [astro-ph.HE]

Kitajima N, Lee J, Murai K et al (2024) Gravitational waves from domain wall collapse, and application to nanohertz signals with QCD-coupled axions. Phys Lett B 851:138586. https://doi.org/10.1016/j.physletb.2024.138586. arXiv:2306.17146 [hep-ph]

Kitajima N, Tada Y, Yokoyama S et al (2021) Primordial black holes in peak theory with a non-Gaussian tail. JCAP 10:053. https://doi.org/10.1088/1475-7516/2021/10/053. arXiv:2109.00791 [astro-ph.CO]

Klein A, et al (2022) The last three years: multiband gravitational-wave observations of stellar-mass binary black holes. arXiv e-prints arXiv:2204.03423 [astro-ph.HE]

Kocsis B, Gaspar ME, Marka S (2006) Detection rate estimates of gravity-waves emitted during parabolic encounters of stellar black holes in globular clusters. Astrophys J 648:411–429. https://doi.org/10.1086/505641. arXiv:astro-ph/0603441

Kocsis B, Sesana A (2011) Gas-driven massive black hole binaries: signatures in the nHz gravitational wave background. Mon Not R Astron Soc 411(3):1467–1479. https://doi.org/10.1111/j.1365-2966.2010.17782.x. arXiv:1002.0584 [astro-ph.CO]

Kocsis B, Suyama T, Tanaka T et al (2018) Hidden universality in the merger rate distribution in the primordial black hole scenario. Astrophys J 854(1):41. https://doi.org/10.3847/1538-4357/aaa7f4. arXiv:1709.09007 [astro-ph.CO]

Kofman L, Linde AD, Starobinsky AA (1994) Reheating after inflation. Phys Rev Lett 73:3195–3198. https://doi.org/10.1103/PhysRevLett.73.3195. arXiv:hep-th/9405187
Kofman L, Linde AD, Starobinsky AA (1997) Towards the theory of reheating after inflation. Phys Rev D 56:3258–3295. https://doi.org/10.1103/PhysRevD.56.3258. arXiv:hep-ph/9704452
Kohri K, Nakama T, Suyama T (2014) Testing scenarios of primordial black holes being the seeds of supermassive black holes by ultracompact minihalos and CMB μ-distortions. Phys Rev D 90 (8):083514. https://doi.org/10.1103/PhysRevD.90.083514. arXiv:1405.5999 [astro-ph.CO]
Kohri K, Terada T (2018) Semianalytic calculation of gravitational wave spectrum nonlinearly induced from primordial curvature perturbations. Phys Rev D 97(12):123532. https://doi.org/10.1103/PhysRevD.97.123532. arXiv:1804.08577 [gr-qc]
Kohri K, Terada T (2021) Solar-mass primordial black holes explain NANOGrav hint of gravitational waves. Phys Lett B 813:136040. https://doi.org/10.1016/j.physletb.2020.136040. arXiv:2009.11853 [astro-ph.CO]
Kohri K, Yokoyama J (2000) Primordial black holes and primordial nucleosynthesis. 1. Effects of hadron injection from low mass holes. Phys Rev D 61:023501. https://doi.org/10.1103/PhysRevD.61.023501. arXiv:astro-ph/9908160
Kokubu T, Kyutoku K, Kohri K et al (2018) Effect of inhomogeneity on primordial black hole formation in the matter dominated era. Phys Rev D 98(12):123024. https://doi.org/10.1103/PhysRevD.98.123024. arXiv:1810.03490 [astro-ph.CO]
Kolb EW, Tkachev II (1994) Large amplitude isothermal fluctuations and high density dark matter clumps. Phys Rev D 50:769–773. https://doi.org/10.1103/PhysRevD.50.769. arXiv:astro-ph/9403011
Kopp M, Hofmann S, Weller J (2011) Separate universes do not constrain primordial black hole formation. Phys Rev D 83:124025. https://doi.org/10.1103/PhysRevD.83.124025. arXiv:1012.4369 [astro-ph.CO]
Kotok E, Naselsky P (1998) Blue spectra and induced formation of primordial black holes. Phys Rev D 58:103517. https://doi.org/10.1103/PhysRevD.58.103517. arXiv:astro-ph/9806139
Kou XX, Tian C, Zhou SY (2021) Oscillon preheating in full general relativity. Class Quant Grav 38 (4):045005. https://doi.org/10.1088/1361-6382/abd09f. arXiv:1912.09658 [gr-qc]
Koushiappas SM, Loeb A (2017a) Dynamics of dwarf galaxies disfavor stellar-mass black holes as dark matter. Phys Rev Lett 119(4):041102. https://doi.org/10.1103/PhysRevLett.119.041102. arXiv:1704.01668 [astro-ph.GA]
Koushiappas SM, Loeb A (2017b) Maximum redshift of gravitational wave merger events. Phys Rev Lett 119(22):221104. https://doi.org/10.1103/PhysRevLett.119.221104. arXiv:1708.07380 [astro-ph.CO]
Kouvaris C, Tinyakov P, Tytgat MHG (2018) NonPrimordial solar mass black holes. Phys Rev Lett 121 (22):221102. https://doi.org/10.1103/PhysRevLett.121.221102. arXiv:1804.06740 [astro-ph.HE]
Kozaczuk J, Lin T, Villarama E (2022) Signals of primordial black holes at gravitational wave interferometers. Phys Rev D 105(12):123023. https://doi.org/10.1103/PhysRevD.105.123023. arXiv:2108.12475 [astro-ph.CO]
Kristiano J, Yokoyama J (2024a) Constraining primordial black hole formation from single-field inflation. Phys Rev Lett 132(22):221003. https://doi.org/10.1103/PhysRevLett.132.221003. arXiv:2211.03395 [hep-th]
Kristiano J, Yokoyama J (2024b) Note on the bispectrum and one-loop corrections in single-field inflation with primordial black hole formation. Phys Rev D 109(10):103541. https://doi.org/10.1103/PhysRevD.109.103541. arXiv:2303.00341 [hep-th]
Kritos K, De Luca V, Franciolini G et al (2021) The astro-primordial black hole merger rates: a reappraisal. JCAP 05:039. https://doi.org/10.1088/1475-7516/2021/05/039. arXiv:2012.03585 [gr-qc]
Kuhnel F, Matas A, Starkman GD et al (2020) Waves from the centre: probing PBH and other macroscopic dark matter with LISA. Eur Phys J C 80(7):627. https://doi.org/10.1140/epjc/s10052-020-8183-4. arXiv:1811.06387 [gr-qc]
Labbé I, van Dokkum P, Nelson E et al (2023) A population of red candidate massive galaxies 600 myr after the big bang. Nature 616(7956):266–269. https://doi.org/10.1038/s41586-023-05786-2. arXiv:2207.12446 [astro-ph.GA]
Laguna P, Larson SL, Spergel D et al (2010) Integrated Sachs-Wolfe effect for gravitational radiation. Astrophys J Lett 715:L12. https://doi.org/10.1088/2041-8205/715/1/L12. arXiv:0905.1908 [gr-qc]
Laha R (2019) Primordial black holes as a dark matter candidate are severely constrained by the galactic center 511 keV γ -ray line. Phys Rev Lett 123(25):251101. https://doi.org/10.1103/PhysRevLett.123.251101. arXiv:1906.09994 [astro-ph.HE]

Laha R, Lu P, Takhistov V (2021) Gas heating from spinning and non-spinning evaporating primordial black holes. Phys Lett B 820:136459. https://doi.org/10.1016/j.physletb.2021.136459. arXiv:2009.11837 [astro-ph.CO]

Laha R, Muñoz JB, Slatyer TR (2020) INTEGRAL constraints on primordial black holes and particle dark matter. Phys Rev D 101(12):123514. https://doi.org/10.1103/PhysRevD.101.123514. arXiv:2004.00627 [astro-ph.CO]

Lazarides G, Maji R, Shafi Q (2023) Superheavy quasistable strings and walls bounded by strings in the light of NANOGrav 15 year data. Phys Rev D 108(9):095041. https://doi.org/10.1103/PhysRevD.108.095041. arXiv:2306.17788 [hep-ph]

Lewicki M, Toczek P, Vaskonen V (2023) Primordial black holes from strong first-order phase transitions. JHEP 09:092. https://doi.org/10.1007/JHEP09(2023)092. arXiv:2305.04924 [astro-ph.CO]

Li TS et al (2017) Farthest neighbor: The distant Milky Way satellite Eridanus II. Astrophys J 838(1):8. https://doi.org/10.3847/1538-4357/aa6113. arXiv:1611.05052 [astro-ph.GA]

Li T, Liao J (2022) Electron-target experiment constraints on light dark matter produced in primordial black hole evaporation. Phys Rev D 106(5):055043. https://doi.org/10.1103/PhysRevD.106.055043. arXiv:2203.14443 [hep-ph]

Li SL, Shao L, Wu P et al (2021) NANOGrav signal from first-order confinement-deconfinement phase transition in different QCD-matter scenarios. Phys Rev D 104(4):043510. https://doi.org/10.1103/PhysRevD.104.043510. arXiv:2101.08012 [astro-ph.CO]

Libanore S, Artale MC, Karagiannis D et al (2022) Clustering of gravitational wave and supernovae events: a multitracer analysis in luminosity distance space. JCAP 02(02):003. https://doi.org/10.1088/1475-7516/2022/02/003. arXiv:2109.10857 [astro-ph.CO]

Libanore S, Liguori M, Raccanelli A (2023) Signatures of primordial black holes in gravitational wave clustering. JCAP 08:055. https://doi.org/10.1088/1475-7516/2023/08/055. arXiv:2306.03087 [astro-ph.CO]

Lin J, Gao Q, Gong Y et al (2020) Primordial black holes and secondary gravitational waves from k and G inflation. Phys Rev D 101(10):103515. https://doi.org/10.1103/PhysRevD.101.103515. arXiv:2001.05909 [gr-qc]

Lin J, Gao S, Gong Y et al (2023) Primordial black holes and scalar induced gravitational waves from Higgs inflation with noncanonical kinetic term. Phys Rev D 107(4):043517. https://doi.org/10.1103/PhysRevD.107.043517. arXiv:2111.01362 [gr-qc]

Linde AD (1994) Hybrid inflation. Phys Rev D 49:748–754. https://doi.org/10.1103/PhysRevD.49.748. arXiv:astro-ph/9307002

Linde A, Mooij S, Pajer E (2013) Gauge field production in supergravity inflation: local non-gaussianity and primordial black holes. Phys Rev D 87(10):103506. https://doi.org/10.1103/PhysRevD.87.103506. arXiv:1212.1693 [hep-th]

Linde AD, Westphal A (2008) Accidental inflation in string theory. JCAP 03:005. https://doi.org/10.1088/1475-7516/2008/03/005. arXiv:0712.1610 [hep-th]

Liu J, Bian L, Cai RG et al (2022) Primordial black hole production during first-order phase transitions. Phys Rev D 105(2):L021303. https://doi.org/10.1103/PhysRevD.105.L021303. arXiv:2106.05637 [astro-ph.CO]

Liu B, Bromm V (2020a) Gravitational waves from Population III binary black holes formed by dynamical capture. Mon Not R Astron Soc 495(2):2475–2495. https://doi.org/10.1093/mnras/staa1362. arXiv:2003.00065 [astro-ph.CO]

Liu B, Bromm V (2020b) The population III origin of GW190521. Astrophys J Lett 903(2):L40. https://doi.org/10.3847/2041-8213/abc552. arXiv:2009.11447 [astro-ph.GA]

Liu B, Bromm V (2022) Accelerating early massive galaxy formation with primordial black holes. Astrophys J Lett 937(2):L30. https://doi.org/10.3847/2041-8213/ac927f. arXiv:2208.13178 [astro-ph.CO]

Liu L, Chen ZC, Huang QG (2024) Implications for the non-Gaussianity of curvature perturbation from pulsar timing arrays. Phys Rev D 109(6):L061301. https://doi.org/10.1103/PhysRevD.109.L061301. arXiv:2307.01102 [astro-ph.CO]

Liu J, Guo ZK, Cai RG (2020) Primordial black holes from cosmic domain walls. Phys Rev D 101(2):023513. https://doi.org/10.1103/PhysRevD.101.023513. arXiv:1908.02662 [astro-ph.CO]

Lovell CC, Harrison I, Harikane Y et al (2022) Extreme value statistics of the halo and stellar mass distributions at high redshift: are JWST results in tension with ΛCDM? Mon Not R Astron Soc 518(2):2511–2520. https://doi.org/10.1093/mnras/stac3224. arXiv:2208.10479 [astro-ph.GA]

Lu Y, Ali A, Gong Y et al (2020) Gauge transformation of scalar induced gravitational waves. Phys Rev D 102(8):083503. https://doi.org/10.1103/PhysRevD.102.083503(2020). arXiv:2006.03450 [gr-qc]
Lu P, Takhistov V, Gelmini GB et al (2021) Constraining primordial black holes with dwarf galaxy heating. Astrophys J Lett 908(2):L23. https://doi.org/10.3847/2041-8213/abdcb6. arXiv:2007.02213 [astro-ph.CO]
Lucca M, Schöneberg N, Hooper DC et al (2020) The synergy between CMB spectral distortions and anisotropies. JCAP 02:026. https://doi.org/10.1088/1475-7516/2020/02/026. arXiv:1910.04619 [astro-ph.CO]
Luo Y, Hanasoge S, Tromp J et al (2012) Detectable seismic consequences of the interaction of a primordial black hole with Earth. Astrophys J 751:16. https://doi.org/10.1088/0004-637X/751/1/16. arXiv:1203.3806 [astro-ph.CO]
Lyth DH (2012) The hybrid inflation waterfall and the primordial curvature perturbation. JCAP 05:022. https://doi.org/10.1088/1475-7516/2012/05/022. arXiv:1201.4312 [astro-ph.CO]
Lyth DH, Malik KA, Sasaki M (2005) A general proof of the conservation of the curvature perturbation. JCAP 05:004. https://doi.org/10.1088/1475-7516/2005/05/004. arXiv:astro-ph/0411220
Lyth DH, Riotto A (1999) Particle physics models of inflation and the cosmological density perturbation. Phys Rept 314:1–146. https://doi.org/10.1016/S0370-1573(98)00128-8. arXiv:hep-ph/9807278
Lyth DH, Wands D (2002) Generating the curvature perturbation without an inflaton. Phys Lett B 524:5–14. https://doi.org/10.1016/S0370-2693(01)01366-1. arXiv:hep-ph/0110002
López-Coto R, Doro M, de Angelis A et al (2021) Prospects for the observation of Primordial Black Hole evaporation with the Southern Wide field of view Gamma-ray Observatory. JCAP 08:040. https://doi.org/10.1088/1475-7516/2021/08/040. arXiv:2103.16895 [astro-ph.HE]
MacGibbon JH, Brandenberger RH, Wichoski UF (1998) Limits on black hole formation from cosmic string loops. Phys Rev D 57:2158–2165. https://doi.org/10.1103/PhysRevD.57.2158. arXiv:astro-ph/9707146
Mack KJ, Ostriker JP, Ricotti M (2007) Growth of structure seeded by primordial black holes. Astrophys J 665:1277–1287. https://doi.org/10.1086/518998. arXiv:astro-ph/0608642
Madge E, Morgante E, Puchades-Ibáñez C et al (2023) Primordial gravitational waves in the nano-Hertz regime and PTA data–towards solving the GW inverse problem. JHEP 10:171. https://doi.org/10.1007/JHEP10(2023)171. arXiv:2306.14856 [hep-ph]
Maeso DN, Marzola L, Raidal M et al (2022) Primordial black holes from spectator field bubbles. JCAP 02 (02):017. https://doi.org/10.1088/1475-7516/2022/02/017. arXiv:2112.01505 [astro-ph.CO]
Maggiore M (2000) Gravitational wave experiments and early universe cosmology. Phys Rept 331:283–367. https://doi.org/10.1016/S0370-1573(99)00102-7. arXiv:gr-qc/9909001
Maggiore M et al (2020) Science case for the einstein telescope. JCAP 03:050. https://doi.org/10.1088/1475-7516/2020/03/050. arXiv:1912.02622 [astro-ph.CO]
Maggiore M (2008) Gravitational Waves: Volume 1: Theory and Experiments. Gravitational Waves, OUP Oxford
Maldacena J (2021) Comments on magnetic black holes. JHEP 04:079. https://doi.org/10.1007/JHEP04(2021)079. arXiv:2004.06084 [hep-th]
Mandic V, Bird S, Cholis I (2016) Stochastic gravitational-wave background due to primordial binary black hole mergers. Phys Rev Lett 117(20):201102. https://doi.org/10.1103/PhysRevLett.117.201102. arXiv:1608.06699 [astro-ph.CO]
Manshanden J, Gaggero D, Bertone G et al (2019) Multi-wavelength astronomical searches for primordial black holes. JCAP 06:026. https://doi.org/10.1088/1475-7516/2019/06/026. arXiv:1812.07967 [astro-ph.HE]
Margalit A, Contaldi CR, Pieroni M (2020) Phase decoherence of gravitational wave backgrounds. Phys Rev D 102(8):083506. https://doi.org/10.1103/PhysRevD.102.083506. arXiv:2004.01727 [astro-ph.CO]
Martin J, Papanikolaou T, Pinol L et al (2020a) Metric preheating and radiative decay in single-field inflation. JCAP 05:003. https://doi.org/10.1088/1475-7516/2020/05/003. arXiv:2002.01820 [astro-ph.CO]
Martin J, Papanikolaou T, Vennin V (2020b) Primordial black holes from the preheating instability in single-field inflation. JCAP 01:024. https://doi.org/10.1088/1475-7516/2020/01/024. arXiv:1907.04236 [astro-ph.CO]
Martinelli M, Scarcella F, Hogg NB et al (2022) Dancing in the dark: detecting a population of distant primordial black holes. JCAP 08(08):006. https://doi.org/10.1088/1475-7516/2022/08/006. arXiv:2205.02639 [astro-ph.CO]

Matarrese S, Pantano O, Saez D (1994) General relativistic dynamics of irrotational dust: cosmological implications. Phys Rev Lett 72:320–323. https://doi.org/10.1103/PhysRevLett.72.320. arXiv:astro-ph/9310036

Matsubara T, Sasaki M (2022) Non-Gaussianity effects on the primordial black hole abundance for sharply-peaked primordial spectrum. JCAP 10:094. https://doi.org/10.1088/1475-7516/2022/10/094. arXiv:2208.02941 [astro-ph.CO]

Mavromatos NE, Spanos VC, Stamou ID (2022) Primordial black holes and gravitational waves in multiaxion-Chern-Simons inflation. Phys Rev D 106(6):063532. https://doi.org/10.1103/PhysRevD.106.063532. arXiv:2206.07963 [hep-th]

McClelland J, Silk J (1977) The correlation function for density perturbations in an expanding universe. II. Nonlinear theory. Astrophys J 217:331–352. https://doi.org/10.1086/155583

Mena O, Palomares-Ruiz S, Villanueva-Domingo P et al (2019) Constraining the primordial black hole abundance with 21 cm cosmology. Phys Rev D 100(4):043540. https://doi.org/10.1103/PhysRevD.100.043540. arXiv:1906.07735 [astro-ph.CO]

Menci N, Castellano M, Santini P et al (2022) High-redshift galaxies from early JWST observations: constraints on dark energy models. Astrophys J Lett 938(1):L5. https://doi.org/10.3847/2041-8213/ac96e9. arXiv:2208.11471 [astro-ph.CO]

Meng DS, Yuan C, Huang Qg (2022) One-loop correction to the enhanced curvature perturbation with local-type non-Gaussianity for the formation of primordial black holes. Phys Rev D 106(6):063508. https://doi.org/10.1103/PhysRevD.106.063508. arXiv:2207.07668 [astro-ph.CO]

Miller AL, Aggarwal N, Clesse S et al (2022) Constraints on planetary and asteroid-mass primordial black holes from continuous gravitational-wave searches. Phys Rev D 105(6):062008. https://doi.org/10.1103/PhysRevD.105.062008. arXiv:2110.06188 [gr-qc]

Miller AL, Clesse S, De Lillo F et al (2021) Probing planetary-mass primordial black holes with continuous gravitational waves. Phys Dark Univ 32:100836. https://doi.org/10.1016/j.dark.2021.100836. arXiv:2012.12983 [astro-ph.HE]

Mirbabayi M, Gruzinov A, Noreña J (2020) Spin of primordial black holes. JCAP 03:017. https://doi.org/10.1088/1475-7516/2020/03/017. arXiv:1901.05963 [astro-ph.CO]

Misner CW, Thorne K, Wheeler J (1973) Gravitation. W. H. Freeman, San Francisco

Mittal S, Ray A, Kulkarni G et al (2022) Constraining primordial black holes as dark matter using the global 21 cm signal with X-ray heating and excess radio background. JCAP 03:030. https://doi.org/10.1088/1475-7516/2022/03/030. arXiv:2107.02190 [astro-ph.CO]

Miyama S, Sato K (1978) An upper bound on the number density of primordial black holes from the big bang nucleosynthesis. Prog Theor Phys 59(3):1012–1013. https://doi.org/10.1143/PTP.59.1012

Mocz P et al (2020) Galaxy formation with BECDM - II. Cosmic filaments and first galaxies. Mon Not R Astron Soc 494(2):2027–2044. https://doi.org/10.1093/mnras/staa738. arXiv:1911.05746 [astro-ph.CO]

Mollerach S, Harari D, Matarrese S (2004) CMB polarization from secondary vector and tensor modes. Phys Rev D 69:063002. https://doi.org/10.1103/PhysRevD.69.063002. arXiv:astro-ph/0310711

Monroy-Rodríguez MA, Allen C (2014) The end of the MACHO era, revisited: new limits on MACHO masses from halo wide binaries. Astrophys J 790(2):159. https://doi.org/10.1088/0004-637X/790/2/159. arXiv:1406.5169 [astro-ph.GA]

Montanari F, García-Bellido J (2022) Mass classification of dark matter perturbers of stellar tidal streams. Phys Dark Univ 35:100978. https://doi.org/10.1016/j.dark.2022.100978. arXiv:2012.11482 [astro-ph.GA]

Montero-Camacho P, Fang X, Vasquez G et al (2019) Revisiting constraints on asteroid-mass primordial black holes as dark matter candidates. JCAP 08:031. https://doi.org/10.1088/1475-7516/2019/08/031. arXiv:1906.05950 [astro-ph.CO]

Moore C, Cole R, Berry C (2015) Gravitational-wave sensitivity curves. Class Quant Grav 32(1):015014. https://doi.org/10.1088/0264-9381/32/1/015014. arXiv:1408.0740 [gr-qc]

Moradinezhad Dizgah A, Franciolini G, Riotto A (2019) Primordial black holes from broad spectra: abundance and clustering. JCAP 11:001. https://doi.org/10.1088/1475-7516/2019/11/001. arXiv:1906.08978 [astro-ph.CO]

Moroi T, Takahashi T (2001) Effects of cosmological moduli fields on cosmic microwave background. Phys Lett B 522:215–221. https://doi.org/10.1016/S0370-2693(01)01295-3. [Erratum: Phys. Lett. B 539, 303-303 (2002)] arXiv:hep-ph/0110096

Morras G et al (2023) Analysis of a subsolar-mass compact binary candidate from the second observing run of Advanced LIGO. Phys Dark Univ 42:101285. https://doi.org/10.1016/j.dark.2023.101285. arXiv:2301.11619 [gr-qc]

Morscher M, Pattabiraman B, Rodriguez C et al (2015) The dynamical evolution of stellar black holes in globular clusters. Astrophys J 800(1):9. https://doi.org/10.1088/0004-637X/800/1/9. arXiv:1409.0866 [astro-ph.GA]

Motohashi H, Hu W (2017) Primordial black holes and slow-roll violation. Phys Rev D 96(6):063503. https://doi.org/10.1103/PhysRevD.96.063503. arXiv:1706.06784 [astro-ph.CO]

Mróz P et al (2024a) Microlensing optical depth and event rate toward the large magellanic cloud based on 20 yr of OGLE observations. Astrophys J Suppl 273(1):4. https://doi.org/10.3847/1538-4365/ad452e. arXiv:2403.02398 [astro-ph.GA]

Mróz P et al (2024b) No massive black holes in the Milky Way halo. Nature 632(8026):749–751. https://doi.org/10.1038/s41586-024-07704-6. arXiv:2403.02386 [astro-ph.GA]

Mukherjee S, Mitra S, Chatterjee S (2021) Gravitational Wave observatories may be able to detect hyperbolic encounters of Black Holes. Mon Not R Astron Soc 508:5064–5073. https://doi.org/10.1093/mnras/stab2721. arXiv:2010.00916 [gr-qc]

Mukherjee S, Silk J (2020) Time-dependence of the astrophysical stochastic gravitational wave background. Mon Not R Astron Soc 491(4):4690–4701. https://doi.org/10.1093/mnras/stz3226. arXiv:1912.07657 [gr-qc]

Mukherjee S, Silk J (2021) Can we distinguish astrophysical from primordial black holes via the stochastic gravitational wave background? Mon Not R Astron Soc 506(3):3977–3985. https://doi.org/10.1093/mnras/stab1932. arXiv:2105.11139 [gr-qc]

Murai K, Yin W (2023) A novel probe of supersymmetry in light of nanohertz gravitational waves. JHEP 10:062. https://doi.org/10.1007/JHEP10(2023)062. arXiv:2307.00628 [hep-ph]

Murgia R, Scelfo G, Viel M et al (2019) Lyman-α forest constraints on primordial black holes as dark matter. Phys Rev Lett 123(7):071102. https://doi.org/10.1103/PhysRevLett.123.071102. arXiv:1903.10509 [astro-ph.CO]

Musco I (2019) Threshold for primordial black holes: dependence on the shape of the cosmological perturbations. Phys Rev D 100(12):123524. https://doi.org/10.1103/PhysRevD.100.123524. arXiv:1809.02127 [gr-qc]

Musco I, Jedamzik K, Young S (2024) Primordial black hole formation during the QCD phase transition: threshold, mass distribution, and abundance. Phys Rev D 109(8):083506. https://doi.org/10.1103/PhysRevD.109.083506. arXiv:2303.07980 [astro-ph.CO]

Musco I, De Luca V, Franciolini G et al (2021) Threshold for primordial black holes. II. A simple analytic prescription. Phys Rev D 103(6):063538. https://doi.org/10.1103/PhysRevD.103.063538. arXiv:2011.03014 [astro-ph.CO]

Musco I, Miller JC (2013) Primordial black hole formation in the early universe: critical behaviour and self-similarity. Class Quant Grav 30:145009. https://doi.org/10.1088/0264-9381/30/14/145009. arXiv:1201.2379 [gr-qc]

Musco I, Miller JC, Polnarev AG (2009) Primordial black hole formation in the radiative era: investigation of the critical nature of the collapse. Class Quant Grav 26:235001. https://doi.org/10.1088/0264-9381/26/23/235001. arXiv:0811.1452 [gr-qc]

Musco I, Miller JC, Rezzolla L (2005) Computations of primordial black hole formation. Class Quant Grav 22:1405–1424. https://doi.org/10.1088/0264-9381/22/7/013. arXiv:gr-qc/0412063

Musco I, Papanikolaou T (2022) Primordial black hole formation for an anisotropic perfect fluid: initial conditions and estimation of the threshold. Phys Rev D 106(8):083017. https://doi.org/10.1103/PhysRevD.106.083017. arXiv:2110.05982 [gr-qc]

Naidu RP, Oesch PA, Setton DJ, et al (2022) Schrodinger's galaxy candidate: puzzlingly luminous at $z \approx 17$, or dusty/quenched at $z \approx 5$? arXiv e-prints arXiv:2208.02794 [astro-ph.GA]

Nakai Y, Suzuki M, Takahashi F et al (2021) Gravitational waves and dark radiation from dark phase transition: connecting NANOGrav pulsar timing data and hubble tension. Phys Lett B 816:136238. https://doi.org/10.1016/j.physletb.2021.136238. arXiv:2009.09754 [astro-ph.CO]

Nakama T, Carr B, Silk J (2018) Limits on primordial black holes from μ distortions in cosmic microwave background. Phys Rev D 97(4):043525. https://doi.org/10.1103/PhysRevD.97.043525. arXiv:1710.06945 [astro-ph.CO]

Nakama T, Kohri K, Silk J (2019) Ultracompact minihalos associated with stellar-mass primordial black holes. Phys Rev D 99(12):123530. https://doi.org/10.1103/PhysRevD.99.123530. arXiv:1905.04477 [astro-ph.CO]

Nakama T, Silk J, Kamionkowski M (2017) Stochastic gravitational waves associated with the formation of primordial black holes. Phys Rev D 95(4):043511. https://doi.org/10.1103/PhysRevD.95.043511. arXiv:1612.06264 [astro-ph.CO]

Nakama T, Suyama T, Yokoyama J (2016) Supermassive black holes formed by direct collapse of inflationary perturbations. Phys Rev D 94(10):103522. https://doi.org/10.1103/PhysRevD.94.103522. arXiv:1609.02245 [gr-qc]

Nakamura T et al (2016) Pre-DECIGO can get the smoking gun to decide the astrophysical or cosmological origin of GW150914-like binary black holes. PTEP 9:093E01. https://doi.org/10.1093/ptep/ptw127. arXiv:1607.00897 [astro-ph.HE]

Namba R, Peloso M, Shiraishi M et al (2016) Scale-dependent gravitational waves from a rolling axion. JCAP 01:041. https://doi.org/10.1088/1475-7516/2016/01/041. arXiv:1509.07521 [astro-ph.CO]

Namba R, Suzuki M (2020) Implications of gravitational-wave production from dark photon resonance to pulsar-timing observations and effective number of relativistic species. Phys Rev D 102:123527. https://doi.org/10.1103/PhysRevD.102.123527. arXiv:2009.13909 [astro-ph.CO]

Namigata T, Horowitz CJ, Widmer-Schnidrig R (2022) Gravitational search for near Earth black holes or other compact dark objects. arXiv e-prints arXiv:2201.06511 [gr-qc]

Nanopoulos DV, Spanos VC, Stamou ID (2020) Primordial black holes from no-scale supergravity. Phys Rev D 102(8):083536. https://doi.org/10.1103/PhysRevD.102.083536. arXiv:2008.01457 [astro-ph.CO]

Narayan R, Yi I (1995) Advection dominated accretion: underfed black holes and neutron stars. Astrophys J 452:710. https://doi.org/10.1086/176343. arXiv:astro-ph/9411059

Natwariya PK, Nayak AC, Srivastava T (2021) Constraining spinning primordial black holes with global 21 cm signal. Mon Not R Astron Soc 510:4236. https://doi.org/10.1093/mnras/stab3754. arXiv:2107.12358 [astro-ph.CO]

Nayak B, Singh LP (2012) Brans-dicke theory and primordial black holes in early matter-dominated era. Int J Theor Phys 51:1386–1395. https://doi.org/10.1007/s10773-011-1014-5. arXiv:0905.3657 [gr-qc]

Neilsen DW, Choptuik MW (2000) Critical phenomena in perfect fluids. Class Quant Grav 17:761–782. https://doi.org/10.1088/0264-9381/17/4/303. arXiv:gr-qc/9812053

Nelson PE, Etienne ZB, McWilliams ST et al (2019) Induced spins from scattering experiments of initially nonspinning black holes. Phys Rev D 100(12):124045. https://doi.org/10.1103/PhysRevD.100.124045. arXiv:1909.08621 [gr-qc]

Nesseris S, Sapone D, Sypsas S (2020) Evaporating primordial black holes as varying dark energy. Phys Dark Univ 27:100413. https://doi.org/10.1016/j.dark.2019.100413. arXiv:1907.05608 [astro-ph.CO]

Ng KKY et al (2023) Measuring properties of primordial black hole mergers at cosmological distances: effect of higher order modes in gravitational waves. Phys Rev D 107(2):024041. https://doi.org/10.1103/PhysRevD.107.024041. arXiv:2210.03132 [astro-ph.CO]

Ng KKY, Chen S, Goncharov B et al (2022a) On the single-event-based identification of primordial black hole mergers at cosmological distances. Astrophys J Lett 931(1):L12. https://doi.org/10.3847/2041-8213/ac6bea. arXiv:2108.07276 [astro-ph.CO]

Ng KKY, Franciolini G, Berti E et al (2022b) Constraining high-redshift stellar-mass primordial black holes with next-generation ground-based gravitational-wave detectors. Astrophys J Lett 933(2):L41. https://doi.org/10.3847/2041-8213/ac7aae. arXiv:2204.11864 [astro-ph.CO]

Ng KW, Wu YP (2021) Constant-rate inflation: primordial black holes from conformal weight transitions. JHEP 11:076. https://doi.org/10.1007/JHEP11(2021)076. arXiv:2102.05620 [astro-ph.CO]

Niemeyer JC, Jedamzik K (1998) Near-critical gravitational collapse and the initial mass function of primordial black holes. Phys Rev Lett 80:5481–5484. https://doi.org/10.1103/PhysRevLett.80.5481. arXiv:astro-ph/9709072

Niikura H et al (2019b) Microlensing constraints on primordial black holes with Subaru/HSC Andromeda observations. Nat Astron 3(6):524–534. https://doi.org/10.1038/s41550-019-0723-1. arXiv:1701.02151 [astro-ph.CO]

Niikura H, Takada M, Yokoyama S et al (2019a) Constraints on Earth-mass primordial black holes from OGLE 5-year microlensing events. Phys Rev D 99(8):083503. https://doi.org/10.1103/PhysRevD.99.083503. arXiv:1901.07120 [astro-ph.CO]

Nitz AH, Wang YF (2021a) Search for gravitational waves from high-mass-ratio compact-binary mergers of stellar mass and subsolar mass black holes. Phys Rev Lett 126(2):021103. https://doi.org/10.1103/PhysRevLett.126.021103. arXiv:2007.03583 [astro-ph.HE]

Nitz AH, Wang YF (2021b) Search for gravitational waves from the coalescence of subsolar-mass binaries in the first half of advanced LIGO and Virgo's third observing run. Phys Rev Lett 127(15):151101. https://doi.org/10.1103/PhysRevLett.127.151101. arXiv:2106.08979 [astro-ph.HE]

Nitz AH, Wang YF (2022) Broad search for gravitational waves from subsolar-mass binaries through LIGO and Virgo's third observing run. Phys Rev D 106(2):023024. https://doi.org/10.1103/PhysRevD.106.023024. arXiv:2202.11024 [astro-ph.HE]

Novikov ID, Polnarev AG (1978) The hydrodynamics of primordial black hole formation. Soviet Astron 22:129–138

Novikov ID, Polnarev AG (1980) The hydrodynamics of primordial black hole formation: dependence on the equation of state. Soviet Astron 24:147–151

Novikov I, Thorne K (1973) Astrophysics of black holes. In: DeWitt C, DeWitt B (eds) Black holes / Les astres occlus (Les Houches 1972). Gordon and Breach, pp 343–550

Nurmi S, Schiappacasse ED, Yanagida TT (2021) Radio signatures from encounters between neutron stars and QCD-axion minihalos around primordial black holes. JCAP 09:004. https://doi.org/10.1088/1475-7516/2021/09/004. arXiv:2102.05680 [hep-ph]

Oguri M (2016) Measuring the distance-redshift relation with the cross-correlation of gravitational wave standard sirens and galaxies. Phys Rev D 93(8):083511. https://doi.org/10.1103/PhysRevD.93.083511. arXiv:1603.02356 [astro-ph.CO]

Oguri M, Diego JM, Kaiser N et al (2018) Understanding caustic crossings in giant arcs: characteristic scales, event rates, and constraints on compact dark matter. Phys Rev D 97(2):023518. https://doi.org/10.1103/PhysRevD.97.023518. arXiv:1710.00148 [astro-ph.CO]

Oguri M, Takhistov V, Kohri K (2023) Revealing dark matter dress of primordial black holes by cosmological lensing. Phys Lett B 847:138276. https://doi.org/10.1016/j.physletb.2023.138276. arXiv:2208.05957 [astro-ph.CO]

Oh S, Haiman Z (2003) Fossil HII regions: self-limiting star formation at high redshift. Mon Not R Astron Soc 346:456. https://doi.org/10.1046/j.1365-2966.2003.07103.x. arXiv:astro-ph/0307135

Oncins M, Miralda-Escudé J, Gutiérrez JL et al (2022) Primordial black holes capture by stars and induced collapse to low-mass stellar black holes. Mon Not R Astron Soc 517(1):28–37. https://doi.org/10.1093/mnras/stac2647. arXiv:2205.13003 [astro-ph.GA]

O'Leary RM, Kocsis B, Loeb A (2009) Gravitational waves from scattering of stellar-mass black holes in galactic nuclei. Mon Not R Astron Soc 395(4):2127–2146. https://doi.org/10.1111/j.1365-2966.2009.14653.x. arXiv:0807.2638 [astro-ph]

Özsoy O (2021) Synthetic gravitational waves from a rolling axion monodromy. JCAP 04:040. https://doi.org/10.1088/1475-7516/2021/04/040. arXiv:2005.10280 [astro-ph.CO]

Özsoy O, Lalak Z (2021) Primordial black holes as dark matter and gravitational waves from bumpy axion inflation. JCAP 01:040. https://doi.org/10.1088/1475-7516/2021/01/040. arXiv:2008.07549 [astro-ph.CO]

Özsoy O, Parameswaran S, Tasinato G et al (2018) Mechanisms for primordial black hole production in string theory. JCAP 07:005. https://doi.org/10.1088/1475-7516/2018/07/005. arXiv:1803.07626 [hep-th]

Özsoy O, Tasinato G (2020) On the slope of the curvature power spectrum in non-attractor inflation. JCAP 04:048. https://doi.org/10.1088/1475-7516/2020/04/048. arXiv:1912.01061 [astro-ph.CO]

Özsoy O, Tasinato G (2023) Inflation and primordial black holes. Universe 9(5):203. https://doi.org/10.3390/universe9050203. arXiv:2301.03600 [astro-ph.CO]

Paczynski B (1986) Gravitational microlensing by the galactic halo. Astrophys J 304:1–5. https://doi.org/10.1086/164140

Padilla ND, Magaña J, Sureda J et al (2021) Power spectrum of density fluctuations, halo abundances, and clustering with primordial black holes. Mon Not R Astron Soc 504(3):3139–3155. https://doi.org/10.1093/mnras/stab1115. arXiv:2010.06470 [astro-ph.CO]

Palma GA, Sypsas S, Zenteno C (2020) Seeding primordial black holes in multifield inflation. Phys Rev Lett 125(12):121301. https://doi.org/10.1103/PhysRevLett.125.121301. arXiv:2004.06106 [astro-ph.CO]

Pani P, Loeb A (2013) Constraining primordial black-hole bombs through spectral distortions of the cosmic microwave background. Phys Rev D 88:041301. https://doi.org/10.1103/PhysRevD.88.041301. arXiv:1307.5176 [astro-ph.CO]

Pani P, Loeb A (2014) Tidal capture of a primordial black hole by a neutron star: implications for constraints on dark matter. JCAP 06:026. https://doi.org/10.1088/1475-7516/2014/06/026. arXiv:1401.3025 [astro-ph.CO]

Papanikolaou T (2022a) Gravitational waves induced from primordial black hole fluctuations: the effect of an extended mass function. JCAP 10:089. https://doi.org/10.1088/1475-7516/2022/10/089. arXiv:2207.11041 [astro-ph.CO]

Papanikolaou T (2022b) Toward the primordial black hole formation threshold in a time-dependent equation-of-state background. Phys Rev D 105(12):124055. https://doi.org/10.1103/PhysRevD.105.124055. arXiv:2205.07748 [gr-qc]

Papanikolaou T (2023a) Primordial black holes in loop quantum cosmology: the effect on the threshold. Class Quant Grav 40(13):134001. https://doi.org/10.1088/1361-6382/acd97d. arXiv:2301.11439 [gr-qc]

Papanikolaou T, Banerjee S, Cai YF et al (2024a) Primordial black holes and induced gravitational waves in non-singular matter bouncing cosmology. JCAP 06:066. https://doi.org/10.1088/1475-7516/2024/06/066. arXiv:2404.03779 [gr-qc]

Papanikolaou T, Gourgouliatos KN (2023a) Constraining supermassive primordial black holes with magnetically induced gravitational waves. Phys Rev D 108(6):063532. https://doi.org/10.1103/PhysRevD.108.063532. arXiv:2306.05473 [astro-ph.CO]

Papanikolaou T, Gourgouliatos KN (2023b) Primordial magnetic field generation via primordial black hole disks. Phys Rev D 107(10):103532. https://doi.org/10.1103/PhysRevD.107.103532. arXiv:2301.10045 [astro-ph.CO]

Papanikolaou T, He XC, Ma XH et al (2024b) New probe of non-Gaussianities with primordial black hole induced gravitational waves. Phys Lett B 857:138997. https://doi.org/10.1016/j.physletb.2024.138997. arXiv:2403.00660 [astro-ph.CO]

Papanikolaou T, Lymperis A, Lola S et al (2023a) Primordial black holes and gravitational waves from non-canonical inflation. JCAP 03:003. https://doi.org/10.1088/1475-7516/2023/03/003. arXiv:2211.14900 [astro-ph.CO]

Papanikolaou T, Tzerefos C, Basilakos S et al (2022) Scalar induced gravitational waves from primordial black hole Poisson fluctuations in f(R) gravity. JCAP 10:013. https://doi.org/10.1088/1475-7516/2022/10/013. arXiv:2112.15059 [astro-ph.CO]

Papanikolaou T, Tzerefos C, Basilakos S et al (2023b) No constraints for $f(T)$ gravity from gravitational waves induced from primordial black hole fluctuations. Eur Phys J C 83(1):31. https://doi.org/10.1140/epjc/s10052-022-11157-4. arXiv:2205.06094 [gr-qc]

Papanikolaou T, Tzerefos C, Basilakos S et al (2024c) Revisiting string-inspired running-vacuum models under the lens of light primordial black holes. Phys Rev D 110(2):024055. https://doi.org/10.1103/PhysRevD.110.024055. arXiv:2402.19373 [gr-qc]

Papanikolaou T, Vennin V, Langlois D (2021) Gravitational waves from a universe filled with primordial black holes. JCAP 03:053. https://doi.org/10.1088/1475-7516/2021/03/053. arXiv:2010.11573 [astro-ph.CO]

Papanikolaou T (2023b) The H_0 tension alleviated through ultra-light primordial black holes: an information insight through gravitational waves. In: CORFU2022: 22th Hellenic School and Workshops on Elementary Particle Physics and Gravity, arXiv:2303.00600

Park K, Ricotti M (2011) Accretion onto intermediate mass black holes regulated by radiative feedback I. Parametric study for spherically symmetric accretion. Astrophys J 739(1):2. https://doi.org/10.1088/0004-637x/739/1/2

Park K, Ricotti M (2012) Accretion onto black holes from large scales regulated by radiative feedback. II. Growth rate and duty cycle. Astrophys J 747(1):9. https://doi.org/10.1088/0004-637x/747/1/9

Park K, Ricotti M (2013) Accretion onto black holes from large scales regulated by radiative feedback. III. Enhanced luminosity of intermediate mass black holes moving at supersonic speeds. Astrophys J 767(2):163. https://doi.org/10.1088/0004-637x/767/2/163

Passaglia S, Hu W, Motohashi H (2019) Primordial black holes and local non-Gaussianity in canonical inflation. Phys Rev D 99(4):043536. https://doi.org/10.1103/PhysRevD.99.043536. arXiv:1812.08243 [astro-ph.CO]

Passaglia S, Hu W, Motohashi H (2020) Primordial black holes as dark matter through Higgs field criticality. Phys Rev D 101(12):123523. https://doi.org/10.1103/PhysRevD.101.123523. arXiv:1912.02682 [astro-ph.CO]

Pattison C, Vennin V, Assadullahi H et al (2017) Quantum diffusion during inflation and primordial black holes. JCAP 10:046. https://doi.org/10.1088/1475-7516/2017/10/046. arXiv:1707.00537 [hep-th]

Pattison C, Vennin V, Wands D et al (2021) Ultra-slow-roll inflation with quantum diffusion. JCAP 04:080. https://doi.org/10.1088/1475-7516/2021/04/080. arXiv:2101.05741 [astro-ph.CO]

Peebles PJE (1974) The nature of the distribution of galaxies. Astron Astrophys 32:197

Peloso M, Sorbo L, Ünal C (2016) Rolling axions during inflation: perturbativity and signatures. JCAP 09:001. https://doi.org/10.1088/1475-7516/2016/09/001. arXiv:1606.00459 [astro-ph.CO]
Perrodin D, Sesana A (2018) Radio pulsars: testing gravity and detecting gravitational waves. In: Rezzolla L, Pizzochero P, Jones DI, et al (eds) The Physics and Astrophysics of Neutron Stars. Astrophysics and Space Science Library, vol 457. Springer, Cham, p 95–148, https://doi.org/10.1007/978-3-319-97616-7_3, arXiv:1709.02816
Petač M, Lavalle J, Jedamzik K (2022) Microlensing constraints on clustered primordial black holes. Phys Rev D 105(8):083520. https://doi.org/10.1103/PhysRevD.105.083520. arXiv:2201.02521 [astro-ph.CO]
Phinney ES (2001) A practical theorem on gravitational wave backgrounds. arXiv e-prints arXiv:astro-ph/0108028
Phukon KS, Baltus G, Caudill S, et al (2021) The hunt for sub-solar primordial black holes in low mass ratio binaries is open. arXiv e-prints arXiv:2105.11449 [astro-ph.CO]
Pi S, Sasaki M (2020) Gravitational waves induced by scalar perturbations with a lognormal peak. JCAP 09:037. https://doi.org/10.1088/1475-7516/2020/09/037. arXiv:2005.12306 [gr-qc]
Pi S, Sasaki M (2023) Primordial black hole formation in nonminimal curvaton scenarios. Phys Rev D 108 (10):L101301. https://doi.org/10.1103/PhysRevD.108.L101301. arXiv:2112.12680 [astro-ph.CO]
Pi S, Zhang Yl, Huang QG et al (2018) Scalaron from R^2-gravity as a heavy field. JCAP 05:042. https://doi.org/10.1088/1475-7516/2018/05/042. arXiv:1712.09896 [astro-ph.CO]
Piga L, Lucca M, Bellomo N et al (2022) The effect of outflows on CMB bounds from Primordial Black Hole accretion. JCAP 12:016. https://doi.org/10.1088/1475-7516/2022/12/016. arXiv:2210.14934 [astro-ph.CO]
Pilipenko S, Tkachev M, Ivanov P (2022) Evolution of a primordial binary black hole due to interaction with cold dark matter and the formation rate of gravitational wave events. Phys Rev D 105 (12):123504. https://doi.org/10.1103/PhysRevD.105.123504. arXiv:2205.10792 [astro-ph.CO]
Pirvu D, Braden J, Johnson MC (2022) Bubble clustering in cosmological first order phase transitions. Phys Rev D 105(4):043510. https://doi.org/10.1103/PhysRevD.105.043510. arXiv:2109.04496 [hep-th]
Pitrou C, Cusin G, Uzan JP (2020) Unified view of anisotropies in the astrophysical gravitational-wave background. Phys Rev D 101(8):081301. https://doi.org/10.1103/PhysRevD.101.081301. arXiv:1910.04645 [astro-ph.CO]
Polnarev AG, Khlopov MY (1985) Cosmology, primordial black holes, and supermassive particles. Sov Phys Usp 28:213–232. https://doi.org/10.1070/PU1985v028n03ABEH003858
Polnarev AG, Musco I (2007) Curvature profiles as initial conditions for primordial black hole formation. Class Quant Grav 24:1405–1432. https://doi.org/10.1088/0264-9381/24/6/003. arXiv:gr-qc/0605122
Polnarev A, Zembowicz R (1991) Formation of Primordial Black Holes by Cosmic Strings. Phys Rev D 43:1106–1109. https://doi.org/10.1103/PhysRevD.43.1106
Poulin V, Serpico PD, Calore F et al (2017) CMB bounds on disk-accreting massive primordial black holes. Phys Rev D 96(8):083524. https://doi.org/10.1103/PhysRevD.96.083524. arXiv:1707.04206 [astro-ph.CO]
Poulter H, Ali-Haïmoud Y, Hamann J, et al (2019) CMB constraints on ultra-light primordial black holes with extended mass distributions. arXiv e-prints arXiv:1907.06485 [astro-ph.CO]
Press WH, Schechter P (1974) Formation of galaxies and clusters of galaxies by selfsimilar gravitational condensation. Astrophys J 187:425–438. https://doi.org/10.1086/152650
Pujolas O, Vaskonen V, Veermäe H (2021) Prospects for probing gravitational waves from primordial black hole binaries. Phys Rev D 104(8):083521. https://doi.org/10.1103/PhysRevD.104.083521. arXiv:2107.03379 [astro-ph.CO]
Qiu ZY, Yu ZH (2023) Gravitational waves from cosmic strings associated with pseudo-Nambu-Goldstone dark matter*. Chin Phys C 47(8):085104. https://doi.org/10.1088/1674-1137/acd9bf. arXiv:2304.02506 [hep-ph]
Quinn DP, Wilkinson MI, Irwin MJ et al (2009) On the reported death of the MACHO era. Mon Not R Astron Soc 396(1):L11–L15. https://doi.org/10.1111/j.1745-3933.2009.00652.x. arXiv:0903.1644 [astro-ph.GA]
Quinn DP, Wilkinson MI, Irwin MJ et al (2009) On the reported death of the MACHO Era. Mon Not R Astron Soc 396:11. https://doi.org/10.1111/j.1745-3933.2009.00652.x. arXiv:0903.1644 [astro-ph.GA]

Quintin J, Brandenberger RH (2016) Black hole formation in a contracting universe. JCAP 11:029. https://doi.org/10.1088/1475-7516/2016/11/029. arXiv:1609.02556 [astro-ph.CO]
Raccanelli A (2017) Gravitational wave astronomy with radio galaxy surveys. Mon Not R Astron Soc 469 (1):656–670. https://doi.org/10.1093/mnras/stx835. arXiv:1609.09377 [astro-ph.CO]
Raccanelli A, Kovetz ED, Bird S et al (2016a) Determining the progenitors of merging black-hole binaries. Phys Rev D 94(2):023516. https://doi.org/10.1103/PhysRevD.94.023516. arXiv:1605.01405 [astro-ph.CO]
Raccanelli A, Montanari F, Bertacca D et al (2016b) Cosmological measurements with general relativistic galaxy correlations. JCAP 05:009. https://doi.org/10.1088/1475-7516/2016/05/009. arXiv:1505.06179 [astro-ph.CO]
Ragavendra HV, Saha P, Sriramkumar L et al (2021) Primordial black holes and secondary gravitational waves from ultraslow roll and punctuated inflation. Phys Rev D 103(8):083510. https://doi.org/10.1103/PhysRevD.103.083510. arXiv:2008.12202 [astro-ph.CO]
Raidal M, Spethmann C, Vaskonen V et al (2019) Formation and evolution of primordial black hole binaries in the early universe. JCAP 02:018. https://doi.org/10.1088/1475-7516/2019/02/018. arXiv:1812.01930 [astro-ph.CO]
Raidal M, Vaskonen V, Veermäe H (2017) Gravitational waves from primordial black hole mergers. JCAP 09:037. https://doi.org/10.1088/1475-7516/2017/09/037. arXiv:1707.01480 [astro-ph.CO]
Ramazanov S, Babichev E, Gorbunov D et al (2022) Beyond freeze-in: dark matter via inverse phase transition and gravitational wave signal. Phys Rev D 105(6):063530. https://doi.org/10.1103/PhysRevD.105.063530. arXiv:2104.13722 [hep-ph]
Reardon DJ et al (2023a) Search for an isotropic gravitational-wave background with the parkes pulsar timing array. Astrophys J Lett 951(1):L6. https://doi.org/10.3847/2041-8213/acdd02. arXiv:2306.16215 [astro-ph.HE]
Reardon DJ et al (2023b) The gravitational-wave background null hypothesis: characterizing noise in millisecond pulsar arrival times with the parkes pulsar timing array. Astrophys J Lett 951(1):L7. https://doi.org/10.3847/2041-8213/acdd03. arXiv:2306.16229 [astro-ph.HE]
Reitze D et al (2019) Cosmic explorer: the U.S. contribution to gravitational-wave astronomy beyond LIGO. Bull Am Astron Soc 51(7):035 arXiv:1907.04833 [astro-ph.IM]
Renaux-Petel S (2022) Inflation with strongly non-geodesic motion: theoretical motivations and observational imprints. PoS EPS-HEP 2021:128. https://doi.org/10.22323/1.398.0128. arXiv:2111.00989 [astro-ph.CO]
Renzini A, Contaldi C (2019) Improved limits on a stochastic gravitational-wave background and its anisotropies from Advanced LIGO O1 and O2 runs. Phys Rev D 100(6):063527. https://doi.org/10.1103/PhysRevD.100.063527. arXiv:1907.10329 [gr-qc]
Rezazadeh K, Teimoori Z, Karimi S et al (2022) Non-Gaussianity and secondary gravitational waves from primordial black holes production in α-attractor inflation. Eur Phys J C 82(8):758. https://doi.org/10.1140/epjc/s10052-022-10735-w. arXiv:2110.01482 [gr-qc]
Riccardi F, Taoso M, Urbano A (2021) Solving peak theory in the presence of local non-gaussianities. JCAP 08:060. https://doi.org/10.1088/1475-7516/2021/08/060. arXiv:2102.04084 [astro-ph.CO]
Ricciardone A, Tasinato G (2018) Anisotropic tensor power spectrum at interferometer scales induced by tensor squeezed non-Gaussianity. JCAP 02:011. https://doi.org/10.1088/1475-7516/2018/02/011. arXiv:1711.02635 [astro-ph.CO]
Ricotti M (2007) Bondi accretion in the early universe. Astrophys J 662:53–61. https://doi.org/10.1086/516562. arXiv:0706.0864 [astro-ph]
Ricotti M, Gould A (2009) A new probe of dark matter and high-energy universe using microlensing. Astrophys J 707:979–987. https://doi.org/10.1088/0004-637X/707/2/979. arXiv:0908.0735 [astro-ph.CO]
Ricotti M, Ostriker JP, Mack KJ (2008) Effect of primordial black holes on the cosmic microwave background and cosmological parameter estimates. Astrophys J 680:829. https://doi.org/10.1086/587831. arXiv:0709.0524 [astro-ph]
Rigopoulos G, Shellard E (2003) The separate universe approach and the evolution of nonlinear superhorizon cosmological perturbations. Phys Rev D 68:123518. https://doi.org/10.1103/PhysRevD.68.123518. arXiv:astro-ph/0306620
Ringwald A, Schütte-Engel J, Tamarit C (2021) Gravitational waves as a big bang thermometer. JCAP 03:054. https://doi.org/10.1088/1475-7516/2021/03/054. arXiv:2011.04731 [hep-ph]
Riotto A (2023a) The primordial black hole formation from single-field inflation is not ruled out. arXiv e-prints arXiv:2301.00599 [astro-ph.CO]

Riotto A (2023b) The primordial black hole formation from single-field inflation is still not ruled out. arXiv e-prints arXiv:2303.01727 [astro-ph.CO]
Rodriguez CL et al (2022) Modeling dense star clusters in the milky way and beyond with the cluster monte carlo code. Astrophys J Supp 258(2):22. https://doi.org/10.3847/1538-4365/ac2edf. arXiv:2106.02643 [astro-ph.GA]
Romero-Rodriguez A, Martinez M, Pujolàs O et al (2022) Search for a scalar induced stochastic gravitational wave background in the third LIGO-Virgo observing run. Phys Rev Lett 128(5):051301. https://doi.org/10.1103/PhysRevLett.128.051301. arXiv:2107.11660 [gr-qc]
Rubin SG, Khlopov MY, Sakharov AS (2000) Primordial black holes from nonequilibrium second order phase transition. Grav Cosmol 6:51–58 arXiv:hep-ph/0005271
Safarzadeh M, Naoz S, Sadowski A et al (2018) Primordial black holes as seeds of magnetic fields in the universe. Mon Not R Astron Soc 479(1):315–318. https://doi.org/10.1093/mnras/sty1486. arXiv:1701.03800 [astro-ph.HE]
Saga S, Tashiro H, Yokoyama S (2020) Limits on primordial magnetic fields from primordial black hole abundance. JCAP 05:039. https://doi.org/10.1088/1475-7516/2020/05/039. arXiv:2002.01286 [astro-ph.CO]
Saito R, Yokoyama J (2009) Gravitational wave background as a probe of the primordial black hole abundance. Phys Rev Lett 102:161101. https://doi.org/10.1103/PhysRevLett.102.161101. [Erratum: Phys. Rev. Lett. 107, 069901 (2011)] arXiv:0812.4339 [astro-ph]
Saito R, Yokoyama J (2010) Gravitational-wave constraints on the abundance of primordial black holes. Prog Theor Phys 123:867–886. https://doi.org/10.1143/PTP.126.351. [Erratum: Prog. Theor. Phys. 126, 351-352 (2011)] arXiv:0912.5317 [astro-ph.CO]
Sakharov AS, Eroshenko YN, Rubin SG (2021) Looking at the NANOGrav signal through the anthropic window of axionlike particles. Phys Rev D 104(4):043005. https://doi.org/10.1103/PhysRevD.104.043005. arXiv:2104.08750 [hep-ph]
Salopek D, Bond J (1990) Nonlinear evolution of long wavelength metric fluctuations in inflationary models. Phys Rev D 42:3936–3962. https://doi.org/10.1103/PhysRevD.42.3936
Samanta R, Datta S (2021) Gravitational wave complementarity and impact of NANOGrav data on gravitational leptogenesis. JHEP 05:211. https://doi.org/10.1007/JHEP05(2021)211. arXiv:2009.13452 [hep-ph]
Sasaki M, Stewart ED (1996) A General analytic formula for the spectral index of the density perturbations produced during inflation. Prog Theor Phys 95:71–78. https://doi.org/10.1143/PTP.95.71. arXiv:astro-ph/9507001
Sasaki M, Suyama T, Tanaka T et al (2016) Primordial black hole scenario for the gravitational-wave event GW150914. Phys Rev Lett 117(6):061101. https://doi.org/10.1103/PhysRevLett.117.061101. [Erratum: Phys. Rev. Lett. 121, 059901 (2018)] arXiv:1603.08338 [astro-ph.CO]
Sasaki M, Suyama T, Tanaka T et al (2018) Primordial black holes–perspectives in gravitational wave astronomy. Class Quant Grav 35(6):063001. https://doi.org/10.1088/1361-6382/aaa7b4. arXiv:1801.05235 [astro-ph.CO]
Sasaki M, Takhistov V, Vardanyan V et al (2022) Establishing the nonprimordial origin of black hole-neutron star mergers. Astrophys J 931(1):2. https://doi.org/10.3847/1538-4357/ac66da. arXiv:2110.09509 [astro-ph.CO]
Sasaki M, Valiviita J, Wands D (2006) Non-Gaussianity of the primordial perturbation in the curvaton model. Phys Rev D 74:103003. https://doi.org/10.1103/PhysRevD.74.103003. arXiv:astro-ph/0607627
Sathyaprakash B et al (2012) Scientific objectives of einstein telescope. Class Quant Grav 29:124013. https://doi.org/10.1088/0264-9381/29/12/124013. [Erratum: Class. Quant. Grav. 30, 079501 (2013)] arXiv:1206.0331 [gr-qc]
Scelfo G, Bellomo N, Raccanelli A et al (2018) GW×LSS: chasing the progenitors of merging binary black holes. JCAP 09:039. https://doi.org/10.1088/1475-7516/2018/09/039. arXiv:1809.03528 [astro-ph.CO]
Scelfo G, Boco L, Lapi A et al (2020) Exploring galaxies-gravitational waves cross-correlations as an astrophysical probe. JCAP 10:045. https://doi.org/10.1088/1475-7516/2020/10/045. arXiv:2007.08534 [astro-ph.CO]
Scelfo G, Spinelli M, Raccanelli A et al (2022) Gravitational waves x HI intensity mapping: cosmological and astrophysical applications. JCAP 01(01):004. https://doi.org/10.1088/1475-7516/2022/01/004. arXiv:2106.09786 [astro-ph.CO]

Schmitz K (2021) New sensitivity curves for gravitational-wave signals from cosmological phase transitions. JHEP 97. https://doi.org/10.1007/JHEP01(2021)097, arXiv:2002.04615 [hep-ph]
Schneider R, Ferrara A, Ciardi B et al (2000) Gravitational waves signals from the collapse of the first stars. Mon Not R Astron Soc 317:385. https://doi.org/10.1046/j.1365-8711.2000.03596.x. arXiv:astro-ph/9909419
Schneider R, Ferrara A, Natarajan P et al (2002) First stars, very massive black holes and metals. Astrophys J 571:30–39. https://doi.org/10.1086/339917. arXiv:astro-ph/0111341
Schneider R, Ferrara A, Salvaterra R et al (2003) Low-mass relics of early star formation. Nature 422:869–871. https://doi.org/10.1038/nature01579. arXiv:astro-ph/0304254
Schneider R, Valiante R, Trinca A et al (2023) Are we surprised to find SMBHs with JWST at $z \geq 9$? Mon Not R Astron Soc 526(3):3250–3261. https://doi.org/10.1093/mnras/stad2503. arXiv:2305.12504 [astro-ph.GA]
Scholtz J, Unwin J (2020) What if planet 9 is a primordial black hole? Phys Rev Lett 125(5):051103. https://doi.org/10.1103/PhysRevLett.125.051103. arXiv:1909.11090 [hep-ph]
Schwarz DJ, Terrero-Escalante CA, Garcia AA (2001) Higher order corrections to primordial spectra from cosmological inflation. Phys Lett B 517:243–249. https://doi.org/10.1016/S0370-2693(01)01036-X. arXiv:astro-ph/0106020 [astro-ph]
Serpico PD, Poulin V, Inman D et al (2020) Cosmic microwave background bounds on primordial black holes including dark matter halo accretion. Phys Rev Res 2(2):023204. https://doi.org/10.1103/PhysRevResearch.2.023204. arXiv:2002.10771 [astro-ph.CO]
Sesana A (2016) Prospects for multiband gravitational-wave astronomy after GW150914. Phys Rev Lett 116(23):231102. https://doi.org/10.1103/PhysRevLett.116.231102. arXiv:1602.06951 [gr-qc]
Sesana A, Vecchio A, Colacino CN (2008) The stochastic gravitational-wave background from massive black hole binary systems: implications for observations with Pulsar Timing Arrays. Mon Not R Astron Soc 390:192. https://doi.org/10.1111/j.1365-2966.2008.13682.x. arXiv:0804.4476 [astro-ph]
Seto N, Cooray A (2004) Search for small-mass black hole dark matter with space-based gravitational wave detectors. Phys Rev D 70:063512. https://doi.org/10.1103/PhysRevD.70.063512. arXiv:astro-ph/0405216
Shakura N, Sunyaev R (1973) Black holes in binary systems. Observational appearance. Astron Astrophys 24:337–355
Shandera S, Jeong D, Gebhardt HSG (2018) Gravitational waves from binary mergers of subsolar mass dark black holes. Phys Rev Lett 120(24):241102. https://doi.org/10.1103/PhysRevLett.120.241102. arXiv:1802.08206 [astro-ph.CO]
Shibata M, Sasaki M (1999) Black hole formation in the Friedmann universe: formulation and computation in numerical relativity. Phys Rev D 60:084002. https://doi.org/10.1103/PhysRevD.60.084002. arXiv:gr-qc/9905064
Silverstein E, Westphal A (2008) Monodromy in the CMB: gravity waves and string inflation. Phys Rev D 78:106003. https://doi.org/10.1103/PhysRevD.78.106003. arXiv:0803.3085 [hep-th]
Singh N, Bulik T, Belczynski K et al (2022a) Exploring compact binary populations with the Einstein Telescope. Astron Astrophys 667:A2. https://doi.org/10.1051/0004-6361/202142856. arXiv:2112.04058 [astro-ph.HE]
Singh S, Nambissan TJ, Subrahmanyan R et al (2022b) On the detection of a cosmic dawn signal in the radio background. Nature Astron 6(5):607–617. https://doi.org/10.1038/s41550-022-01610-5. arXiv:2112.06778 [astro-ph.CO]
Siraj A, Loeb A (2020) Searching for black holes in the outer solar system with LSST. Astrophys J Lett 898(1):L4. https://doi.org/10.3847/2041-8213/aba119. arXiv:2005.12280 [astro-ph.HE]
Sirunyan AM et al (2020) Measurement of $t\bar{t}$ normalised multi-differential cross sections in pp collisions at $\sqrt{s} = 13$ TeV, and simultaneous determination of the strong coupling strength, top quark pole mass, and parton distribution functions. Eur Phys J C 80(7):658. https://doi.org/10.1140/epjc/s10052-020-7917-7. arXiv:1904.05237 [hep-ex]
Smirnov J, Goobar A, Linden T et al (2024) White dwarfs in dwarf spheroidal galaxies: a new class of compact-dark-matter detectors. Phys Rev Lett 132(15):151401. https://doi.org/10.1103/PhysRevLett.132.151401. arXiv:2211.00013 [astro-ph.CO]
Smyth N, Profumo S, English S et al (2020) Updated constraints on asteroid-mass primordial black holes as dark matter. Phys Rev D 101(6):063005. https://doi.org/10.1103/PhysRevD.101.063005. arXiv:1910.01285 [astro-ph.CO]

Sorbo L (2011) Parity violation in the Cosmic Microwave Background from a pseudoscalar inflaton. JCAP 06:003. https://doi.org/10.1088/1475-7516/2011/06/003. arXiv:1101.1525 [astro-ph.CO]
de Souza RS, Yoshida N, Ioka K (2011) Population III.1 and III.2 gamma-ray bursts: constraints on the event rate for future radio and X-ray surveys. Astron Astrophys 533:A32. https://doi.org/10.1051/0004-6361/201117242. arXiv:1105.2395 [astro-ph.CO]
Stamou I, Clesse S (2024a) Can primordial black holes form in the standard model? Phys Rev D 109 (12):123501. https://doi.org/10.1103/PhysRevD.109.123501. arXiv:2312.06873 [astro-ph.CO]
Stamou I, Clesse S (2024b) Primordial black holes without fine-tuning from a light stochastic spectator field. Phys Rev D 109(4):043522. https://doi.org/10.1103/PhysRevD.109.043522. arXiv:2310.04174 [astro-ph.CO]
Starobinsky AA (1982) Dynamics of Phase transition in the new inflationary universe scenario and generation of perturbations. Phys Lett B 117:175–178. https://doi.org/10.1016/0370-2693(82)90541-X
Starobinsky AA (1985) Multicomponent de sitter (Inflationary) stages and the generation of perturbations. JETP Lett 42:152–155
Stegmann J, Capelo PR, Bortolas E et al (2020) Improved constraints from ultra-faint dwarf galaxies on primordial black holes as dark matter. Mon Not R Astron Soc 492(4):5247–5260. https://doi.org/10.1093/mnras/staa170. arXiv:1910.04793 [astro-ph.GA]
Sten Delos M, Silk J (2023) Ultradense dark matter haloes accompany primordial black holes. Mon Not R Astron Soc 520(3):4370–4375. https://doi.org/10.1093/mnras/stad356. arXiv:2210.04904 [astro-ph.CO]
Stone NC, Leigh NWC (2019) A statistical solution to the chaotic, non-hierarchical three-body problem. Nature 576(7787):406–410. https://doi.org/10.1038/s41586-019-1833-8. arXiv:1909.05272 [astro-ph.GA]
Stöcker P, Krämer M, Lesgourgues J et al (2018) Exotic energy injection with ExoCLASS: application to the Higgs portal model and evaporating black holes. JCAP 03:018. https://doi.org/10.1088/1475-7516/2018/03/018. arXiv:1801.01871 [astro-ph.CO]
Sugiyama S, Takhistov V, Vitagliano E et al (2021) Testing stochastic gravitational wave signals from primordial black holes with optical telescopes. Phys Lett B 814:136097. https://doi.org/10.1016/j.physletb.2021.136097. arXiv:2010.02189 [astro-ph.CO]
Suyama T, Tanaka T, Bassett B et al (2005) Are black holes over-produced during preheating? Phys Rev D 71:063507. https://doi.org/10.1103/PhysRevD.71.063507. arXiv:hep-ph/0410247 [hep-ph]
Suyama T, Yokoyama S (2019) Clustering of primordial black holes with non-Gaussian initial fluctuations. PTEP 10:103E02. https://doi.org/10.1093/ptep/ptz105. arXiv:1906.04958 [astro-ph.CO]
Takhistov V, Lu P, Murase K et al (2022) Impacts of Jets and winds from primordial black holes. Mon Not R Astron Soc 517(1):L1–L4. https://doi.org/10.1093/mnrasl/slac097. arXiv:2111.08699 [astro-ph.HE]
Tanikawa A, Susa H, Yoshida T et al (2021) Merger rate density of Population III binary black holes below, above, and in the pair-instability mass gap. Astrophys J 910(1):30. https://doi.org/10.3847/1538-4357/abe40d. arXiv:2008.01890 [astro-ph.HE]
Taoso M, Urbano A (2021) Non-gaussianities for primordial black hole formation. JCAP 08:016. https://doi.org/10.1088/1475-7516/2021/08/016. arXiv:2102.03610 [astro-ph.CO]
Tashiro H, Kadota K (2021a) CMB and 21 cm bounds on early structure formation boosted by primordial black hole entropy fluctuations. Phys Rev D 104(6):063522. https://doi.org/10.1103/PhysRevD.104.063522. arXiv:2105.08462 [astro-ph.CO]
Tashiro H, Kadota K (2021b) Constraining mixed dark-matter scenarios of WIMPs and primordial black holes from CMB and 21 cm observations. Phys Rev D 103(12):123532. https://doi.org/10.1103/PhysRevD.103.123532. arXiv:2104.09738 [astro-ph.CO]
Tasinato G (2021) An analytic approach to non-slow-roll inflation. Phys Rev D 103(2):023535. https://doi.org/10.1103/PhysRevD.103.023535. arXiv:2012.02518 [hep-th]
Tasinato G (2023) Large $|\eta|$ approach to single field inflation. Phys Rev D 108(4):043526. https://doi.org/10.1103/PhysRevD.108.043526. arXiv:2305.11568 [hep-th]
Tavernier T, Glicenstein JF, Brun F (2020) Search for primordial black hole evaporations with H.E.S.S. PoS ICRC2019:804. https://doi.org/10.22323/1.358.0804, arXiv:1909.01620 [astro-ph.HE]
Tegmark M, Peebles PJE (1998) The Time evolution of bias. Astrophys J Lett 500:L79. https://doi.org/10.1086/311426. arXiv:astro-ph/9804067
Thorne KS (1974) Disk accretion onto a black hole. 2. Evolution of the hole. Astrophys J 191:507–520. https://doi.org/10.1086/152991

Thoss V, Burkert A, Kohri K (2024) Breakdown of hawking evaporation opens new mass window for primordial black holes as dark matter candidate. Mon Not R Astron Soc 532(1):451–459. https://doi.org/10.1093/mnras/stae1098. arXiv:2402.17823 [astro-ph.CO]

Tian HJ, El-Badry K, Rix HW et al (2020) The separation distribution of ultrawide binaries across galactic populations. Astrophys J S 246(1):4. https://doi.org/10.3847/1538-4365/ab54c4. arXiv:1909.04765 [astro-ph.GA]

Tisserand P et al (2007) Limits on the macho content of the galactic halo from the EROS-2 survey of the magellanic clouds. Astron Astrophys 469:387–404. https://doi.org/10.1051/0004-6361:20066017. arXiv:astro-ph/0607207

Tomikawa K, Kobayashi T (2020) Gauge dependence of gravitational waves generated at second order from scalar perturbations. Phys Rev D 101(8):083529. https://doi.org/10.1103/PhysRevD.101.083529. arXiv:1910.01880 [gr-qc]

Tomita K (1975) Evolution of irregularities in a chaotic early universe. Prog Theor Phys 54:730. https://doi.org/10.1143/PTP.54.730

Tornatore L, Borgani S, Dolag K et al (2007) Chemical enrichment of galaxy clusters from hydrodynamical simulations. Mon Not R Astron Soc 382:1050. https://doi.org/10.1111/j.1365-2966.2007.12070.x. arXiv:0705.1921 [astro-ph]

Torres-Lomas E, Hidalgo JC, Malik KA et al (2014) Formation of subhorizon black holes from preheating. Phys Rev D 89(8):083008. https://doi.org/10.1103/PhysRevD.89.083008. arXiv:1401.6960 [astro-ph.CO]

Torres-Lomas E, Urena-LAlpez L (2013) Primordial black hole production during preheating in a chaotic inflationary model. AIP Conf Proc 1548(1):238–243. https://doi.org/10.1063/1.4817051. arXiv:1308.1268 [astro-ph.CO]

Trashorras M, García-Bellido J, Nesseris S (2021) The clustering dynamics of primordial black boles in N-body simulations. Universe 7(1):18. https://doi.org/10.3390/universe7010018. arXiv:2006.15018 [astro-ph.CO]

Trenti M, Stiavelli M (2009) The formation rates of population III stars and chemical enrichment of halos during the reionization era. Astrophys J 694:879–892. https://doi.org/10.1088/0004-637X/694/2/879. arXiv:0901.0711 [astro-ph.CO]

Tzerefos C, Papanikolaou T, Saridakis EN et al (2023) Scalar induced gravitational waves in modified teleparallel gravity theories. Phys Rev D 107(12):124019. https://doi.org/10.1103/PhysRevD.107.124019. arXiv:2303.16695 [gr-qc]

Ünal C (2019) Imprints of primordial non-gaussianity on gravitational wave spectrum. Phys Rev D 99(4):041301. https://doi.org/10.1103/PhysRevD.99.041301. arXiv:1811.09151 [astro-ph.CO]

Ünal C, Kovetz ED, Patil SP (2021) Multimessenger probes of inflationary fluctuations and primordial black holes. Phys Rev D 103(6):063519. https://doi.org/10.1103/PhysRevD.103.063519. arXiv:2008.11184 [astro-ph.CO]

Ünal C, Papageorgiou A, Obata I (2024) Axion-gauge dynamics during inflation as the origin of pulsar timing array signals and primordial black holes. Phys Lett B 856:138873. https://doi.org/10.1016/j.physletb.2024.138873. arXiv:2307.02322 [astro-ph.CO]

Ünal C (2023) Superradiance properties of light black holes and 10^{-12}-10^{5} eV Bosons. arXiv e-prints arXiv:2301.08267 [hep-ph]

Vagnozzi S (2021) Implications of the NANOGrav results for inflation. Mon Not R Astron Soc 502(1):L11–L15. https://doi.org/10.1093/mnrasl/slaa203. arXiv:2009.13432 [astro-ph.CO]

Vagnozzi S (2023) Inflationary interpretation of the stochastic gravitational wave background signal detected by pulsar timing array experiments. JHEAp 39:81–98. https://doi.org/10.1016/j.jheap.2023.07.001. arXiv:2306.16912 [astro-ph.CO]

Vainer BV, Naselskii PD (1978) Cosmological implications of the process of primordial black hole evaporation. Soviet Astron 22:138–140

Vaskonen V, Veermäe H (2020) Lower bound on the primordial black hole merger rate. Phys Rev D 101(4):043015. https://doi.org/10.1103/PhysRevD.101.043015. arXiv:1908.09752 [astro-ph.CO]

Vaskonen V, Veermäe H (2021) Did NANOGrav see a signal from primordial black hole formation? Phys Rev Lett 126(5):051303. https://doi.org/10.1103/PhysRevLett.126.051303. arXiv:2009.07832 [astro-ph.CO]

Vattis K, Goldstein IS, Koushiappas SM (2020) Could the 2.6 $M_{\odot}$ object in GW190814 be a primordial black hole? Phys Rev D 102(6):061301. https://doi.org/10.1103/PhysRevD.102.061301. arXiv:2006.15675 [astro-ph.HE]

Vennin V, Starobinsky AA (2015) Correlation Functions in stochastic inflation. Eur Phys J C 75:413. https://doi.org/10.1140/epjc/s10052-015-3643-y. arXiv:1506.04732 [hep-th]
Villanueva-Domingo P, Ichiki K (2022) 21 cm forest constraints on primordial black holes. Publ Astron Soc Japan 75(Supplement–1):S33–S49. https://doi.org/10.1093/pasj/psab119. arXiv:2104.10695 [astro-ph.CO]
Vitale S, Gerosa D, Haster CJ et al (2017) Impact of bayesian priors on the characterization of binary black hole coalescences. Phys Rev Lett 119(25):251103. https://doi.org/10.1103/PhysRevLett.119.251103. arXiv:1707.04637 [gr-qc]
Volonteri M, Madau P, Quataert E et al (2005) The distribution and cosmic evolution of massive black hole spins. Astrophys J 620:69–77. https://doi.org/10.1086/426858. arXiv:astro-ph/0410342
Wands D, Malik KA, Lyth DH et al (2000) A new approach to the evolution of cosmological perturbations on large scales. Phys Rev D 62:043527. https://doi.org/10.1103/PhysRevD.62.043527. arXiv:astro-ph/0003278
Wang YF, Nitz AH (2021) Prospects for detecting gravitational waves from eccentric subsolar mass compact binaries. Astrophys J 912(1):53. https://doi.org/10.3847/1538-4357/abe939. arXiv:2101.12269 [astro-ph.HE]
Wang Y, Robberto M, Dickinson M et al (2019) ATLAS probe: breakthrough science of galaxy evolution, cosmology, milky way, and the solar system. Publ Astron Soc Australia 36:e015. https://doi.org/10.1017/pasa.2019.5. arXiv:1802.01539 [astro-ph.IM]
Wang S, Terada T, Kohri K (2019) Prospective constraints on the primordial black hole abundance from the stochastic gravitational-wave backgrounds produced by coalescing events and curvature perturbations. Phys Rev D 99(10):103531. https://doi.org/10.1103/PhysRevD.99.103531. [Erratum: Phys. Rev. D 101, 069901 (2020)] arXiv:1903.05924 [astro-ph.CO]
Wang S, Wang YF, Huang QG et al (2018) Constraints on the primordial black hole abundance from the first advanced LIGO observation run using the stochastic gravitational-wave background. Phys Rev Lett 120(19):191102. https://doi.org/10.1103/PhysRevLett.120.191102. arXiv:1610.08725 [astro-ph.CO]
Wang S, Xia DM, Zhang X et al (2021) Constraining primordial black holes as dark matter at JUNO. Phys Rev D 103(4):043010. https://doi.org/10.1103/PhysRevD.103.043010. arXiv:2010.16053 [hep-ph]
Wang S, Zhao ZC, Li JP et al (2024a) Implications of pulsar timing array data for scalar-induced gravitational waves and primordial black holes: primordial non-Gaussianity fNL considered. Phys Rev Res 6(1):L012060. https://doi.org/10.1103/PhysRevResearch.6.L012060. arXiv:2307.00572 [astro-ph.CO]
Wang S, Zhao ZC, Zhu QH (2024b) Constraints on scalar-induced gravitational waves up to third order from a joint analysis of BBN, CMB, and PTA data. Phys Rev Res 6(1):013207. https://doi.org/10.1103/PhysRevResearch.6.013207. arXiv:2307.03095 [astro-ph.CO]
Weinberg S (2004) Damping of tensor modes in cosmology. Phys Rev D 69:023503. https://doi.org/10.1103/PhysRevD.69.023503. arXiv:astro-ph/0306304
Weltman A et al (2020) Fundamental physics with the Square Kilometre Array. Publ Astron Soc Austral 37:e002. https://doi.org/10.1017/pasa.2019.42. arXiv:1810.02680 [astro-ph.CO]
Wenzl L, Doux C, Heinrich C et al (2022) Cosmology with the roman space telescope - synergies with CMB lensing. Mon Not R Astron Soc 512(4):5311–5328. https://doi.org/10.1093/mnras/stac790. arXiv:2112.07681 [astro-ph.CO]
Witkowski LT, Domènech G, Fumagalli J et al (2022) Expansion history-dependent oscillations in the scalar-induced gravitational wave background. JCAP 05(05):028. https://doi.org/10.1088/1475-7516/2022/05/028. arXiv:2110.09480 [astro-ph.CO]
Witten E (2020) Searching for a black hole in the outer solar system. arXiv e-prints arXiv:2004.14192 [astro-ph.EP]
Wong KWK, Franciolini G, De Luca V et al (2021) Constraining the primordial black hole scenario with Bayesian inference and machine learning: the GWTC-2 gravitational wave catalog. Phys Rev D 103(2):023026. https://doi.org/10.1103/PhysRevD.103.023026. arXiv:2011.01865 [gr-qc]
Wyrzykowski L et al (2010) The OGLE View of Microlensing towards the Magellanic Clouds. II. OGLE-II SMC data. Mon Not R Astron Soc 407:189–200. https://doi.org/10.1111/j.1365-2966.2010.16936.x. arXiv:1004.5247 [astro-ph.GA]
Wyrzykowski L et al (2011a) The OGLE view of microlensing towards the magellanic clouds. III. Ruling out sub-solar MACHOs with the OGLE-III LMC data. Mon Not R Astron Soc 413:493. https://doi.org/10.1111/j.1365-2966.2010.18150.x. arXiv:1012.1154 [astro-ph.GA]

Wyrzykowski L et al (2011b) The OGLE view of microlensing towards the Magellanic Clouds IV OGLE-III SMC Data and final conclusions on MACHOs. Mon Not R Astron Soc 416:2949. https://doi.org/10.1111/j.1365-2966.2011.19243.x. arXiv:1106.2925 [astro-ph.GA]

Wyrzykowski L et al (2016) Black hole, neutron star and white dwarf candidates from microlensing with OGLE-III. Mon Not R Astron Soc 458(3):3012–3026. https://doi.org/10.1093/mnras/stw426. arXiv:1509.04899 [astro-ph.SR]

Wyrzykowski L, Mandel I (2020) Constraining the masses of microlensing black holes and the mass gap with Gaia DR2. Astron Astrophys 636:A20. https://doi.org/10.1051/0004-6361/201935842. arXiv:1904.07789 [astro-ph.SR]

Xu H et al (2023) Searching for the nano-hertz stochastic gravitational wave background with the chinese pulsar timing array data release I. Res Astron Astrophys 23(7):075024. https://doi.org/10.1088/1674-4527/acdfa5. arXiv:2306.16216 [astro-ph.HE]

Xue X et al (2021) Constraining cosmological phase transitions with the parkes pulsar timing array. Phys Rev Lett 127(25):251303. https://doi.org/10.1103/PhysRevLett.127.251303. arXiv:2110.03096 [astro-ph.CO]

Yan H, Ma Z, Ling C et al (2023) First batch of $z \approx 11$–20 candidate objects revealed by the james webb space telescope early release observations on SMACS 0723–73. Astrophys J Lett 942(1):L9. https://doi.org/10.3847/2041-8213/aca80c. arXiv:2207.11558 [astro-ph.GA]

Yang Y (2020) Constraints on primordial black holes and curvature perturbations from the global 21 cm signal. Phys Rev D 102(8):083538. https://doi.org/10.1103/PhysRevD.102.083538. arXiv:2009.11547 [astro-ph.CO]

Yang Y (2021) Constraints on accreting primordial black holes with the global 21 cm signal. Phys Rev D 104(6):063528. https://doi.org/10.1103/PhysRevD.104.063528. arXiv:2108.11130 [astro-ph.CO]

Yang KZ, Mandic V, Scarlata C et al (2020) Searching for cross-correlation between stochastic gravitational wave background and galaxy number counts. Mon Not R Astron Soc 500(2):1666–1672. https://doi.org/10.1093/mnras/staa3159. arXiv:2007.10456 [astro-ph.CO]

Yi Z (2023) Primordial black holes and scalar-induced gravitational waves from the generalized Brans-Dicke theory. JCAP 03:048. https://doi.org/10.1088/1475-7516/2023/03/048. arXiv:2206.01039 [gr-qc]

Yi Z, Fei Q (2023) Constraints on primordial curvature spectrum from primordial black holes and scalar-induced gravitational waves. Eur Phys J C 83(1):82. https://doi.org/10.1140/epjc/s10052-023-11233-3. arXiv:2210.03641 [astro-ph.CO]

Yokoyama J (1997) Formation of MACHO primordial black holes in inflationary cosmology. Astron Astrophys 318:673 arXiv:astro-ph/9509027

Yokoyama J (1998) Formation of primordial black holes in the inflationary universe. Phys Rept 307:133–139. https://doi.org/10.1016/S0370-1573(98)00044-1

Yoo CM, Gong JO, Yokoyama S (2019) Abundance of primordial black holes with local non-Gaussianity in peak theory. JCAP 09:033. https://doi.org/10.1088/1475-7516/2019/09/033. arXiv:1906.06790 [astro-ph.CO]

Yoo CM, Harada T, Garriga J et al (2018) Primordial black hole abundance from random Gaussian curvature perturbations and a local density threshold. PTEP 12:123E01. https://doi.org/10.1093/ptep/pty120. arXiv:1805.03946 [astro-ph.CO]

You ZQ, Yi Z, Wu Y (2023) Constraints on primordial curvature power spectrum with pulsar timing arrays. JCAP 11:065. https://doi.org/10.1088/1475-7516/2023/11/065. arXiv:2307.04419 [gr-qc]

Young S (2019) The primordial black hole formation criterion re-examined: parametrisation, timing and the choice of window function. Int J Mod Phys D 29(02):2030002. https://doi.org/10.1142/S0218271820300025. arXiv:1905.01230 [astro-ph.CO]

Young S (2022) Peaks and primordial black holes: the effect of non-Gaussianity. JCAP 05(05):037. https://doi.org/10.1088/1475-7516/2022/05/037. arXiv:2201.13345 [astro-ph.CO]

Young S, Byrnes CT (2013) Primordial black holes in non-Gaussian regimes. JCAP 08:052. https://doi.org/10.1088/1475-7516/2013/08/052. arXiv:1307.4995 [astro-ph.CO]

Young S, Byrnes CT (2015) Signatures of non-gaussianity in the isocurvature modes of primordial black hole dark matter. JCAP 04:034. https://doi.org/10.1088/1475-7516/2015/04/034. arXiv:1503.01505 [astro-ph.CO]

Young S, Byrnes CT (2020) Initial clustering and the primordial black hole merger rate. JCAP 03:004. https://doi.org/10.1088/1475-7516/2020/03/004. arXiv:1910.06077 [astro-ph.CO]

Young S, Byrnes CT, Sasaki M (2014) Calculating the mass fraction of primordial black holes. JCAP 07:045. https://doi.org/10.1088/1475-7516/2014/07/045. arXiv:1405.7023 [gr-qc]

Young S, Musco I, Byrnes CT (2019) Primordial black hole formation and abundance: contribution from the non-linear relation between the density and curvature perturbation. JCAP 11:012. https://doi.org/10.1088/1475-7516/2019/11/012. arXiv:1904.00984 [astro-ph.CO]

Yuan C, Chen ZC, Huang QG (2019) Probing primordial-black-hole dark matter with scalar induced gravitational waves. Phys Rev D 100(8):081301. https://doi.org/10.1103/PhysRevD.100.081301. arXiv:1906.11549 [astro-ph.CO]

Yuan C, Chen ZC, Huang QG (2020) Scalar induced gravitational waves in different gauges. Phys Rev D 101(6):063018. https://doi.org/10.1103/PhysRevD.101.063018. arXiv:1912.00885 [astro-ph.CO]

Yuan C, Huang QG (2021a) A topic review on probing primordial black hole dark matter with scalar induced gravitational waves. iScience 24:102860. https://doi.org/10.1016/j.isci.2021.102860. arXiv:2103.04739 [astro-ph.GA]

Yuan C, Huang QG (2021b) Gravitational waves induced by the local-type non-Gaussian curvature perturbations. Phys Lett B 821:136606. https://doi.org/10.1016/j.physletb.2021.136606. arXiv:2007.10686 [astro-ph.CO]

Zagorac JL, Easther R, Padmanabhan N (2019) GUT-scale primordial black holes: mergers and gravitational waves. JCAP 06:052. https://doi.org/10.1088/1475-7516/2019/06/052. arXiv:1903.05053 [astro-ph.CO]

Zel'dovich ID, Novikov YB (1967) The hypothesis of cores retarded during expansion and the hot cosmological model. Soviet Astron 10:602

Zeng ZM, Liu J, Guo ZK (2023) Enhanced curvature perturbations from spherical domain walls nucleated during inflation. Phys Rev D 108(6):063005. https://doi.org/10.1103/PhysRevD.108.063005. arXiv:2301.07230 [astro-ph.CO]

Zhang F (2022) Primordial black holes and scalar induced gravitational waves from the E model with a Gauss-Bonnet term. Phys Rev D 105(6):063539. https://doi.org/10.1103/PhysRevD.105.063539. arXiv:2112.10516 [gr-qc]

Zhang F, Feng JX, Gao X (2022) Circularly polarized scalar induced gravitational waves from the Chern-Simons modified gravity. JCAP 10:054. https://doi.org/10.1088/1475-7516/2022/10/054. arXiv:2205.12045 [gr-qc]

Zhao JX, Liu XH, Li N (2023) Primordial black holes and scalar-induced gravitational waves from the perturbations on the inflaton potential in peak theory. Phys Rev D 107(4):043515. https://doi.org/10.1103/PhysRevD.107.043515. arXiv:2302.06886 [astro-ph.CO]

Zhao ZC, Wang S (2023) Bayesian implications for the primordial black holes from NANOGrav's pulsar-timing data using the scalar-induced gravitational waves. Universe 9(4):157. https://doi.org/10.3390/universe9040157. arXiv:2211.09450 [astro-ph.CO]

Zhao W, Zhang Y, You XP et al (2013) Constraints of relic gravitational waves by pulsar timing arrays: Forecasts for the FAST and SKA projects. Phys Rev D 87(12):124012. https://doi.org/10.1103/PhysRevD.87.124012. arXiv:1303.6718 [astro-ph.CO]

Zhao ZC, Zhu QH, Wang S, et al (2024) Exploring the equation of state of the early universe: insights from BBN, CMB, and PTA observations. Chinese Phys C https://doi.org/10.1088/1674-1137/ad79d5, arXiv:2307.13574 [astro-ph.CO]

Zhou Z, Jiang J, Cai YF et al (2020) Primordial black holes and gravitational waves from resonant amplification during inflation. Phys Rev D 102(10):103527. https://doi.org/10.1103/PhysRevD.102.103527. arXiv:2010.03537 [astro-ph.CO]

Zic A et al (2023) The parkes pulsar timing array third data release. Publ Astron Soc Austral 40:e049. https://doi.org/10.1017/pasa.2023.36. arXiv:2306.16230 [astro-ph.HE]

Ziparo F, Gallerani S, Ferrara A et al (2022) Cosmic radiation backgrounds from primordial black holes. Mon Not R Astron Soc 517(1):1086–1097. https://doi.org/10.1093/mnras/stac2705. arXiv:2209.09907 [astro-ph.CO]

Zumalacarregui M, Seljak U (2018) Limits on stellar-mass compact objects as dark matter from gravitational lensing of type Ia supernovae. Phys Rev Lett 121(14):141101. https://doi.org/10.1103/PhysRevLett.121.141101. arXiv:1712.02240 [astro-ph.CO]

Authors and Affiliations

Eleni Bagui[1] · Sébastien Clesse[1] · Valerio De Luca[2] · Jose María Ezquiaga[3] · Gabriele Franciolini[4] · Juan García-Bellido[5] · Cristian Joana[6,7] · Rajeev Kumar Jain[8] · Sachiko Kuroyanagi[5,9] · Ilia Musco[10,11] · Theodoros Papanikolaou[12,13,14] · Alvise Raccanelli[4,15,16,17] · Sébastien Renaux-Petel[18] · Antonio Riotto[19] · Ester Ruiz Morales[5,20] · Marco Scalisi[21] · Olga Sergijenko[22,23,24,25] · Caner Ünal[26,27,28] · Vincent Vennin[29] · David Wands[30] · For the LISA Cosmology Working Group

✉ Juan García-Bellido
juan.garciabellido@uam.es

Sébastien Clesse
sebastien.clesse@ulb.be

[1] Service de Physique Théorique, Université Libre de Bruxelles (ULB), Boulevard du Triomphe, CP225, 1050 Brussels, Belgium

[2] Center for Particle Cosmology, Department of Physics and Astronomy, University of Pennsylvania, 209 S. 33rd St., Philadelphia, PA 19104, USA

[3] Niels Bohr International Academy, Niels Bohr Institute, Blegdamsvej 17, 2100 Copenhagen, Denmark

[4] Theoretical Physics Department, CERN, 1 Esplanade des Particules, 1211 Geneva 23, Switzerland

[5] Instituto de Física Teórica UAM/CSIC, Universidad Autónoma de Madrid, Cantoblanco, 28049 Madrid, Spain

[6] CAS Key Laboratory of Theoretical Physics, Institute of Theoretical Physics, Chinese Academy of Sciences, Beijing 100190, China

[7] Cosmology, Universe and Relativity at Louvain (CURL), Institute of Mathematics and Physics, University of Louvain, Chemin du Cyclotron 2, 1348 Louvain-la-Neuve, Belgium

[8] Department of Physics, Indian Institute of Science, C. V. Raman Road, Bangalore 560012, India

[9] Department of Physics, Nagoya University, Furo-cho Chikusa-ku, Nagoya 464-8602, Japan

[10] Dipartimento di Fisica, Sapienza Università di Roma, Piazzale Aldo Moro 5, 00185 Roma, Italy

[11] INFN, Sezione di Roma, Piazzale Aldo Moro 2, 00185 Roma, Italy

[12] Scuola Superiore Meridionale, Largo S. Marcellino 10, 80138 Napoli, Italy

[13] Laboratoire Astroparticule et Cosmologie, CNRS Université de Paris, 75013 Paris, France

[14] National Observatory of Athens, Lofos Nymfon, 11852 Athens, Greece

[15] Dipartimento di Fisica Galileo Galilei, Università di Padova, 35131 Padova, Italy

[16] INFN Sezione di Padova, 35131 Padova, Italy

[17] INAF-Osservatorio Astronomico di Padova, Padova, Italy

[18] Institut d'Astrophysique de Paris, GReCO, UMR 7095 du CNRS et de Sorbonne Université, 98bis boulevard Arago, 75014 Paris, France

[19] Département de Physique Théorique and Gravitational Wave Science Center (GWSC), Université de Genève, 1211 Geneva, Switzerland

[20] Department of Physics-ETSIDI, Universidad Politécnica de Madrid, 28012 Madrid, Spain

[21] Max-Planck-Institut für Physik (Werner-Heisenberg-Institut), Föhringer Ring 6, 80805 München, Germany

[22] Main Astronomical Observatory of the National Academy of Sciences of Ukraine, Zabolotnoho str., 27, 03143 Kyiv, Ukraine

[23] AGH University of Krakow, Aleja Mickiewicza, 30, 30-059 Krakow, Poland

[24] Faculty of Natural Sciences, National University "Kyiv Mohyla Academy", Skovorody str., 2, 04070 Kyiv, Ukraine

[25] Astronomical Observatory of Taras Shevchenko National University of Kyiv, Observatorna str., 3, 04053 Kyiv, Ukraine

[26] Department of Physics, Ben-Gurion University of the Negev, Beer Sheva 84105, Israel

[27] CEICO, FZU–Institute of Physics of the Czech Academy of Sciences, Na Slovance 2, 182 21 Prague, Czech Republic

[28] Feza Gursey Institute, Bogazici University, Kandilli, Istanbul, Turkey

[29] Laboratoire de Physique de l'École Normale Supérieure, ENS, CNRS, Université PSL, Sorbonne Université, Université Paris Cité, 75005 Paris, France

[30] Institute of Cosmology and Gravitation, University of Portsmouth, Dennis Sciama Building, Burnaby Road, Portsmouth PO1 3FX, UK